

Geochemistry of diamonds and their mineral inclusions constraining the composition of the lithospheric mantle and recycling of crustal materials

by

Mei Yan Lai

A thesis submitted in partial fulfillment of the requirements for the degree of

Doctor of Philosophy

Department of Earth and Atmospheric Sciences

University of Alberta

© Mei Yan Lai, 2022

Abstract

Bimineralic eclogite xenoliths from Koidu have been extensively studied previously, but less attention has been directed towards diamondiferous eclogite xenoliths as well as eclogitic and peridotitic diamonds from this locality. To gain insight into the geologic history of the lithospheric mantle of the West African Craton beneath Koidu, a suite of 105 diamonds and their mineral inclusions and six diamond-bearing eclogites from Koidu are analyzed for major element, trace element and stable isotopic compositions in this study.

Of 105 Koidu diamonds, 78% contain eclogitic mineral inclusions, 17% contain peridotitic mineral inclusions and 5% contain co-occurring eclogitic and peridotitic mineral inclusions indicating a mixed paragenesis. All diamonds were analyzed *in situ* for carbon ($\delta^{13}\text{C}$) and nitrogen ($\delta^{15}\text{N}$) isotope compositions, nitrogen concentrations and nitrogen aggregation states. Based on the $\delta^{13}\text{C}$ - $\delta^{15}\text{N}$ systematics, Koidu diamonds can be classified into three distinct compositional clusters: (1) diamonds derived from recycled crustal carbon and nitrogen ($\delta^{13}\text{C} = -33.2$ to -14.4% ; $\delta^{15}\text{N} = -5.3$ to $+10.1\%$); (2) diamonds derived from mixing of carbon and nitrogen from subducted and mantle sources ($\delta^{13}\text{C} = -6.0$ to -1.1% ; $\delta^{15}\text{N} = -4.2$ to $+9.7\%$); and (3) diamonds derived from mantle-derived carbon and nitrogen ($\delta^{13}\text{C} = -7.8$ to -3.6% ; $\delta^{15}\text{N} = -7.9$ to -2.1%). The distinct isotopic signatures of the three diamond clusters suggest episodic diamond growth during multiple fluid/melt pulses.

Peridotitic diamonds contain olivine inclusions with high Mg# (92.2–94.7), indicating highly-depleted dunites or harzburgites as the preferred substrates for peridotitic diamond formation at Koidu. High-Ti spinel inclusions ($\text{TiO}_2 = 2.8$ wt%) occurring in one peridotitic diamond indicate melt-metasomatic Ti re-enrichment which may have converted some dunites or

harzburgites into lherzolites, as lherzolic garnet dominates in heavy mineral concentrate recovered from Koidu. Eclogitic diamonds with coexisting garnet and omphacite inclusions were used to estimate the depth distribution of eclogitic substrates through the Koidu lithospheric mantle. Diamond-bearing eclogites with gabbroic oceanic crust protoliths derived from shallower lithospheric depths (150 to 190 km) compared to those with basaltic protoliths (≥ 200 km). Eclogite whole-rock trace-element compositions reconstructed from co-existing garnet and omphacite inclusions indicate that a subset of eclogites experienced a high-degree of melt extraction ($> 20\%$ batch melting), followed by metasomatic LREE re-enrichment prior to or coeval with diamond formation. A high abundance of coesite inclusions (in 44% of studied diamonds) is in apparent contradiction to the high modeled melt degrees but can be reconciled if the coesite is of secondary nature, introduced via metasomatism subsequent to melt extraction.

A set of 16 eclogitic garnet inclusions were analyzed for oxygen isotope composition ($\delta^{18}\text{O}$). One eclogitic garnet inclusion has a positive Eu-anomaly and $\delta^{18}\text{O}$ of +5.4 ‰, suggesting derivation from gabbroic layers of oceanic crust. Fourteen eclogitic garnet inclusions have much higher $\delta^{18}\text{O}$ (+9.9 to +12.1 ‰) consistent with extensive low-temperature seawater alteration of upper basaltic layers of oceanic crust protoliths. The one remaining garnet inclusion has a mild majorite component (Si = 3.03), with $\delta^{18}\text{O}$ of +6.3 ‰ and relatively high Mg# (79.0) and Cr# (0.90), suggesting its formation involved interaction with ambient peridotitic mantle. Covariations between major element compositions (Mg#, Ca# and Cr#) and $\delta^{18}\text{O}$ in garnet inclusions suggest possible chemical exchange between eclogite and ambient mantle, which may have been facilitated by eclogite-derived melt. However, $\delta^{13}\text{C}$ of the host diamonds do not show correlations with $\delta^{18}\text{O}$ of these garnets, suggesting that there was no significant mixing between crust- and mantle-derived carbon during diamond formation.

Preface

(1) A modified version of Chapter 2 has been published as

Lai, M. Y., Stachel, T., Stern, R. A., Hardman, M. F., Pearson, D. G., and Harris, J. W. (2022) Formation of mixed paragenesis diamonds during multistage growth – Constraints from *in situ* $\delta^{13}\text{C}$ – $\delta^{15}\text{N}$ –[N] analyses of Koidu diamonds. *Geochimica et Cosmochimica Acta*, **323**, 20-39.

I was responsible for sample preparation and analysis, data interpretation and manuscript composition. Thomas Stachel guided the project and assisted with data interpretation and preparation of the manuscript. Richard A. Stern assisted in determination of isotope compositions of diamonds by SIMS. Matthew F. Hardman and D. Graham Pearson contributed to manuscript edits. Jeff W. Harris provided the samples for this research and reviewed the manuscript.

(2) Supplementary data can be found in University of Alberta Libraries collections:

(a) Descriptions of Koidu diamonds and their mineral inclusions

<https://doi.org/10.7939/r3-fwvg-pb91>

(b) Photos of Koidu diamonds

<https://doi.org/10.7939/r3-cr9f-r922>

(c) Infrared absorption spectra of Koidu diamonds

<https://doi.org/10.7939/r3-2yn4-yw02>

(d) Cathodoluminescence images of Koidu diamonds

<https://doi.org/10.7939/r3-07g6-nw92>

(e) Major element compositions of mineral inclusions in Koidu diamonds

<https://doi.org/10.7939/r3-4fdy-kz82>

(f) Trace element compositions of mineral inclusions in Koidu diamonds

<https://doi.org/10.7939/r3-14p4-8t17>

Acknowledgements

I am very grateful to my supervisor, Thomas Stachel, for giving me the opportunity to work with him on interesting diamond projects. Even though I did not have any background in Geology before I came to Canada, Thomas has been very patient and understanding during my MSc and PhD studies. I really enjoy working with him because he is very efficient. His guidance and advice also greatly improved my writing. Thank you for always being so supportive and encouraging during my journey.

Thank you to Graham Pearson for providing me with all necessary resources for my projects, as well as meeting with me to discuss my data. Thank you to Bob Luth for explaining carbonation of eclogite to me. I would also like to thank Jeff Harris for donating his invaluable collection of Koidu diamonds for my PhD study, these samples are absolutely fascinating and I have learned so much from studying them. Jeff is a delight and we always enjoy his lectures on the history and development of diamond research. In addition, thank you Jeff for your kind words that bring me comfort and confidence.

During the past few years, I was fortunate to have the opportunities to work as an intern at Dominion Diamond Mines (now Arctic Canadian Diamond Company) and GIA. I am grateful to Jon Carlson and Kimberly Ferguson (Dominion Diamond Mines), for teaching me a lot about diamond mining, as well as letting me visit the Ekati diamond mines in the Lac de Gras region, the facilities for diamond processing in Saskatchewan, and the diamond sorting centre in Toronto. Thank you to Mike Breeding (GIA) for guiding me throughout my research project during my internship. I would also like to thank Anetta Banas for organizing the DERTS program. The internship component of this program definitely broadens our horizon and assists our future career.

I am really glad to be part of the DERTS program.

Andrew Locock is thanked for helping me with EPMA work. Working with Andrew has been delightful and I have learned a lot from him about minerals. I would also like to thank Richard Stern for all the efficient and high-quality SIMS analyses, as well as Robert Dokken for his excellent sample preparation skills. A huge thank you to Mark Labbe for helping me in many respects. I would also like to thank Yan Luo and H el ene Legros for assistance with LA-ICP-MS.

Matthew Hardman is thanked for sharing his knowledge about eclogite with me, reviewing my drafts and providing many helpful comments, as well as recommending relevant articles that help me with my writing. Thank you to Nicole Meyer, for showing me how to mount mineral inclusions; and to Kan Li, for sharing his knowledge about stable isotope with me. Special thanks to my friends in the Diamond Research Group/DERTS program – Sarah, Melissa, Fiona, Kristi, Kelsey, Mandy, Irina, Suzette, Andrea, Daoheng, Ji, Qiwei and Alex, for the laughter and friendship. I will definitely miss the days when we got London fog/frosty/ice cream together.

Thank you everyone for making my journey in Canada so memorable. I will miss you all, and Edmonton of course, but maybe not the cold weather. I am excited to start a new chapter in my life!

Contents

Chapter 1 Introduction and background	1
1.1 Diamond as a probe into Earth's mantle	1
1.2 Diamond as a recorder of Earth's geotectonic history	1
1.3 Diamond as a tracer of volatile recycling.....	2
1.4 Rock types in Earth's upper mantle.....	3
1.5 Paragenesis of diamond.....	5
1.6 Study area and geologic background.....	6
1.7 Existing data	7
1.8 Layout.....	8
References.....	12
Chapter 2 Formation of mixed paragenesis diamonds during multistage growth – constraints from <i>in situ</i> $\delta^{13}\text{C}$ – $\delta^{15}\text{N}$ –[N] analyses of Koidu diamonds	20
2.1 Introduction	20
2.2 Sample description	21
2.3 Analytical methods.....	23
2.3.1 Mineral inclusions	23
2.3.2 Host diamonds	24
2.4 Results	26
2.4.1 Mineral inclusions from mixed paragenesis diamonds	26
2.4.2 $\delta^{13}\text{C}$, $\delta^{15}\text{N}$ and N concentrations in Koidu diamonds.....	28
2.4.3 Nitrogen aggregation in episodically grown diamonds.....	32
2.5 Discussion	32
2.5.1 Origin of eclogitic mineral inclusions in Koidu mixed paragenesis diamonds.....	33
2.5.2 Progressive precipitation of eclogitic and then peridotitic inclusions from an evolving	

eclogite-derived fluid.....	35
2.5.3 Covariation of $\delta^{13}\text{C}$ values and N abundance.....	36
2.5.4 Sources of C and N in Koidu diamonds	37
2.5.5 Growth episodes of Koidu diamonds	41
2.6 Conclusions	44
References.....	61
Chapter 3 Nature of slab-mantle interaction recorded by coupled $\delta^{13}\text{C}$ – $\delta^{15}\text{N}$ – $\delta^{18}\text{O}$ signatures and elemental compositions of diamonds and their inclusions	73
3.1 Introduction	73
3.2 Samples and methods	75
3.3 Results	77
3.3.1 Major element composition	77
3.3.2 Trace element composition.....	78
3.3.3 Oxygen isotope composition	79
3.4 Discussion	80
3.4.1 Origin of Koidu eclogites	80
3.4.2 Slab-mantle interaction during diamond formation.....	82
3.4.3 Variation of $\delta^{18}\text{O}$ – $\delta^{13}\text{C}$: mixing between AOC- and mantle-derived carbon?.....	84
3.4.4 Variation of $\delta^{18}\text{O}$ – $\delta^{15}\text{N}$: mixing between AOC- and mantle-derived nitrogen?	87
3.5 Conclusions	89
References.....	104
Chapter 4 Composition and evolution of the lithospheric mantle and its subducted components beneath the Koidu kimberlite, West African Craton	117
4.1 Introduction.....	117
4.2 Samples and analytical methods	119
4.3 Results	121

4.3.1 Major element compositions of minerals	121
4.3.2 Trace element compositions of minerals	126
4.3.3 Reconstructed whole-rock compositions.....	128
4.3.4 Geothermobarometry.....	129
4.3.5 Oxygen isotope compositions.....	130
4.4 Discussion	130
4.4.1 Mantle substrates for diamond formation beneath the West African Craton.....	131
4.4.2 Evolution of subducted oceanic crust beneath the West African Craton	136
4.5 Conclusions	140
References.....	160
Chapter 5 Conclusions	171
5.1 Volatile recycling recorded by diamonds.....	171
5.2 Diamond formation mechanisms	171
5.3 The lithospheric mantle beneath Koidu	173
5.4 Future directions.....	175
Appendix A.....	176
Appendix B.....	201
Appendix C.....	208

List of Figures

1.1 Geological map of the southern part of the West African Craton	11
2.1 Diamonds with co-occurring eclogitic and peridotitic mineral inclusions	46
2.2 Ternary diagram of omphacite inclusions from mixed paragenesis diamond	47
2.3 REE concentrations in omphacites from mixed paragenesis diamond	48
2.4 Concentrations of LILE and HFSE in omphacites from mixed paragenesis diamond	49
2.5 Ternary diagram of garnet inclusions from mixed paragenesis diamond	50
2.6 REE concentrations in garnets from mixed paragenesis diamond	51
2.7 Concentrations of LILE and HFSE in garnets from mixed paragenesis diamond	52
2.8 Distribution of $\delta^{13}\text{C}$ values in peridotitic, eclogitic and mixed paragenesis diamonds	53
2.9 $\delta^{13}\text{C}$ versus $\delta^{15}\text{N}$ for peridotitic, eclogitic and mixed paragenesis diamonds	54
2.10 Examples of cathodoluminescence images of Koidu eclogitic diamonds	55
2.11 Core-to-rim transects across the four fragments of mixed paragenesis diamond	56
2.12 Infrared absorption spectra of diamond collected through its centre and rim	58
2.13 Schematic diagram showing the growth episodes reflected by Koidu diamonds	59
3.1 Plot of Ti against Na cations in garnet inclusions in Koidu diamonds	92
3.2 Plot of Al against Ti cations in garnet inclusions in Koidu diamonds	93
3.3 Variation between Si and Al+Cr in garnets	94
3.4 REE concentrations in eclogitic garnets from Koidu diamonds	95
3.5 Distribution of $\delta^{18}\text{O}$ values in garnet inclusions from Koidu diamonds	97
3.6 $\delta^{18}\text{O}$ of eclogitic garnet inclusions in diamonds worldwide	98
3.7 Covariations of $\delta^{18}\text{O}$ and molar Mg#, Ca# and Cr# in Koidu garnet inclusions	99
3.8 $\delta^{18}\text{O}$ of garnet inclusions and $\delta^{13}\text{C}$ of their host diamonds	101
3.9 Cathodoluminescence image of diamond showing inner and outer growth zones	102

3.10 $\delta^{18}\text{O}$ of eclogitic garnet inclusions and $\delta^{15}\text{N}$ of their host diamonds.....	103
4.1 Histograms of molar Mg# of olivine inclusions in diamonds.....	143
4.2 Molar Cr# vs molar Mg# of spinel inclusions in Koidu diamonds.....	144
4.3 Jadeite component vs molar Mg# of omphacite in diamonds and xenoliths	145
4.4 Ternary diagram of omphacite in diamonds and xenoliths.....	146
4.5 Molar Ca# vs molar Mg# of garnets in diamonds and xenoliths	147
4.6 Fe-Ni-S quadrilateral for sulphide inclusions from Koidu	148
4.7 REE concentrations of garnet in diamonds and xenoliths	149
4.8 REE concentrations of omphacite in diamonds and xenoliths.....	151
4.9 Ternary diagram for reconstructed bulk rock compositions	153
4.10 REE concentrations in reconstructed whole-rocks	154
4.11 Equilibration temperatures for minerals in diamonds and xenoliths	155
4.12 Batch melting residues compared to REE _N patterns of reconstructed whole-rocks	156
4.13 Fractional melting residues compared to REE _N patterns of reconstructed whole-rocks	158
4.14 Extended trace element patterns for reconstructed whole-rocks	159
A.1 Common surface textures of Koidu diamonds.....	200
B.1 Major element composition of Koidu majoritic garnet.....	207
C.1 Texture of Koidu diamondiferous eclogite xenolith	228
C.2 Accessory phlogopite in a Koidu diamondiferous eclogite xenolith	229
C.3 Common mineral inclusions in Koidu diamonds.....	230

List of Tables

A.1 Characteristics of Koidu diamonds.....	177
A.2 Major element compositions of mineral inclusions in other mixed paragenesis diamonds...	181
A.3 Major element compositions of mineral inclusions in diamond 133-6 and 138-7.....	182
A.4 Trace element compositions of mineral inclusions in diamond 133-6 and 138-7.....	183
A.5 Summary of SIMS analysis of Koidu diamonds.....	184
A.6 SIMS analysis of Koidu diamonds.....	185
B.1 Major element composition of garnet inclusions in 16 Koidu diamonds.....	202
B.2 Trace element concentration of garnet inclusions in 16 Koidu diamonds.....	203
B.3 Average $\delta^{18}\text{O}$ values and nitrogen concentrations, $\delta^{13}\text{C}$ and $\delta^{15}\text{N}$ values of garnet inclusions and their host diamonds.....	204
B.4 SIMS analysis of garnet inclusions in 16 Koidu diamonds.....	205
C.1 Inclusion abundance in Koidu diamonds.....	209
C.2 Major element compositions of representative silicate and oxide inclusions from Koidu diamonds, and of constituent garnet and omphacite from Koidu diamond-bearing eclogite xenoliths.....	210
C.3 Trace element compositions of representative garnet and omphacite inclusions from Koidu diamonds, and constituent garnet and omphacite from Koidu xenoliths.....	215
C.4 Major element and trace element compositions of reconstructed whole-rocks from garnet and omphacite inclusions.....	220
C.5 Average $\delta^{18}\text{O}$ values of garnet grains in six Koidu diamondiferous eclogites.....	224
C.6 SIMS analysis of garnet grains in six Koidu diamondiferous eclogites.....	225

List of abbreviations and symbols

~	approximately
°C	degree Celsius
‰	per mil; parts per thousand
r^2	r-squared; coefficient of determination
σ	sigma; one standard deviation of the mean
Σ	sum
A-centre	lattice defect in diamond with a structure of paired nitrogen atoms
AOC	altered oceanic crust
at.ppm	atomic parts per million
b.d.l.	below detection limit
B-centre	lattice defect in diamond with a structure of four nitrogen atoms surrounding a vacancy
BSE	back-scattered electron
Ca#	$100 \times \text{Ca}/(\text{Ca} + \text{Mg} + \text{Fe})$
C-centre	lattice defect in diamond in the form of single substitutional nitrogen
CL	cathodoluminescence
Cr#	$100 \times \text{Cr}/(\text{Cr} + \text{Al})$
e.g.	for example
EDS	energy-dispersive spectroscopy
EPMA	electron probe microanalyzer
Eu/Eu*	Europium anomaly; $\text{Eu}_N/(\text{Sm}_N \times \text{Gd}_N)^{0.5}$
FTIR	Fourier transform infrared

Ga	giga-annum; billion years
GPa	gigapascal
HFSE	high-field-strength element
HREE	heavy rare earth element
i.e.	that is
$K_N^{\text{diamond-fluid}}$	partition coefficient of nitrogen between diamond and diamond-forming fluid
LA-ICP-MS	laser ablation inductively coupled plasma mass spectrometer
LILE	large-ion lithophile element
LREE	light rare earth element
Ma	mega-annum; million years
Mg#	$100 \times \text{Mg}/(\text{Mg} + \text{Fe})$
mol%	mole percent
MORB	mid-ocean ridge basalt
MREE	middle rare earth element
μ_A	absorption coefficient at 1282 cm^{-1} for the A-centre
μ_B	absorption coefficient at 1282 cm^{-1} for the B-centre
N	subscript to denote normalized values
$[N_A]$	concentration of nitrogen in A-centre
$[N_B]$	concentration of nitrogen in B-centre
n.d.	not determined
N3 centre	lattice defect in diamond with a structure of three nitrogen atoms surrounding a vacancy

NIST	National Institute of Standards and Technology
NMORB	normal-type mid-ocean ridge basalt
%B	percentage of nitrogen in B-centre
ppb	parts per billion
P-T	pressure-temperature
SEM	scanning electron microscope
SIMS	secondary ion mass spectrometry
Type IaA	type of diamond with proportion of A-centre > 90%
Type IaAB	type of diamond with proportion of A-centre between 10 and 90%
Type IaB	type of diamond with proportion of B-centre > 90%
vol%	volume percent
VPDB	Vienna Pee Dee Belemnite
VSMOW	Vienna Standard Mean Ocean Water
WDS	wavelength-dispersive spectrometer
wt%	weight percent
$\delta^{13}\text{C}$	carbon isotope composition ($^{13}\text{C}/^{12}\text{C}$) normalized to VPDB
$\delta^{15}\text{N}$	nitrogen isotope composition ($^{15}\text{N}/^{14}\text{N}$) normalized to atmosphere
$\delta^{18}\text{O}$	oxygen isotope composition ($^{18}\text{O}/^{16}\text{O}$) normalized to VSMOW

Chapter 1 Introduction and background

1.1 Diamond as a probe into Earth's mantle

Diamond is one of the most valuable minerals due to its superb physical and chemical properties, and scarcity worldwide (typically at the ppb level even in volcanic host rocks that carry minable diamond contents; Gurney, 1989; Read and Janse, 2009). Most diamonds form in the subcratonic lithospheric mantle (approximately 99% of diamonds recovered globally; Stachel and Harris, 2008), at depths of 140–200 km (Stachel and Harris, 2009). These depths cannot be directly sampled by any physical method. However, about a century ago, researchers noticed that some diamonds contain mineral inclusions similar to minerals in their host rocks, encapsulated during diamond formation (e.g. Sutton, 1907, 1921). Since then, scientists have been using inclusion-bearing diamond as a tool to interpret the composition of Earth's mantle.

Due to their extreme hardness, diamonds are likely to survive the journey from the mantle to Earth's surface, entrained by kimberlite magma as xenocrysts. Occasionally, fragments of mantle rocks such as peridotite and eclogite are also transported as xenoliths, but their compositions may be modified by kimberlite infiltration and/or other mantle processes, such as mantle metasomatism (e.g., MacDougall and Haggerty, 1999; Barth et al., 2001; Aulbach et al., 2019a). In contrast, inclusions trapped inside diamond preserve the most pristine information about the conditions in the mantle at the time of diamond formation, and are not affected by post-formation mantle processes.

1.2 Diamond as a recorder of Earth's geotectonic history

Minerals encapsulated by diamonds are isolated from their host rocks, thus preventing further diffusive exchange of elements and isotopes. Based on mantle residence above closure

temperature in the presence of fluid, radiogenic isotope systems in minerals (e.g., Re–Os isotope system in sulphide inclusions; Pearson et al., 1998) start at the time of diamond formation, giving a synchronous age of mineral inclusions and their host diamonds (Nestola et al., 2017). Age dating of diamonds, utilizing radiogenic isotope systems in their inclusions, has provided important constraints on tectonothermal events on the local and global scale. Peridotitic diamonds occur since ~3.5–3.3 Ga, whereas the oldest eclogitic diamonds found to date formed at ~2.9 Ga (Richardson et al., 2001; Shirey et al., 2001; Westerlund et al., 2006; Aulbach et al., 2009).

As formation of eclogitic diamonds is linked to subducted and metamorphosed oceanic crust (e.g., Jaques et al., 1989), the oldest age of eclogitic diamonds (2.9 Ga) implies that global plate tectonic processes, known as Wilson cycles, began at ~3 Ga (Shirey and Richardson, 2011). This is consistent with sulphur isotope signatures of sulphide inclusions in diamonds, where mass-independently fractionated sulphur isotopes indicate that surficial sulphur was transported into the mantle through subduction processes prior to the great oxidation event at ~2.5 Ga (Farquhar et al., 2002). Plate tectonic processes involving rifting and assembly of continents often facilitate diamond formation, and these processes may have been more prominent from 2.2 to 0.8 Ga, as inferred by the formation ages of most eclogitic diamonds worldwide (Gurney et al., 2010; Shirey and Richardson, 2011; Smit and Shirey, 2020; Howell et al., 2020).

1.3 Diamond as a tracer of volatile recycling

Diamond is composed of carbon but usually contains nitrogen as a substitutional impurity (concentrations of nitrogen in diamonds can reach 5200 at.ppm; e.g., Smart et al., 2011), as nitrogen has similar ionic radius and charge to carbon. Isotopic compositions of carbon and nitrogen, denoted as $\delta^{13}\text{C}$ and $\delta^{15}\text{N}$, respectively, are robust tracers of their origins. Mantle-derived carbon and nitrogen have a narrow range of isotopic compositions (both about $-5 \pm 3\%$; Cartigny

et al., 2014), whereas crust-derived carbon and nitrogen, involving contributions from biogenic carbonate, organic matter and low- and high-temperature clay, can have very extreme isotopic compositions (e.g., Kirkley et al., 1991; Boyd and Phillinger 1994; Busigny et al., 2005; Li et al., 2007; Li et al., 2019).

Diamonds usually grow episodically, as observed in their internal growth textures imaged by cathodoluminescence, in which multiple growth layers resembling tree rings are caused by intermittent growth, and possibly changes in diamond-forming fluid/melt composition. In some extreme cases, diamonds resume growth after residing in the mantle for very long periods of time (up to ~ 1 Ga; Wiggers de Vries et al., 2013). This can result in diamond cores with long mantle residence times (tens of millions to > 1 billion years) coated by a much younger overgrowth (mantle residence times of years to tens of thousands of years) with distinct isotopic compositions, indicating formation from fluids/melts with different composition (e.g., cores with crustal carbon isotope signatures and overgrowths with mantle carbon isotope signatures; Lai et al., 2020). By *in situ* analysis of diamonds cut and polished through the centre along a $\{110\}$ plane, the variation of isotopic compositions of diamond through time can be detected, thus allowing to trace the sources of carbon and nitrogen that contributed during the diamond formation processes.

1.4 Rock types in Earth's upper mantle

Earth's upper mantle is mainly composed of peridotite, with minor proportions of eclogite and pyroxenite (Schulze, 1989). Peridotite is further divided into dunite (olivine > 90 vol%), harzburgite (olivine + orthopyroxene), lherzolite (olivine + orthopyroxene + clinopyroxene) and wehrlite (olivine + clinopyroxene). Common accessory phases in peridotite include (from low- to high-pressure) plagioclase, spinel and garnet. The evolution of lherzolite to harzburgite to dunite represents the compositional evolution associated with an increasing degree of broadly basaltic

melt extraction in the mantle, where the melt is enriched in CaO, Al₂O₃ and Na₂O, and depleted in MgO and NiO, leading to the increase of molar Mg# [Mg/(Mg+Fe)] in the residual rocks (McDonough and Rudnick, 1998).

Eclogite consists of approximately equal proportions of garnet and omphacite (the sodic nature of the clinopyroxene differentiates it from garnet clinopyroxenite), with the ratio of garnet to omphacite typically ranging from 70:30 to 40:60 (Jacob, 2004). Formation of eclogites has been attributed to subduction and high-pressure metamorphism of oceanic crust (Helmstaedt and Doig, 1975; MacGregor and Manton, 1986). The presence of positive or negative europium anomalies (i.e., on a chondrite normalized basis, Eu is enriched or depleted relative to the neighbouring rare earth elements Sm and Gd) and of fractionated oxygen isotope compositions (¹⁸O/¹⁶O, denoted by δ¹⁸O relative to Vienna Standard Mean Ocean Water; VSMOW) in some eclogites unequivocally supports a crustal origin for their protoliths. Europium is the only rare earth element in nature that can occur in the divalent state, which readily substitutes for Ca²⁺ in plagioclase as both elements have similar ionic radius. During oceanic crust formation, accumulation and fractionation of plagioclase in intrusive and extrusive portions of oceanic crust may create positive and negative europium anomalies, respectively (Philpotts and Schnetzler, 1968; Jacob, 2004; Aulbach and Jacob, 2016). Subsequently, alteration of oceanic crust by seawater results in shifts of its oxygen isotope composition away from that of fresh mid-ocean ridge basalt (average δ¹⁸O value of +5.5 ‰; Eiler et al., 2000). Minerals formed in eclogites during prograde metamorphism of altered oceanic crust inherit these trace element and oxygen isotopic signatures from their precursor. Eclogite elemental compositions can, however, be modified by additional processes, including devolatilization and partial melting during and after subduction, which may lead to depletion in incompatible element contents, or mantle metasomatism that may affect major, trace element and

oxygen isotope compositions and may also introduce new minerals (Jacob, 2004).

1.5 Paragenesis of diamond

Mineral inclusions in diamond reflect the composition of their source rocks in the mantle. Diamonds encapsulating minerals associated with peridotite or eclogite are referred to as peridotitic or eclogitic diamonds, respectively. The most common minerals found in diamond are garnet, olivine, clinopyroxene, orthopyroxene, spinel and sulphide (Meyer, 1987; Stachel and Harris, 2008).

Similar to their mantle source rocks, peridotitic diamonds can be further divided into dunitic/harzburgitic, lherzolitic and wehrlitic diamonds. Based on the composition of garnet inclusions in peridotitic diamonds (Sobolev et al. 1973; Grütter et al., 2004), dunitic/harzburgitic diamonds are the most abundant and constitute approximately 86% of the studied diamonds worldwide, whereas wehrlitic diamonds (1%) are uncommon (Stachel and Harris, 2008). It is not possible to separate dunitic and harzburgitic diamonds based solely on their olivine or garnet inclusions, as these inclusions have overlapping Mg# and Cr₂O₃ and CaO contents for both paragenesis.

As for eclogitic diamonds, the composition of garnet inclusions alone cannot always unambiguously distinguish between eclogitic and pyroxenitic host rocks; the composition of clinopyroxene is crucial, as a Na-rich character (i.e., omphacite) is a requirement for eclogite (Desmons and Smulikowski 2004). A single garnet inclusion with low Cr₂O₃ (< 1 wt%) and CaO (2 to < 6 wt%) content (G4 garnet; Grütter et al. 2004), for example, has an equivocal host rock, which may correspond to relatively calcium-poor eclogite (omphacite-bearing) or pyroxenite (diopside-bearing).

A minor proportion of diamonds contain inclusions of websteritic (pyroxenitic) paragenesis, which have mineral compositions intermediate between peridotitic and eclogitic inclusions (Gurney et al., 1984; Deines et al., 1993) and which may result from the reaction of eclogite-derived melts/fluids with surrounding peridotite in the mantle (Aulbach et al., 2002; Mikhail et al., 2021) or from ultramafic (kimberlite) metasomatism of original eclogites (Aulbach et al., 2019a).

Combining all studied inclusion-bearing lithospheric diamonds worldwide, 65% are peridotitic, 33% are eclogitic, and 2% are websteritic (Stachel and Harris, 2008). Given the small proportion of eclogite in the lithospheric mantle, such high abundance of eclogitic diamond implies that eclogite provides a more suitable environment for diamond growth than peridotite (Stachel and Luth, 2015; Stachel et al., 2022).

1.6 Study area and geologic background

Earth's upper mantle is compositionally, lithologically and structurally heterogeneous. The chemical and physical properties of the subcratonic lithospheric mantle at different localities, even within the same craton, can be very different due to localized geodynamic processes (e.g., subduction, melt depletion, metasomatism and plume activity). Thus, a compilation of geologic data from different regions of a craton is necessary for understanding its origin and evolution.

My research focuses on samples derived from the lithospheric mantle of the West African Craton (Fig. 1.1). Diamondiferous eclogite xenoliths were obtained from the Koidu kimberlite complex, while inclusion-bearing diamonds were collected from both the Koidu kimberlite complex and an adjacent sedimentary basin, in the Kono District of eastern Sierra Leone, situated on the Archean Man Shield in the southern part of the West African Craton.

The Archean rocks in the Man Shield are comprised mainly of 3.26–2.85 Ga tonalite-

trondhjemite-granodiorite (TTG) gneisses (up to 3.6–3.5 Ga in age), supracrustal belts containing a basalt-komatiite sequence overlain by sediments, and ca. 2.8 Ga granitoids formed in a craton-wide thermal event (Rollinson, 2016). The whole rock Re–Os isochron age of low-MgO eclogite xenoliths from the Koidu kimberlite complex was found to be 3.4 ± 0.8 Ga, indicating the possibility of their formation during Archean subduction (Barth et al., 2002a). Strontium-U-Pb dating of clinopyroxenes from Koidu eclogite xenoliths also suggested at least Proterozoic and possibly Archean ages, with a preferred age of 2.7 Ga (Aulbach et al., 2019b). The Neoproterozoic break-up of Rodinia may have led to infiltration of the West African lithospheric mantle by a kimberlite-like metasomatic agent (Aulbach et al., 2019a). This metasomatic event may have prompted diamond formation at ca. 0.6 Ga, as indicated by Re–Os isochron ages of sulphide inclusions in diamonds from Zimmi, West Africa, with radiogenic and sulphur stable isotope compositions requiring an Archean subduction origin (Smit et al., 2016, 2019a).

The Koidu kimberlite complex is one of few localities worldwide where eclogites constitute the only type of mantle xenoliths (Tompkins and Haggerty, 1984; Hills and Haggerty, 1989; Fung and Haggerty, 1995). Despite the absence of peridotite xenoliths, indicator minerals (heavy media separates) from the Koidu kimberlites are both peridotitic and eclogitic (Skinner et al., 2004). A more recent study of Koidu indicator minerals documented a large proportion of garnets with high chromium and low calcium contents, indicating the presence of strongly depleted harzburgites or dunites in the underlying lithospheric mantle (Harder et al., 2013).

1.7 Existing data

A small number of diamonds with either eclogitic or peridotitic inclusions has previously been recovered from Sierra Leone, containing olivine, enstatite, Cr-pyrope garnet, chromite (Meyer and Boyd, 1972) and sulphide inclusions (Deines and Harris, 1995; Smit et al., 2016).

These inclusions were analyzed for their major element compositions, but trace element compositions have not been determined. Carbon isotope analyses of Sierra Leone diamonds are also scarce, with only a few chromite- and sulphide-bearing diamonds from Koidu and Zimmi (Deines and Harris, 1995; Smit et al., 2019b, respectively) being analyzed and no nitrogen isotope compositions reported.

Eclogite xenoliths collected from the Koidu kimberlite complex were first systematically studied by Hills and Haggerty (1989), with the authors identifying both low-MgO (6–13 wt%) and high-MgO (16–20 wt%) eclogites. Accessory minerals including diamond, graphite, kyanite, corundum and quartz (after coesite) were reported in some low-MgO eclogites. Major element and selected trace element compositions of xenolith minerals and whole rocks are included in their study. Subsets of Koidu eclogites (bimineralic, kyanite-bearing, and graphite-bearing) were further studied by Fung and Haggerty (1995), Barth et al. (2001, 2002b) and Aulbach et al. (2019a). In addition to expanding the database of major and trace element compositions, oxygen isotope compositions of garnets from these samples were also reported.

1.8 Layout

This research aims to fill an important gap in our understanding of the geologic history of the lithospheric mantle of the West African Craton beneath the Koidu kimberlite complex: There has been a lack of information in the published literature on the geochemistry of Koidu diamonds and their mineral inclusions. Thus, Koidu inclusion-bearing diamonds are the main subject of this study. As mentioned above, inclusion-bearing diamonds are an essential tool to understand the composition of the mantle and the potential recycling of crustal materials. Diamond-bearing eclogites, as the host rocks for eclogitic diamonds, are also analyzed for comparison, in order to better constrain the origin(s) of Koidu eclogites and post-diamond-forming mantle processes

beneath the West African Craton.

The following chapters are dedicated to experimental results and data interpretation, summarized below.

Chapter 2: Formation of mixed paragenesis diamonds during multistage growth – Constraints from *in situ* $\delta^{13}\text{C}$ – $\delta^{15}\text{N}$ –[N] analyses of Koidu diamonds

In a suite of 105 inclusion-bearing Koidu diamonds, five contained co-occurring eclogitic and peridotitic mineral inclusions, classifying them as “mixed paragenesis” diamonds. Worldwide, mixed paragenesis diamonds are extremely rare, and the mechanism of their formation is unclear. This chapter focuses on the compositions of mineral inclusions in Koidu mixed paragenesis diamonds, as well as variations in carbon and nitrogen isotope signatures and nitrogen concentrations in different growth zones of the host diamonds, to trace the sources of diamond-forming fluids/melts and constrain the mechanism of their formation.

Chapter 3: Nature of slab-mantle interactions recorded by coupled $\delta^{13}\text{C}$ – $\delta^{15}\text{N}$ – $\delta^{18}\text{O}$ signatures and elemental compositions of diamonds and their inclusions

Eclogitic diamond formation could be associated with interactions between subducted oceanic crust-derived fluids/melts and ambient mantle (Mikhail et al., 2021), or interactions between eclogitic diamond substrates and mantle-derived fluids/melts (Aulbach et al., 2011), but the extent of these interactions has not been fully investigated. This chapter focuses on major element, trace element and oxygen isotope compositions of a subset of eclogitic garnet inclusions, as well as carbon and nitrogen isotope compositions of their 16 host diamonds. The coupled $\delta^{13}\text{C}$ – $\delta^{15}\text{N}$ – $\delta^{18}\text{O}$ signatures and elemental compositions of diamonds and their inclusions reflect the degree of crust-mantle interaction and are used to identify mixing of crust- and mantle-derived

carbon and nitrogen during diamond formation.

Chapter 4: Composition and evolution of the lithospheric mantle and its subducted components beneath the Koidu kimberlite, West African Craton

Scarcely any geochemical data for inclusions in diamonds from the Koidu kimberlite complex have been reported previously, hindering a thorough understanding of composition and early geologic history of the local lithospheric mantle. This chapter focuses on the major and trace element composition of mineral inclusions in Koidu diamonds. Inclusions in this study are predominantly eclogitic, implying that eclogites are the preferred diamond substrate beneath Koidu. Eclogitic garnet and omphacite inclusions coexisting in the same diamonds are used for whole-rock reconstructions. The reconstructed whole rocks are compared with biminerally and diamond-bearing eclogite xenoliths, to identify the geologic processes (e.g., melt depletion and metasomatism) experienced by their oceanic crustal protoliths after subduction and prograde metamorphism.

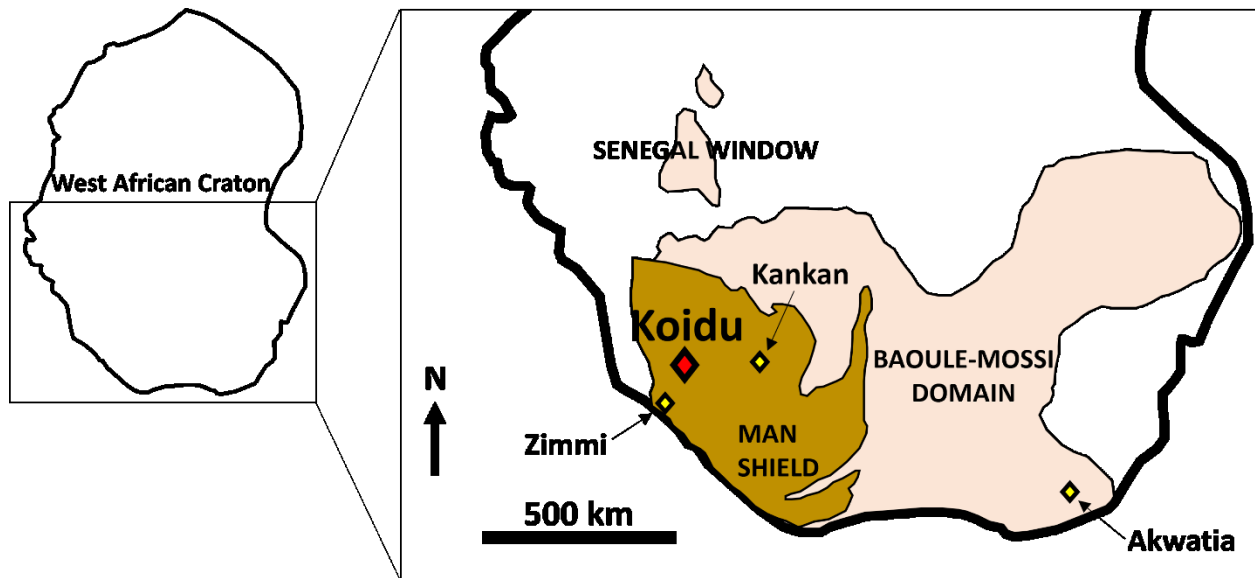


Figure 1.1 Geological map of the southern part of the West African Craton showing the locations of diamond deposits: Koidu, Zimmi, Kankan and Akwatia, after Rollinson (2016) and Smit et al. (2016).

References

- Aulbach S. and Jacob D. E. (2016) Major- and trace-elements in cratonic mantle eclogites and pyroxenites reveal heterogeneous sources and metamorphic processing of low-pressure protoliths. *Lithos* **262**, 586–605.
- Aulbach S., Stachel T., Viljoen K. S., Brey G. P. and Harris J. W. (2002) Eclogitic and websteritic diamond sources beneath the Limpopo Belt – Is slab-melting the link? *Contrib. to Mineral. Petrol.* **143**, 56–70.
- Aulbach S., Stachel T., Creaser R. A., Heaman L. M., Shirey S. B., Muehlenbachs K., Eichenberg D. and Harris J.W. (2009) Sulphide survival and diamond genesis during formation and evolution of Archaean subcontinental lithosphere: A comparison between the Slave and Kaapvaal cratons. *Lithos* **112**, 747–757.
- Aulbach S., Stachel T., Heaman L. M. and Carlson J. A. (2011) Microxenoliths from the Slave craton: archives of diamond formation along fluid conduits. *Lithos* **126**, 419-434.
- Aulbach S., Höfer H. E. and Gerdes A. (2019a) High-Mg and Low-Mg mantle eclogites from Koidu (West African Craton) linked by Neoproterozoic ultramafic melt metasomatism of subducted Archaean plateau-like oceanic crust. *J. Petrol.* **60**, 723–754.
- Aulbach S., Heaman L. M., Jacob D. E. and Viljoen K. S. (2019b) Ages and sources of mantle eclogites: ID-TIMS and in situ MC-ICPMS Pb-Sr isotope systematics of clinopyroxene. *Chem. Geol.* **503**, 15–28.
- Barth M. G., Rudnick R. L., Horn I., McDonough W. F., Spicuzza M. J., Valley J. W. and Haggerty S. E. (2001) Geochemistry of xenolithic eclogites from West Africa, part I: A link

- between low MgO eclogites and Archean crust formation. *Geochim. Cosmochim. Acta* **65**, 1499–1527.
- Barth M. G., Rudnick R. L., Carlson R. W., Horn I. and McDonough W. F. (2002a) Re-Os and U-Pb geochronological constraints on the eclogite-tonalite connection in the Archean Man Shield, West Africa. *Precambrian Res.* **118**, 267–283.
- Barth M. G., Rudnick R. L., Horn I., McDonough W. F., Spicuzza M. J., Valley J. W. and Haggerty S. E. (2002b) Geochemistry of xenolithic eclogites from West Africa, part 2: Origins of the high MgO eclogites. *Geochim. Cosmochim. Acta* **66**, 4325–4345.
- Boyd S. R. and Pillinger C. T. (1994) A preliminary study of $^{15}\text{N}/^{14}\text{N}$ in octahedral growth form diamonds. *Chem. Geol.* **116**, 43–59.
- Busigny V., Laverne C. and Bonifacie M. (2005) Nitrogen content and isotopic composition of oceanic crust at a superfast spreading ridge: A profile in altered basalts from ODP Site 1256, Leg 206. *Geochem. Geophys. Geosystems* **6**, 1–16.
- Cartigny P., Palot M., Thomassot E. and Harris J. W. (2014) Diamond formation: a stable isotope perspective. *Annu. Rev. Earth Planet. Sci.* **42**, 699–732.
- Deines P. and Harris J. W. (1995) Sulfide inclusion chemistry and carbon isotopes of African diamonds. *Geochim. Cosmochim. Acta* **59**, 3173–3188.
- Deines P., Harris J. W. and Gurney J. J. (1993) Depth-related carbon isotope and nitrogen concentration variability in the mantle below the Orapa kimberlite, Botswana, Africa. *Geochim. Cosmochim. Acta* **57**, 2781–2796.
- Desmons J. and Smulikowski W. (2007) High P/T Metamorphic Rocks. In *Metamorphic Rocks:*

A Classification and Glossary of Terms, pp. 32–35.

Eiler J. M., Schiano P., Kitchen N. and Stolper E. M. (2000) Oxygen-isotope evidence for recycled crust in the sources of mid-ocean-ridge basalts. *Nature* **403**, 530–534.

Farquhar J., Wing B. A., McKeegan K. D., Harris J. W., Cartigny P. and Thiemens M. H. (2002) Mass-independent sulfur of inclusions in diamond and sulfur recycling on early Earth. *Science* **298**, 2369–2372.

Fung A. T. and Haggerty S. E. (1995) Petrography and mineral compositions of eclogites from the Koidu Kimberlite Complex, Sierra Leone. *J. Geophys. Res.* **100**, 20451–20473.

Grütter H. S., Gurney J. J., Menzies A. H. and Winter F. (2004) An updated classification scheme for mantle-derived garnet, for use by diamond explorers. *Lithos* **77**, 841–857.

Gurney J. J., (1989) Diamonds. In *Kimberlites and related rocks (vol 2)*, pp. 935–965.

Gurney J. J., Harris J. W. and Rickard R. S. (1984) Silicate and oxide inclusions in diamonds from the Orapa Mine, Botswana. In *Kimberlites II: the mantle and crust-mantle relationships*, pp. 3–9.

Gurney J. J., Helmstaedt H. H., Richardson S. H. and Shirey S. B. (2010) Diamonds through Time. *Econ. Geol.* **105**, 689–712.

Harder M., Nowicki T. E., Hetman C. M., Freeman L. and Abedu B. (2013) Geology and Evaluation of the K2 Kimberlite, Koidu Mine, Sierra Leone, West Africa. *Proc. 10th Int. Kimberl. Conf.*, 191–208.

Helmstaedt H. and Doig R. (1975) Eclogite nodules from kimberlite pipes of the Colorado plateau - samples of subducted Franciscan-type oceanic lithosphere. *Phys. Chem. Earth*,

95–111.

Hills D. V. and Haggerty S. E. (1989) Petrochemistry of eclogites from the Koidu kimberlite complex, Sierra Leone. *Contrib. to Mineral. Petrol.* **103**, 397–422.

Howell D., Stachel T., Stern R. A., Pearson D. G., Nestola F., Hardman M. F., Harris J. W., Jaques A. L., Shirey S. B., Cartigny P., Smit K. V., Aulbach S., Brenker F. E., Jacob D. E., Thomassot E., Walter M. J. and Navon O. (2020) Deep carbon through time: Earth's diamond record and its implications for carbon cycling and fluid speciation in the mantle. *Geochim. Cosmochim. Acta* **275**, 99–122.

Jacob D. E. (2004) Nature and origin of eclogite xenoliths from kimberlites. *Lithos* **77**, 295–316.

Jaques A. L., Hall A. E., Sheraton J. W., Smith C. B., Sun S-S, Drew R. M., Foudoulis C. and Ellingsen K. (1989) Composition of crystalline inclusions and C-isotopic composition of Argyle and Ellendale diamonds. In *Kimberlites and related rocks (vol 2)*, pp. 966–989.

Kirkley M. B., Gurney J. J., Otter M. L., Hill S. J. and Daniels L. R. (1991) The application of C isotope measurements to the identification of the sources of C in diamonds: a review. *Appl. Geochem.* **6**, 477–494.

Lai M. Y., Stachel T., Breeding C. M. and Stern R. A. (2020) Yellow diamonds with colourless cores – evidence for episodic diamond growth beneath Chidliak and the Ekati Mine, Canada. *Mineral. Petrol.* **114**, 91–103.

Li K., Li L., Pearson D. G. and Stachel T. (2019) Diamond isotope compositions indicate altered igneous oceanic crust dominates deep carbon recycling. *Earth Planet. Sci. Lett.* **516**, 190–201.

- Li L., Bebout G. E. and Idleman B. D. (2007) Nitrogen concentration and $\delta^{15}\text{N}$ of altered oceanic crust obtained on ODP Legs 129 and 185: insights into alteration-related nitrogen enrichment and the nitrogen subduction budget. *Geochim. Cosmochim. Acta* **71**, 2344–2360.
- MacDougall J. D. and Haggerty S. E. (1999) Ultradeep xenoliths from African kimberlites: Sr and Nd isotopic compositions suggest complex history. *Earth Planet. Sci. Lett.* **170**, 73–82.
- MacGregor I. D. and Manton W. I. (1986) Roberts Victor eclogites: ancient oceanic crust. *J. Geophys. Res.* **91**, 14063–14079.
- McDonough W. F. and Rudnick R. L. (1998) Mineralogy and composition of the upper mantle. *Rev. Mineral.* **37**, 139–164.
- Meyer H. O. A. (1987) Inclusions in diamond. In *Nixon PH Mantle xenoliths*, John Wiley Sons, Chichester, pp. 501–522.
- Meyer H. O. A. and Boyd F. R. (1972) Composition and origin of crystalline inclusions in natural diamonds. *Geochim. Cosmochim. Acta* **36**, 1255–1273.
- Mikhail S., Rinaldi M., Mare E. R. and Sverjensky D. A. (2021) A genetic metasomatic link between eclogitic and peridotitic diamond inclusions. *Geochemical Perspect. Lett.* **17**, 33–38.
- Nestola F., Jung H. and Taylor L. A. (2017) Mineral inclusions in diamonds may be synchronous but not syngenetic. *Nat. Commun.* **8**, 1–6.
- Pearson D. G., Shirey S. B., Harris J. W. and Carlson R. W. (1998) Sulphide inclusions in diamonds from the Koffiefontein kimberlite, S Africa: Constraints on diamond ages and

- mantle Re-Os systematics. *Earth Planet. Sci. Lett.* **160**, 311–326.
- Philpotts J. A. and Schnetzler C. C. (1968) Europium anomalies and the genesis of basalt. *Chem. Geol.* **3**, 5–13.
- Read G. H. and Janse A. J. A. (2009) Diamonds: Exploration, mines and marketing. *Lithos* **112**, 1–9.
- Richardson S. H., Shirey S. B., Harris J.W. and Carlson R.W. (2001) Archean subduction recorded by Re-Os isotopes in eclogitic sulfide inclusions in Kimberley diamonds. *Earth Planet. Sci. Lett.* **191**, 257–266.
- Rollinson H. (2016) Archaean crustal evolution in West Africa: a new synthesis of the Archaean geology in Sierra Leone, Liberia, Guinea and Ivory Coast. *Precambrian Res.* **281**, 1–12.
- Schulze D. J. (1989) Constraints on the abundance of eclogite in the upper mantle. *J. Geophys. Res.* **94**, 4205–4212.
- Shirey S. B. and Richardson S. H. (2011) Start of the Wilson cycle at 3 Ga shown by diamonds from subcontinental mantle. *Science* **333**, 434–436.
- Shirey S. B., Carlson R. W., Richardson S. H., Menzies A., Gurney J. J., Pearson D. G. and Harris J. W. (2001) Archean emplacement of eclogitic components into the lithospheric mantle during formation of the Kaapvaal Craton. *Geophys. Res. Lett.* **28**, 2509–2512.
- Skinner E. M. W., Apter D. B., Morelli C. and Smithson N. K. (2004) Kimberlites of the Man craton, West Africa. *Lithos* **76**, 233–259.
- Smart K. A., Chacko T., Stachel T., Muehlenbachs K., Stern R. A. and Heaman L. M. (2011) Diamond growth from oxidized carbon sources beneath the Northern Slave Craton, Canada:

- a $\delta^{13}\text{C}$ -N study of eclogite-hosted diamonds from the Jericho kimberlite. *Geochim. Cosmochim. Acta* **75**, 6027–6047.
- Smit K. V. and Shirey S. B. (2020) What have diamond ages taught us? *Gems Gemol.* **56**, 534–541.
- Smit K. V., Shirey S. B. and Wang W. (2016) Type Ib diamond formation and preservation in the West African lithospheric mantle: Re–Os age constraints from sulphide inclusions in Zimmi diamonds. *Precambrian Res.* **286**, 152–166.
- Smit K. V., Shirey S. B., Hauri E. H. and Stern R. A. (2019a) Sulfur isotopes in diamonds reveal differences in continent construction. *Science* **364**, 383–385.
- Smit K. V., Stachel T., Luth R. W. and Stern R. A. (2019b) Evaluating mechanisms for eclogitic diamond growth: an example from Zimmi Neoproterozoic diamonds (West African craton). *Chem. Geol.* **520**, 21–32.
- Sobolev N. V., Lavrent'Ev Y. G., Pokhilenko N. P. and Usova L. V. (1973) Chrome-rich garnets from the kimberlites of Yakutia and their paragenesis. *Contrib. to Mineral. Petrol.* **40**, 39–52.
- Stachel T. and Harris J. W. (2008) The origin of cratonic diamonds – Constraints from mineral inclusions. *Ore Geol. Rev.* **34**, 5–32.
- Stachel T. and Harris J. W. (2009) Formation of diamond in the Earth's mantle. *J. Phys. Condens. Matter* **21**, 364206.
- Stachel T. and Luth R. W. (2015) Diamond formation – Where, when and how? *Lithos* **220–223**, 200–220.

Stachel T., Aulbach S. and Harris J. W. (2022) Mineral inclusions in lithospheric diamonds. *Rev. Mineral. Geochemistry* **88**, 307–391.

Sutton J. R. (1907) The relationship between diamonds and garnets. *Nature* **75**, 488.

Sutton J. R. (1921) Inclusions in diamond from South Africa. *Mineral. Mag.* **19**, 208–210.

Tompkins L. A. and Haggerty S. E. (1984) The Koidu kimberlite complex, Sierra Leone: geological setting, petrology and mineral chemistry. In *Developments in Petrology (vol 11)*, pp. 83–105.

Westerlund K. J., Shirey S. B., Richardson S. H., Carlson R. W., Gurney J. J. and Harris J. W. (2006) A subduction wedge origin for Paleoproterozoic peridotitic diamonds and harzburgites from the Panda kimberlite, Slave craton: Evidence from Re-Os isotope systematics. *Contrib. to Mineral. Petrol.* **152**, 275–294.

Wiggers de Vries D. F., Pearson D. G., Bulanova G. P., Smelov A. P., Pavlushin A. D. and Davies G. R. (2013) Re–Os dating of sulphide inclusions zonally distributed in single Yakutian diamonds: Evidence for multiple episodes of Proterozoic formation and protracted timescales of diamond growth. *Geochim. Cosmochim. Acta* **120**, 363–394.

Chapter 2 Formation of mixed paragenesis diamonds during multistage growth – constraints from *in situ* $\delta^{13}\text{C}$ – $\delta^{15}\text{N}$ –[N] analyses of Koidu diamonds

2.1 Introduction

Mineral inclusions encapsulated within diamonds preserve pristine information about the conditions of the mantle at the time of diamond formation, as they cannot re-equilibrate with their surroundings during mantle residence or kimberlite eruption. Based on inclusion mineralogy and composition, a first order division can be drawn between common lithospheric diamonds that form within the thick lithospheric mantle keels underpinning long-term stable continental areas (cratons) and rare superdeep diamonds originating from beneath (> 250 km depth) (Stachel and Harris, 2008). Lithospheric diamonds are divided into peridotitic, eclogitic and websteritic suites, which represent the mantle substrates for their crystallization. Common peridotitic mineral inclusions are Cr-pyrope garnet, Cr-diopside, forsterite, enstatite, Mg-chromite and Ni-rich sulphide. The eclogitic suite includes, but is not limited to, pyrope-almandine-grossular garnet, omphacite, kyanite, rutile, coesite, corundum and Ni-poor sulphide. The websteritic suite contains minerals that have compositions that are transitional between the peridotitic and eclogitic suites (Meyer, 1987; Taylor and Anand, 2004; Stachel and Harris, 2008).

Any given lithospheric diamond crystal typically hosts mineral inclusions that are derived from a single suite only (Stachel and Harris, 2008). On some occasions, diamond formation occurs in compositionally changing environments caused by the interaction of metasomatic melts with diamond substrates, which may result in eclogitic and websteritic inclusions being trapped in the same diamond at different stages during diamond growth (Aulbach et al., 2002; Davies et al., 2004a). Diamonds containing both peridotitic and eclogitic mineral inclusions (referred to as

“mixed paragenesis” hereafter) are rare and have only been documented from a few localities, e.g., West Africa (Prinz et al., 1975), Argyle in Western Australia (Hall and Smith, 1984), Monastery in South Africa (Moore and Gurney, 1986), Sloan in USA (Otter and Gurney, 1986), Shengli 1 and Pipe 50 in China (Wang, 1998) and the Lac de Gras area in Canada (Davies et al., 2004b). Diamonds of mixed paragenesis are thought to document multiple diamond growth events that occurred in different substrates (Wang, 1998) although other origins are possible, such as modification of mineral compositions by melt-rock reaction in the mantle, accompanied by diamond growth (Mikhail et al., 2021).

In this study, I identify five diamonds from the Koidu kimberlite complex in Sierra Leone that contain both eclogitic and peridotitic mineral inclusions – an unusually high number of diamonds relative to the majority of those recovered. I investigate their formation by imaging diamond growth textures, assessing the chemical compositions of the mixed paragenesis mineral inclusions and by comparing the N concentrations, N aggregation states and stable isotope compositions of these unusual diamonds to single-paragenesis diamonds from the same locality. This is the first study to employ multi-collector secondary ion mass spectrometry (SIMS) to measure variations in $\delta^{13}\text{C}$, $\delta^{15}\text{N}$ and N concentration in different growth zones of Koidu diamonds (including peridotitic, eclogitic and mixed paragenesis diamonds) at high spatial resolution, enabling detection of changing growth conditions and therefore the dynamic environment of diamond formation.

2.2 Sample description

A total of 111 inclusion-bearing rough diamonds 2–4 mm in size were studied. The total

weight of the diamonds is 10.7 carats. All diamonds in the sample suite are colourless except for one pale yellow and one light brown diamond. Their morphology is dominated by octahedra (n = 85), followed by rounded dodecahedra (n = 11), transitional octahedra-dodecahedra (n = 7), irregular shapes (n = 4), macles (n = 2), an aggregate (n = 1) and an intergrowth of two octahedra (n = 1). Descriptions of diamonds are summarized in Table A.1.

Resorption features are observed on all diamonds, with negative trigons occurring on all octahedral faces and aligning in parallel rows where plastic deformation lines are present. Other common resorption features include shield-shaped laminae and hexagonal pits on octahedral faces, hillocks, corrosion sculptures and micro-disk patterns on rounded dodecahedral faces, terraces around the three-fold axes of dodecahedral crystals, and tetragons on presumed {100} faces of irregular-shaped diamonds. Surface textures not restricted to specific crystal faces include deformation lines (observed in nine diamonds), ruts, fractures, and a green irradiation spot on an octahedral diamond. Voids of cubo-octahedral shapes are found on the surface of some diamonds, likely representing cavities previously occupied by mineral inclusions. Examples of common surface textures of Koidu diamonds can be found in Fig. A.1.

Six diamonds contained only crustal mineral inclusions (epigenetic) and thus they were not further investigated. From 105 diamonds, 370 primary mineral inclusions were recovered, and I found that 82 diamonds (78%) contained eclogitic inclusions, 18 diamonds (17%) contained peridotitic inclusions, and five diamonds (5%) contained both eclogitic and peridotitic inclusions.

The five diamonds of mixed paragenesis are 130-9 (omphacite + olivine), 130-31 (coesite + olivine), 133-6 (omphacite + Mg-chromite), 138-7 (eclogitic garnet + olivine) and 146-1 (olivine + Mg-chromite + coesite). Omphacite, olivine and coesite inclusions are all colourless, but were identified using their chemical compositions. The spatial distribution of particular inclusions

within their host diamonds and consequently the direction of changes in inclusion composition could only be investigated for two diamonds containing mineral inclusions with clearly distinguishable colours — diamonds 133-6 and 138-7. The chemical composition of the mineral inclusions in these two diamonds are discussed in detail below, whereas the inclusion compositions of the other mixed paragenesis diamonds are reported in Table A.2. In both diamonds, eclogitic inclusions are located in the centre and peridotitic inclusions near the rim (Fig. 2.1).

2.3 Analytical methods

2.3.1 Mineral inclusions

Mineral inclusions were mounted with epoxy resin in 6 mm diameter brass tubes and polished. Initial mineral identification was achieved by back-scattered electron (BSE) imaging and energy dispersive spectroscopy (EDS). Major and minor element compositions were determined using CAMECA SX100 and JEOL JXA-8900R electron probe microanalyzers (EPMA), both equipped with five wavelength-dispersive spectrometers (WDS). The instruments were operated at an accelerating voltage of 20 kV, a beam current of 20 nA, and a fully-focussed beam with a diameter < 1 μm . Reference materials include metals and natural and synthetic minerals. For all elements, the $K\alpha$ emission lines were employed for analysis. The counting time was 20–100 s on the peak, with resulting oxide detection limits typically ≤ 0.02 wt%. Three spots were measured on each grain and, after assessing compositional homogeneity, the compositions of the spots were averaged.

Trace elements (including REE, Ti, V, Ni, Rb, Sr, Zr, Nb, Ba and Hf) in garnet and clinopyroxene inclusions were determined using a Resonetics M-50-LR 193 nm ArF excimer laser

ablation system, with a Laurin-Technic S-155 two-volume ablation cell, coupled with a Thermo Scientific Element IIXR inductively coupled plasma mass spectrometer (LA-ICP-MS). Mineral inclusions were ablated with a spot size of 23–90 μm at a frequency of 10 Hz and a laser fluence of $\sim 4 \text{ J/cm}^2$. Analysis of each sample includes 40 s background collection followed by 60 s sample ablation/measurement and 40 s washout. Detection limits are typically ≤ 40 ppb for REE, V, Rb, Sr, Zr, Nb, Ba and Hf, and ≤ 1 ppm for Ti and Ni. Calibration was achieved using the NIST SRM 612 glass standard and ^{43}Ca as internal standard for data processing. USGS reference glass BIR-1G was analysed as an unknown and the results were compared to the GeoRem preferred values (Jochum et al., 2005) to assess repeatability and accuracy.

2.3.2 Host diamonds

Infrared absorption spectra of diamonds were obtained before crushing, using a Thermo Fisher Nexus 470 Fourier transform infrared (FTIR) spectrometer equipped with a Continuum IR microscope. An aperture size of $100 \times 100 \mu\text{m}$ was used in transmission mode. Spectra were acquired by averaging 200 scans at a spectral resolution of 1 cm^{-1} with a spectral range of $4000\text{--}650 \text{ cm}^{-1}$. Baseline-corrected spectra were normalized to 1 cm diamond thickness, where the absorption coefficient for the intrinsic absorption of diamond at 1995 cm^{-1} is approximately 11.94 cm^{-1} (e.g., Howell et al., 2012). Nitrogen concentrations and aggregation states of diamonds were calculated by deconvolution of the normalized spectra, where $[\text{N}_\text{A}] = 16.5 \times \mu\text{A}$ (absorption coefficient at 1282 cm^{-1} for the A-centre; Boyd et al., 1994a) and $[\text{N}_\text{B}] = 79.4 \times \mu\text{B}$ (absorption coefficient at 1282 cm^{-1} for the B-centre; Boyd et al., 1995). The detection limit for N is ~ 5 at.ppm. More than one spectrum was collected for diamonds at different spots. Note that the N distribution in diamond may be heterogeneous, and the infrared absorption spectrum is an integrated signal collected over the optical path of the diamond, which may contain different growth zones with

distinctly different N contents.

Diamond fragments were first cast in epoxy and then ground and polished. Subsequently, the fragments were co-mounted in indium with a SIMS reference material – diamond S0270. Prior to analysis, cathodoluminescence (CL) images of diamond fragments were obtained using a Zeiss EVO MA15 scanning electron microscope (SEM) equipped with a parabolic mirror coupled to a high sensitivity broadband photomultiplier tube to reveal the diamond internal growth textures. The mount was coated with Au to prevent charging during SEM operation. The scanning electron microscope was operated at a voltage of 15 kV and a beam current of 3–5 nA. Subsequently, C and N isotope compositions and N abundances of the mounted diamond fragments were determined using a CAMECA IMS-1280 multi-collector ion microprobe. Two to eight measurement spots were set on each diamond fragment to cover all growth zones. The primary beam of 20 keV $^{133}\text{Cs}^+$ ions was focused to a beam diameter of approximately 10 μm , with beam currents of 2 nA, 2.5–3.0 nA and 0.6 nA for the analyses of C isotope composition, N isotope composition and N abundance, respectively. Carbon isotopes were analyzed first, followed by N abundance and N isotope measurements from the same spot location. The detection limit for N abundance is ~ 0.1 at.ppm. Nitrogen isotope compositions were only measured on spots with N abundance > 65 at.ppm. Carbon isotope compositions are reported as $\delta^{13}\text{C}_{\text{VPDB}}$, which is the normalized difference of the $^{13}\text{C}/^{12}\text{C}$ ratio of the sample relative to that of the Vienna Pee Dee Belemnite standard ($^{13}\text{C}/^{12}\text{C}_{\text{VPDB}} = 0.01118$; Coplen et al., 2002). Nitrogen isotope compositions are reported as $\delta^{15}\text{N}_{\text{AIR}}$, which is the normalized difference of the $^{15}\text{N}/^{14}\text{N}$ ratio of the sample relative to that of the atmosphere ($^{15}\text{N}/^{14}\text{N}_{\text{AIR}} = 0.003677$; Junk and Svec, 1958). The analytical sequences for C and N isotopes interspersed measurements of unknowns with diamond reference S0270 ($\delta^{13}\text{C}_{\text{VPDB}} = -8.88 \pm 0.10$ ‰; $\delta^{15}\text{N}_{\text{AIR}} = -0.40 \pm 0.50$ ‰; Stern et al., 2014) in a 4:1 ratio.

Uncertainties of individual $\delta^{13}\text{C}_{\text{VPDB}}$ analyses for diamond S0270 and unknowns are typically $\pm 0.14\text{‰}$ (2σ). Uncertainties of individual $\delta^{15}\text{N}_{\text{AIR}}$ analyses are typically $\pm 0.60\text{‰}$ (2σ) for diamond S0270, and typically range from ± 0.50 to $\pm 4.0\text{‰}$ (2σ) for unknowns with N concentration ranging from 2500 to 50 at.ppm, respectively. Additional details of the analytical procedure were outlined in Stern et al. (2014).

2.4 Results

2.4.1 Mineral inclusions from mixed paragenesis diamonds

2.4.1.1 Diamond 133-6

Diamond 133-6 contains four omphacites (clinopyroxenes with a jadeite component ≥ 20 and < 80 mol%; Clark and Papike, 1968) within a radius of $\sim 500\text{ }\mu\text{m}$ in the centre and one Mg-chromite in the rim (Fig. 2.1a). The omphacites were surrounded by small fractures, which did not extend to the surface of the diamond. Backscattered electron images indicated that all inclusions have homogeneous compositions throughout the grains. Inter-grain variation among the four omphacites was negligible, thus an average major element composition is reported.

The omphacites have high molar Mg# ($100 \times \text{Mg}/[\text{Mg}+\text{Fe}] = 82.2$) and jadeite component ($100 \times 2\text{Na}/[2\text{Na}+\text{Ca}+\text{Mg}+\text{Fe}] = 63.9$ mol%). The Ca-Mg-Fe compositions of these omphacites are similar to the omphacites from Koidu gabbroic eclogites (classified based on bulk-rock $[\text{Eu}/\text{Eu}^*]_{\text{N}} \geq 1.05$, where $\text{Eu}^* = [\text{Sm}_{\text{N}} \times \text{Gd}_{\text{N}}]^{0.5}$; Aulbach et al., 2019b) and low-MgO eclogites (bulk-rock MgO content = 6–13 wt%; Hills and Haggerty, 1989; Aulbach et al., 2019b) (Fig. 2.2). The average Cr_2O_3 content in these omphacites is very low (≤ 0.02 wt%) (Table A.3).

Trace element compositions were determined for three of the omphacites from diamond 133-6 (Table A.4). They have very similar REE_N patterns and show positive Eu anomalies (defined as $[\text{Eu}/\text{Eu}^*]_{\text{N}} > 1$), with $[\text{Eu}/\text{Eu}^*]_{\text{N}} = 1.63\text{--}1.78$. The REE_N patterns of these omphacites are clearly different from omphacites in Koidu eclogite xenoliths (Aulbach et al., 2019b) (Fig. 2.3). The omphacite inclusions are enriched in LREE relative to CI-chondrite, but have unusually low MREE and HREE compared to clinopyroxene inclusions in diamonds worldwide (Stachel and Harris, 2008), resulting in high LREE/HREE ratios. The concentrations of the HREE Tm, Yb and Lu are below the limit of detection, except for Yb in one omphacite. They also are enriched in Nb, Sr, Ti and V relative to CI-chondrite (Fig. 2.4).

The Mg-chromite inclusion has a cubo-octahedral morphology and no associated fractures, implying a synchronous relationship with the growth zone of the host diamond in which it occurs. It has high Mg# (65.2) and Cr# ($100 \times \text{Cr}/[\text{Cr} + \text{Al}] = 85.5$), typical for peridotitic spinel inclusions in diamond worldwide (Stachel and Harris, 2008).

2.4.1.2 Diamond 138-7

Diamond 138-7 contains five eclogitic garnets in the centre and one olivine in the rim (Fig. 2.1b). No fractures are observed around the inclusions nor elsewhere in this diamond. All inclusion grains are internally compositionally homogeneous, without any sign of alteration.

Garnets show significant grain to grain compositional variations in SiO₂ (39.5–41.9 wt%), Al₂O₃ (21.9–23.9 wt%), MgO (8.1–9.7 wt%) and CaO (16.7–19.3 wt%) (Table A.3). The very high CaO contents are unusual. Worldwide, diamond-hosted garnet inclusions with CaO contents ≥ 17 wt% have been reported only from a few localities, most prominently Klipspringer in South Africa (Westerlund and Gurney, 2004), the New South Wales alluvials (Davies et al., 2003) and

Argyle in Australia (Jaques et al., 1989), but have not been observed at other localities on the West African Craton. Among Koidu eclogite xenoliths, similar high CaO in garnet is only seen in a few low-MgO kyanite or corundum eclogites (Hills and Haggerty, 1989) (Fig. 2.5).

Trace element compositions of three garnets from diamond 138-7 were determined (Table A.4). Their REE_N patterns are very similar to one another, with small differences in La and from Eu to Lu (Fig. 2.6). All garnets have positive Eu anomalies, with $[Eu/Eu^*]_N = 1.10\text{--}1.41$. They have REE_N patterns typical of cratonic eclogite xenoliths, characterised by increasing abundances from subchondritic La to about 10x chondritic MREE and HREE (Sm to Lu). Their MREE to HREE contents overlap with the field of garnets from Koidu gabbroic eclogites (Aulbach et al., 2019b), with the LREE La to Pr above the xenolith garnet range. Strontium and Nb abundances are subchondritic (Fig. 2.7). There are positive correlations between trace element and major element compositions, where Nb and Ti increase with CaO abundance in these garnets (Tables A.3 and A.4).

The single olivine inclusion is elongated in shape. It has a very high Mg# (94.5), documenting the strongly depleted nature of the harzburgitic to dunitic diamond substrate. On the West African Craton, such high Mg# have only been reported for retrograde olivines occurring as inclusions in sublithospheric diamonds (Kankan, Guinea; after primary wadsleyite or ringwoodite; Stachel et al., 2000a), but not for olivine in lithospheric diamonds (Meyer and Boyd, 1972 ; Stachel and Harris, 1997; Stachel et al., 2000b).

2.4.2 $\delta^{13}\text{C}$, $\delta^{15}\text{N}$ and N concentrations in Koidu diamonds

2.4.2.1 Peridotitic diamonds

Peridotitic diamonds from Koidu (18 diamonds; 54 SIMS analyses; Tables A.5 and A.6)

have a restricted range in $\delta^{13}\text{C}$ values from -6.0 to -1.1 ‰, well within the range of peridotitic diamond worldwide (Stachel et al., 2009) (Fig. 2.8a). Their N abundances (all values stated in section 2.5.2 were obtained by SIMS) and $\delta^{15}\text{N}$ values range from 0.4 to 920 at.ppm (median = 80 at.ppm) and -4.2 to +9.7 ‰, respectively, and define one of three clusters (Cluster 2) shown in Fig. 2.9 (see Section 2.5.4 for detailed discussion). Three peridotitic diamonds have mantle-like isotopic signatures (defined as $\delta^{13}\text{C} = -5 \pm 3$ ‰ and $\delta^{15}\text{N} = -5 \pm 3$ ‰; Cartigny et al., 2014) with $\delta^{13}\text{C}$ values of -5.7 to -2.6 ‰ and $\delta^{15}\text{N}$ values of -4.2 to -2.1 ‰ (Fig. 2.9), accompanied by variable N contents (1–680 at.ppm). Most diamonds have small internal variations in C isotope composition (average $\sigma < 0.2$ ‰), except for four diamonds (130-21, 130-25, 134-2 and 136-1; Table A.6) which have intra-diamond $\delta^{13}\text{C}$ variations up to 2.8 ‰.

2.4.2.2 Eclogitic diamonds

Koidu eclogitic diamonds in this study (82 diamonds, 321 SIMS analyses; Tables A.5 and A.6) show highly variable isotope compositions and N concentrations, indicating growth during multiple events. Based on their $\delta^{13}\text{C}$ and $\delta^{15}\text{N}$ values, they define two additional clusters (Clusters 1 and 3; Fig. 2.9), which will be discussed in Section 2.5.4 in detail.

Based solely on their $\delta^{13}\text{C}$ values, the eclogitic diamonds can be separated into three subgroups:

^{13}C -enriched diamond: This group contains only a single diamond with the highest $\delta^{13}\text{C}$ values among Koidu eclogitic diamonds. The bulk of this diamond has $\delta^{13}\text{C}$ values from -1.8 to 0.0 ‰ and negligible N content. Lower $\delta^{13}\text{C}$ values (-4.2 ‰) are observed in a more N-rich (50–80 at.ppm) growth zone. $\delta^{15}\text{N}$ values were not determined for this overall N-poor diamond.

^{13}C -depleted diamond: Diamonds in this group have $\delta^{13}\text{C}$ values from -33.2 to -15.1 ‰,

with ~80% of the data falling in the range of -30 to -25 ‰ (Fig. 2.8b). Compared to Koidu peridotitic diamonds, this group has a broader range of N abundances (0.4 to 2080 at.ppm; median = 30 at.ppm) and $\delta^{15}\text{N}$ values (-5.3 to +9.9 ‰; Fig. 2.9). Most diamonds are internally homogeneous in carbon isotope composition, but with a spread in $\delta^{15}\text{N}$ values of up to 5.4 ‰. Six diamonds in this group have a less ^{13}C -depleted outermost growth zone ($\delta^{13}\text{C} = -19.2$ to -15.1 ‰) compared to the core ($\delta^{13}\text{C} = -29.6$ to -24.9 ‰).

Diamonds with cores depleted in ^{13}C and rims with mantle-like C isotopic signature: Twenty-four diamonds have a clear core-rim structure (core and rim have distinctly different CL brightness), where the core zone has low $\delta^{13}\text{C}$ values (-30.2 to -14.4 ‰) and generally low N concentrations (1–890 at.ppm; median = 30 at.ppm), while the rim has higher, mantle-like $\delta^{13}\text{C}$ values (-7.8 to -5.6 ‰) and high N concentrations (610–2200 at.ppm; median = 870 at.ppm) (Figs. 2.8c and 2.10). For the core zones, only 12 diamonds have sufficiently high N abundances (> 65 at.ppm) to allow for precise N isotope analysis; $\delta^{15}\text{N}$ values in the cores range from -5.6 to +8.1 ‰, overlapping with the range for the subgroup of ^{13}C -depleted eclogitic diamonds (see above). The high N abundances in the rims allow the measurement of N isotope compositions for all diamonds in this group, indicating mantle-like $\delta^{15}\text{N}$ values between -7.9 and -2.6 ‰ (Fig. 2.9). One diamond in this group has a distinct intermediate layer between the core and the rim, with an average $\delta^{13}\text{C}$ value of -15.3 ‰ that is ~10 ‰ higher than the core zone and ~8 ‰ lower than the rim, but similar to the outermost growth zones of the six zoned ^{13}C -depleted eclogitic diamonds (see above). $\delta^{15}\text{N}$ values of this diamond fluctuate from -0.5 ‰ in the core zone to +10.1 ‰ in the intermediate layer to -5.5 ‰ in the rim.

2.4.2.3 Mixed paragenesis diamonds

The isotope compositions of all studied mixed paragenesis diamonds (5 diamonds, 89

SIMS analyses) are shown in Figs. 2.8d and 2.9, and together with N concentrations listed in Tables A.5 and A.6. These mixed paragenesis diamonds lie within the three clusters (Fig. 2.9) mentioned above and will be discussed in detail in Section 2.5.4.

Diamond 133-6 (omphacite and Mg-chromite included) is comprised of inner growth zones and a rim with similar $\delta^{13}\text{C}$ (-4.8 to -3.6 ‰) but distinct $\delta^{15}\text{N}$ values and N contents. The inner growth zones have a broad range of N isotope compositions ($\delta^{15}\text{N} = -6.2$ to $+4.8$ ‰) and low N contents (1–380 at.ppm). The rim has a restricted, mantle-like N isotopic signature ($\delta^{15}\text{N} = -7.9$ to -6.7 ‰) and high N contents (520–750 at.ppm). Core-to-rim transects show that within the innermost zone of this diamond (fragments 1 and 3 in Fig. 2.11) a minor outward increase in $\delta^{13}\text{C}$ values (from -4.7 to -3.7 ‰) is accompanied by decreasing N concentrations (from 330 to 20 at.ppm), but no trend in $\delta^{13}\text{C}$ values is observed for the intermediate or rim zones.

Diamond 138-7 (eclogitic garnet and olivine inclusions) does not have a discernible core-rim zonation. Carbon and N isotope compositions vary ($\delta^{13}\text{C} = -5.3$ to -4.1 ‰; $\delta^{15}\text{N} = -9.8$ to -5.3 ‰) within the mantle range. Nitrogen abundance varies widely, from 1 to 1050 at.ppm. Although multiple growth zones and some mild resorption at the outer boundary of the inner growth zone are observed, the zones generally have a homogeneous CL response and transects across them do not reveal coherent trends in $\delta^{13}\text{C}$ values.

Diamonds 130-31 (with coesite and olivine inclusions) and 146-1 (coesite, Mg-chromite and olivine) have isotope compositions ($\delta^{13}\text{C} = -4.7$ to -1.3 ‰; $\delta^{15}\text{N} = -2.3$ to $+5.8$ ‰) and N contents (0.3–340 at.ppm) within the range of peridotitic Koidu diamonds. Diamond 130-9 (omphacite and olivine) has an isotopic signature ($\delta^{13}\text{C} = -24.8$ to -22.6 ‰; $\delta^{15}\text{N} = -4.1$ ‰) and N contents (0.9–180 at.ppm) similar to the ^{13}C -depleted eclogitic diamonds in this study.

2.4.3 Nitrogen aggregation in episodically grown diamonds

Nitrogen is incorporated into the diamond lattice in the form of single substitutional N (C-centres; Taylor et al., 1996; Type Ib) during crystallization. Residence in the mantle at high temperature leads to the diffusion and combination of single N atoms into pairs (A-centres; Davies, 1976; Type IaA). Nitrogen pairs further aggregate to a structure of four N atoms surrounding a vacancy (B-centre; Jones et al., 1992; Type IaB), along with the generation of two side products – the N₃ centre (three N atoms surrounding a vacancy) and platelets (aggregations of interstitial C atoms) (Woods, 1986). The rate of N aggregation depends on three major factors – mantle residence temperature, mantle residence time and N concentration in diamonds (e.g., Taylor et al., 1990).

Cathodoluminescence images of the episodically-grown diamonds show bright cores and dark rims (Fig. 2.10), indicating low concentrations of optically active lattice defects to cause CL in the rims. Infrared absorption spectra (Table A.1 and Fig. 2.12) show that the brighter cores contain N in higher aggregation states (Type IaAB with ≥ 30 %B), where N₃ centres (with a luminescent wavelength at 415 nm; Zaitsev, 2001) are present, while the rims represent overgrowths of diamond with lower N aggregation states dominated by A-centres, which are known to quench luminescence (Vasil'ev et al., 2004). Enhanced N aggregation states in the cores indicate that they had longer mantle residence times or higher mantle storage temperatures compared to the rims (Taylor et al., 1990; Leahy and Taylor, 1997), requiring that cores and rims in these diamonds formed during distinct growth events separated in time or in temperature.

2.5 Discussion

2.5.1 Origin of eclogitic mineral inclusions in Koidu mixed paragenesis diamonds

Positive Eu anomalies in omphacites from diamond 133-6 and garnets from diamond 138-7 indicate accumulation of plagioclase in their protoliths (Schmickler et al., 2004), suggesting a protolith origin as gabbro cumulates. Major element compositions of both omphacite and garnet inclusions are similar to some Koidu kyanite- and corundum-bearing low-MgO eclogite xenoliths (Hills and Haggerty 1989), and trace element compositions (MREE to HREE) of garnet inclusions are similar to garnet from Koidu gabbroic eclogite xenoliths (Aulbach et al., 2019b), suggesting that the eclogitic inclusions in mixed paragenesis diamonds inherited compositional characteristics of their eclogitic diamond substrates.

Omphacites from diamond 133-6 have highly fractionated REE_N patterns ($La_N/Yb_N = 422$) that are very different from typical eclogitic clinopyroxenes, which usually have humped patterns with $La_N/Nd_N < 1$ and higher HREE contents (e.g., Jacob, 2004). Omphacites with very similar REE_N and HFSE_N patterns at lower LREE (Figs. 2.3 and 2.4) were, however, observed in two low-MgO eclogites from Obnazhennaya in Siberia (Sun et al., 2020) and a kyanite eclogite from Bellsbank in South Africa (Shu et al., 2016). This similarity in trace element patterns does not fully extend to major element compositions, where the omphacites from diamond 133-6 and from Obnazhennaya and Bellsbank are distinct in their Mg# (82.2 versus 88.8 and 88.4, respectively) and jadeite content (63.9 versus 22.1 and 46.5 mol%, respectively). The protoliths of Obnazhennaya low-MgO and Bellsbank kyanite eclogites were suggested to be olivine gabbro cumulates (Shu et al., 2016; Sun et al., 2020). Eclogites with cumulate protoliths are inferred to have incorporated a trapped melt component and subsequently, during subduction, to have experienced eclogite-facies melt extraction (Aulbach et al., 2007; Aulbach and Jacob, 2016; Sun et al., 2020). Without coexisting garnet, I cannot evaluate the origin of the clinopyroxene

inclusions in diamond 133-6 in detail, but based on their similarity in trace element composition to the Obnazhennaya and Bellsbank clinopyroxenes I suggest a similar origin, i.e., that the clinopyroxene inclusions derived from oceanic cumulates (possibly with trapped melt) that were subducted and metamorphosed. In addition, the diamond substrate could have been affected by a subsequent stage of metasomatic LREE enrichment to explain the significantly higher contents in La to Pr relative to Obnazhennaya and Bellsbank clinopyroxenes (Fig. 2.3).

The high and variable CaO contents in the garnets from diamond 138-7 may reflect continuous metasomatic enrichment during diamond growth. This was previously suggested for an eclogitic diamond from the Mir kimberlite containing 35 garnet inclusions with a wide range of CaO contents (Sobolev et al., 1998). Multiple olivine inclusions with different CaO contents in a single Kankan diamond were also attributed to metasomatic Ca enrichment during diamond growth (Stachel et al., 2000b). The observed positive correlations of Ca with Nb and Ti for the garnets from diamond 138-7 indicate that the metasomatic process accompanying diamond formation could have affected trace elements. Elevated LREE in the garnet inclusions relative to garnets from Koidu gabbroic eclogite xenoliths (Aulbach et al., 2019b) appear to support this interpretation. A possible metasomatic agent driving diamond precipitation and enrichment in Ca and LREE could be a low-Mg carbonatitic high-density fluid or a carbonatitic melt (Sobolev et al., 1998; Stachel et al., 2000b; Klein-BenDavid et al., 2009). Alternatively, the difference in LREE concentrations between inclusion and gabbroic eclogite xenolith garnets may be attributed to crystal-chemical effects: the $Ca\#$ ($Ca/[Ca+Mg+Fe+Mn]$) of garnet strongly influences partitioning of trace elements between garnet and pyroxene, with both the REE concentrations and the LREE/HREE ratio in garnet increasing together with $Ca\#_{\text{garnet}}$ (Harte and Kirkley 1997; Aulbach et al., 2017).

Either way, two key observations suggest that the garnet inclusions in diamond 138-7 predominantly reflect their substrate composition: (1) the presence of positive Eu anomalies and (2) the overall shape of the REE_N patterns, which are typical for garnets in eclogites with low-pressure protoliths that experienced some cumulate enrichment (lowering the REE overall) and possibly partial melting during or after subduction (preferentially extracting LREE) (Ireland et al., 1994; Barth et al., 2001; Stachel et al., 2004; Aulbach and Jacob, 2016).

2.5.2 Progressive precipitation of eclogitic and then peridotitic inclusions from an evolving eclogite-derived fluid

Geochemical modelling, based on the Extended Deep Earth Water (DEW) model, indicated that the interaction between eclogite-derived fluids and a range of mantle peridotite compositions may result in the progressive formation of eclogitic, websteritic and peridotitic minerals (Mikhail et al., 2021). If captured in the form of inclusions during associated diamond growth, this model predicts the occurrence of inclusions of different paragenesis in single diamonds. The calculated models predict 2-3 vol% spinel in the final mineralogy resulting from fluid-peridotite interactions, which seemingly appears to fit with my observation of spinel (chromite) in mixed paragenesis diamond 133-6. With the caveat that the minor element Cr is not included in the DEW model runs, the predicted spinel-group mineral, however, is magnetite, which is a very rare inclusion in diamond (Stachel et al., 1998). Instead, the spinel inclusion found in the rim of diamond 133-6 is a Mg-chromite, with the high Mg# (65.2) and Cr# (85.5) typical of garnet-facies spinels found in cratonic peridotite xenoliths and as inclusions in diamonds (McDonough and Rudnick, 1998; Stachel and Harris 2008). Similarly, the olivine inclusion near the rim of mixed paragenesis diamond 138-7 bears the highly magnesian character (Mg# 94.5) of strongly depleted cratonic peridotites, very much unlike the expected product of a process that converts depleted peridotite

into websterite (Mallik and Dasgupta, 2012, 2013). As discussed in the preceding section, the centrally located eclogitic garnet and omphacite inclusions also are very much like eclogite xenolith minerals and bear the characteristics of subducted gabbroic protoliths rather than those of an eclogite-derived fluid. The very high CaO content of the eclogitic garnet inclusions precludes equilibration with orthopyroxene and consequently, derivation from websterite, which is the product of the modelled fluid-rock interactions (Mikhail et al., 2021). Thus, I conclude that the peridotitic inclusions in my samples are not the result of extended eclogitic fluid-peridotite reactions but instead must have a separate origin from the “coexisting” eclogitic inclusions. The contrasting CL responses and N concentrations of the core and rim zones of diamond 133-6 (Fig. 11) implicate episodic diamond growth rather than fluid evolution during a single metasomatic event.

2.5.3 Covariation of $\delta^{13}\text{C}$ values and N abundance

In the literature, N is generally considered as a compatible element in diamond, incorporated through equilibrium partitioning with the diamond-forming fluid/melt, with $K_{\text{N}}^{\text{diamond-fluid}} \geq 2$ for diamond crystallization from a reduced medium (Thomassot et al., 2007; Smit et al., 2019b), and $K_{\text{N}}^{\text{diamond-fluid}} \geq 4$ for diamond growth from an oxidized medium (Stachel et al., 2009; Smart et al., 2011; Petts et al., 2015). Therefore, progressive diamond formation from a single pulse of fluid/melt should lead to a gradual decrease in N concentration.

Assuming precipitation from a single C species in the fluid/melt, diamond showing a trend of outward decreasing N concentration accompanied by increasing or decreasing $\delta^{13}\text{C}$ values reflects diamond formation from an oxidized (CO_2 or CO_3^{2-}) or a reduced medium (CH_4), respectively (Deines, 1980). Thus, the core-to-rim transects showing progressively decreasing N concentrations and increasing $\delta^{13}\text{C}$ values within the innermost growth zone of diamond 133-6

may indicate an oxidized diamond-forming medium (Fig. 2.11). Alternatively, precipitation from a mixed CHO fluid, containing both CH₄ and CO₂ in variable ratios, would also lead to ¹³C enrichment during diamond precipitation under fluid-limited conditions (Stachel et al., 2017). The same covariation is not observed in the intermediate zones and the rim of this diamond (Fig. 2.11), suggesting that they did not form from the same pulse of fluid/melt as the innermost zone. In addition, N abundance within the rim of diamond 133-6 is consistently high and systematic variations in stable isotope composition are absent, implying that the final growth stage did not occur in a fluid/melt-limited system, in contrast with the innermost growth zone showing systematic N and δ¹³C variations that point to a fluid/melt-limited system.

Diamond 138-7 has overall high N concentrations, except for minor growth zones that have N < 100 at.ppm. The absence of a systematic covariations in δ¹³C and N abundance again suggests diamond formation in a system that was not fluid/melt-limited. Although mild resorption is observed at the outer boundary of the inner growth zone, this diamond has homogeneous CL brightness and shows overall small variations in isotope compositions, suggesting that it either formed from two pulses of a related fluid or during protracted growth from fluids with similar isotope compositions and N contents.

2.5.4 Sources of C and N in Koidu diamonds

The variation of δ¹³C–δ¹⁵N in Koidu diamonds indicates the presence of three major clusters (Fig. 2.9). Cluster 1 is characterised by depletion in ¹³C and highly variable δ¹⁵N values (δ¹³C = -33.2 to -14.4 ‰; δ¹⁵N = -5.3 to +10.1 ‰); it comprises diamonds with eclogitic inclusions and mixed paragenesis diamond 130-9 (Fig. 2.13a). Cluster 2 shows mantle-like to mildly ¹³C-enriched C isotope compositions and again a large spread of δ¹⁵N values (δ¹³C = -6.0 to -1.1 ‰; δ¹⁵N = -4.2 to +9.7 ‰); it includes mainly peridotitic diamonds and three mixed paragenesis

diamonds – 133-6 (core zone only), 130-31 and 146-1 (Fig. 2.13a). Cluster 3 has a mantle-like isotopic signature ($\delta^{13}\text{C} = -7.8$ to -3.6 ‰; $\delta^{15}\text{N} = -7.9$ to -2.1 ‰) and includes the rims of eclogitic diamonds and mixed paragenesis diamonds 138-7 and 133-6 (rim only) (Fig. 2.13b). The assignment of mixed paragenesis diamonds to either Cluster 2 or 3 is entirely based on their N isotope composition, with their $\delta^{13}\text{C}$ values remaining approximately constant over the entire $\delta^{15}\text{N}$ range from ~ -10 to $+10$ ‰.

Cluster 1: The ^{13}C -depleted signature of my Koidu eclogitic diamonds is also observed in previously studied sulphide-bearing eclogitic diamonds from Koidu ($\delta^{13}\text{C} = -33.0$ to -16.3 ‰; Deines and Harris, 1995). In a suite of five sulphide-bearing eclogitic diamonds from Zimmi (Sierra Leone), which are alluvial diamonds thought to derive from a subcontinental lithospheric mantle source similar to Koidu, three show similar ^{13}C -depleted signatures ($\delta^{13}\text{C} = -24.5$ to -16.1 ‰) while the remaining two have $\delta^{13}\text{C}$ between -8.3 and -6.7 ‰ (Smit et al., 2019b). Since $\delta^{15}\text{N}$ was not analysed in these two previous studies, it is not possible to assign these diamonds to the three clusters defined in this study. The much wider range of $\delta^{13}\text{C}$ values of eclogitic diamonds compared to peridotitic diamonds has been attributed to fractionation of mantle C during CO_2 -escape from a carbonated fluid/melt before diamond formation (Cartigny et al., 2001). This fractionation model, however, is not likely to produce diamonds with $\delta^{13}\text{C} < -14$ ‰ from a source with initial mantle-like C isotope compositions (Smart et al., 2011). A more probable source of ^{13}C -depleted C for Koidu eclogitic diamonds is recycled crustal material (Milledge et al., 1983; Kirkley et al., 1991), in particular biogenic carbonate \pm organic matter from subducted altered oceanic crust (AOC; Li et al., 2019).

The major reservoirs for crustal C in AOC include normal marine carbonate ($\delta^{13}\text{C} \sim 0$ ‰; Schidlowski, 2001; Cartigny et al., 2014), ^{13}C -depleted biogenic carbonate ($\delta^{13}\text{C}$ as low as -24 ‰;

Li et al., 2019) and organic matter (average $\delta^{13}\text{C}$ of -26 ± 7 ‰; Schidlowski, 2001). Similarly, crustal N from clay minerals formed by low-temperature ($< 100^\circ\text{C}$) and high-temperature ($> 250^\circ\text{C}$) alteration of oceanic crust has high $\delta^{15}\text{N}$ and low $\delta^{15}\text{N}$ values, respectively (Busigny et al., 2005; Li et al., 2019). Devolatilization of C and N from AOC during subduction further decreases $\delta^{13}\text{C}$ and increases $\delta^{15}\text{N}$ values in the residue (Bebout and Fogel, 1992; Li et al., 2014; Cartigny et al., 2014). Devolatilization and mixing of C and N from these various AOC reservoirs (\pm a mantle component) can explain the diverse $\delta^{13}\text{C}$ and $\delta^{15}\text{N}$ values of the eclogitic diamonds contained in Cluster 1 (Fig. 2.13a).

Cluster 3: Mantle-derived fluids/melts (i.e., fluids/melts that ultimately derive from the convecting upper mantle) associated with kimberlitic or carbonatitic magmatism are invoked for the crystallization of fibrous diamonds (Boyd et al., 1987; Navon et al., 1988; Boyd et al., 1994b). The confined ranges of $\delta^{13}\text{C}$ and $\delta^{15}\text{N}$ values (both are close to -5 ‰; Boyd et al., 1987; Cartigny, 2005; Cartigny et al., 2014; Petts et al., 2016) in fibrous diamonds worldwide indicate that the mantle reservoir of their parental fluids/melts has homogeneous C and N isotope compositions. The $\delta^{13}\text{C}$ and $\delta^{15}\text{N}$ values of rocks that are sourced directly from the convecting upper mantle, i.e. fresh mid-ocean ridge basalts (MORB), also fall in similar ranges (Marty and Zimmermann, 1999; Cartigny et al., 2014), suggesting that they are the isotopic signature of the convecting depleted mantle. Thus, Koidu diamonds in Cluster 3, with C and N isotope compositions similar to fibrous diamonds and MORB, likely formed from relatively homogeneous, mantle-derived fluids/melts (Fig. 2.13b).

The observation that the eclogitic diamond rims fall into “mantle-like” Cluster 3 suggests that the diamond-forming melts/fluids switched from slab-derived to mantle-derived. Decoupling between mineral inclusion composition (related to the eclogitic diamond substrates) and diamond

C and N (derived externally, from deeper portions of a slab and/or the lithospheric or convecting mantle) is common, as revealed by a prominent mode in $\delta^{13}\text{C}$ at -5 ‰ and mostly negative $\delta^{15}\text{N}$ values for eclogitic inclusion-bearing diamonds worldwide (Cartigny, 2005; Stachel et al., 2009; Cartigny et al., 2014). Although mixed paragenesis diamond 138-7 (in Cluster 3) contains both eclogitic and peridotitic inclusions, none of its growth zones show isotope compositions clearly indicative of subducted C and N, again indicating decoupling between an evolving/changing substrate and the apparently constant source of the diamond-forming fluid.

Cluster 2: Mixing of C and N derived from the convecting mantle with subducted components shifts diamond $\delta^{13}\text{C}$ and $\delta^{15}\text{N}$ away from the mantle value, following mixing arrays that are controlled in their curvature by the ratio $(\text{N/C})_{\text{Mantle}}/(\text{N/C})_{\text{AOC}}$ (Li et al., 2019) (Fig. 2.13a). Almost two-thirds of the diamonds in Cluster 2 have $\delta^{13}\text{C} > -4$ ‰ and the majority have positive $\delta^{15}\text{N}$ values, possibly reflecting variable degrees of mixing between a mantle-derived component ($\delta^{13}\text{C} = -5$ ‰ and $\delta^{15}\text{N} = -5$ ‰) and a normal marine carbonate- ($\delta^{13}\text{C} \approx 0$ ‰) and low-temperature clay-derived ($\delta^{15}\text{N} > 0$ ‰) subducted component (Li et al., 2019). Generally, diamonds showing only minor ^{13}C enrichment relative to the mantle value but strongly variable $\delta^{15}\text{N}$ values suggest decoupling of C and N (Mikhail et al., 2014). Alternatively, the slightly ^{13}C -enriched character of Cluster 2 could be a mantle signature unique to the West African Craton, since similar mild shifts to elevated $\delta^{13}\text{C}$ values were also observed for peridotitic diamonds from Kankan (Guinea; Stachel et al., 2002) and Akwatia (Ghana; Stachel and Harris, 1997). The observation that this signature extends to lower mantle diamonds from Kankan (Stachel et al., 2002; Palot et al., 2014) may indicate a plume source of mildly ^{13}C -enriched C, possibly ultimately linked to deeply subducted crustal material. The spread in N isotope composition of Cluster 2 could then also be linked to mixing between asthenosphere-derived ($\delta^{15}\text{N}$ of -5 ± 2 ‰; Cartigny and Marty, 2013) and plume-

derived components ($\delta^{15}\text{N}$ of $+3 \pm 2$ ‰; Dauphas and Marty, 1999; Marty and Dauphas, 2003).

2.5.5 Growth episodes of Koidu diamonds

The three distinct clusters in $\delta^{13}\text{C}$ – $\delta^{15}\text{N}$ space suggest that multiple diamond growth events occurred in the lithospheric mantle beneath Koidu (Fig. 2.13). Eclogitic diamond cores formed from subducted crustal material (Cluster 1) and rims from mantle-derived fluids/melts (Cluster 3). This sequence indicates eclogitic diamond growth in at least two distinct episodes. One mixed paragenesis diamond (133-6) shows inner growth zones indicative of mixed C and N sources (mantle and subducted; Cluster 2) and a rim that again has a purely mantle-like signature (Cluster 3). The abrupt change of isotopic signature between core and rim in these diamonds documents that their growth followed two sequences: Cluster 1 \rightarrow Cluster 3 and Cluster 2 \rightarrow Cluster 3, with the temporal relationship between Clusters 1 and 2 remaining unconstrained.

Crystallization of the earlier generation of eclogitic diamonds (Cluster 1) may have been coeval with or subsequent to Archean subduction and eclogite emplacement beneath the Man Shield (Barth et al., 2002a; Aulbach et al., 2019a). For eclogitic sulphide-bearing diamonds from nearby Zimmi, Re-Os dating indicated formation only in the Neoproterozoic (~650 Ma; Smit et al., 2016), but involving S that had experienced mass independent isotopic fractionation in the Archean atmosphere (Smit et al., 2019a), thereby documenting an indirect link to Archean subduction processes. Given the subduction signature of Cluster 1 diamonds, their formation likely is associated with C contained within the Archean slab, but an additional fluid/melt pulse may still be required to facilitate mobilization and re-precipitation of the subducted C and to add a mantle-like N component to the compositional array.

A detailed study of Koidu eclogites (Aulbach et al., 2019b) indicated that a subset of

diamondiferous low-MgO eclogites and gabbroic eclogites were transformed to barren high-MgO eclogites and pyroxenites as a consequence of metasomatic overprint associated with the Neoproterozoic break-up of Rodinia. The 650 Ma age obtained for Zimmi diamonds (Smit et al., 2016) correlates with the timing of this event. Mixed paragenesis diamonds with a mantle-like stable isotope composition, either throughout (138-7) or in a distinct rim zone (133-6), and the mantle-like composition of the secondary overgrowth on eclogitic diamonds suggest that these metasomatic processes and the transition to diamond formation with mantle-like C and N isotopic signatures may be linked.

I propose that after initial growth of eclogitic diamonds (Cluster 1), there were at least two pulses of metasomatic agents involved in the growth of diamonds, the first resulting in Cluster 2 and the second in Cluster 3. The first pulse of carbonated ultrabasic melt, derived possibly from either a mantle plume or melting initiated by subduction-related fluids, infiltrated eclogite lenses in the lithospheric mantle, converting some low-MgO and gabbroic eclogites to high-MgO eclogites and pyroxenites (Hills and Haggerty, 1989; Barth et al., 2002b). Some of the original diamond content of the low-MgO and gabbroic eclogites may have been destroyed by the infiltrating melt (Aulbach et al., 2019b). The same pulse of carbonated melt also infiltrated surrounding peridotites (possibly evolving into an aqueous CHO fluid upon equilibration with subsolidus harzburgites). This metasomatic event was associated with the precipitation of Cluster 2 diamonds (peridotitic suite and the core of mixed paragenesis diamond 133-6) with mild ^{13}C enrichment and variable ^{15}N enrichment. The trend of outward increasing $\delta^{13}\text{C}$ values and decreasing N concentrations in the central portion of diamond 133-6 suggests that this melt pulse was relatively oxidizing (Fig. 2.11), driven by carbonate reduction, or redox-neutral precipitation from coexisting CH_4 and CO_2 during cooling.

A second pulse of melt/fluid with an asthenosphere-derived C and N isotope signature infiltrated the local lithospheric mantle after a significant period of time, documented by the different N aggregation states of cores and rims of some diamonds (Fig. 2.12). This pulse was more N-rich and a lack of covariation between $\delta^{13}\text{C}$ values and N abundance in precipitated Cluster 3 diamonds indicates that fluid-limited conditions did not occur. Infiltration of this melt/fluid is documented in the rims of eclogitic diamonds and some mixed paragenesis diamonds (133-6 (rim) and 138-7).

The two instances of peridotitic inclusions in the rims of mixed paragenesis diamonds are both related to this second metasomatic event, based on mantle-like $\delta^{13}\text{C}$ and $\delta^{15}\text{N}$ values and high N contents of these diamond growth zones. As discussed above, the earlier eclogitic and later peridotitic inclusions in the studied mixed paragenesis diamonds have the respective chemical signatures of eclogitic and peridotitic mantle xenolith minerals, requiring that the diamonds involved must have physically moved between different diamond substrates. Infiltration of an eclogite-derived fluid into a peridotitic diamond substrate (Mikhail et al. 2021) is neither consistent with the clearly crust-derived signatures of the eclogitic inclusions nor with the very Mg- and Cr-rich character of the peridotitic inclusions. Physical transport may have been associated with melt injection, as documented by polymict mantle breccias (juxtaposition of minerals and rock clasts from strongly disparate lithologies) observed as xenoliths from the Kaapvaal craton (Zhang et al., 2003; Giuliani et al., 2014). Alternatively, intense deformation involving small eclogite bodies may have achieved transport of resistant minerals such as diamond into surrounding peridotite along high-strain shear zones. Partial melting of eclogites during fluid influx (Spetsius, 1998) and segregation of such melts may also have allowed for physical transport of originally eclogitic diamonds into peridotitic substrates, followed by renewed diamond growth and encapsulation of

peridotitic minerals (Wang, 1998). As indicated by a mild resorption boundary within the one mixed paragenesis diamond entirely associated with Cluster 3 (138-7), this second fluid/melt infiltration may have occurred as repeated pulses over an extended period of time.

2.6 Conclusions

Combined C and N isotope composition of diamond is a robust tracer of the source of diamond-forming fluids/melts. The distinct isotopic signatures, CL responses and N aggregation states observed in the cores and rims of Koidu diamonds suggest episodic diamond growth during multiple pulses of melts/fluids. In their stable isotope compositions, Koidu diamonds of peridotitic, eclogitic and mixed paragenesis form three major clusters: Cluster 1 (cores of eclogitic diamonds) has low $\delta^{13}\text{C}$ and highly variable $\delta^{15}\text{N}$ values ($\delta^{13}\text{C} = -33.2$ to -14.4 ‰; $\delta^{15}\text{N} = -5.3$ to $+10.1$ ‰), suggesting derivation from recycled crustal material (\pm a mantle component). Cluster 2 (peridotitic diamonds and core of mixed paragenesis diamond 133-6) has mantle-like to mildly ^{13}C -enriched C isotope compositions and a wide range of $\delta^{15}\text{N}$ values ($\delta^{13}\text{C} = -6.0$ to -1.1 ‰; $\delta^{15}\text{N} = -4.2$ to $+9.7$ ‰), likely reflecting mixing of C and N from subducted and mantle sources. Cluster 3 (rims of eclogitic diamonds and of mixed paragenesis diamond 133-6, and mixed paragenesis diamond 138-7) has a homogeneous isotopic signature similar to fibrous diamonds and MORB ($\delta^{13}\text{C} = -7.8$ to -3.6 ‰; $\delta^{15}\text{N} = -7.9$ to -2.1 ‰), pointing to precipitation from mantle-derived fluids/melts. Transects across mixed paragenesis diamond 133-6 indicate that the fluid/melt pulse responsible for the growth of its innermost zones (Cluster 2) was relatively oxidizing (gradual outward increase in $\delta^{13}\text{C}$ and decrease in N), whereas diamonds in Clusters 1 and 3 likely precipitated in systems that were not fluid-limited, precluding isotopic fractionation, and thus the redox states of their growth media cannot be constrained.

Mixed paragenesis diamonds are associated with all three clusters (1, 2 and 3), but the two examples where I could document a transition from an eclogitic paragenesis core to a peridotitic paragenesis rim either show a transition from mixed source-type Cluster 2 (core) to mantle-like Cluster 3 (rim) or fall entirely into Cluster 3. Based on the major and trace element composition of the mineral inclusions in these mixed paragenesis diamonds, which provide good matches to the equivalent minerals in a subset of Koidu eclogites and in cratonic peridotites, I exclude precipitation during a single intense metasomatic event but instead invoke physical transport of diamonds from eclogitic to peridotitic substrates between separate growth events. The highly depleted character of the peridotitic inclusions precludes that diamond transport involved significant interaction between the peridotitic substrates and either eclogite or melt, which favours either mechanical shearing of small eclogite pods residing in lithospheric peridotites or diamond transport and injection into peridotite through small melt volumes.

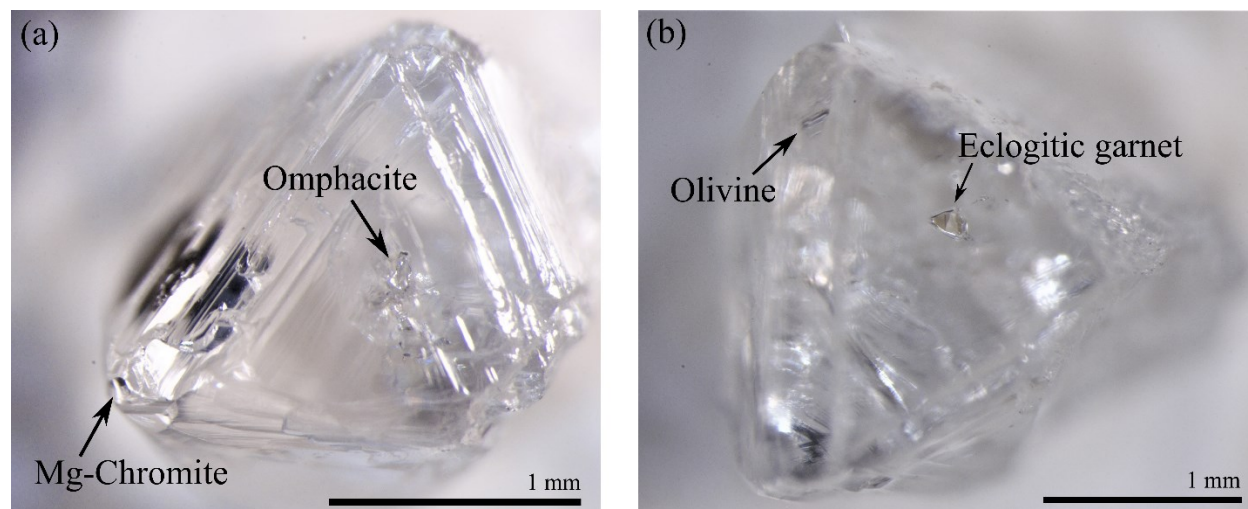


Figure 2.1 Diamonds with co-occurring eclogitic and peridotitic mineral inclusions. (a) Diamond 133-6 with multiple omphacites in the centre and a Mg-chromite in the rim. (b) Diamond 138-7 with eclogitic garnets in the centre and an olivine near the rim.

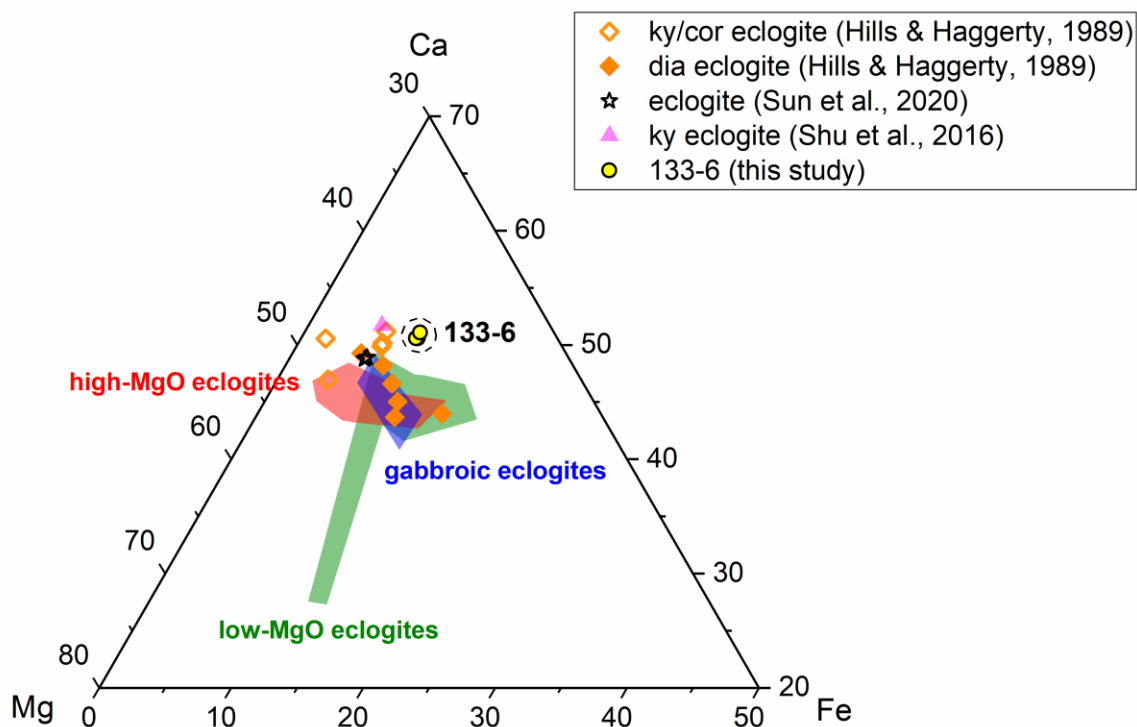


Figure 2.2 Ternary diagram showing the major element composition (molar Ca-Mg-Fe) of omphacite inclusions from mixed paragenesis diamond 133-6 in this study (circles). The fields for omphacites from high-MgO (red), low-MgO (green) and gabbroic eclogites (blue) (Aulbach et al., 2019b), and from kyanite- and corundum-bearing low-MgO eclogites (open diamonds) and diamond-bearing low-MgO eclogites (solid diamonds) (Hills and Haggerty, 1989) are shown for comparison. Also shown are omphacites from two low-MgO eclogites from the Obnazhennaya kimberlite in Siberia (overlapping stars; Sun et al., 2020) and from a kyanite eclogite from the Bellsbank kimberlite in South Africa (triangle; Shu et al., 2016).

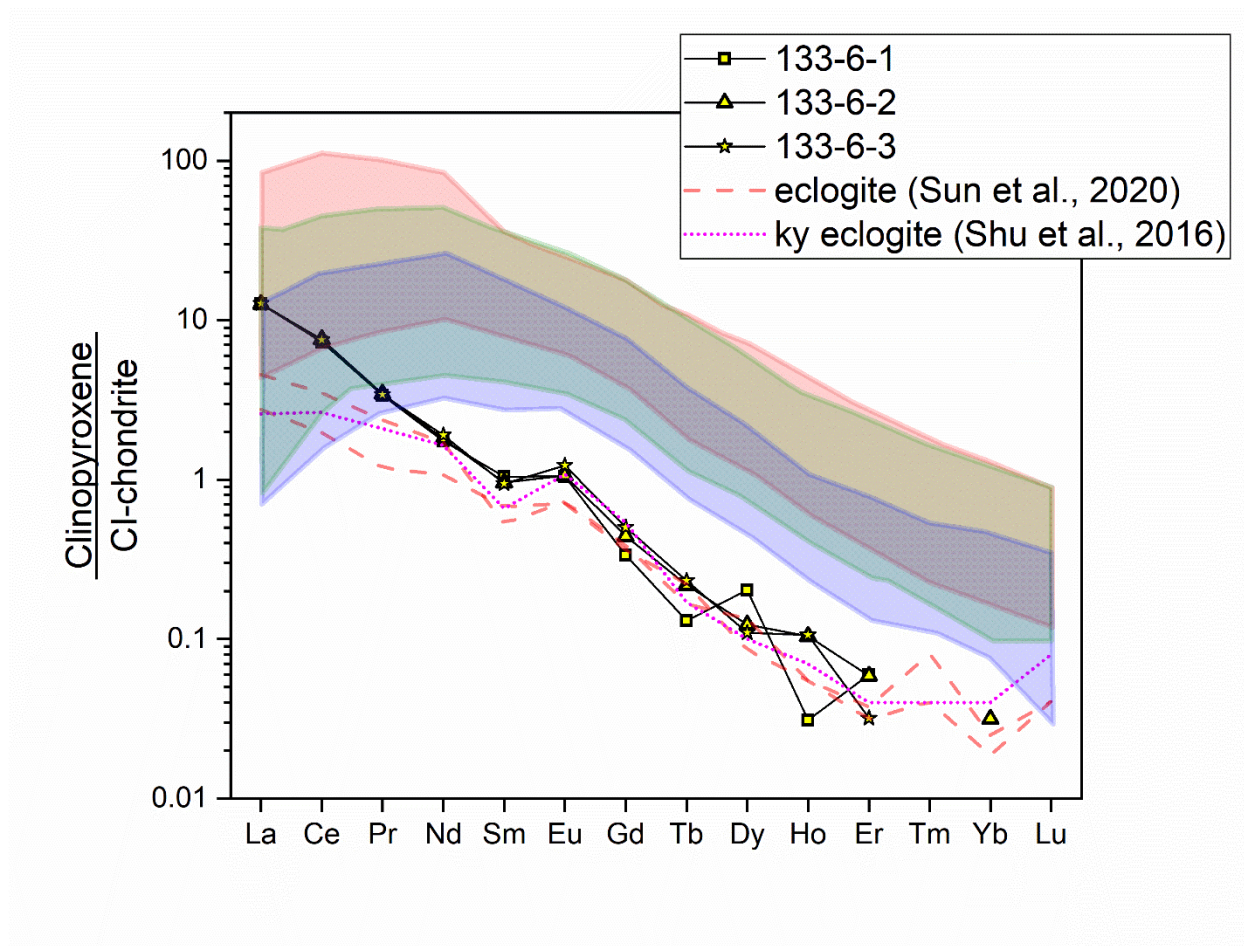


Figure 2.3 REE concentrations in omphacites from mixed paragenesis diamond 133-6, normalized to CI-chondrite (McDonough and Sun, 1995). These omphacites have highly fractionated ($\text{La}_N/\text{Yb}_N = 422$) REE_N patterns. The fields for omphacites from high-MgO (red), low-MgO (green) and gabbroic eclogites (blue) (Aulbach et al., 2019b) are shown for comparison. Also shown are the REE_N patterns of omphacites from two low-MgO eclogites from the Obnazhennaya kimberlite in Siberia (red dashed lines; Sun et al., 2020) and from a kyanite eclogite from the Bellsbank kimberlite in South Africa (magenta dotted line; Shu et al. 2016), which are very similar to my Koidu samples.

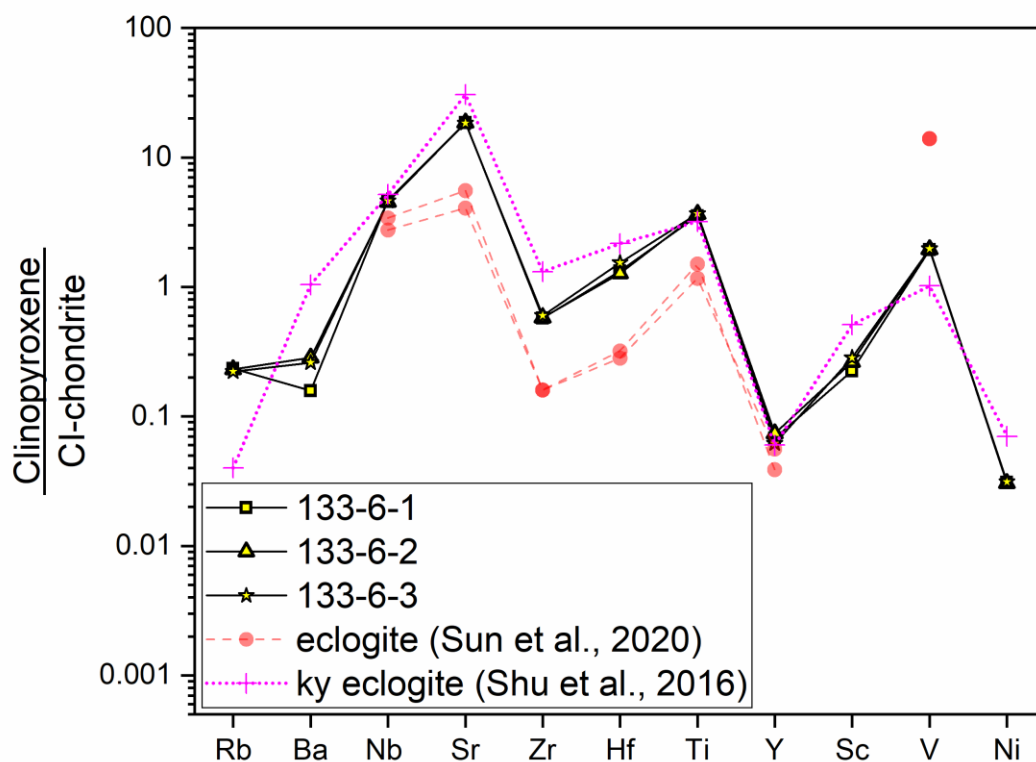


Figure 2.4 Concentrations of other trace elements including LILE and HFSE in omphacites from mixed paragenesis diamond 133-6, normalized to CI-chondrite (McDonough and Sun, 1995). Also shown are the omphacites from two low-MgO eclogites from the Obnazhennaya kimberlite in Siberia (red dashed lines; Sun et al., 2020) and from a kyanite eclogite from the Bellsbank kimberlite in South Africa (magenta dotted line; Shu et al., 2016). As already seen for the REE, these omphacites have overall very similar trace element patterns to my samples. Elements are arranged in increasing compatibility in the clinopyroxene structure (Green, 1994).

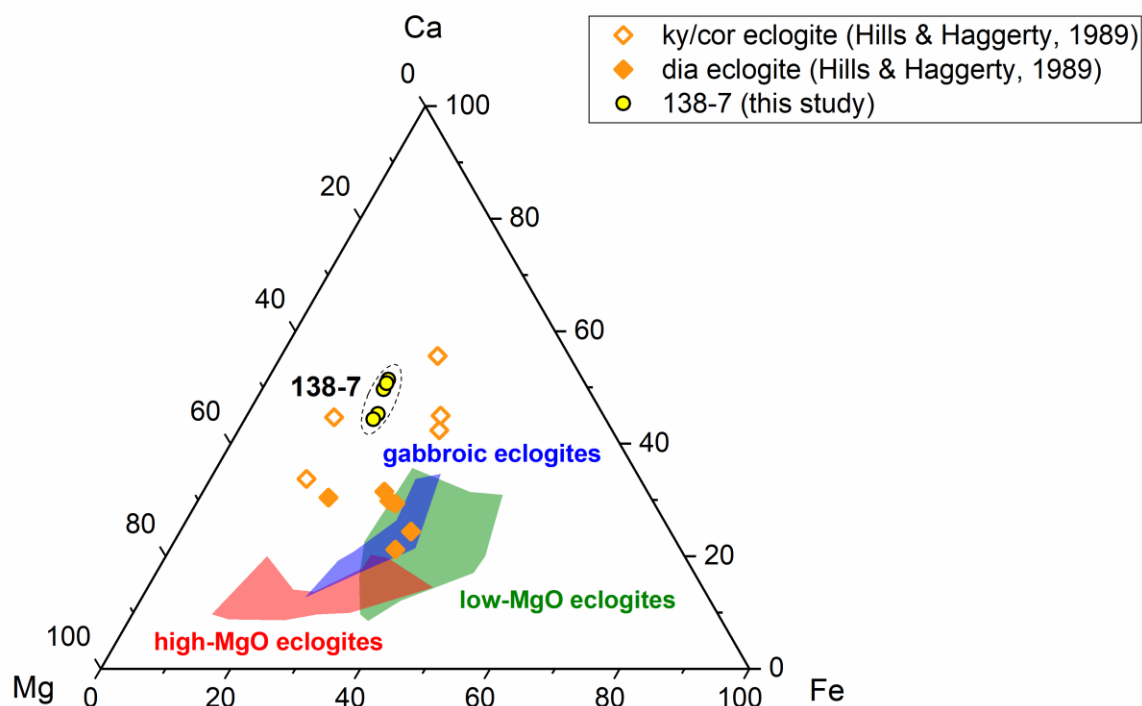


Figure 2.5 Ternary diagram showing the major element compositions (molar Ca-Mg-Fe) of garnet inclusions from mixed paragenesis diamond 138-7 (open circles). The fields for garnets from high-MgO (red), low-MgO (green) and gabbroic eclogites (blue) (Aulbach et al., 2019b) and from kyanite- and corundum-bearing low-MgO eclogites (open diamonds) and diamond-bearing low-MgO eclogites (solid diamonds) (Hills and Haggerty, 1989) are shown for comparison.

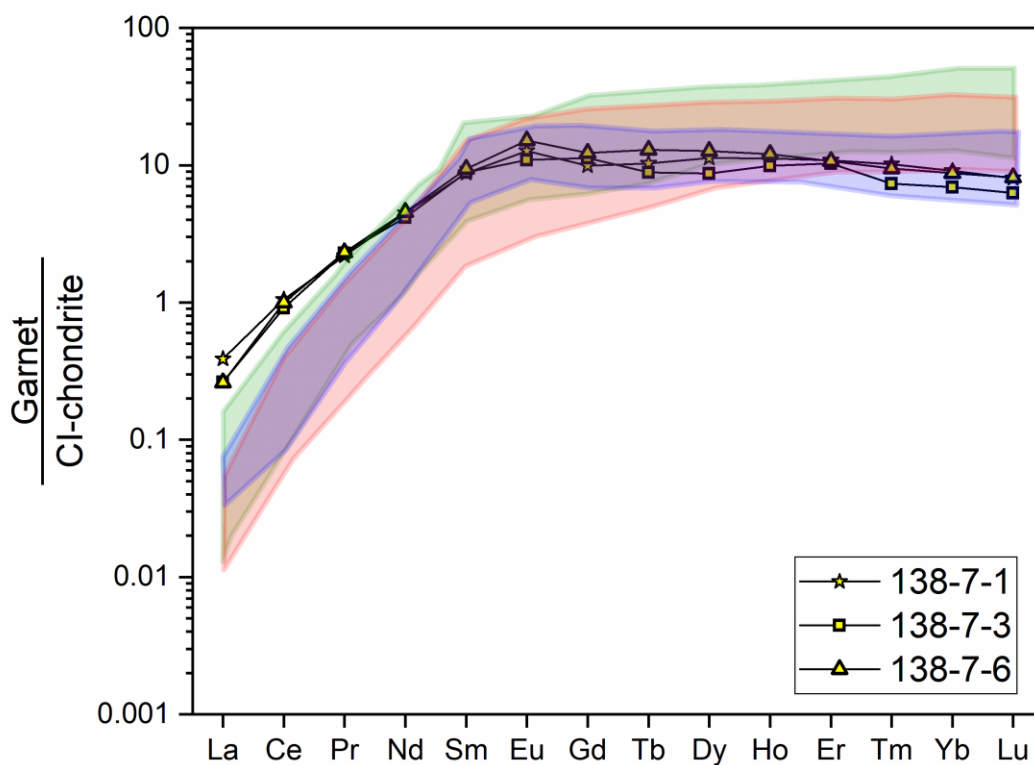


Figure 2.6 REE concentrations in garnets from mixed paragenesis diamond 138-7, normalized to CI-chondrite (McDonough and Sun, 1995). The fields for garnets from high-MgO (red), low-MgO (green) and gabbroic eclogites (blue) (Aulbach et al., 2019b) are shown for comparison.

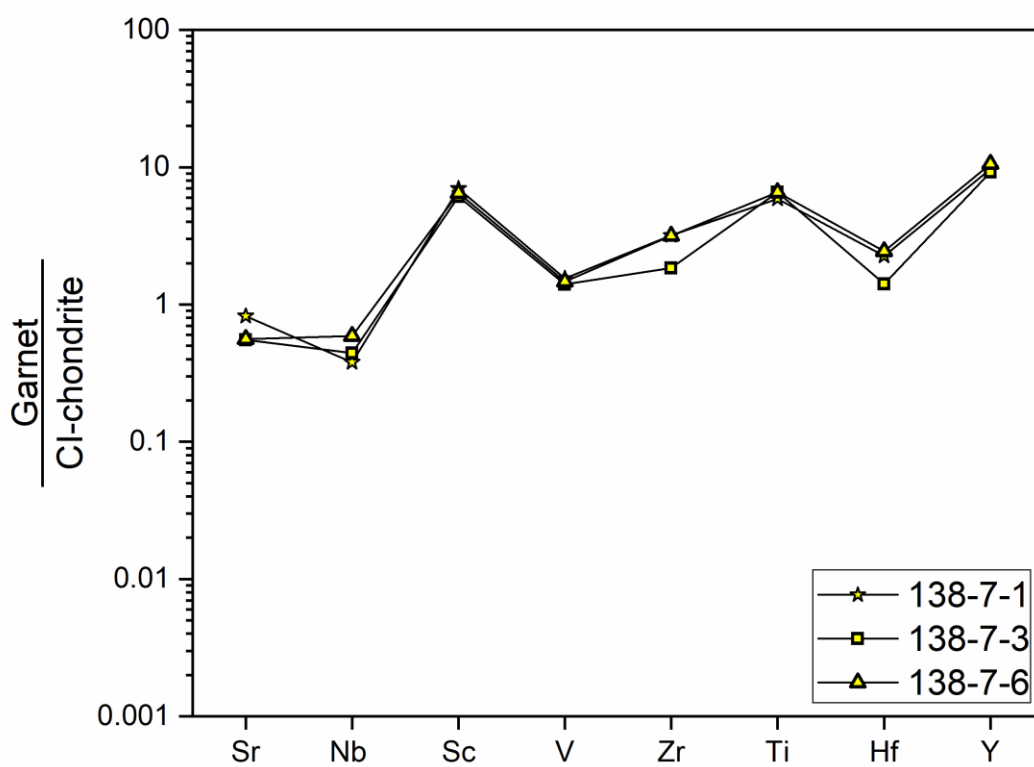


Figure 2.7 Concentrations of other trace elements including LILE and HFSE in garnets from mixed paragenesis diamond 138-7, normalized to CI-chondrite (McDonough and Sun, 1995). Elements are arranged in increasing compatibility in the garnet structure (Green, 1994).

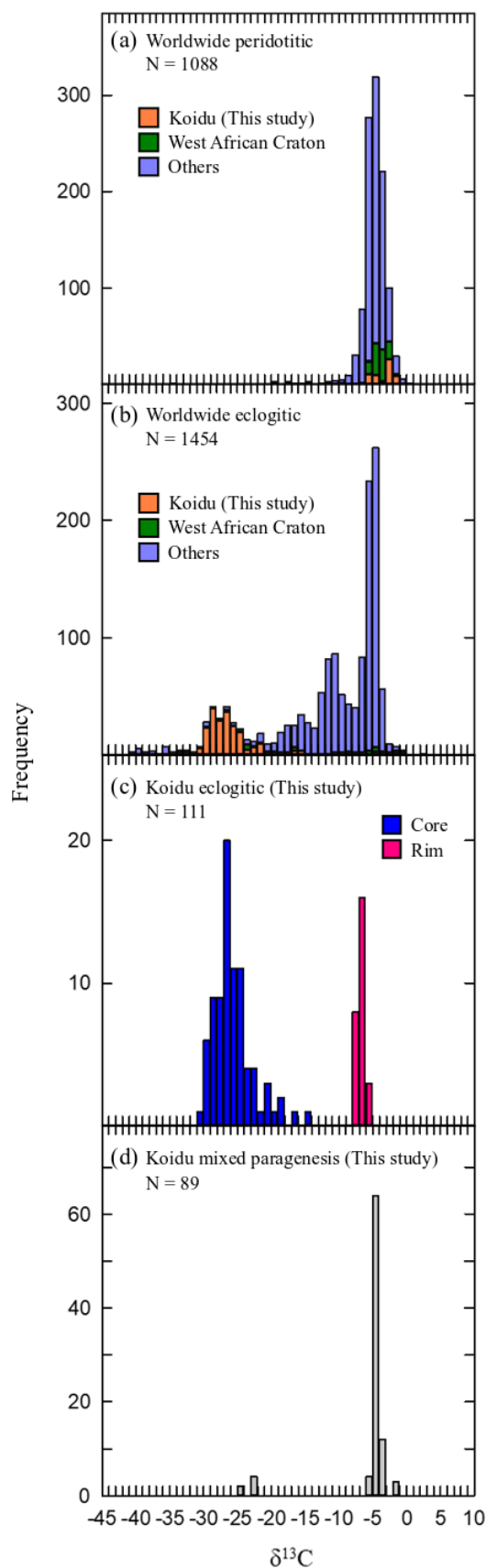


Figure 2.8 Distribution of $\delta^{13}\text{C}$ values (individual SIMS analysis spots) in (a) peridotitic diamonds, (b) eclogitic diamonds (only diamonds without a core-rim structure are shown), (c) eclogitic diamonds with a core-rim structure and (d) mixed paragenesis diamonds in this study. Both peridotitic (a) and unzoned eclogitic (b) Koidu diamonds are compared to diamonds from other localities on the West African Craton and from worldwide sources (database of Stachel et al., 2022).

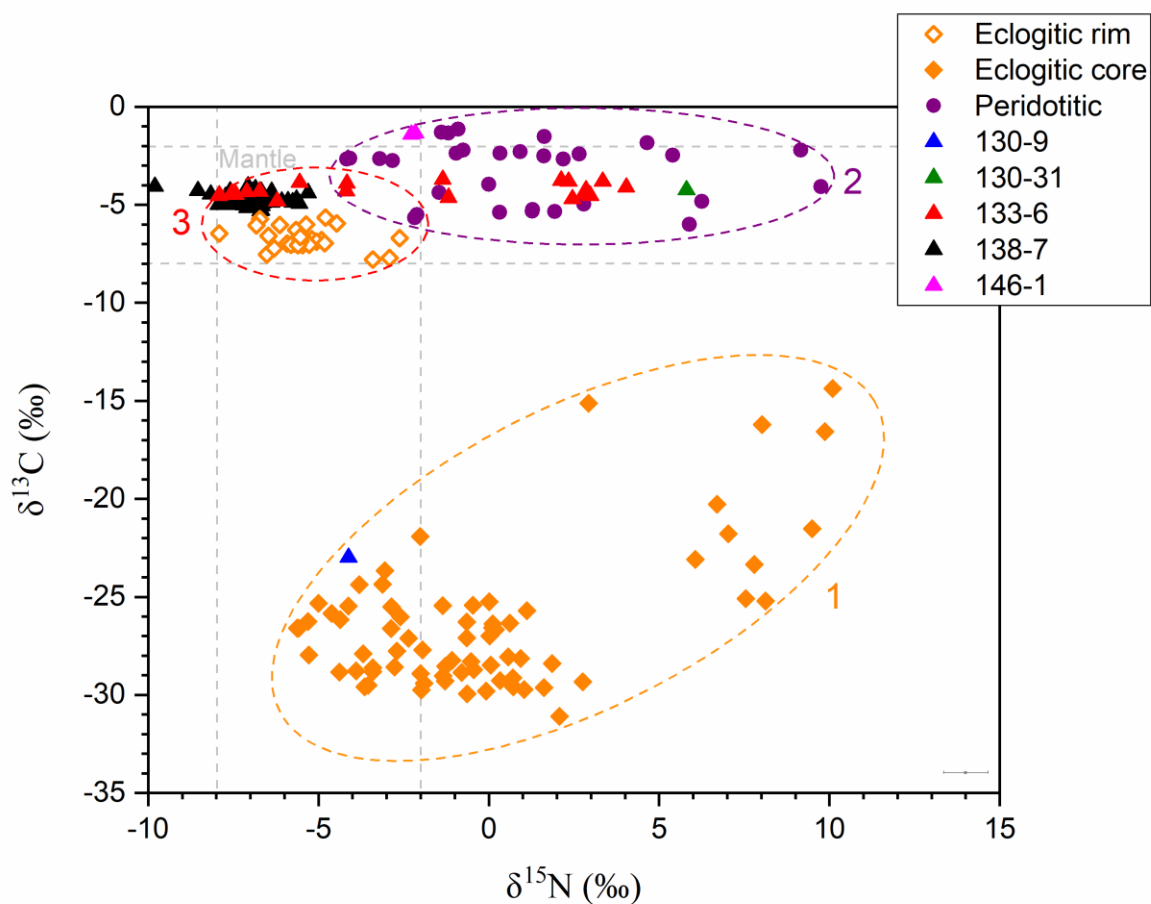


Figure 2.9 $\delta^{13}\text{C}$ versus $\delta^{15}\text{N}$ for peridotitic (circles), eclogitic (solid diamonds: core; open diamonds: rim) and mixed paragenesis diamonds (triangles) from Koidu. The error bars in the lower right corner indicated the typical total analytical uncertainties (95% confidence level). Three major compositional clusters are identified for Koidu diamonds: Cluster 1 ($\delta^{13}\text{C} = -33.2$ to -14.4% ; $\delta^{15}\text{N} = -5.3$ to $+10.1\%$), Cluster 2 ($\delta^{13}\text{C} = -6.0$ to -1.1% ; $\delta^{15}\text{N} = -4.2$ to $+9.7\%$) and Cluster 3 ($\delta^{13}\text{C} = -7.8$ to -3.6% ; $\delta^{15}\text{N} = -7.9$ to -2.1%).

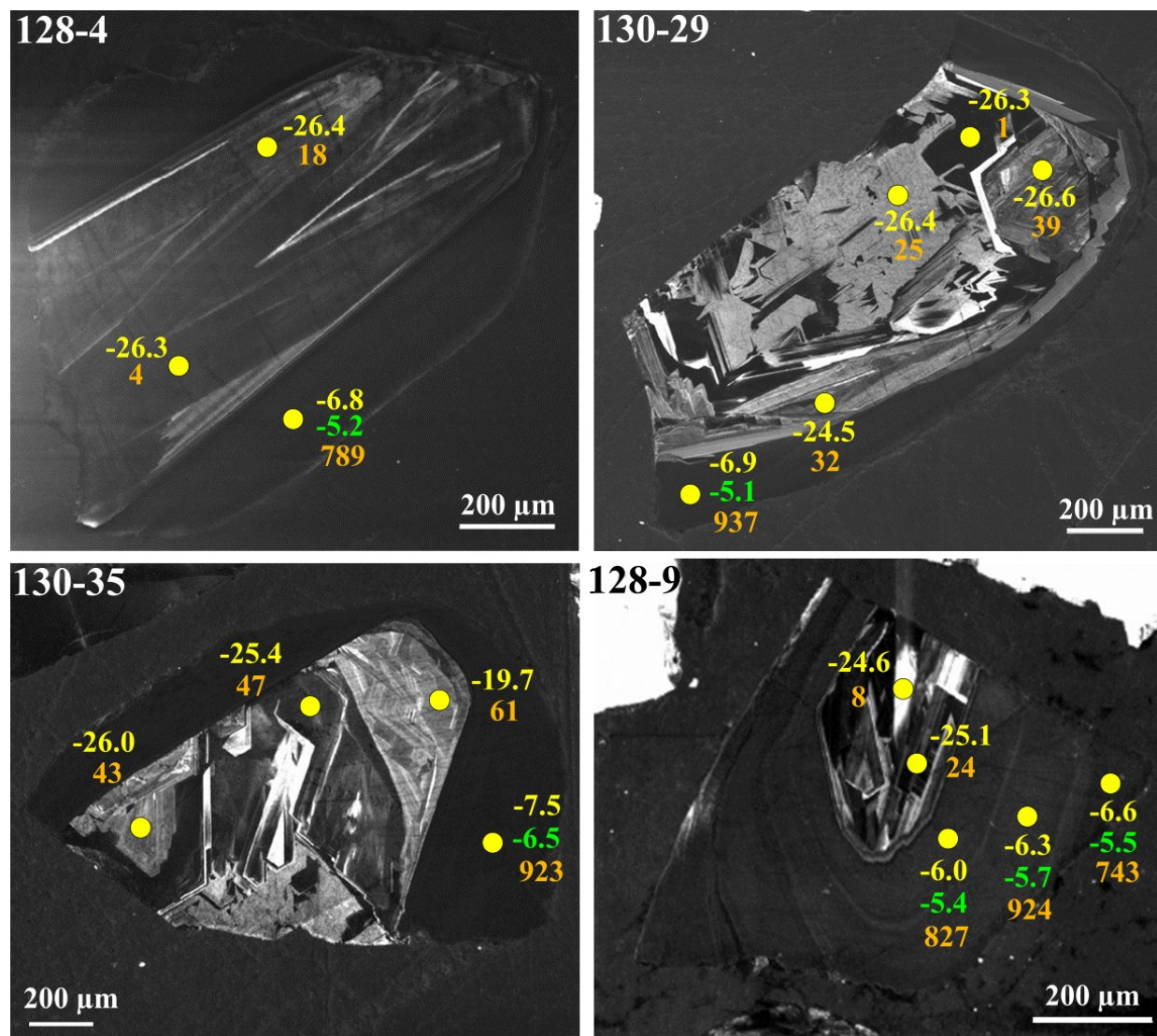


Figure 2.10 Examples of cathodoluminescence images of Koidu eclogitic diamonds (128-4, 128-9, 130-29 and 130-35) showing core–rim structures. SIMS measurement spots with $\delta^{13}\text{C}$ values (‰; yellow), $\delta^{15}\text{N}$ values (‰; green) and N concentrations (at.ppm; orange) are indicated.

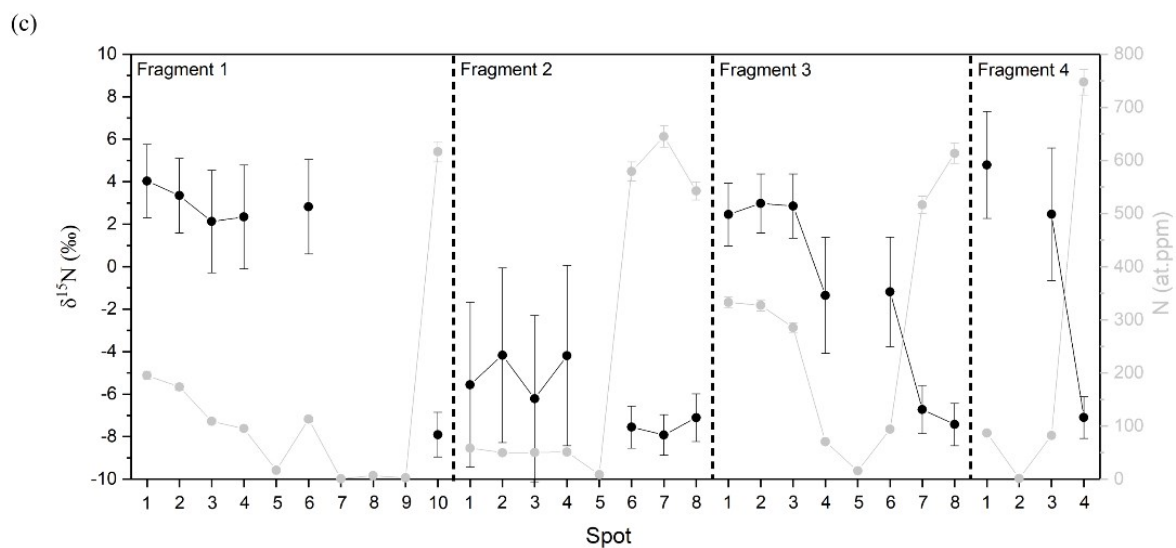
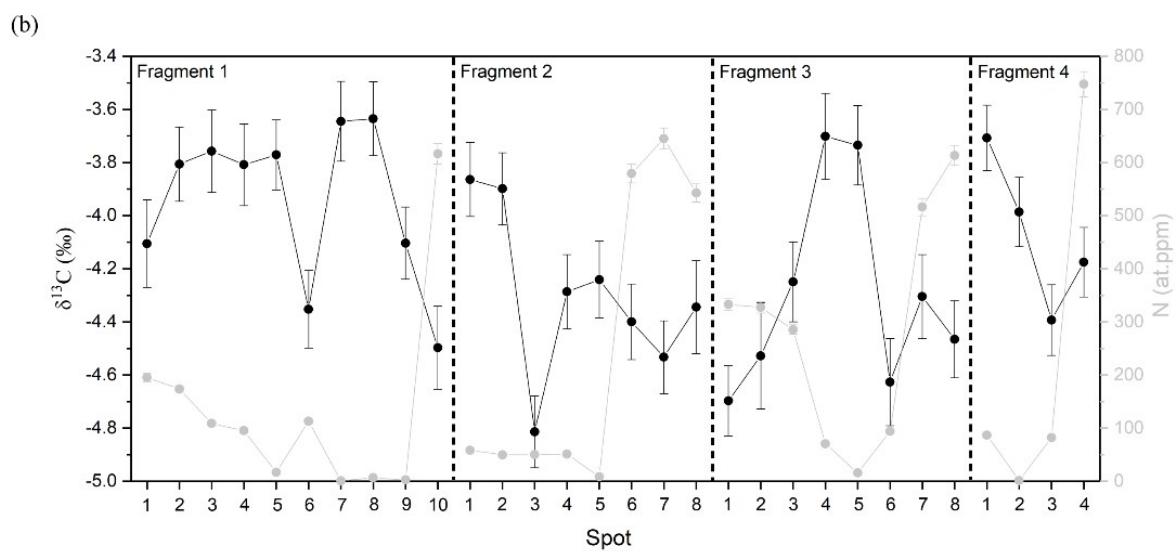
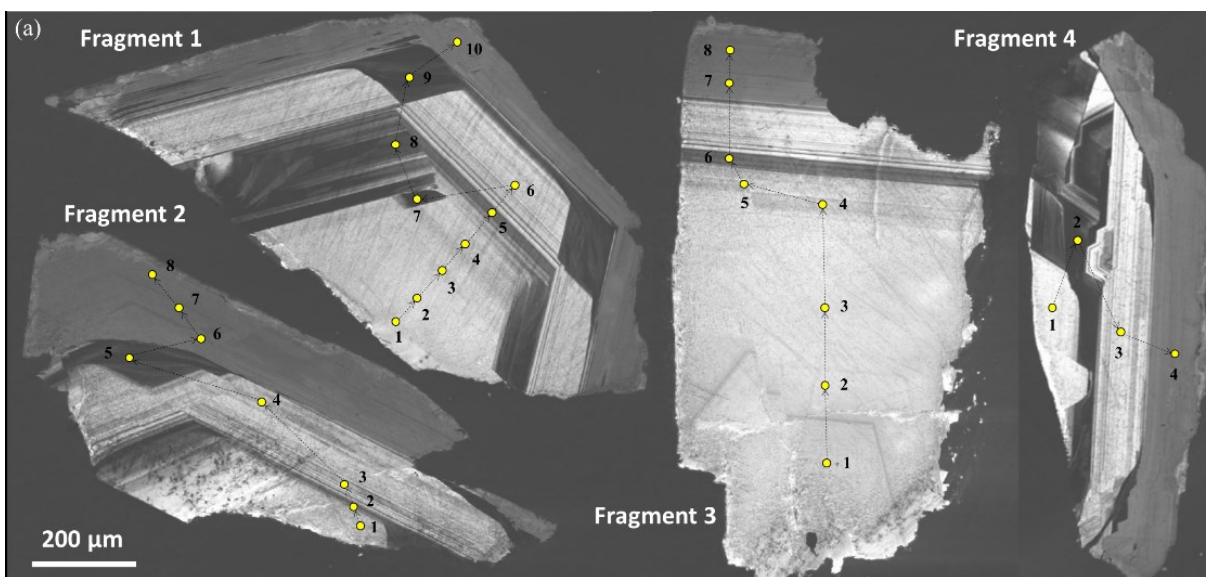


Figure 2.11 (a) Cathodoluminescence images of four fragments of mixed paragenesis diamond 133-6. The yellow dots indicate the spots of SIMS analyses. (b) Core-to-rim transects across the four fragments showing variations in $\delta^{13}\text{C}$ (‰; black) and N concentration (at.ppm; grey). (c) Core to rim variations across the same fragments for $\delta^{15}\text{N}$ (‰; black) and N concentration (at.ppm; grey). The total uncertainty (95% confidence level) for each point is indicated by error bars unless they are smaller than the size of the symbol.

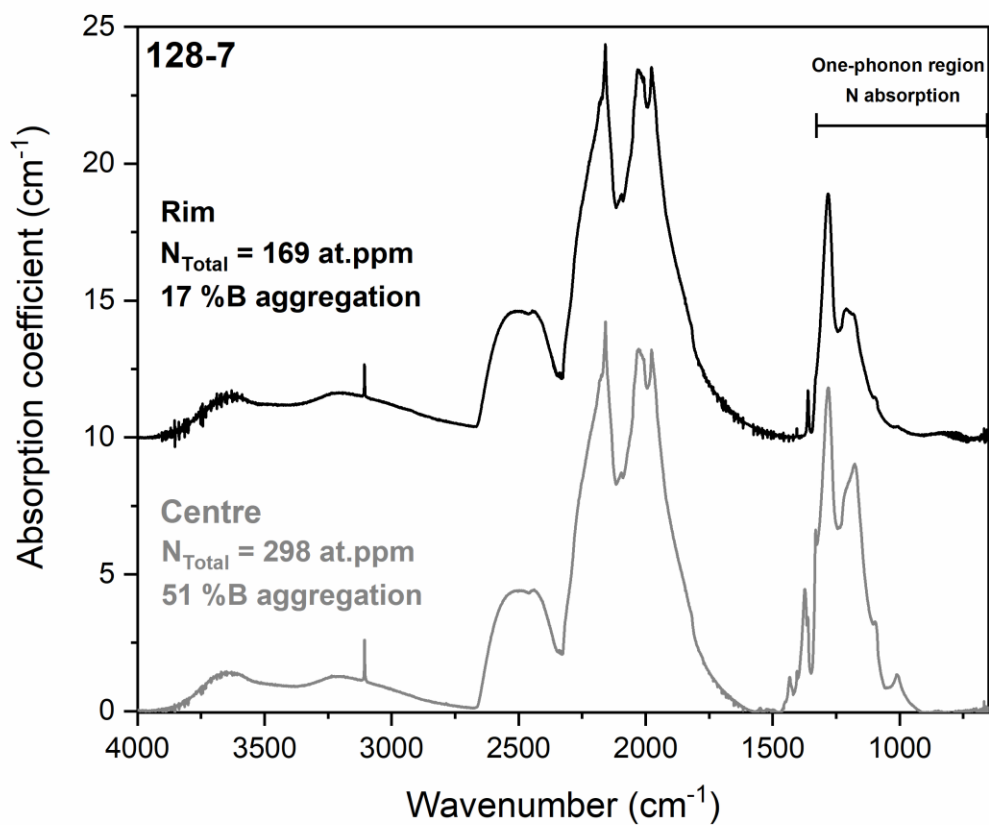


Figure 2.12 Infrared absorption spectra of a Koidu diamond (diamond 128-7) collected through its centre (grey) and rim (black). Nitrogen absorption bands in the one-phonon region (~ 1332 to ~ 400 cm^{-1}) of the spectra show a higher degree of N aggregation (higher percentage of N in B aggregation) in the centre compared to the rim.

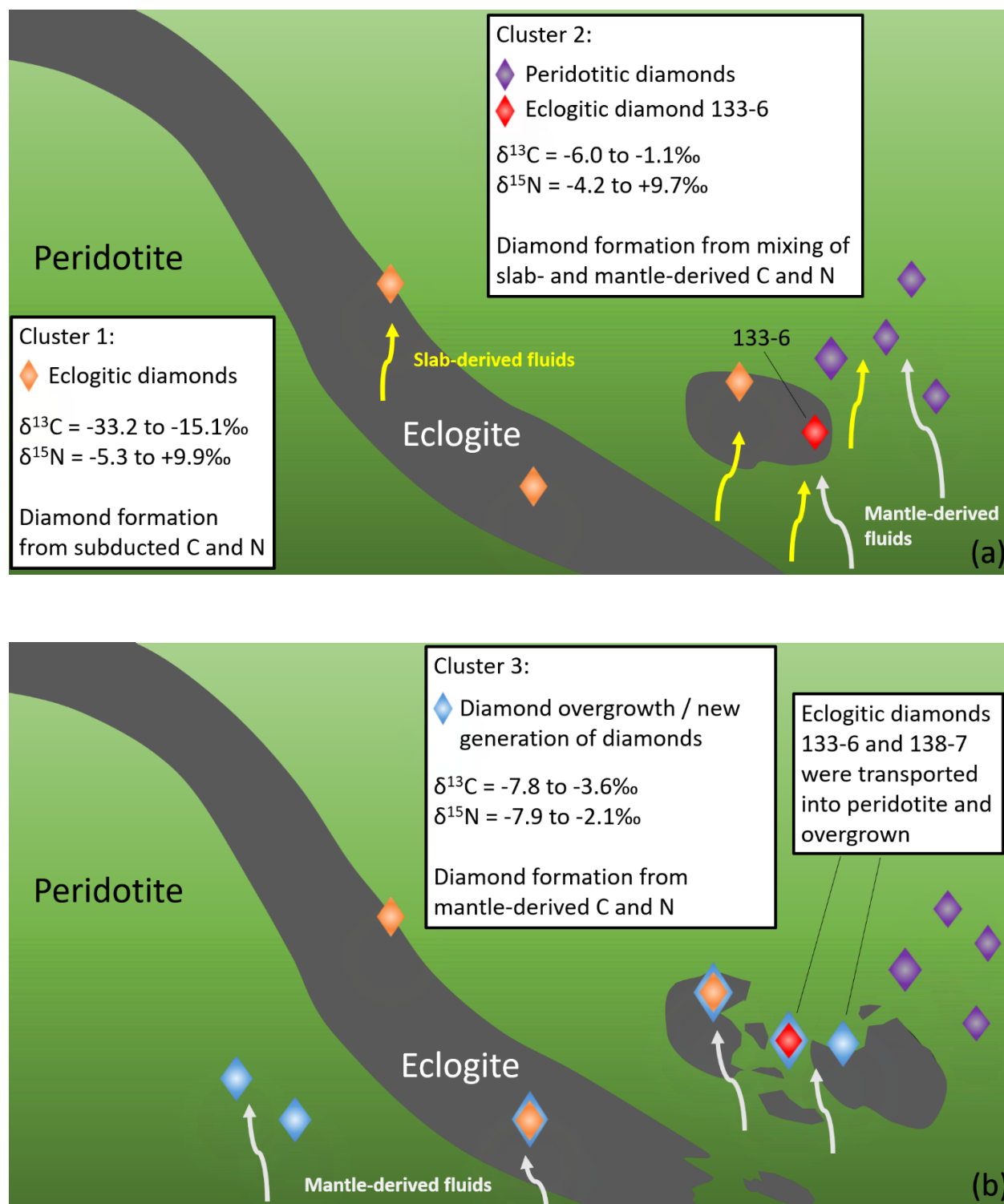


Figure 2.13 Schematic diagram showing the growth episodes reflected by Koidu diamonds. (a) Cluster 1 diamonds (cores of eclogitic diamonds indicated by orange diamond symbol) formed

from subducted crustal material (\pm a mantle component). Cluster 2 diamonds (core of mixed paragenesis diamond 133-6 indicated by red diamond symbol, and peridotitic diamonds indicated by purple diamond symbol) formed from mixing of slab- and mantle-derived C and N. Note that the temporal relationship between Cluster 1 and 2 is unconstrained. (b) Cluster 3 diamonds (rims of eclogitic diamonds and of mixed paragenesis diamond 133-6, mixed paragenesis diamond 138-7 and potentially some peridotitic diamonds indicated by blue diamond symbol) formed from purely mantle-derived C and N. Mixed paragenesis diamonds 133-6 and 138-7 originally formed in eclogite (encapsulating omphacites and eclogitic garnets, respectively) and were then physically transported into surrounding peridotites, where renewed diamond growth encapsulated peridotitic minerals (Mg-chromite and olivine, respectively).

References

- Aulbach S. and Jacob D. E. (2016) Major- and trace-elements in cratonic mantle eclogites and pyroxenites reveal heterogeneous sources and metamorphic processing of low-pressure protoliths. *Lithos* **262**, 586–605.
- Aulbach S., Stachel T., Viljoen K. S., Brey G. P. and Harris J. W. (2002) Eclogitic and websteritic diamond sources beneath the Limpopo Belt - Is slab-melting the link? *Contrib. to Mineral. Petrol.* **143**, 56–70.
- Aulbach S., Pearson N. J., O'Reilly S. Y., and Doyle B. J. (2007) Origins of xenolithic eclogites and pyroxenites from the Central Slave Craton, Canada. *J. Petrol.* **48**, 1843–1873.
- Aulbach S., Jacob D. E., Cartigny P., Stern R. A., Simonetti S. S., Wörner G., and Viljoen K. S. (2017) Eclogite xenoliths from Orapa: ocean crust recycling, mantle metasomatism and carbon cycling at the western Zimbabwe craton margin. *Geochim. Cosmochim. Acta* **213**, 574-592.
- Aulbach S., Heaman L. M., Jacob D. E., and Viljoen K. S. (2019a) Ages and sources of mantle eclogites: ID-TIMS and in situ MC-ICPMS Pb-Sr isotope systematics of clinopyroxene. *Chem. Geol.* **503**, 15–28.
- Aulbach S., Höfer H. E. and Gerdes A. (2019b) High-Mg and Low-Mg Mantle eclogites from Koidu (West African Craton) linked by neoproterozoic ultramafic melt metasomatism of subducted archaean plateau-like oceanic crust. *J. Petrol.* **60**, 723–754.
- Barth M. G., Rudnick R. L., Horn I., McDonough W. F., Spicuzza M. J., Valley J. W. and Haggerty S. E. (2001) Geochemistry of xenolithic eclogites from West Africa, part I: A link

between low MgO eclogites and Archean crust formation. *Geochim. Cosmochim. Acta* **65**, 1499–1527.

Barth M. G., Rudnick R. L., Carlson R. W., Horn I. and McDonough W. F. (2002a) Re-Os and U-Pb geochronological constraints on the eclogite-tonalite connection in the Archean Man Shield, West Africa. *Precambrian Res.* **118**, 267–283.

Barth M. G., Rudnick R. L., Horn I., McDonough W. F., Spicuzza M. J., Valley J. W. and Haggerty S. E. (2002b) Geochemistry of xenolithic eclogites from West Africa, part 2: origins of the high MgO eclogites. *Geochim. Cosmochim. Acta* **66**, 4325–4345.

Bebout G. E. and Fogel M. L. (1992) Nitrogen-isotope compositions of metasedimentary rocks in the Catalina Schist, California: implications for metamorphic devolatilization history. *Geochim. Cosmochim. Acta* **56**, 2839–2849.

Boyd S. R., Matthey D. P., Pillinger C. T., Milledge H. J., Mendelsohn M. and Seal M. (1987) Multiple growth events during diamond genesis: an integrated study of carbon and nitrogen isotopes and nitrogen aggregation state in coated stones. *Earth Planet. Sci. Lett.* **86**, 341–353.

Boyd S. R., Kiflawi I. and Woods G. S. (1994a) The relationship between infrared absorption and the A defect concentration in diamond. *Philos. Mag. B* **69**, 1149–1153.

Boyd S. R., Pineau F. and Javoy M. (1994b) Modelling the growth of natural diamonds. *Chem. Geol.* **116**, 29–42.

Boyd S. R., Kiflawi I. and Woods G. S. (1995) Infrared absorption by the B nitrogen aggregate in diamond. *Philos. Mag. B* **72**, 351–361.

- Busigny V., Laverne C. and Bonifacie M. (2005) Nitrogen content and isotopic composition of oceanic crust at a superfast spreading ridge: A profile in altered basalts from ODP Site 1256, Leg 206. *Geochemistry, Geophys. Geosystems* **6**, 1–16.
- Cartigny P. (2005) Stable isotopes and the origin of diamond. *Elements* **1**, 79–84.
- Cartigny P. and Marty B. (2013) Nitrogen isotopes and mantle geodynamics: the emergence of life and the atmosphere-crust-mantle connection. *Elements* **9**, 359–366.
- Cartigny P., Harris J. W. and Javoy M. (2001) Diamond genesis, mantle fractionations and mantle nitrogen content: a study of $\delta^{13}\text{C-N}$ concentrations in diamonds. *Earth Planet. Sci. Lett.* **185**, 85–98.
- Cartigny P., Palot M., Thomassot E. and Harris J. W. (2014) Diamond formation: a stable isotope perspective. *Annu. Rev. Earth Planet. Sci.* **42**, 699–732.
- Clark J. R. and Papike J. J. (1968) Crystal-chemical characterization of omphacites. *Am. Mineral.* **53**, 840–868.
- Coplen T.B., Böhlke J.K., De Bièvre P., Ding T., Holden N.E., Hopple J.A., Krouse H.R., Lamberty A., Peiser H.S., Revesz K. and Rieder S.E. (2002) Isotope-abundance variations of selected elements (IUPAC Technical Report). *Pure Appl. Chem.* **74**, 1987–2017.
- Dauphas N. and Marty B. (1999) Heavy nitrogen in carbonatites of the Kola Peninsula: a possible signature of the deep mantle. *Science*. **286**, 2488–2490.
- Davies G. (1976) The A nitrogen aggregate in diamond-its symmetry and possible structure. *J. Phys. C Solid State Phys.* **9**, L537–L542.
- Davies R. M., Griffin W. L., O'Reilly S. Y. and Andrew A. S. (2003) Unusual mineral inclusions

- and carbon isotopes of alluvial diamonds from Bingara, eastern Australia. *Lithos* **69**, 51–66.
- Davies R. M., Griffin W. L., O'Reilly S. Y. and McCandless T. E. (2004a) Inclusions in diamonds from the K14 and K10 kimberlites, Buffalo Hills, Alberta, Canada: Diamond growth in a plume? *Lithos* **77**, 99–111.
- Davies R. M., Griffin W. L., O'Reilly S. Y. and Doyle B. J. (2004b) Mineral inclusions and geochemical characteristics of microdiamonds from the DO27, A154, A21, A418, DO18, DD17 and Ranch Lake kimberlites at Lac de Gras, Slave Craton, Canada. *Lithos* **77**, 39–55.
- Deines P. (1980) The carbon isotopic composition of diamonds: relationship to diamond shape, color, occurrence and vapor composition. *Geochim. Cosmochim. Acta* **44**, 943–961.
- Deines P. and Harris J. W. (1995) Sulfide inclusion chemistry and carbon isotopes of African diamonds. *Geochim. Cosmochim. Acta* **59**, 3173–3188.
- Fung A. T. and Haggerty S. E. (1995) Petrography and mineral compositions of eclogites from the Koidu Kimberlite Complex, Sierra Leone. *J. Geophys. Res.* **100**.
- Giuliani, A., Phillips, D., Kamenetsky, V. S., Kendrick, M. A., Wyatt, B. A., Goemann, K. and Hutchinson, G. (2014) Petrogenesis of mantle polymict breccias: insights into mantle processes coeval with kimberlite magmatism. *J. Petrol.* **55**, 831-858.
- Green T. H. (1994) Experimental studies of trace-element partitioning applicable to igneous petrogenesis - Sedona 16 years later. *Chem. Geol.* **117**, 1–36.
- Hall A. E. and Smith C. B. (1984) Lamproite diamonds - Are they different? *Univ. West. Aust. Dep. Geol. Publ.* **8**, 167–212.
- Harder M., Nowicki T. E., Hetman C. M., Freeman L. and Abedu B. (2013) Geology and

- Evaluation of the K2 Kimberlite, Koidu Mine, Sierra Leone, West Africa. *Proc. 10th Int. Kimberl. Conf.*, 191–208.
- Harte B., and Kirkley M. B. (1997) Partitioning of trace elements between clinopyroxene and garnet: data from mantle eclogites. *Chem. Geol.* **136**, 1-24.
- Hills D. V. and Haggerty S. E. (1989) Petrochemistry of eclogites from the Koidu Kimberlite Complex, Sierra Leone. *Contrib. to Mineral. Petrol.* **103**, 397–422.
- Howell D., O'Neill C. J., Grant K. J., Griffin W. L., Pearson N. J. and O'Reilly S. Y. (2012) μ -FTIR mapping : Distribution of impurities in different types of diamond growth. *Diam. Relat. Mater.* **29**, 29–36.
- Ireland T. R., Rudnick R. L. and Spetsius Z. (1994) Trace elements in diamond inclusions from eclogites reveal link to Archean granites. *Earth Planet. Sci. Lett.* **128**, 199–213.
- Jacob D. E. (2004) Nature and origin of eclogite xenoliths from kimberlites. *Lithos* **77**, 295–316.
- Jaques A., Hall A., Sheraton J., Smith C., Sun S.-S., Drew R., Foudoulis C. and Ellingsen K. (1989) Composition of crystalline inclusions and C-isotopic composition of Argyle and Ellendale diamonds. *Ross J, al. Kimberlites Relat. rocks GSA Spec Publ 14, vol 2. Blackwell, Carlt.*, 966–989.
- Jochum K. P., Nohl U., Herwig K., Lammel E., Stoll B., and Hofmann A. W. (2005) GeoReM: a new geochemical database for reference materials and isotopic standards. *Geostand. Geoanal. Res.* **29**, 333–338.
- Jones R., Briddon P. R. and Öberg S. (1992) First-principles theory of nitrogen aggregates in diamond. *Philos. Mag. Lett.* **66**, 67–74.

- Junk G. and Svec H. J. (1958) The absolute abundance of the nitrogen isotopes in the atmosphere and compressed gas from various sources. *Geochim. Cosmochim. Acta* **14**, 234–243.
- Kirkley M. B., Gurney J. J., Otter M. L., Hill S. J. and Daniels L. R. (1991) The application of C isotope measurements to the identification of the sources of C in diamonds: a review. *Appl. Geochemistry* **6**, 477–494.
- Klein-BenDavid O., Logvinova A. M., Schrauder M., Spetius Z. V., Weiss Y., Hauri E. H., Kaminsky F. V., Sobolev N. V. and Navon O. (2009) High-Mg carbonatitic microinclusions in some Yakutian diamonds—a new type of diamond-forming fluid. *Lithos* **112S**, 648–659.
- Leahy K. and Taylor W. R. (1997) The influence of the Glennie domain deep structure on the diamonds in Saskatchewan kimberlites. *Geol. i Geofiz.* **38**, 451–460.
- Li K., Li L., Pearson D. G. and Stachel T. (2019) Diamond isotope compositions indicate altered igneous oceanic crust dominates deep carbon recycling. *Earth Planet. Sci. Lett.* **516**, 190–201.
- Li L., Zheng Y. F., Cartigny P. and Li J. (2014) Anomalous nitrogen isotopes in ultrahigh-pressure metamorphic rocks from the Sulu orogenic belt: Effect of abiotic nitrogen reduction during fluid-rock interaction. *Earth Planet. Sci. Lett.* **403**, 67–78.
- Mallik A. and Dasgupta R. (2012) Reaction between MORB-eclogite derived melts and fertile peridotite and generation of ocean island basalts. *Earth Planet. Sci. Lett.* **329–330**, 97–108.
- Mallik A. and Dasgupta R. (2013) Reactive infiltration of MORB-eclogite-derived carbonated silicate melt into fertile peridotite at 3 GPa and genesis of alkalic magmas. *J. Petrol.* **54**, 2267–2300.

- Marty B. and Zimmermann L. (1999) Volatiles (He, C, N, Ar) in mid-ocean ridge basalts: Assessment of shallow-level fractionation and characterization of source composition. *Geochim. Cosmochim. Acta* **63**, 3619–3633.
- Marty B. and Dauphas N. (2003) The nitrogen record for crust-mantle interaction and mantle convection from Archean to present. *Earth Planet. Sci. Lett.* **206**, 397–410.
- McDonough W. F. and Sun S. S. (1995) The composition of the Earth. *Chem. Geol.* **120**, 223–253.
- McDonough W. F. and Rudnick R. L. (1998) Mineralogy and composition of the upper mantle. *Rev. Mineral.* **37**, 139–164.
- Meyer H. O. A. (1987) Inclusions in diamond. *Nixon PH Mantle xenoliths, John Wiley Sons, Chichester*, 501–522.
- Meyer H. O. A. and Boyd F. R. (1972) Composition and origin of crystalline inclusions in natural diamonds. *Geochim. Cosmochim. Acta* **36**, 1255–1273.
- Mikhail S., Verchovsky A. B., Howell D., Hutchison M. T., Southworth R., Thomson A. R., Warburton P., Jones A. P. and Milledge H. J. (2014) Constraining the internal variability of the stable isotopes of carbon and nitrogen within mantle diamonds. *Chem. Geol.* **366**, 14–23.
- Mikhail S., Rinaldi M., Mare E. R. and Sverjensky D. A. (2021) A genetic metasomatic link between eclogitic and peridotitic diamond inclusions. *Geochemical Perspect. Lett.* **17**, 33–38.
- Milledge H. J., Mendelsohn M. J., Seal M., Rouse J. E., Swart P. K. and Pillinger C. T. (1983)

- Carbon isotopic variation in spectral type II diamonds. *Nature* **303**, 791–792.
- Moore R. O. and Gurney J. J. (1986) Mineral inclusions in diamonds from the Monastery kimberlite, South Africa. *Int. Kimberl. Conf. Ext. Abstr.* **4**, 406–408.
- Navon O., Hutcheon I. D., Rossman G. R. and Wasserburg G. J. (1988) Mantle-derived fluids in diamond micro-inclusions. *Nature* **335**, 784–789.
- Otter M. L. and Gurney J. J. (1986) Mineral inclusions in diamonds from the Sloan diatremes, Colorado-Wyoming State Line kimberlite district, North America. *Int. Kimberl. Conf. Ext. Abstr.* **4**, 415–417.
- Palot M., Pearson D. G., Stern R. A., Stachel T., and Harris J. W. (2014) Isotopic constraints on the nature and circulation of deep mantle C–H–O–N fluids: Carbon and nitrogen systematics within ultra-deep diamonds from Kankan (Guinea). *Geochim. Cosmochim. Acta* **139**, 26–46.
- Petts D. C., Chacko T., Stachel T., Stern R. A. and Heaman L. M. (2015) A nitrogen isotope fractionation factor between diamond and its parental fluid derived from detailed SIMS analysis of a gem diamond and theoretical calculations. *Chem. Geol.* **410**, 188–200.
- Petts D. C., Stachel T., Stern R. A., Hunt L. and Fomradas G. (2016) Multiple carbon and nitrogen sources associated with the parental mantle fluids of fibrous diamonds from Diavik, Canada, revealed by SIMS microanalysis. *Contrib. to Mineral. Petrol.* **171**, 1–15.
- Prinz M., Vincent Manson D., Hlava P. F. and Keil K. (1975) Inclusions in diamonds: Garnet lherzolite and eclogite assemblages. *Phys. Chem. Earth* **9**, 797–815.
- Rollinson H. (2016) Archaean crustal evolution in West Africa: a new synthesis of the Archaean

- geology in Sierra Leone, Liberia, Guinea and Ivory Coast. *Precambrian Res.* **281**, 1–12.
- Schidlowski M. (2001) Carbon isotopes as biogeochemical recorders of life over 3.8 Ga of earth history: evolution of a concept. *Precambrian Res.* **106**, 117–134.
- Schmickler B., Jacob D. E. and Foley S. F. (2004) Eclogite xenoliths from the Kuruman kimberlites, South Africa: geochemical fingerprinting of deep subduction and cumulate processes. *Lithos* **75**, 173–207.
- Shu Q., Brey G. P., Hoefler H. E., Zhao Z. and Pearson D. G. (2016) Kyanite/corundum eclogites from the Kaapvaal Craton: subducted troctolites and layered gabbros from the Mid- to Early Archean. *Contrib. to Mineral. Petrol.* **171**, 1–24.
- Skinner E. M. W., Apter D. B., Morelli C. and Smithson N. K. (2004) Kimberlites of the Man craton, West Africa. *Lithos* **76**, 233–259.
- Smart K. A., Chacko T., Stachel T., Muehlenbachs K., Stern R. A. and Heaman L. M. (2011) Diamond growth from oxidized carbon sources beneath the Northern Slave Craton, Canada: a $\delta^{13}\text{C-N}$ study of eclogite-hosted diamonds from the Jericho kimberlite. *Geochim. Cosmochim. Acta* **75**, 6027–6047.
- Smit K. V., Shirey S. B. and Wang W. (2016) Type Ib diamond formation and preservation in the West African lithospheric mantle: Re–Os age constraints from sulphide inclusions in Zimmi diamonds. *Precambrian Res.* **286**, 152–166.
- Smit K. V., Shirey S. B., Hauri E. H. and Stern R. A. (2019a) Sulfur isotopes in diamonds reveal differences in continent construction. *Science* **364**, 383–385.
- Smit K. V., Stachel T., Luth R. W. and Stern R. A. (2019b) Evaluating mechanisms for eclogitic

- diamond growth: An example from Zimmi Neoproterozoic diamonds (West African craton). *Chem. Geol.* **520**, 21–32.
- Sobolev N. V., Snyder G. A., Taylor L. A., Keller R. A., Yefimova E. S., Sobolev V. N. and Shimizu N. (1998) Extreme chemical diversity in the mantle during eclogitic diamond formation: Evidence from 35 garnet and 5 pyroxene inclusions in a single diamond. *Int. Geol. Rev.* **40**, 567–578.
- Spetsius Z. V. (1998) Two generations of diamonds in eclogitic xenoliths from Yakutia. *Proc. 7th Int. Kimberl. Conf.*, 844–846.
- Stachel T. and Harris J. W. (1997) Syngenetic inclusions in diamond from the Birim field (Ghana) - A deep peridotitic profile with a history of depletion and re-enrichment. *Contrib. to Mineral. Petrol.* **127**, 336–352.
- Stachel T. and Harris J. W. (2008) The origin of cratonic diamonds — Constraints from mineral inclusions. *Ore Geol. Rev.* **34**, 5–32.
- Stachel T., Harris J. W. and Brey G. P. (1998) Rare and unusual mineral inclusions in diamonds from Mwadui, Tanzania. *Contrib. to Mineral. Petrol.* **132**, 34–47.
- Stachel T., Harris J. W., Brey G. P. and Joswig W. (2000a) Kankan diamonds (Guinea) II: lower mantle inclusion parageneses. *Contrib. to Mineral. Petrol.* **140**, 16–27.
- Stachel T., Brey G. P. and Harris J. W. (2000b) Kankan diamonds (Guinea) I: From the lithosphere down to the transition zone. *Contrib. to Mineral. Petrol.* **140**, 1–15.
- Stachel T., Harris J. W., Aulbach S. and Deines P. (2002) Kankan diamonds (Guinea) III: $\delta^{13}\text{C}$ and nitrogen characteristics of deep diamonds. *Contrib. to Mineral. Petrol.* **142**, 465–475.

- Stachel T., Aulbach S., Brey G. P., Harris J. W., Leost I., Tappert R. and Viljoen K. S. (2004) The trace element composition of silicate inclusions in diamonds: a review. *Lithos* **77**, 1–19.
- Stachel T., Harris J. W. and Muehlenbachs K. (2009) Sources of carbon in inclusion bearing diamonds. *Lithos* **112S**, 625–637.
- Stachel T., Chacko T. and Luth R. W. (2017) Carbon isotope fractionation during diamond growth in depleted peridotite: counterintuitive insights from modelling water-maximum CHO fluids as multi-component systems. *Earth Planet. Sci. Lett.* **473**, 44–51.
- Stachel T., Aulbach S. and Harris J. W. (2022) Mineral inclusions in lithospheric diamonds. *Rev. Mineral. Geochem.* **88**, 307–391.
- Stern R. A., Palot M., Howell D., Stachel T., Pearson D. G., Cartigny P. and Oh A. (2014) Methods and reference materials for SIMS diamond C- and N-isotope analysis: Canadian Centre for Isotopic Microanalysis, Research Report 14-01. *Univ. Alberta, Educ. Res. Arch.*
- Sun J., Rudnick R. L., Kostrovitsky S., Kalashnikova T., Kitajima K., Li R. and Shu Q. (2020) The origin of low-MgO eclogite xenoliths from Obnazhennaya kimberlite, Siberian craton. *Contrib. to Mineral. Petrol.* **175**, 1–22.
- Taylor L. A. and Anand M. (2004) Diamonds: Time capsules from the Siberian mantle. *Chemie der Erde* **64**, 1–74.
- Taylor W. R., Jaques A. L. L. and Ridd M. (1990) Nitrogen-defect aggregation characteristics of some Australasian diamonds: time-temperature constraints on the source regions of pipe and alluvial diamonds. *Am. Mineral.* **75**, 1290–1310.
- Taylor W. R., Canil D. and Milledge H. J. (1996) Kinetics of Ib to IaA nitrogen aggregation in

diamond. *Geochim. Cosmochim. Acta* **60**, 4725–4733.

Thomassot E., Cartigny P., Harris J. W. and Viljoen K. S. (2007) Methane-related diamond crystallization in the Earth's mantle: stable isotope evidences from a single diamond-bearing xenolith. *Earth Planet. Sci. Lett.* **257**, 362–371.

Tompkins L. A. and Haggerty S. E. (1984) *The Koidu kimberlite complex, Sierra Leone: geological setting, petrology and mineral chemistry.*, Elsevier Science Publishers B.V.

Vasil'ev E. A., Ivanov-Omskii V. I., Pomazanskii B. S. and Bogush I. N. (2004) The N3 center luminescence quenched by nitrogen impurity in natural diamond. *Tech. Phys. Lett.* **30**, 802–803.

Wang W. (1998) Formation of diamond with mineral inclusions of “mixed” eclogite and peridotite paragenesis. *Earth Planet. Sci. Lett.* **160**, 831–843.

Westerlund K. J. and Gurney J. J. (2004) Silicate and oxide inclusion characteristics and infrared absorption analysis of diamonds from the Klipspringer kimberlites, South Africa. *South African J. Geol.* **107**, 131–146.

Woods G. S. (1986) Platelets and the infrared absorption of Type Ia diamonds. *Proc. R. Soc. A Math. Phys. Eng. Sci.* **407**, 219–238.

Zaitsev A. M. (2001) *Optical Properties of Diamond: a data handbook.* Springer Berlin Heidelberg, pp 502.

Zhang H. F., Menzies M. A. and Matthey D. (2003) Mixed mantle provenance: diverse garnet compositions in polymict peridotites, Kaapvaal craton, South Africa. *Earth Planet. Sci. Lett.* **216**, 329–346.

Chapter 3 Nature of slab-mantle interaction recorded by coupled $\delta^{13}\text{C}$ – $\delta^{15}\text{N}$ – $\delta^{18}\text{O}$ signatures and elemental compositions of diamonds and their inclusions

3.1 Introduction

Despite the minor proportion of eclogite within the lithospheric upper mantle (< 1 vol%; Schulze, 1989), eclogite xenoliths provide key information about past geodynamic processes. Subduction and associated metamorphism of oceanic crust in the mantle (Helmstaedt and Doig, 1975; MacGregor and Manton, 1986; Jacob, 2004) has been widely accepted as the origin of most if not all mantle eclogites. Alternate models that invoke direct crystallization of basaltic melts produced from peridotites in the deep mantle (O'Hara and Yoder, 1967; McGetchin and Silver, 1972; Caporuscio and Smyth, 1990) are inconsistent with the major and trace element relationships observed in eclogite xenoliths (Aulbach and Arndt, 2019). In addition, Eu anomalies and oxygen isotope signatures in eclogites are unequivocal evidence for a crustal origin.

Europium anomalies in the rare earth element (REE) patterns of eclogite whole rocks or their minerals indicate that the formation of their protoliths involved accumulation or fractionation of plagioclase – a low-pressure mineral formed in the Earth's crust. Since plagioclase preferentially incorporates Eu from melts relative to other REEs (Weill and Drake, 1973; Bédard, 1994), cumulate gabbros, enriched in plagioclase that crystallized in the lower oceanic crust, often have positive Eu anomalies. This results in depletion of Eu in the residual melts, which subsequently may rise into the upper oceanic crust to form basalts with relatively rare negative Eu anomalies (Philpotts and Schnetzler, 1968).

Since not all eclogites have discernible Eu anomalies (Jacob, 2004; Schmickler et al., 2004), their oxygen isotope compositions are often used to infer a crustal origin. Peridotitic mantle has a

very restricted oxygen isotope composition ($\delta^{18}\text{O}$) of $+5.5 \pm 0.4$ ‰ (Mattey et al., 1994), whereas oceanic crust has a much wider range from 0 to +15 ‰ (Eiler, 2001; Korolev et al., 2018). Oceanic crust with $\delta^{18}\text{O}$ values above or below the peridotitic mantle range is attributed to low-temperature submarine weathering or high-temperature hydrothermal alteration, respectively. Low-temperature weathering occurs at or near the seawater–basalt interface, while high-temperature alteration occurs in the deeper portion of oceanic crust (Muehlenbachs and Clayton, 1972a,b; Gregory and Taylor, 1981; McCulloch et al., 1981; Alt et al., 1986). Previous studies have shown that the $\delta^{18}\text{O}$ values inherited from these processes are generally retained by eclogites metamorphosed from subducted oceanic crust (Putlitz et al., 2000; Jacob, 2004; Russell et al., 2013). The high $\delta^{18}\text{O}$ values in eclogites cannot be formed by isotopic fractionation at mantle temperatures from an initial mantle-like value ($+5.5 \pm 0.4$ ‰) (Mattey et al., 1994; Schulze et al., 2013) nor by mantle metasomatism, as metasomatic fluids with extreme $\delta^{18}\text{O}$ values are not likely to survive unmodified during passage through the dominantly peridotitic mantle (Riches et al., 2016).

Garnet is the preferred proxy for the determination of the oxygen isotope composition of eclogites as it is more resistant than clinopyroxene to metasomatic modification and resetting of its isotopic composition (Jacob et al., 1994; Deines and Haggerty, 2000; Schulze et al., 2000; Barth et al., 2001; Korolev et al., 2018). In this study, we analyse garnet inclusions in diamonds from the Koidu kimberlite complex in Sierra Leone for their oxygen isotope compositions as well as their major element and trace element compositions. Eclogitic diamond formation could be associated with interactions between eclogite and ambient mantle: (1) eclogite-derived carbonated melts may migrate into reducing ambient mantle peridotite and precipitate diamonds (Rohrbach and Schmidt, 2011; Kiseeva et al., 2013; Mikhail et al., 2021); (2) partial melting of eclogite may

facilitate *in situ* diamond formation as well as chemical exchange with surrounding peridotite (Smart et al., 2009); (3) mantle-derived fluids/melts may interact with eclogitic diamond substrates (Aulbach et al., 2011; Lai et al., 2022). Thus, correlations between the $\delta^{18}\text{O}$ values and major element compositions of garnet inclusions may provide insights into the character of slab-mantle interaction during diamond formation. Carbon and nitrogen isotope compositions ($\delta^{13}\text{C}$ and $\delta^{15}\text{N}$, respectively) of the host diamonds of these garnet inclusions are analysed to identify any mixing of crust- and mantle-derived carbon and nitrogen during this process. Here I present the first coupled $\delta^{13}\text{C}$ – $\delta^{15}\text{N}$ – $\delta^{18}\text{O}$ measurements of diamonds and their inclusions, to gain a better understanding of the nature of the interaction between subducted slabs and ambient mantle during diamond formation.

3.2 Samples and methods

The Koidu kimberlite complex is situated in the Kono District of eastern Sierra Leone, in the southern part of the West African Craton. Although eclogites are the only type of mantle xenoliths recovered from Koidu (Tompkins and Haggerty, 1984; Hills and Haggerty, 1989; Fung and Haggerty, 1995), kimberlite indicator minerals and diamonds from this locality are of both peridotitic and eclogitic paragenesis (Deines and Harris, 1995; Skinner et al., 2004; Harder et al., 2013).

A mineral chemistry study on 105 Koidu diamonds revealed a dominance of eclogitic diamonds (78%), followed by lesser proportions of peridotitic (17%) and mixed paragenesis diamonds (5%) which contained co-occurring peridotitic and eclogitic mineral inclusions (Lai et al., 2022). Sixteen eclogitic garnet inclusions from 16 different diamonds, including one mixed

paragenesis sample, were selected for the determination of their oxygen isotope compositions. The selected garnets cover the entire major element compositional range for all Koidu garnet inclusions, and thus are representative of the sample suite.

Methods for determining major, minor and trace element compositions of mineral inclusions were previously described in detail (Lai et al., 2022) and are only summarised here. Garnet inclusions were mounted in epoxy and analysed with a CAMECA SX100 electron probe microanalyzer (EPMA) for their major and minor element compositions at an accelerating voltage of 20 kV, a beam current of 20 nA, and a fully focused beam with a diameter $< 1 \mu\text{m}$. Oxide detection limits are typically $\leq 0.02 \text{ wt}\%$. Trace element compositions of garnet inclusions were determined using a Resonetics M-50-LR 193 nm ArF excimer laser ablation system coupled with a Thermo Scientific Element IIXR inductively coupled plasma mass spectrometer (LA-ICP-MS). Samples were ablated with a spot size of 23–90 μm at a frequency of 10 Hz and a laser fluence of $\sim 4 \text{ J}/\text{cm}^2$. Calcium contents of garnet inclusions determined with EPMA were used as an internal standard. Detection limits for trace element concentrations are typically $\leq 40 \text{ ppb}$ for REE, V, Rb, Sr, Zr, Nb, Ba and Hf, and $\leq 1 \text{ ppm}$ for Ti and Ni.

Selected eclogitic garnet inclusions were then mounted into a single 25 mm epoxy mount with reference materials S0068 (pyrope garnet from the Gore Mountain area; Bartholomé, 1960) and S0088B (grossular garnet from the Jeffrey mine; Akizuki, 1989). The epoxy mount was polished and coated with 25 nm of Au prior to scanning electron microscopy (SEM). Secondary electron (SE) and backscattered electron (BSE) images were obtained using a Zeiss EVO MA15 SEM operating at a voltage of 20 kV and a beam current of 3–4 nA. After imaging, the epoxy mount was coated with 100 nm of Au. Oxygen isotope compositions were then determined using a CAMECA IMS-1280 multi-collector ion microprobe. Three to six spots were analysed on each

garnet inclusion to assess compositional homogeneity. A $^{133}\text{Cs}^+$ primary beam with an impact energy of 20 keV and a beam current of 2 nA was focused to a beam diameter of approximately 12 μm . Analysis of each spot took 240 s. Oxygen isotope compositions are reported as $\delta^{18}\text{O}_{\text{VSMOW}}$ (normalized difference of the $^{18}\text{O}/^{16}\text{O}$ ratio of the sample relative to that of Vienna Standard Mean Ocean Water (VSMOW), where $^{18}\text{O}/^{16}\text{O}_{\text{VSMOW}} = 2005.20 (\pm 0.45) \times 10^{-6}$ (Baertschi, 1976)). Reference materials S0068 (with $\delta^{18}\text{O}_{\text{VSMOW}} = +5.72 \text{ ‰}$) and S0088B (with $\delta^{18}\text{O}_{\text{VSMOW}} = +4.13 \text{ ‰}$) were analysed after every four and eight unknowns, respectively, to monitor the instrumental mass fractionation (IMF). The 95% confidence uncertainty estimates for $\delta^{18}\text{O}_{\text{VSMOW}}$ of analysed garnet inclusions average $\pm 0.26 \text{ ‰}$, which include errors related to within-spot counting statistics, between-spot (geometric) effects, correction for IMF, and matrix effects associated with Ca# (i.e., molar $\text{Ca}/(\text{Ca}+\text{Mg}+\text{Fe})$). The analytical procedure and matrix calibration are described in Ickert and Stern (2013).

3.3 Results

3.3.1 Major element composition

The selected garnet inclusions show large variations in CaO (3.6–18.6 wt%), MgO (8.5–20.6 wt%), FeO (9.0–18.6 wt%) and Mg# (49.1–79.0), with the garnet (138-7-3) from a mixed paragenesis diamond having the highest CaO and lowest MgO and FeO (Table B.1). The garnet (140-2-1) with the highest MgO content also has the highest TiO_2 concentration (0.86 vs 0.24–0.48 wt% in other garnets). The high Ti in this garnet does not correspond to its relatively low Na_2O (0.13 wt%). Typically, Na increases with Ti in garnet (Fig. 3.1), corresponding to the coupled substitution: $\text{M}^{2+} + \text{Al}^{3+} = \text{Na}^+ + \text{Ti}^{4+}$ (Ringwood and Major, 1971; Bishop et al., 1976,

1978; Grew et al., 2013), however, this positive correlation is not observed for majoritic garnets (Stachel et al., 1998). The concentration of Ti in garnet increases with temperature (Aulbach, 2020) and consequently, along a conductive geotherm, with pressure. This agrees with high pressure-high temperature experiments showing that Ti in garnet increases with both temperature and pressure (Zhang et al., 2003), suggesting that the high Ti content in garnet 140-2-1 corresponds to derivation from higher temperature and pressure. This garnet also has relatively low Al₂O₃ (21.1 wt%) compared with the average Al₂O₃ content (22.9 wt%) of other garnets in this study. A negative correlation ($R^2 = 0.81$) between Al and Ti cations is observed for garnet inclusions from Koidu diamonds (Fig. 3.2), which is consistent with experimental results documenting decreasing Al and increasing Ti with increasing temperature and pressure (Zhang et al., 2003), following the coupled substitution: $2Al^{3+} = M^{2+} + Ti^{4+}$ (Ackerson et al., 2017). In agreement, garnet 140-2-1 has a minor majorite component of 3.4 mol% (calculated following Locock, 2008). Compared to Si and Al + Cr cation contents in experimental majoritic garnets (Akaogi and Akimoto, 1979; Irifune et al., 1986; Irifune, 1987; Collerson et al., 2010), a pressure of 7.8 GPa (corresponding to a depth of 250 km) (Fig. 3.3) is estimated for this garnet. Applying different formulations of the majorite-in-garnet barometer (Collerson et al., 2010; Beyer and Frost, 2017) yields equilibration pressures of 7.8–8.2 GPa, corresponding to a depth between 250 and 260 km. This depth range is slightly below the lithosphere-asthenosphere boundary of the West African Craton (220 ± 10 km), determined from Koidu clinopyroxene xenocryst geothermobarometry (Smit et al., 2016). Backscattered electron imaging of garnet 140-2-1 shows no exsolution, suggesting that it did not re-equilibrate at shallower depth, and was brought to the surface directly from the uppermost asthenosphere.

3.3.2 Trace element composition

Koidu eclogitic garnet inclusions are depleted in LREE with subchondritic La, which is a typical feature observed in eclogitic garnets from mantle xenoliths (Jacob, 2004) and included in diamonds (Stachel et al., 2004) worldwide. The garnet (138-7-3) from the mixed paragenesis diamond is distinct by having the highest LREE ($La_N \sim 0.3$) and lowest HREE ($Lu_N \sim 6$) contents. The remaining garnets have flat $MREE_N$ - $HREE_N$ with $Lu_N > 20$ (Table B.2), and among them, the mildly majoritic garnet 140-2-1 has the highest LREE and lowest HREE.

Three garnets (131-5-8, 138-6-2 and 138-12-1) have negative Eu anomalies (Fig. 3.4a), with $[Eu/Eu^*]_N = 0.80$ – 0.89 , where $Eu^* = [Sm_N \times Gd_N]^{0.5}$ (McLennan, 1989). Garnet 138-7-3 has a small positive Eu anomaly ($[Eu/Eu^*]_N = 1.10$), but two additional garnet inclusions from the same diamond have more prominent positive Eu anomalies ($[Eu/Eu^*]_N = 1.36$ – 1.41). All other garnets in this study have no discernible Eu anomalies (Fig. 3.4b).

3.3.3 Oxygen isotope composition

Backscattered electron images and multiple spot analyses indicate that all garnet inclusions in this study have homogeneous compositions, ruling out alteration by fluid/melt infiltrating through cracks in their host diamonds. The internal variability of $\delta^{18}O$ for individual grains (average $2\sigma = 0.17$ ‰) is within analytical uncertainty ($2\sigma = \sim 0.26$ ‰), thus only average $\delta^{18}O$ values are reported for each grain (Table B.3). Oxygen isotope compositions for all analyzed spots are provided in Table B.4.

The range of $\delta^{18}O$ values of garnet inclusions in this study (+5.4 to +12.1 ‰; Fig. 3.5) is much greater than that of garnets from the Koidu low-MgO (+4.7 to +6.8 ‰) and high-MgO (+5.1 to +5.7 ‰) eclogite xenoliths (Barth et al., 2001, 2002). Garnet 138-7-3 from the mixed paragenesis diamond has the lowest $\delta^{18}O$ value (+5.4 ‰), falling within the mantle range (+5.5 ±

0.4 ‰; Matthey et al., 1994). The mildly majoritic garnet 140-2-1 also has a relatively low $\delta^{18}\text{O}$ value (+6.3 ‰). The other garnets in this study have $\delta^{18}\text{O}$ values from +9.9 to +12.1 ‰, with a median value of +11.6 ‰, which is higher than that of any other eclogitic garnet inclusions in lithospheric diamonds worldwide, including diamonds from the Damtshaa kimberlites (+4.7 to +8.8 ‰; Ickert et al., 2013), Argyle lamproite (+6.0 to +8.3 ‰; Schulze et al., 2013), Finsch kimberlite (+5.7 to +8.0 ‰; Lowry et al., 1999), Siberian placer deposits (+4.8 to +9.6 ‰; Zedgenizov et al., 2016), Jericho kimberlite (+5.2 to +6.0 ‰; Smart et al., 2012) and Guaniamo placer deposit (+7.9 to +11.3 ‰; Schulze et al., 2004) (Fig. 3.6).

A negative correlation between $\delta^{18}\text{O}$ values and Mg# (molar $100 \times \text{Mg}/(\text{Mg}+\text{Fe})$) and a positive correlation between $\delta^{18}\text{O}$ values and Ca# (molar $100 \times \text{Ca}/(\text{Ca}+\text{Mg}+\text{Fe})$) are observed in some garnets (Figs. 3.7a and b). These correlations are especially obvious for three garnets (138-3-1, 138-5-1 and 138-11-1) that also show decreasing LREE contents with decreasing Ca# (Fig. 3.4b). Garnets with the highest $\delta^{18}\text{O}$ values ($\sim +12$ ‰) form a tight cluster in Ca# (0.14–0.18) (Fig. 3.7b). Except for garnet 138-7-3, all garnets follow the trend ($R^2 = 0.77$) of increasing Cr# (molar $100 \times \text{Cr}/(\text{Cr}+\text{Al})$) with decreasing $\delta^{18}\text{O}$ values. The mildly majoritic garnet 140-2-1 has the highest Cr# and lowest $\delta^{18}\text{O}$ along this trend (Fig. 3.7c). Similar relationships between major element compositions and $\delta^{18}\text{O}$ values in eclogitic garnets (xenocrysts, lithospheric diamond inclusions and sublithospheric diamond inclusions) have previously been reported (Schulze et al., 2003; Zedgenizov et al., 2016; Regier et al., 2020).

3.4 Discussion

3.4.1 Origin of Koidu eclogites

Negative Eu anomalies are a typical feature of volcanic rocks in the upper oceanic crust (Philpotts and Schnetzler, 1968). Three garnet inclusions (Fig. 3.4a) with negative Eu anomalies indicate that the protoliths of their host eclogites formed from Eu-depleted residual melts as a result of previous fractionation of plagioclase. The high $\delta^{18}\text{O}$ values in these three samples, and almost all other analyzed garnet inclusions (+9.9 to +12.1 ‰; Fig. 3.5), suggest that their protoliths underwent high degrees of submarine weathering at low temperatures (Muehlenbachs and Clayton, 1972b; Alt et al., 1986; McCulloch et al., 1981). Alteration must have occurred close to the basalt-seawater interface, as $\delta^{18}\text{O}$ values $> +8$ ‰ are restricted to altered oceanic crust (AOC) at depths < 300 m (pillow lavas) (Korolev et al., 2018).

The garnet (140-2-1) with a minor majorite component has a $\delta^{18}\text{O}$ value (+6.3 ‰) that is still elevated relative to the mantle range, but low compared to other garnet inclusions in Koidu eclogitic diamonds. The protolith of this garnet may have been situated slightly deeper in the oceanic crust (e.g., lower portion of the volcanic section), where the water/rock ratio was lower and the alteration temperature was higher, compared to the uppermost portion of the oceanic crust (McCulloch et al., 1981; Alt et al., 1986; Gao et al., 2012). This portion of the oceanic crust then carried the mildly ^{18}O -enriched signature and subducted through the asthenosphere where pyroxene started dissolving into the garnet structure to form majoritic garnet (Akaogi and Akimoto, 1979; Irifune et al., 1986; Moore and Gurney, 1985). The slightly enriched LREE and depleted HREE contents in this garnet (Fig. 3.4b) are consistent with an increasing compatibility of LREE and a decreasing compatibility of HREE in garnet as the depth increases (Stachel and Harris, 1997). Alternatively, the relatively low $\delta^{18}\text{O}$ value and relatively high Cr# in garnet 140-2-1 can be explained by slab-mantle interaction, which will be discussed in the following section.

Positive Eu anomalies and low $\sum\text{HREE}$ of garnets in diamond 138-7 are consistent with

plagioclase accumulation and, consequently, a protolith that originated as cumulate gabbro within the deep oceanic crust (Salisbury and Christensen, 1978; Jacob, 2004; Aulbach and Jacob, 2016). A mantle-like $\delta^{18}\text{O}$ value (+5.4 ‰) indicates a protolith that was located either too deep in the oceanic crust to be altered (Alt and Teagle, 2000), or from the intermediate depth zone where the temperature of alteration creates mantle-like $\delta^{18}\text{O}$ signatures (Schmickler et al., 2004).

3.4.2 Slab-mantle interaction during diamond formation

Based on their low Cr_2O_3 contents (< 1 wt%; Grütter et al., 2004), all garnet inclusions in this study were classified as eclogitic. For majoritic garnets it has, however, been demonstrated that the majority belong to neither a pure eclogitic nor a peridotitic paragenesis, but are intermediate between the two (Kiseeva et al., 2013). An approach based on major element substitutions can better differentiate the parageneses of majoritic garnets, in which peridotitic and pyroxenitic garnets follow the peridotitic majoritic substitution: $2\text{Al}^{3+} = \text{Si}^{4+} + \text{M}^{2+}$, while eclogitic garnets follow the eclogitic majoritic substitution: $\text{M}^{2+} + \text{Al}^{3+} = \text{Na}^{+} + \text{Si}^{4+}$, with increasing pressure (Kiseeva et al., 2013). Garnet 140-2-1 follows the trend of peridotitic-pyroxenitic majoritic substitution (Fig. B.1). Given its high Mg# (79.0) and elevated Cr# (0.90) relative to the other samples (Table B.1) and its low CaO content (4.24 wt%), this combined evidence suggests derivation from a pyroxenitic lithology.

Formation of pyroxenitic inclusions in diamond likely results from the interaction between slab-derived melts and ambient mantle peridotite (Aulbach et al., 2002; Kiseeva et al., 2016). This process is especially prominent in the sublithospheric mantle, as observed from the high abundance of pyroxenitic majoritic garnets (Kiseeva et al., 2013; Regier et al., 2020). This observation was related to a deep depression in the solidus of carbonated oceanic crust, which intersects most slab geotherms and facilitates slab melting at a depth of ~300–700 km (Thomson et al., 2016a).

Carbonatite melts derived from subducting slabs can readily migrate into ambient mantle peridotite because of their low dihedral angle with olivine and low viscosity, resulting in efficient elemental and isotopic exchange between melt and mantle (Minarik and Watson, 1995; Hammouda and Laporte, 2000; Walter et al., 2008; Thomson et al., 2016b). Thus, the relatively low $\delta^{18}\text{O}$ value (+6.3 ‰), and high Mg# and Cr# in garnet 140-2-1 (Fig. 3.7) likely are a consequence of diamond crystallization during carbonatite melt-mantle peridotite interaction. Indeed, at the pressure of formation of this majoritic garnet (~8 GPa), ambient mantle is expected to be very reducing, with a calculated oxygen fugacity ($f\text{O}_2$) close to the iron-wüstite (IW) buffer (Frost and McCammon, 2008). Reduction of carbonates from oxidizing slab-derived melt by the reducing metal-saturated ambient mantle is the likely mechanism of diamond formation in this scenario (Rohrbach and Schmidt, 2011).

The crude correlations between major element compositions and $\delta^{18}\text{O}$ for a subset of garnet inclusions in this study (Fig. 3.7) may be a consequence of seawater alteration in different stratigraphic levels of oceanic crust (Gregory and Taylor, 1981; Aulbach and Jacob, 2016), or kimberlite-like ultramafic metasomatism (Aulbach et al., 2020). Alternatively, these covariations could be associated with elemental and isotopic exchange between eclogitic diamond substrates and surrounding peridotitic lithospheric mantle facilitated by melts (e.g., Smart et al., 2009). In this case, the cluster of garnet inclusions with low Cr# (0.07–0.15) and the highest $\delta^{18}\text{O}$ values (~+12 ‰) may represent the initial compositions of the eclogites, without significant chemical exchange with ambient mantle (Fig. 3.7). Other garnet inclusions that follow the trends of increasing Mg# and Cr# and decreasing Ca# with decreasing $\delta^{18}\text{O}$ could then be explained by various degrees of interaction with surrounding peridotites, in which inward transport of peridotitic components into eclogite were facilitated by eclogite-derived melts, and the extent of chemical

exchange depends on the distance from the eclogite-peridotite interface (Smart et al., 2009). Trace element partitioning between garnet and pyroxene was likely affected by this interaction, as the three garnets (138-3-1, 138-5-1 and 138-11-1) with an obvious positive correlation between Ca# and $\delta^{18}\text{O}$ also show decreasing LREE contents with decreasing Ca# (Figs. 3.4b and 3.7b). The difference in LREE contents could be attributed to crystal-chemical effects, where LREE preferentially partition in garnets with higher Ca# (Harte and Kirkley, 1997; Aulbach et al., 2017).

Garnet 138-7-3 has a mantle-like $\delta^{18}\text{O}$ value (+5.4 ‰) and high Ca# (49.7) (Fig. 3.7b) typical for a cumulate gabbro protolith (e.g., MacGregor and Manton, 1986; Schulze et al., 2000). This garnet originated from deeper layers within oceanic crust that do not show a signature of slab-mantle interaction, implying that its host diamond likely formed during introduction of external carbon, e.g., through asthenosphere-derived fluids/melts (Lai et al., 2022). Alternatively, this diamond may have formed as a result of deserpentinization of altered peridotite in the subducted slab within the diamond stability field, where fluids produced from deserpentinization have mantle-like $\delta^{18}\text{O}$. Deserpentinization fluids can be either oxidizing or reducing (Debret and Sverjensky, 2017; Piccoli et al., 2019). Depending on the redox states of both the overlying crustal portion and the deserpentinization fluids, diamonds can form from reduction of CO_2 or CO_3^{2-} , or oxidation of CH_4 . Mixing of deserpentinization fluids of different redox states within the slab may also facilitate precipitation of diamonds (Aulbach et al., 2012; Stachel et al., 2022).

3.4.3 Variation of $\delta^{18}\text{O}$ – $\delta^{13}\text{C}$: mixing between AOC- and mantle-derived carbon?

Coupled $\delta^{18}\text{O}$ – $\delta^{13}\text{C}$ measurements of garnet-bearing diamonds worldwide (Argyle (Schulze et al., 2013), Damtshaa (Ickert et al., 2013), Siberian placers (Zedgenizov et al., 2016), Finsch (Lowry et al., 1999), Jagersfontein (Ickert et al., 2015), Collier and Juina (Burnham et al., 2015)) exhibit a negative “correlation”, where garnets with $\delta^{18}\text{O}$ near the mantle value are

associated with mantle-like carbon ($\delta^{13}\text{C} = -5 \pm 3 \text{‰}$; Cartigny et al., 2014), whilst distinctly ^{18}O -enriched garnets have ^{13}C -depleted host diamonds (Fig. 3.8). Accordingly, diamonds and their garnet inclusions falling along a trend between these two end-members could be interpreted as mixing products between mantle ($\delta^{13}\text{C} \approx -5 \text{‰}$; $\delta^{18}\text{O} \approx +5.5 \text{‰}$) and AOC ($\delta^{13}\text{C} \approx -30 \text{‰}$; $\delta^{18}\text{O} \approx +12 \text{‰}$) reservoirs, with variable $(\text{O}/\text{C})_{\text{Mantle}}/(\text{O}/\text{C})_{\text{AOC}}$ ratios controlling the curvature of different mixing arrays.

However, instead of following a full mixing array, Koidu diamonds and their garnet inclusions just lie at opposite ends of the supposed trend, where the majority of samples form a cluster with $\delta^{18}\text{O} \geq +9.9 \text{‰}$ and $\delta^{13}\text{C} \leq -19.4 \text{‰}$ (Fig. 3.8 and Table B.3). Since there is no known mantle process that can cause such large ^{18}O enrichment and ^{13}C depletion, this main cluster of Koidu samples represents formation of diamonds and their garnet inclusions in a common surficially-derived geologic environment, i.e., diamond carbon and garnet oxygen both originated from uppermost AOC (Ickert et al., 2013) containing biogenic carbonate \pm organic matter (Milledge et al., 1983; Kirkley et al., 1991; Li et al., 2019). This tight clustering suggests that with respect to oxygen and carbon, the contribution of a mantle-derived component, if present at all, was minor. In slight contrast, the observed negative correlation between Cr# and $\delta^{18}\text{O}$ of garnets in the $\delta^{18}\text{O}$ range of +9.9 to +11.3 ‰ may be attributed to a low degree of eclogite-peridotite interaction during diamond formation (Fig. 3.7c). A possibly associated dilution of AOC carbon with mantle carbon, however, was negligible, which likely relates to elevated carbon concentrations in AOC close to the seawater interface relative to carbon-poor ambient mantle. The diamonds with $\delta^{13}\text{C}$ values of -29.6 to -19.4 ‰ within this cluster thus directly reflect the variable carbon isotope composition of subducted AOC, with e.g., biogenic carbonate having $\delta^{13}\text{C}$ as low as -24 ‰ (Li et al., 2019) and organic matter having $\delta^{13}\text{C}$ of $-26 \pm 7 \text{‰}$ (Schidlowski, 2001).

Possible devolatilization of carbonate from AOC during subduction may decrease $\delta^{13}\text{C}$ values further (Shieh and Taylor, 1969; Li et al., 2019). Although four of the host diamonds of high $\delta^{18}\text{O}$ garnet inclusions (138-5, 138-9, 143-2 and 146-2) have rim zones with mantle-like $\delta^{13}\text{C}$ values (Fig. 3.8), the garnet inclusions were all located in the centres of these diamonds and thus are not related to the rim zones. These abrupt changes in carbon isotope composition from cores (-26.5 to -24.0 ‰) to rims (-7.0 to -6.0 ‰) document distinct stages of diamond formation involving distinct sources of carbon, with the rim zones being precipitated from mantle-derived fluids/melts (Lai et al., 2022).

The mantle-like $\delta^{13}\text{C}$ value (-4.7 ‰) of the host diamond of garnet 138-7-3 can be explained by a low carbon content in the gabbroic layers of subducting slabs (Li et al., 2019), which requires externally sourced, mantle-derived carbon for the formation of diamonds. However, the scarcity of diamond from gabbroic layers implies that the available volume of the required mantle-derived fluids/melts was either small or that the redox conditions in the subducted substrate were not suitable for diamond formation from the carbon species contained in the mantle-derived fluids/melts.

The host diamond of majoritic garnet 140-2-1 has elevated $\delta^{13}\text{C}$ values ranging from -4.2 to 0 ‰ (inner zone: $\delta^{13}\text{C} = -4.2$ ‰; outer zone: $\delta^{13}\text{C} = -1.8$ to 0 ‰; average $\delta^{13}\text{C} = -2.6$ ‰; Fig. 3.9). Similar mildly ^{13}C -enriched carbon isotope compositions were observed on the West African Craton for majoritic garnet-included diamonds from Kankan ($\delta^{13}\text{C} = -3.1$ to +0.9 ‰) and were attributed to diamond formation from subducted normal carbonates (Stachel et al., 2002). As discussed in section 3.4.2, the majoritic garnet with a $\delta^{18}\text{O}$ value of +6.3 ‰ and its ^{13}C -enriched host diamond could have crystallized during the interaction of a slab-derived carbonatitic melt and ambient mantle. The carbon isotope signature of the outer zone of this diamond then may be

attributed to predominantly slab-derived carbon (normal marine carbonates; $\delta^{13}\text{C} \approx 0 \text{ ‰}$). The mantle-like $\delta^{13}\text{C}$ value in the inner zone could be explained by formation of diamond in the peridotitic substrate from mantle-derived carbon prior to or at initial stages of infiltration of slab-derived melt. This was followed by crystallization of the overgrowth layer (outer zone) along with the majoritic garnet inclusion during melt-peridotite interaction. The difference in nitrogen concentrations and cathodoluminescence brightness between the inner ($[\text{N}] = 51\text{--}84 \text{ at.ppm}$) and outer zones ($[\text{N}] = 0.6\text{--}0.7 \text{ at.ppm}$) (Fig. 3.9) in this diamond may be evidence for distinct growth episodes.

3.4.4 Variation of $\delta^{18}\text{O}$ – $\delta^{15}\text{N}$: mixing between AOC- and mantle-derived nitrogen?

Gabbroic diamond 138-7, through its mantle-like $\delta^{13}\text{C}$ (-4.7 ‰) and $\delta^{15}\text{N}$ (-6.9 ‰) values, demonstrates a coupled origin of carbon and nitrogen, likely from asthenosphere-derived fluids/melts (Lai et al., 2022) or from deserpentinization fluids (Aulbach et al., 2012). The association of mantle-like $\delta^{15}\text{N}$ and $\delta^{18}\text{O}$ ($+5.4 \text{ ‰}$) values implies that the gabbroic protolith did not significantly interact with hydrothermal fluids during the seafloor alteration stage (Alt and Teagle, 2000), and thus, in the absence of low-temperature clay formation, did not carry significant nitrogen with a characteristic ^{15}N -enriched signature to depth that could contribute to the diamond-forming process.

Other host diamonds in this study with nitrogen contents sufficiently high for isotopic analysis have $\delta^{15}\text{N}$ values between -5.6 and $+1.3 \text{ ‰}$, except for one outlier with $\delta^{15}\text{N} = +9.9 \text{ ‰}$ (Table B.3). The positive $\delta^{15}\text{N}$ values in Koidu diamonds are attributed to a contribution of nitrogen from clay minerals formed by low-temperature ($< 100 \text{ °C}$) alteration of oceanic crust (Busigny et al., 2005; Bebout et al., 2018; Li et al., 2019). During subduction, devolatilization of nitrogen from AOC further increases $\delta^{15}\text{N}$ values in subducted materials (Bebout and Fogel, 1992;

Cartigny et al., 2014), resulting in diverse $\delta^{15}\text{N}$ values in AOC. Some Koidu diamonds are associated with convecting mantle-like $\delta^{15}\text{N}$ values (-5.6 to -2.0 ‰), but with clearly subducted oxygen ($\delta^{18}\text{O} = +10.3$ to $+11.8$ ‰) and carbon ($\delta^{13}\text{C} = -26.5$ to -22.0 ‰) isotope signatures. This suggests the possibility of independent sources for (1) carbon and oxygen and (2) nitrogen during the diamond-forming process, with carbon and oxygen originating locally from subducted AOC while nitrogen was largely derived from the mantle.

To investigate the extent of mixing of nitrogen derived from AOC and the mantle during diamond precipitation, I model the mixing arrays using different O/N ratios of AOC and the mantle. Mixing models involve two major reservoirs as the endmembers: the mantle ($\delta^{15}\text{N} = -5.0$ ‰; $\delta^{18}\text{O} = +5.5$ ‰) and AOC (represented by diamond 131-2 with $\delta^{15}\text{N} = +9.9$ ‰ and $\delta^{18}\text{O} = +12.1$ ‰). Curvature of the mixing arrays is controlled by $n = (\text{O/N})_{\text{AOC}}/(\text{O/N})_{\text{mantle}}$ ratios. Note that the oxygen contents of eclogite and peridotite are similar (Cartigny et al., 2014), thus the effect of changing oxygen content on the O/N ratio is negligible and the major parameter that controls the mixing model is the nitrogen contents in AOC and the mantle. Koidu diamonds are best fitted by the mixing curves with $n > 1$ (e.g., $n = 10, 25$ and 70 shown in Fig. 3.10). These mixing curves require a mantle reservoir with higher nitrogen content compared to AOC, indicating that the contribution of nitrogen from the mantle during diamond formation is high (mantle-derived nitrogen $> 60\%$; Fig. 3.10). This could be explained by diamond formation in eclogitic substrates facilitated by a mantle-derived fluid/melt pulse, in which the mantle-derived fluid/melt carried a comparatively high concentration of nitrogen but negligible carbon, thus adding a mantle-like $\delta^{15}\text{N}$ signature to the diamonds without affecting their crustal $\delta^{13}\text{C}$ signature.

An alternative explanation is provided by observations of oxygen and nitrogen isotope compositions of the altered basaltic sections recovered at Ocean Drilling Program Site 801, which

are characterized by high $\delta^{18}\text{O}$ (+8.7 to +25.7 ‰; Alt, 2003) and a wide range of $\delta^{15}\text{N}$ (-11.6 to +1.2 ‰; Li et al., 2007) values. The isotope compositions of the super-composite (constructed to represent the bulk composition of the upper oceanic crust; Alt, 2003) at Site 801 show mantle-like $\delta^{15}\text{N}$ values (-5.4 ‰; Li et al., 2007) with very high $\delta^{18}\text{O}$ values (+12.0 ‰; Alt, 2003). This suggests the possibility that mantle-like $\delta^{15}\text{N}$ values of some Koidu diamonds may still derive from an AOC source. Crustal nitrogen remains stable in slabs as NH^{4+} in potassium-bearing minerals and transfers to the deep mantle only in cold subduction zones; in warm subduction zones, however, there is substantial nitrogen loss during slab devolatilization and, thus, the amount of crustal nitrogen left in the downgoing slab for subsequent diamond formation becomes negligible (Labidi, 2022).

3.5 Conclusions

The coupled $\delta^{13}\text{C}$ - $\delta^{15}\text{N}$ - $\delta^{18}\text{O}$ signatures and elemental compositions of diamonds and their eclogitic inclusions from Koidu suggests three possible modes of diamond formation during slab-mantle interaction:

- (1) In the gabbroic layer of oceanic crust where the concentration of crustal carbon is low, diamond formation relies on carbon sourced from mantle-derived fluids/melts, thus the single Koidu diamond formed in this layer has mantle-like carbon and nitrogen isotope compositions ($\delta^{13}\text{C} = -4.7$ ‰; $\delta^{15}\text{N} = -6.9$ ‰). The protolith of this diamond substrate was not significantly altered by seawater and consequently, the gabbroic garnet inclusion has an unperturbed oxygen isotope composition ($\delta^{18}\text{O} = +5.4$ ‰).

- (2) In the uppermost basaltic layer of altered oceanic crust, the concentration of carbon is high and dominates the carbon budget for diamond formation. Invariably strongly ^{13}C -depleted carbon isotope compositions ($\delta^{13}\text{C} = -29.6$ to -19.4 ‰) document that diamond carbon was derived from biogenic carbonate and/or organic matter, with a negligible contribution of normal marine carbonates. Nitrogen isotope compositions of this diamond population fall in an only mildly ^{15}N enriched range with $\delta^{15}\text{N}$ values between -5.6 and $+1.3$ ‰ (one outlier at $+9.9$ ‰). This suggests that either the nitrogen budget during diamond formation was dominated by mantle-derived nitrogen, arriving from an external, mantle-hosted fluid source, or the subducted AOC substrate for Koidu diamonds had an unusual nitrogen isotope composition (without ^{15}N enrichment), similar to that observed at ODP site 801. The basaltic protoliths were intensely altered by seawater at low temperatures prior to subduction, leading to the garnet inclusions derived from this layer having strongly ^{18}O -enriched isotopic compositions ($\delta^{18}\text{O} = +9.9$ to $+12.1$ ‰). If not related to stratigraphic position of the protoliths within the upper oceanic crust or kimberlite-like ultramafic metasomatism, covariations between major element and oxygen isotope compositions of garnet inclusions suggest chemical exchange between eclogite and ambient mantle peridotite coeval with diamond formation. This exchange may have been facilitated by melt generated during partial melting of eclogite, in which the degree of chemical exchange depends on the distance of garnets from the eclogite-peridotite interface, i.e., the distance of melt-assisted inward diffusion of elements from peridotite.
- (3) Exemplified by one Koidu diamond containing a mildly majoritic garnet inclusion, in the sublithospheric mantle fluids/melts derived from slabs infiltrated ambient mantle peridotite and precipitated pyroxenitic diamonds. The core and rim structure of the precipitated

diamond suggests that the core formed from predominantly mantle-derived carbon (core zone $\delta^{13}\text{C} = -4.2 \text{ ‰}$) and the rim from slab-derived crustal carbon (rim zone $\delta^{13}\text{C} = -1.8$ to 0 ‰). Peridotite can efficiently buffer the oxygen isotope composition of infiltrating slab-derived fluids/melts, driving the $\delta^{18}\text{O}$ value of the garnet inclusion ($+6.3 \text{ ‰}$) towards the mantle range. The high Mg#, elevated Cr# and low Ca# of the garnet inclusion are consistent with a high degree of chemical exchange between slab and mantle components.

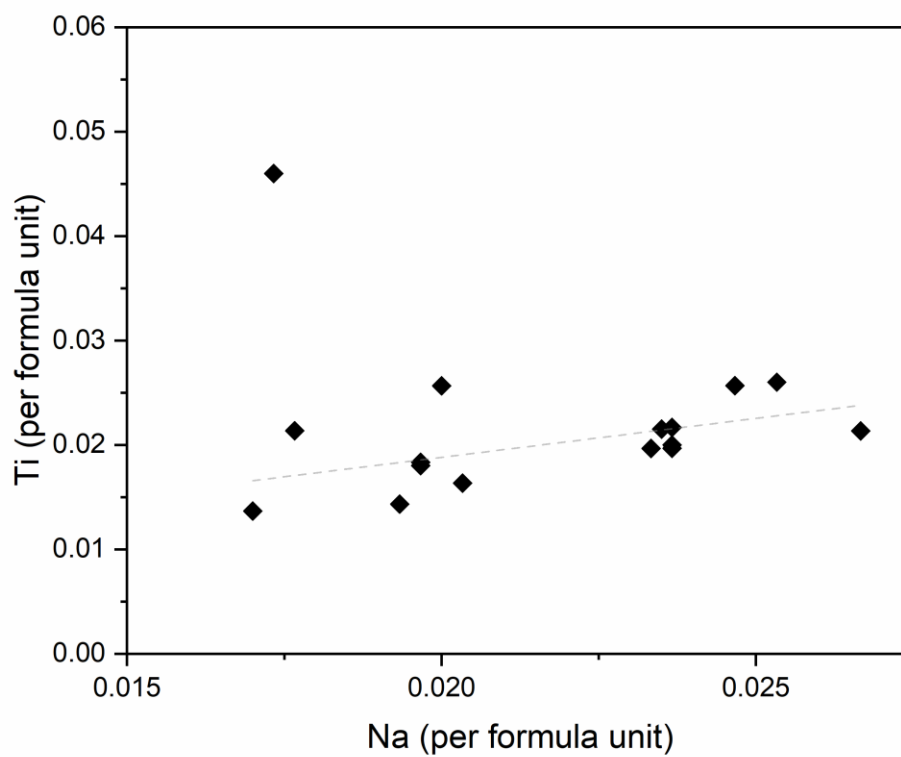


Figure 3.1 Ti versus Na (apfu) for garnet inclusions in Koidu diamonds. Except for one garnet with a minor majorite component, garnets show a crude positive correlation ($R^2 = 0.33$) between Ti and Na.

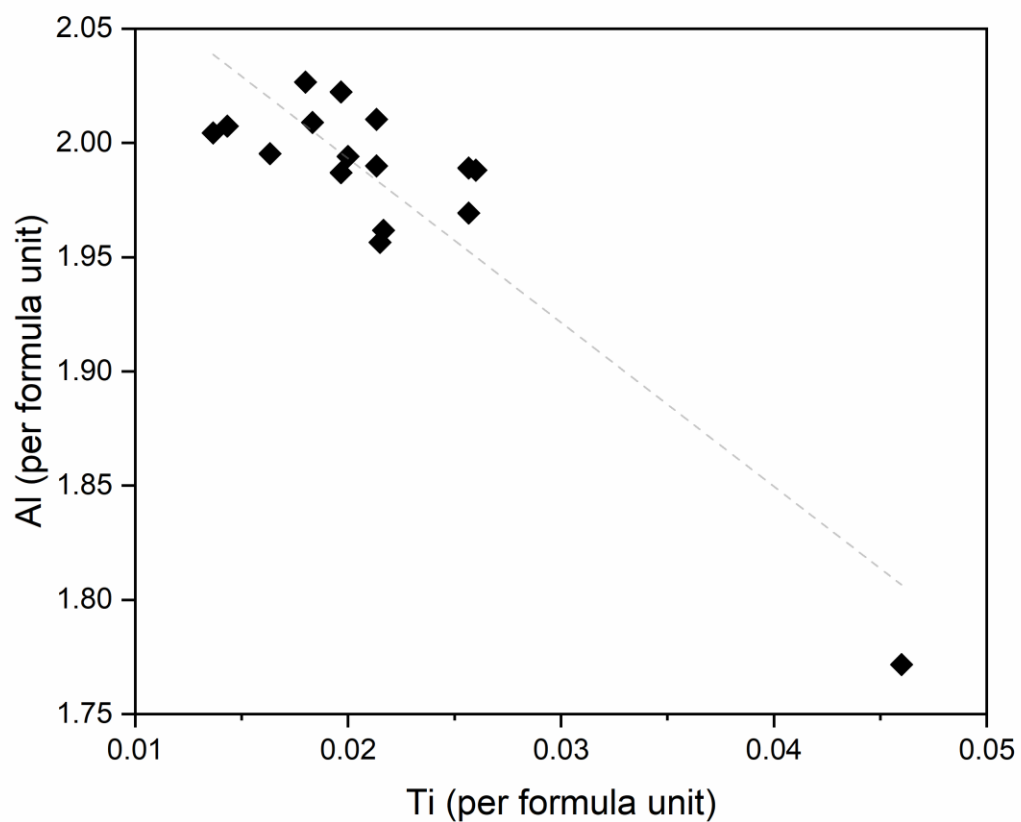


Figure 3.2 Al versus Ti (apfu) in garnet inclusions in Koidu diamonds, based on a formula unit containing twelve oxygen atoms. Al and Ti are strongly negatively correlated ($R^2 = 0.81$). The outlier with high Ti content is the mildly majoritic garnet.

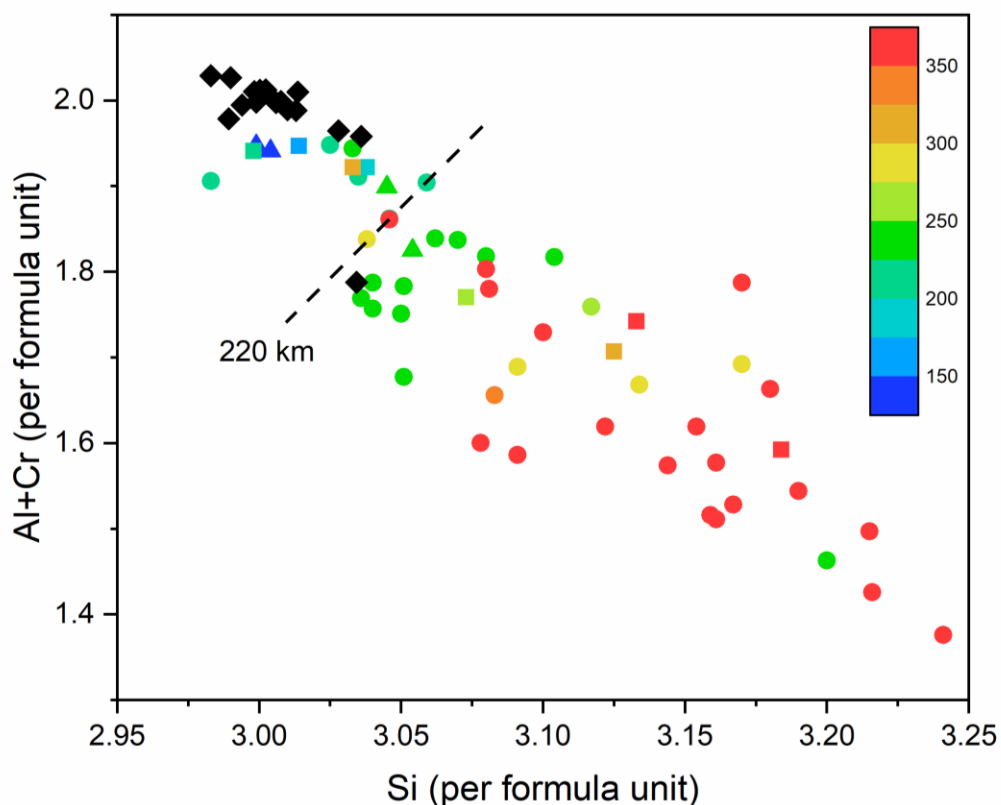
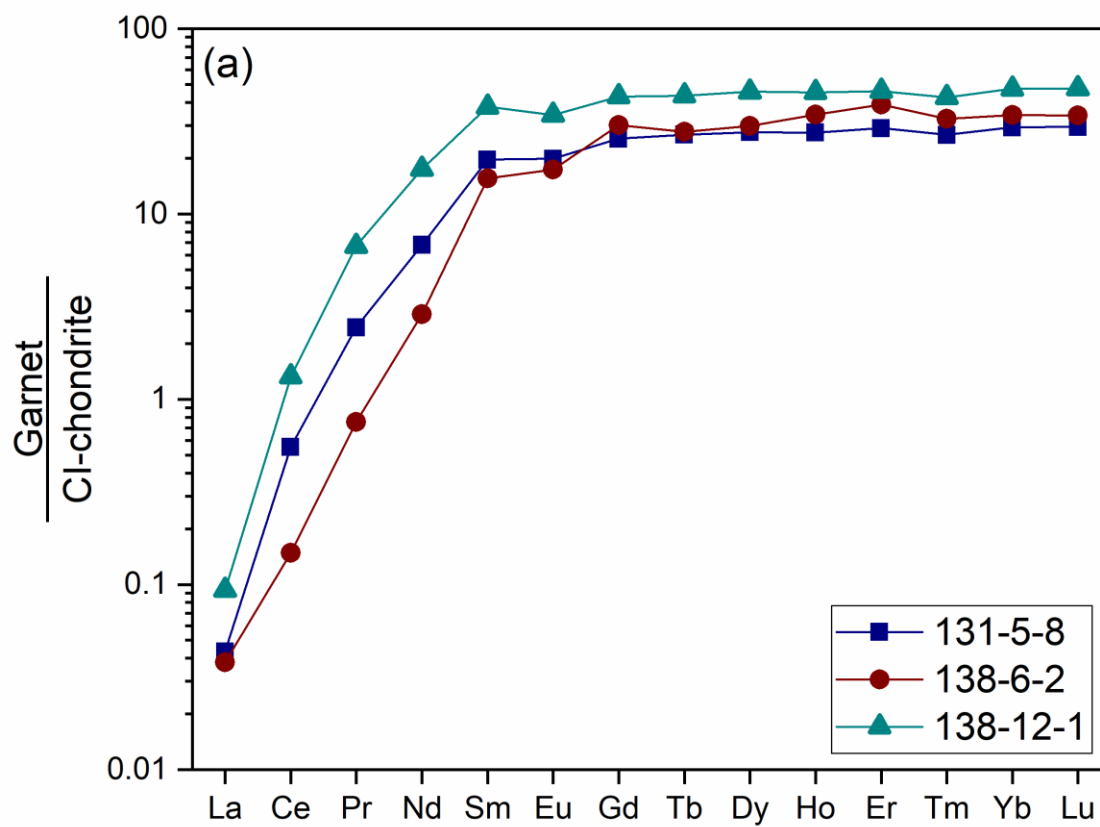


Figure 3.3 Variation between Si and Al+Cr in garnets based on a formula unit containing twelve oxygen atoms. Silicon increases with decreasing Al+Cr, indicating increasing pressure. Symbol colour represents the depths (km) corresponding to equilibration pressures reported in literature: triangles are data from high pressure experiments conducted by Akaogi and Akimoto (1979); squares are data from high pressure experiments conducted by Irifune et al. (1986) and Irifune (1987); circles are data compiled by Collerson et al. (2010) for garnet inclusions in diamonds worldwide. Black diamond symbols represent the chemical compositions of garnet inclusions in this study. The position of the dashed line, indicating a depth of 220 km (lithosphere-asthenosphere boundary of the West African Craton; Smit et al., 2016), is estimated from the garnet inclusions compiled by Collerson et al. (2010). Estimated pressures for garnet 140-2-1 is 7.8–8.2 GPa (Collerson et al., 2010; Beyer and Frost, 2017), corresponding to a depth between 250 and 260 km.



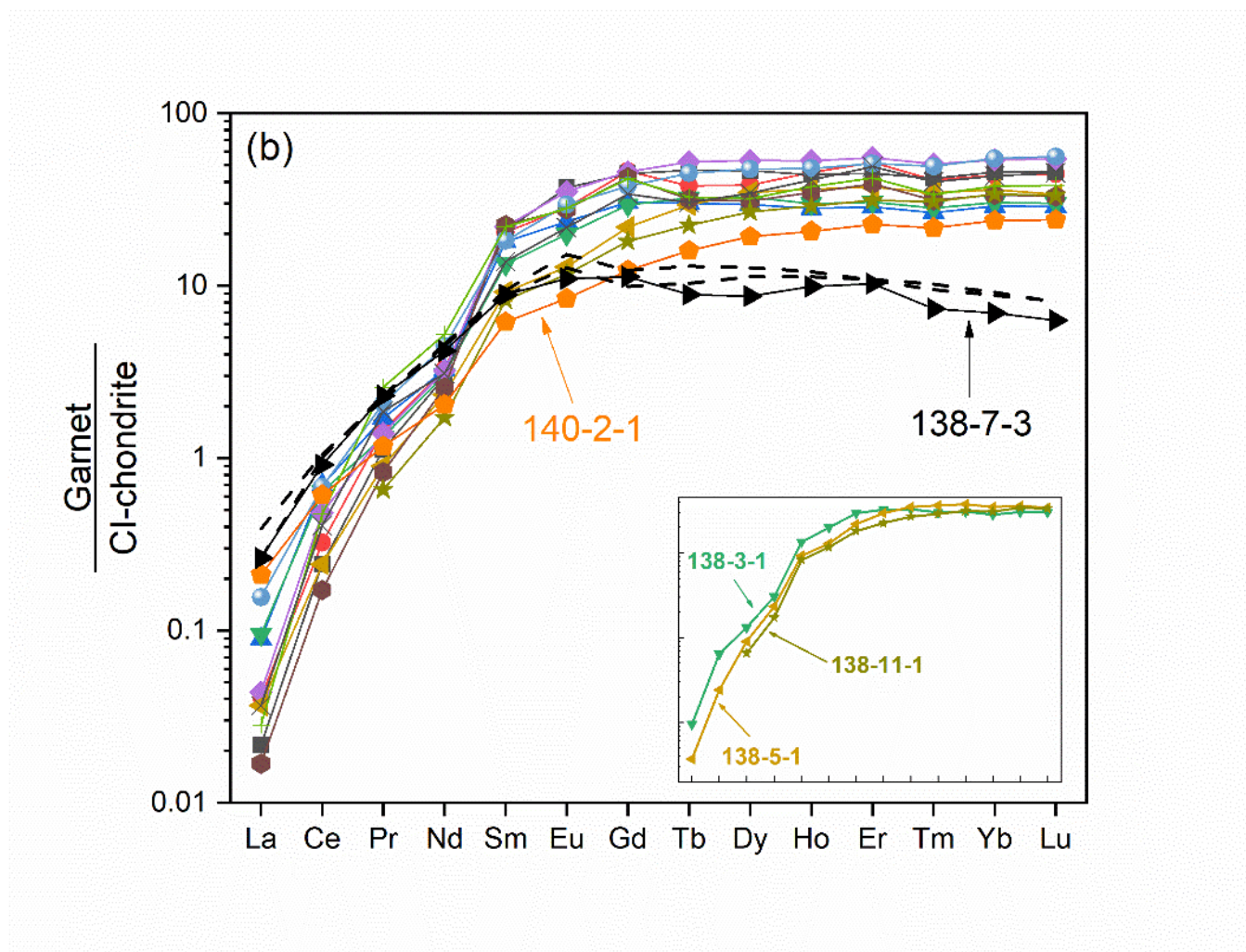


Figure 3.4 REE concentrations in eclogitic garnets from Koidu diamonds normalized to CI-chondrite (McDonough and Sun, 1995). (a) Three garnet inclusions with discernible negative Eu anomalies. (b) Other garnet inclusions lacking obvious Eu anomalies. Garnets from diamond 138-7 (black) are different from other garnets in this study through their negative $MREE_N$ - $HREE_N$ slopes with $Lu_N < 10$. Two garnets (black dashed lines) from diamond 138-7 have discernible positive Eu anomalies. Inset shows three garnets (138-3-1, 138-5-1 and 138-11-1) that follow a clear trend of decreasing Ca# with decreasing $\delta^{18}O$ values (see Fig. 7b).

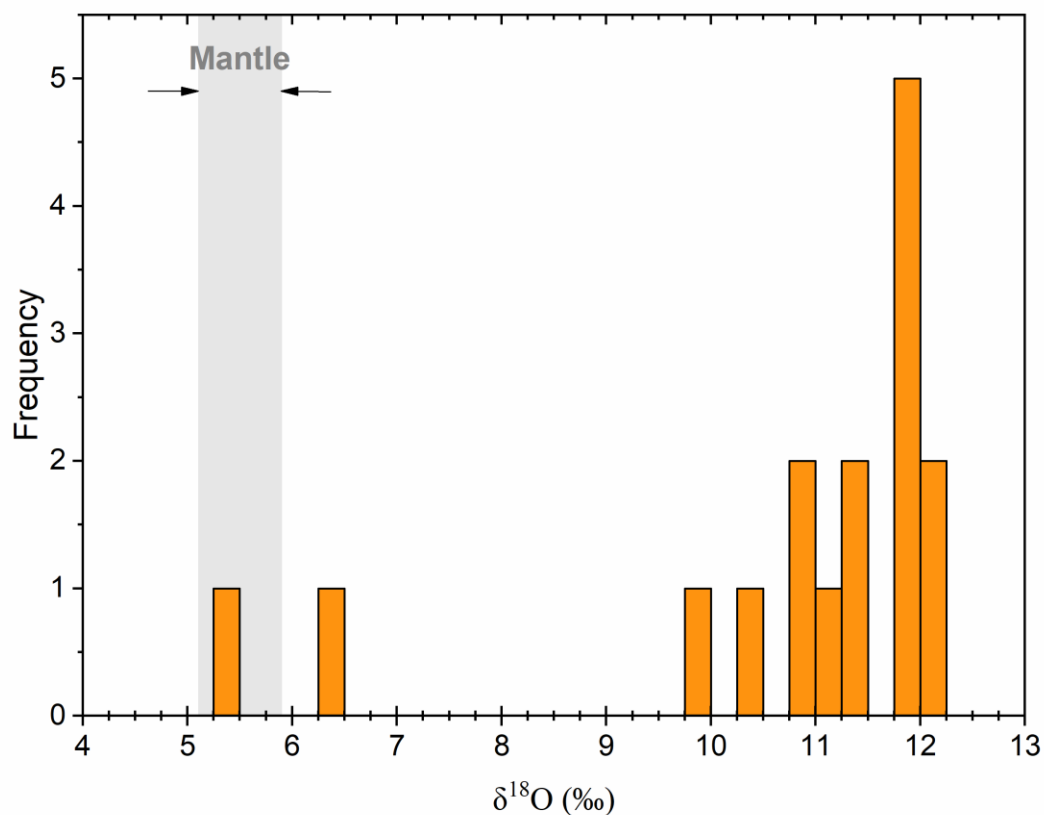


Figure 3.5 Distribution of $\delta^{18}\text{O}$ values in garnet inclusions from Koidu diamonds. The bin size for the histogram is 0.25 ‰. The grey shaded region indicates the canonical $\delta^{18}\text{O}$ range of the mantle ($+5.5 \pm 0.4$ ‰; Matthey et al., 1994). The $\delta^{18}\text{O}$ values of the garnets in this study range from +5.4 to +12.1 ‰, with a mode of +11.8 ‰. Gabbroic garnet 138-7-3 has the lowest $\delta^{18}\text{O}$ value (+5.4 ‰), which falls within the mantle range.

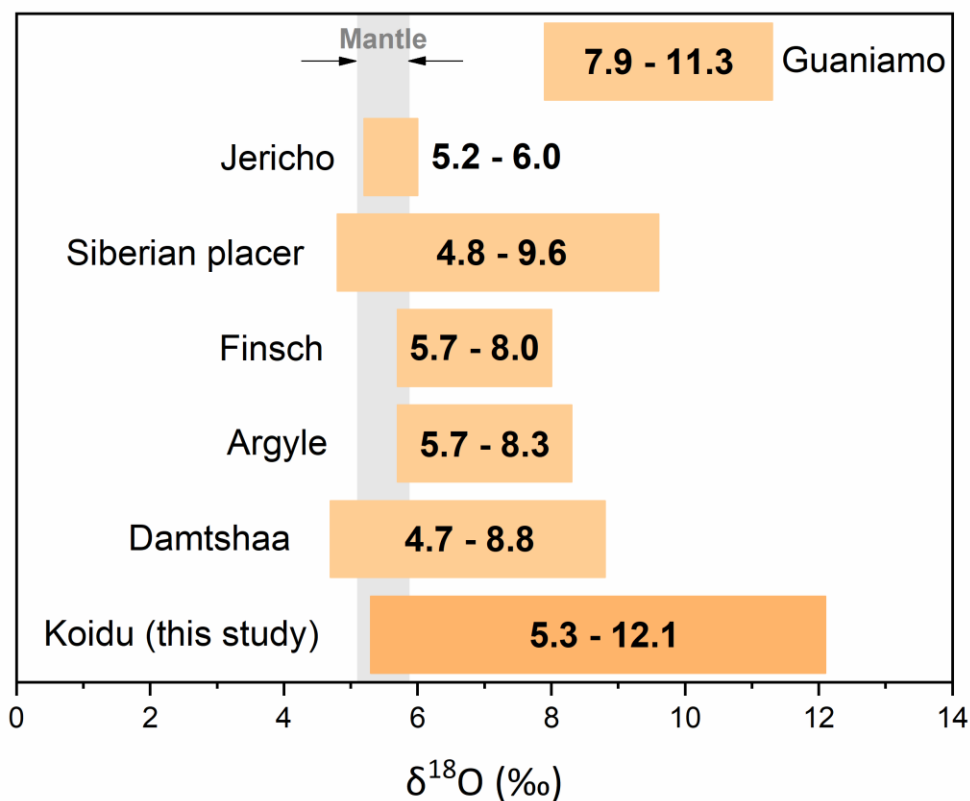


Figure 3.6 Oxygen isotope compositions ($\delta^{18}\text{O}$) of eclogitic garnet inclusions in diamonds from Koidu (this study), Damtshaa (Ickert et al., 2013), Argyle (Schulze et al., 2013), Finsch (Lowry et al., 1999), Siberian placer (Zedgenizov et al., 2016), Jericho (Smart et al., 2012) and the Guaniamo placer deposit ($\delta^{18}\text{O}$ values of multiple garnet inclusions in one single diamond; Schulze et al., 2004). The grey shaded region indicates the canonical $\delta^{18}\text{O}$ range of the mantle ($+5.5 \pm 0.4$ ‰; Matthey et al., 1994).

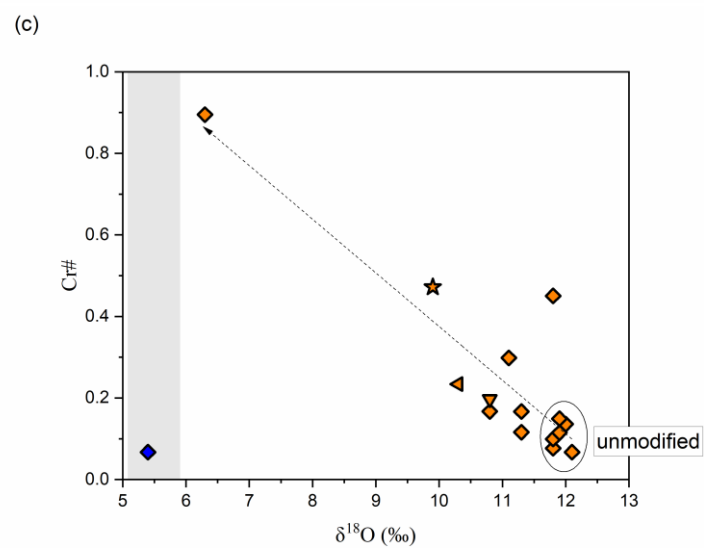
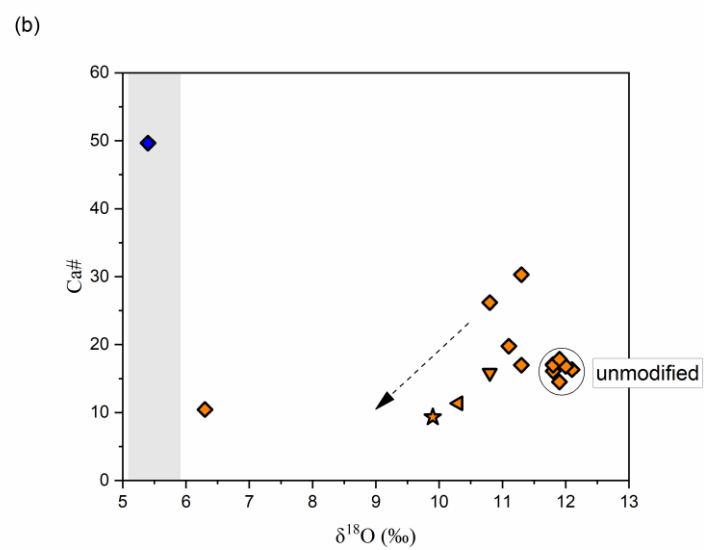
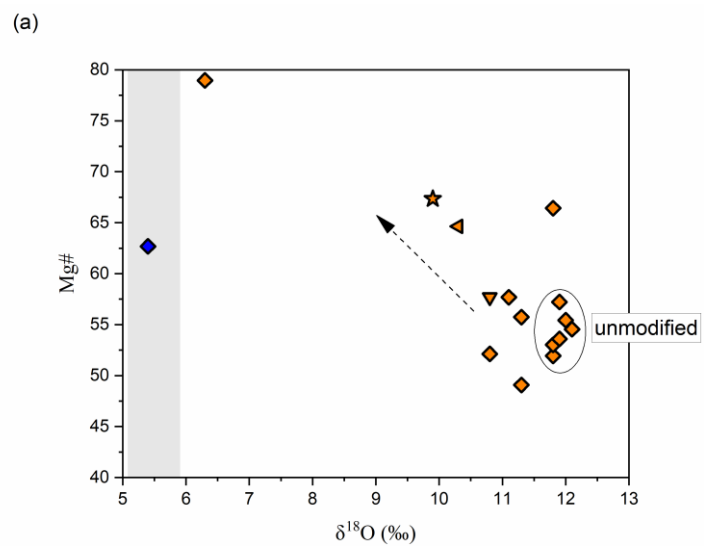


Figure 3.7 Covariations of oxygen isotope composition ($\delta^{18}\text{O}$) and molar Mg# (a), Ca# (b) and Cr# (c) in Koidu garnet inclusions (the gabbroic garnet is shown in blue, other garnets are shown in orange). Three garnets (138-3-1, 138-5-1 and 138-11-1) with clear correlations between $\delta^{18}\text{O}$ and major element compositions are shown with symbols following Fig. 4b. The region shaded in grey indicates the canonical $\delta^{18}\text{O}$ range of the mantle ($+5.5 \pm 0.4 \text{ ‰}$; Matthey et al., 1994). Garnets show a well-defined negative correlation ($r^2 = 0.77$) between Cr# and $\delta^{18}\text{O}$ values.

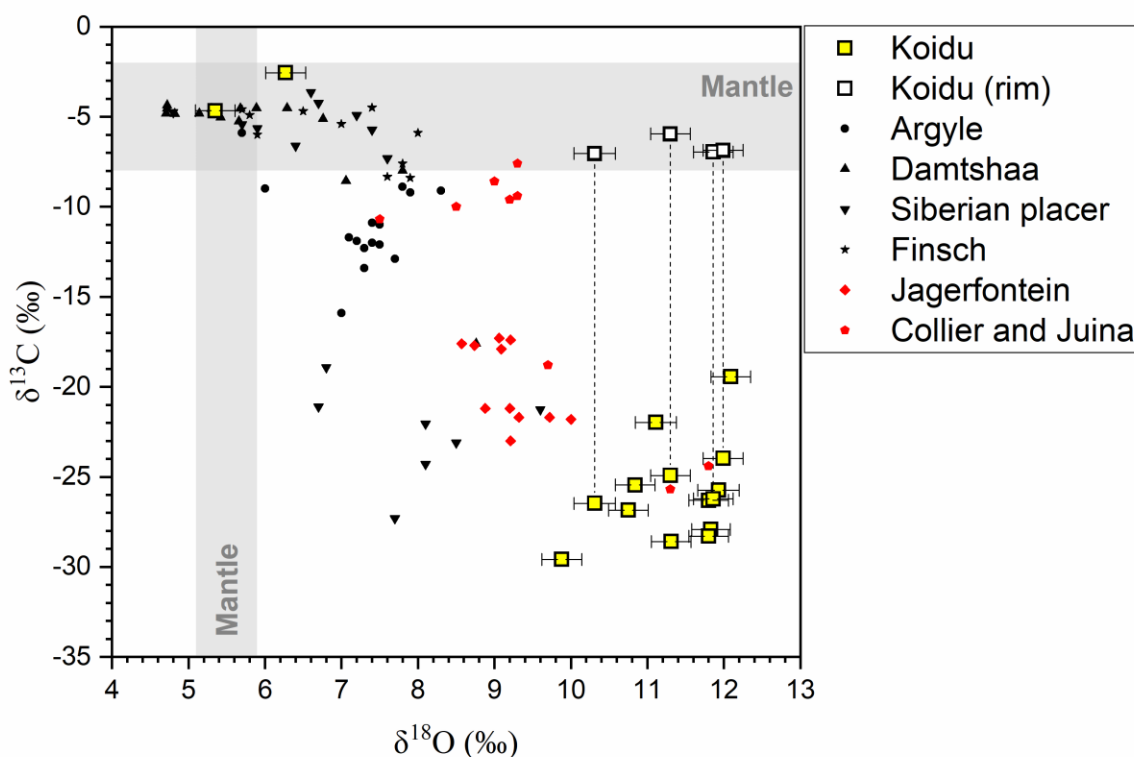


Figure 3.8 Oxygen isotope composition ($\delta^{18}\text{O}$) of garnet inclusions and carbon isotope composition ($\delta^{13}\text{C}$) of their host diamonds in this study. Average $\delta^{18}\text{O}$ and $\delta^{13}\text{C}$ values of multiple analyzed spots of individual garnet grains and diamond fragments are shown. Four diamonds (138-5, 138-9, 143-2 and 146-2) have a core-rim structure and are linked by dashed tie-lines, with $\delta^{13}\text{C}$ values of the rims being indicated by white squares and core-zone values by yellow squares. Error bars reflect total uncertainties (95% confidence level) for the $\delta^{18}\text{O}$ and $\delta^{13}\text{C}$ values of each sample and for $\delta^{13}\text{C}$ are smaller than the symbol size. Also shown are $\delta^{13}\text{C}$ and $\delta^{18}\text{O}$ values of lithospheric (black)/sublithospheric (red) diamonds and their garnet inclusions from Argyle (Schulze et al., 2013), Damtshaa (Ickert et al., 2013), Siberian placers (Zedgenizov et al., 2016), Finsch (Lowry et al., 1999), Jagersfontein (Ickert et al., 2015) and Collier/Juina (Burnham et al., 2015).

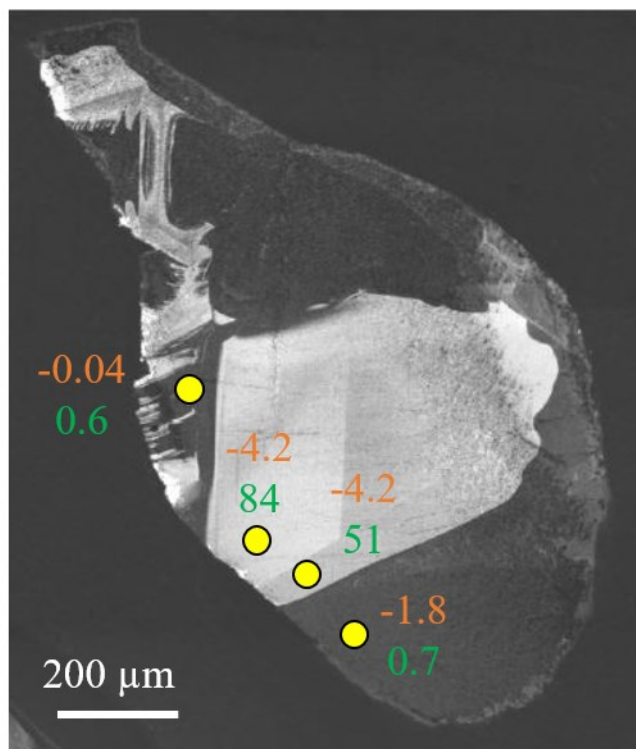


Figure 3.9 Cathodoluminescence image of diamond 140-2-1 showing inner and outer growth zones with distinct $\delta^{13}\text{C}$ values (orange; ‰) and nitrogen concentrations (green; at.ppm).

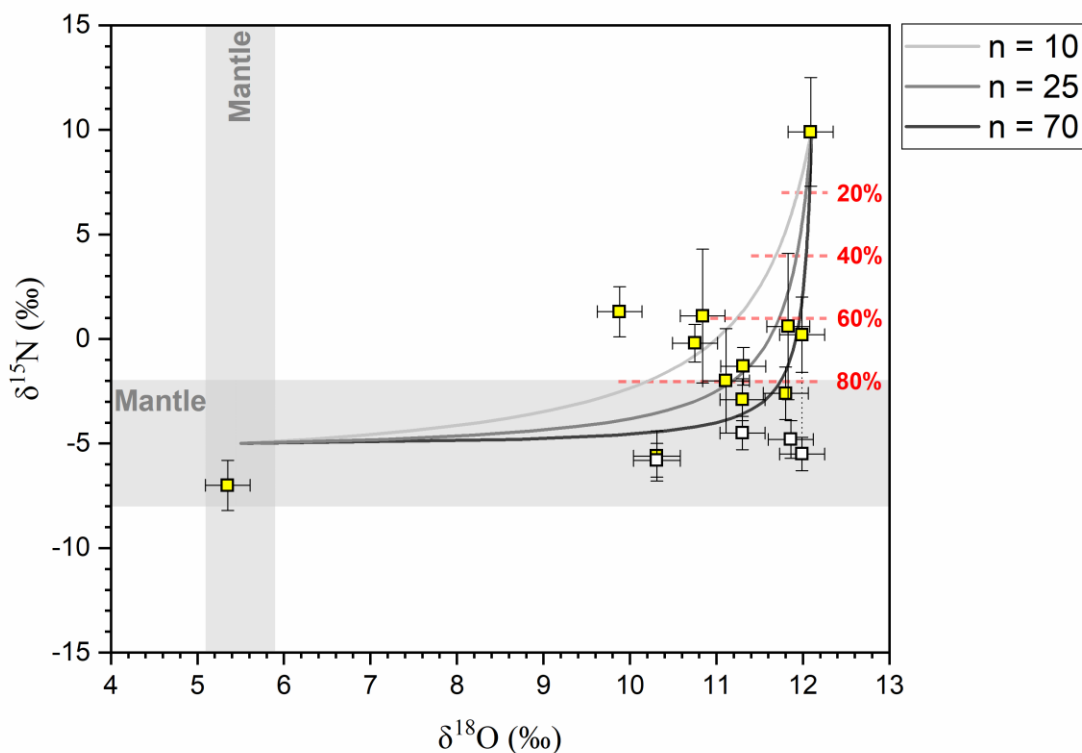


Figure 3.10 Oxygen isotope composition ($\delta^{18}\text{O}$) of eclogitic garnet inclusions and nitrogen isotope composition ($\delta^{15}\text{N}$) of their host diamonds in this study. Average $\delta^{18}\text{O}$ and $\delta^{15}\text{N}$ values of multiple analyzed spots of individual garnet grains and diamond fragments are shown for each sample. Four diamonds (138-5, 138-9, 143-2 and 146-2) have a core-rim structure and are linked by dotted tie-lines, with the compositions of the rims indicated by white squares and core analyses by yellow squares. Error bars reflect total uncertainties (95% confidence level) for the $\delta^{18}\text{O}$ and $\delta^{15}\text{N}$ values of each sample. Solid lines indicate the mixing arrays calculated from different $(\text{O}/\text{N})_{\text{AOC}}/(\text{O}/\text{N})_{\text{mantle}}$ ratios denoted by n : (light grey) $n = 10$; (dark grey) $n = 25$; and (black) $n = 70$. Red dashed lines indicate the percentages of nitrogen contributed by the mantle.

References

- Ackerson M. R., Watson E. B., Tailby N. D. and Spear F. S. (2017) Experimental investigation into the substitution mechanisms and solubility of Ti in garnet. *Am. Mineral.* **102**, 158–172.
- Akaogi M. and Akimoto S. (1979) High-pressure phase equilibria in a garnet lherzolite, with special reference to Mg^{2+} - Fe^{2+} partitioning among constituent minerals. *Phys. Earth Planet. Inter.* **19**, 31–51.
- Akizuki M. (1989) Growth structure and crystal symmetry of grossular garnets from the Jeffrey mine, Asbestos, Quebec, Canada. *Am. Mineral.* **74**, 859–864.
- Alt J. C. (2003) Stable isotopic composition of upper oceanic crust formed at a fast spreading ridge, ODP Site 801. *Geochem. Geophys.* **4**, 1–11.
- Alt J. C. and Teagle D. A. H. (2000) Hydrothermal alteration and fluid fluxes in ophiolites and oceanic crust. *Geol. Soc. Am. Spec. Pap.* **349**, 273–282.
- Alt J. C., Muehlenbachs K. and Honnorez J. (1986) An oxygen isotopic profile through the upper kilometer of the oceanic crust, DSDP Hole 504B. *Earth Planet. Sci. Lett.* **80**, 217–229.
- Aulbach S. (2020) Temperature-dependent rutile solubility in garnet and clinopyroxene from mantle eclogite: implications for continental crust formation and V-based oxybarometry. *J Petrol.* **61**, egaa065.
- Aulbach S. and Jacob D. E. (2016) Major- and trace-elements in cratonic mantle eclogites and pyroxenites reveal heterogeneous sources and metamorphic processing of low-pressure protoliths. *Lithos* **262**, 586–605.
- Aulbach S. and Arndt N. T. (2019) Origin of high-Mg bimineralic eclogite xenoliths in

kimberlite – reply to comment from Claude Herzberg. *Earth Planet. Sci. Lett.* **510**, 234–237.

Aulbach S., Stachel T., Viljoen K. S., Brey G. P. and Harris J. W. (2002) Eclogitic and websteritic diamond sources beneath the Limpopo Belt - Is slab-melting the link? *Contrib. to Mineral. Petrol.* **143**, 56–70.

Aulbach S., Stachel T., Heaman L. M. and Carlson J. A. (2011) Microxenoliths from the Slave craton: archives of diamond formation along fluid conduits. *Lithos* **126**, 419–434.

Aulbach S., Stachel T., Seitz H. M. and Brey G. P. (2012) Chalcophile and siderophile elements in sulphide inclusions in eclogitic diamonds and metal cycling in a Paleoproterozoic subduction zone. *Geochim. Cosmochim. Acta* **93**, 278–299.

Aulbach S., Jacob D. E., Cartigny P., Stern R. A., Simonetti S. S., Wörner G. and Viljoen K. S. (2017) Eclogite xenoliths from Orapa: ocean crust recycling, mantle metasomatism and carbon cycling at the western Zimbabwe craton margin. *Geochim. Cosmochim. Acta* **213**, 574–592.

Aulbach S., Massuyeau M., Garber J. M., Gerdes A., Heaman L. M. and Viljoen K. S. (2020) Ultramafic carbonated melt-and auto-metasomatism in mantle eclogites: compositional effects and geophysical consequences. *Geochem. Geophys.* **21**, e2019GC008774.

Baertschi P. (1976) Absolute ^{18}O content of standard mean ocean water. *Earth Planet. Sci. Lett.* **31**, 341–344.

Barth M. G., Rudnick R. L., Horn I., McDonough W. F., Spicuzza M. J., Valley J. W. and Haggerty S. E. (2001) Geochemistry of xenolithic eclogites from West Africa, part I: A link

- between low MgO eclogites and Archean crust formation. *Geochim. Cosmochim. Acta* **65**, 1499–1527.
- Barth M. G., Rudnick R. L., Horn I., McDonough W. F., Spicuzza M. J., Valley J. W. and Haggerty S. E. (2002) Geochemistry of xenolithic eclogites from West Africa, part 2: Origins of the high MgO eclogites. *Geochim. Cosmochim. Acta* **66**, 4325–4345.
- Bartholomé P. (1960) Genesis of the Gore Mountain garnet deposit, New York. *Econ. Geol.* **55**, 255–277.
- Bebout G. E. and Fogel M. L. (1992) Nitrogen-isotope compositions of metasedimentary rocks in the Catalina Schist, California: implications for metamorphic devolatilization history. *Geochim. Cosmochim. Acta* **56**, 2839–2849.
- Bebout G. E., Banerjee N. R., Izawa M. R. M., Kobayashi K., Lazzeri K., Ranieri L. A. and Nakamura E. (2018) Nitrogen concentrations and isotopic compositions of seafloor-altered terrestrial basaltic glass: implications for astrobiology. *Astrobiology* **18**, 330–342.
- Bédard J. H. (1994) A procedure for calculating the equilibrium distribution of trace elements among the minerals of cumulate rocks, and the concentration of trace elements in the coexisting liquids. *Chem. Geol.* **118**, 143–153.
- Beyer C. and Frost D. J. (2017) The depth of sub-lithospheric diamond formation and the redistribution of carbon in the deep mantle. *Earth Planet. Sci. Lett.* **461**, 30–39.
- Bishop F. C., Smith J. V. and Dawson J. B. (1976) Na, P, Ti and coordination of Si in garnet from peridotite and eclogite xenoliths. *Nature* **260**, 696–697.
- Bishop F. C., Smith J. V. and Dawson J. B. (1978) Na, K, P and Ti in garnet, pyroxene and

olivine from peridotite and eclogite xenoliths from African kimberlites. *Lithos* **11**, 155–173.

Burnham A. D., Thomson A. R., Bulanova G. P., Kohn S. C., Smith C. B. and Walter M. J.

(2015) Stable isotope evidence for crustal recycling as recorded by superdeep diamonds.

Earth Planet. Sci. Lett. **432**, 374–380.

Busigny V., Laverne C. and Bonifacie M. (2005) Nitrogen content and isotopic composition of

oceanic crust at a superfast spreading ridge: A profile in altered basalts from ODP Site

1256, Leg 206. *Geochem. Geophys.* **6**, 1–16.

Caporuscio F. A. and Smyth J. R. (1990) Trace element crystal chemistry of mantle eclogites.

Contrib. to Mineral. Petrol. **105**, 550–561.

Cartigny P., Palot M., Thomassot E. and Harris J. W. (2014) Diamond formation: a stable

isotope perspective. *Annu. Rev. Earth Planet. Sci.* **42**, 699–732.

Collerson K. D., Williams Q., Kamber B. S., Omori S., Arai H. and Ohtani E. (2010) Majoritic

garnet: a new approach to pressure estimation of shock events in meteorites and the

encapsulation of sub-lithospheric inclusions in diamond. *Geochim. Cosmochim. Acta* **74**,

5939–5957.

Debret B. and Sverjensky D. A. (2017) Highly oxidising fluids generated during serpentinite

breakdown in subduction zones. *Sci. Rep.* **7**, 1–6.

Deines P. and Harris J. W. (1995) Sulfide inclusion chemistry and carbon isotopes of African

diamonds. *Geochim. Cosmochim. Acta* **59**, 3173–3188.

Deines P. and Haggerty S. E. (2000) Small-scale oxygen isotope variations and petrochemistry

of ultradeep (>300 km) and transition zone xenoliths. *Geochim. Cosmochim. Acta* **64**, 117–

131.

Eiler J. M. (2001) Oxygen isotope variations of basaltic lavas and upper mantle rocks. *Rev.*

Mineral. Geochemistry **43**, 319–364.

Frost D. J. and McCammon C. A. (2008) The Redox State of earth's mantle. *Annu. Rev. Earth*

Planet. Sci. **36**, 389–420.

Fung A. T. and Haggerty S. E. (1995) Petrography and mineral compositions of eclogites from

the Koidu Kimberlite Complex, Sierra Leone. *J. Geophys. Res.* **100**.

Gao Y., Vils F., Cooper K. M., Banerjee N., Harris M., Hoefs J., Teagle D. A. H., Casey J. F.,

Elliott T., Laverne C., Alt J. C. and Muehlenbachs K. (2012) Downhole variation of lithium and oxygen isotopic compositions of oceanic crust at East Pacific Rise, ODP Site 1256.

Geochem. Geophys. **13**.

Gregory R. T. and Taylor H. P. (1981) An oxygen isotope profile in a section of Cretaceous

oceanic crust, Samail ophiolite, Oman: evidence for $\delta^{18}\text{O}$ buffering of the oceans by deep (>5 km) seawater-hydrothermal circulation at mid-ocean ridges. *J. Geophys. Res. Solid*

Earth **86**, 2737–2755.

Grew E. S., Locock A. J., Mills S. J., Galuskina I. O., Galuskin E. V. and Hålenius U. (2013)

IMA report: Nomenclature of the garnet supergroup. *Am. Mineral.* **98**, 785–810.

Grütter H. S., Gurney J. J., Menzies A. H. and Winter F. (2004) An updated classification

scheme for mantle-derived garnet, for use by diamond explorers. *Lithos* **77**, 841–857.

Hammouda T. and Laporte D. (2000) Ultrafast mantle impregnation by carbonatite melts.

Geology **28**, 283–285.

- Harder M., Nowicki T. E., Hetman C. M., Freeman L. and Abedu B. (2013) Geology and evaluation of the K2 Kimberlite, Koidu Mine, Sierra Leone, West Africa. *Proc. 10th Int. Kimberl. Conf.*, pp. 191–208.
- Harte B. and Kirkley M. B. (1997) Partitioning of trace elements between clinopyroxene and garnet: data from mantle eclogites. *Chem. Geol.* **136**, 1–24.
- Helmstaedt H. and Doig R. (1975) Eclogite nodules from kimberlite pipes of the Colorado plateau - samples of subducted Franciscan-type oceanic lithosphere. *Phys. Chem. Earth*, 95–111.
- Hills D. V. and Haggerty S. E. (1989) Petrochemistry of eclogites from the Koidu Kimberlite Complex, Sierra Leone. *Contrib. to Mineral. Petrol.* **103**, 397–422.
- Ickert R. B. and Stern R. A. (2013) Matrix corrections and error analysis in high-precision SIMS $^{18}\text{O}/^{16}\text{O}$ measurements of Ca-Mg-Fe garnet. *Geostand. Geoanal. Res.* **37**, 429–448.
- Ickert R. B., Stachel T., Stern R. A. and Harris J. W. (2013) Diamond from recycled crustal carbon documented by coupled $\delta^{18}\text{O}$ – $\delta^{13}\text{C}$ measurements of diamonds and their inclusions. *Earth Planet. Sci. Lett.* **364**, 85–97.
- Ickert R. B., Stachel T., Stern R. A. and Harris J. W. (2015) Extreme ^{18}O -enrichment in majorite constrains a crustal origin of transition zone diamonds. *Geochem. Perspect. Lett.* **1**, 65–74.
- Irfune T. (1987) An experimental investigation of the pyroxene-garnet transformation in a pyrolite composition and its bearing on the constitution of the mantle. *Phys. Earth Planet. Inter.* **45**, 324–336.
- Irfune T., Sekine T., Ringwood A. E. and Hibberson W. O. (1986) The eclogite-garnetite

- transformation at high pressure and some geophysical implications. *Earth Planet. Sci. Lett.* **77**, 245–256.
- Jacob D. E. (2004) Nature and origin of eclogite xenoliths from kimberlites. *Lithos* **77**, 295–316.
- Jacob D., Jagoutz E., Lowry D., Matthey D. and Kudrjavitseva G. (1994) Diamondiferous eclogites from Siberia: remnants of Archean oceanic crust. *Geochim. Cosmochim. Acta* **58**, 5191–5207.
- Kirkley M. B., Gurney J. J., Otter M. L., Hill S. J. and Daniels L. R. (1991) The application of C isotope measurements to the identification of the sources of C in diamonds: a review. *Appl. Geochem.* **6**, 477–494.
- Kiseeva E. S., Yaxley G. M., Stepanov A. S., Tkalčić H., Litasov K. D. and Kamenetsky V. S. (2013) Metapyroxenite in the mantle transition zone revealed from majorite inclusions in diamonds. *Geology* **41**, 883–886.
- Kiseeva E. S., Wood B. J., Ghosh S. and Stachel T. (2016) The pyroxenite-diamond connection. *Geochem. Perspect. Lett.* **2**, 1–9.
- Korolev N. M., Melnik A. E., Li X. H. and Skublov S. G. (2018) The oxygen isotope composition of mantle eclogites as a proxy of their origin and evolution: A review. *Earth-Science Rev.* **185**, 288–300.
- Labidi J. (2022) The origin of nitrogen in Earth's mantle: constraints from basalts $^{15}\text{N}/^{14}\text{N}$ and $\text{N}_2/{}^3\text{He}$ ratios. *Chem. Geol.* **597**, 120780.
- Lai M. Y., Stachel T., Stern R. A., Hardman M. F., Pearson D. G. and Harris J. W. (2022) Formation of mixed paragenesis diamonds during multistage growth – Constraints from in

- situ $\delta^{13}\text{C}$ – $\delta^{15}\text{N}$ –[N] analyses of Koidu diamonds. *Geochim. Cosmochim. Acta* **323**, 20–39.
- Li K., Li L., Pearson D. G. and Stachel T. (2019) Diamond isotope compositions indicate altered igneous oceanic crust dominates deep carbon recycling. *Earth Planet. Sci. Lett.* **516**, 190–201.
- Li L., Bebout G. E. and Idleman B. D. (2007) Nitrogen concentration and $\delta^{15}\text{N}$ of altered oceanic crust obtained on ODP Legs 129 and 185: insights into alteration-related nitrogen enrichment and the nitrogen subduction budget. *Geochim. Cosmochim. Acta* **71**, 2344–2360.
- Locock A. J. (2008) An Excel spreadsheet to recast analyses of garnet into end-member components, and a synopsis of the crystal chemistry of natural silicate garnets. *Comput. Geosci.* **34**, 1769–1780.
- Lowry D., Matthey D. P. and Harris J. W. (1999) Oxygen isotope composition of syngenetic inclusions in diamond from the Finsch Mine, RSA. *Geochim. Cosmochim. Acta* **63**, 1825–1836.
- MacGregor I. D. and Manton W. I. (1986) Roberts Victor eclogites: ancient oceanic crust. *J. Geophys. Res.* **91**, 14063–14079.
- Matthey D., Lowry D. and Macpherson C. (1994) Oxygen isotope composition of mantle peridotite. *Earth Planet. Sci. Lett.* **128**, 231–241.
- McCulloch M. T., Gregory R. T., Wasserburg G. J. and Taylor H. P. (1981) Sm-Nd, Rb-Sr, and $^{18}\text{O}/^{16}\text{O}$ isotopic systematics in an oceanic crustal section: evidence from the Samail ophiolite. *J. Geophys. Res.* **86**, 2721–2735.

- McGetchin T. R. and Silver L. T. (1972) A crustal-upper mantle model for the Colorado plateau based on observations of crystalline rock fragments in the Moses Rock Dike. *J. Geophys. Res.* **77**, 7022–7037.
- McLennan S. M. (1989) Rare earth elements in sedimentary rocks: influence of provenance and sedimentary processes. *Rev. Mineral. Geochem.* **21**, 169–200.
- Mikhail S., Rinaldi M., Mare E. R. and Sverjensky D. A. (2021) A genetic metasomatic link between eclogitic and peridotitic diamond inclusions. *Geochem. Perspect. Lett.* **17**, 33–38.
- Milledge H. J., Mendelsohn M. J., Seal M., Rouse J. E., Swart P. K. and Pillinger C. T. (1983) Carbon isotopic variation in spectral type II diamonds. *Nature* **303**, 791–792.
- Minarik W. G. and Watson E. B. (1995) Interconnectivity of carbonate melt at low melt fraction. *Earth Planet. Sci. Lett.* **133**, 423–437.
- Moore R. O. and Gurney J. J. (1985) Pyroxene solid solution in garnets included in diamond. *Nature* **318**, 553–555.
- Muehlenbachs K. and Clayton R. N. (1972a) Oxygen isotope geochemistry of submarine greenstones. *Can. J. Earth Sci.* **9**, 471–478.
- Muehlenbachs K. and Clayton R. N. (1972b) Oxygen isotope studies of fresh and weathered submarine basalts. *Can. J. Earth Sci.* **9**, 172–184.
- O'Hara M. J. and Yoder H. S. (1967) Formation and fractionation of basic magmas at high pressures. *Scottish J. Geol.* **3**, 67–117.
- Philpotts J. A. and Schnetzler C. C. (1968) Europium anomalies and the genesis of basalt. *Chem. Geol.* **3**, 5–13.

- Piccoli F., Hermann J., Pettke T., Connolly J. A. D., Kempf E. D. and Vieira Duarte J. F. (2019) Subducting serpentinites release reduced, not oxidized, aqueous fluids. *Sci. Rep.* **9**, 1–7.
- Putlitz B., Matthews A. and Valley J. W. (2000) Oxygen and hydrogen isotope study of high-pressure metagabbros and metabasalts (Cyclades, Greece): implications for the subduction of oceanic crust. *Contrib. to Mineral. Petrol.* **138**, 114–126.
- Regier M. E., Pearson D. G., Stachel T., Luth R. W., Stern R. A. and Harris J. W. (2020) The lithospheric-to-lower-mantle carbon cycle recorded in superdeep diamonds. *Nature* **585**, 234–238.
- Riches A. J. V., Ickert R. B., Pearson D. G., Stern R. A., Jackson S. E., Ishikawa A., Kjarsgaard B. A. and Gurney J. J. (2016) In situ oxygen-isotope, major-, and trace-element constraints on the metasomatic modification and crustal origin of a diamondiferous eclogite from Roberts Victor, Kaapvaal Craton. *Geochim. Cosmochim. Acta* **174**, 345–359.
- Ringwood A. and Major A. (1971) Synthesis of majorite and other high pressure garnets and perovskites. *Earth Planet. Sci. Lett.* **12**, 411–418.
- Rohrbach A. and Schmidt M. W. (2011) Redox freezing and melting in the Earth's deep mantle resulting from carbon-iron redox coupling. *Nature* **472**, 209–214.
- Russell A. K., Kitajima K., Strickland A., Medaris L. G., Schulze D. J. and Valley J. W. (2013) Eclogite-facies fluid infiltration: constraints from $\delta^{18}\text{O}$ zoning in garnet. *Contrib. to Mineral. Petrol.* **165**, 103–116.
- Salisbury M. H. and Christensen N. I. (1978) The seismic velocity structure of a traverse through the Bay of Islands Ophiolite Complex, Newfoundland, an exposure of oceanic crust and

- upper mantle. *J. Geophys. Res.* **83**, 805–817.
- Schidlowski M. (2001) Carbon isotopes as biogeochemical recorders of life over 3.8 Ga of earth history: evolution of a concept. *Precambrian Res.* **106**, 117–134.
- Schmickler B., Jacob D. E. and Foley S. F. (2004) Eclogite xenoliths from the Kuruman kimberlites, South Africa: geochemical fingerprinting of deep subduction and cumulate processes. *Lithos* **75**, 173–207.
- Schulze D. J. (1989) Constraints on the abundance of eclogite in the upper mantle. *J. Geophys. Res.* **94**, 4205–4212.
- Schulze D. J., Valley J. W. and Spicuzza M. J. (2000) Coesite eclogites from the Roberts Victor kimberlite, South Africa. *Lithos* **54**, 23–32.
- Schulze D. J., Valley J. W., Spicuzza M. J. and Channer D. M. D. (2003) Oxygen isotope composition of eclogitic and peridotitic garnet xenocrysts from the La Ceniza kimberlite, Guaniamo, Venezuela. *Int. Geol. Rev.* **45**, 968–975.
- Schulze D. J., Harte B., Valley J. W. and Channer D. M. D. (2004) Evidence of subduction and crust – mantle mixing from a single diamond. *Lithos* **77**, 349–358.
- Schulze D. J., Harte B., Edinburgh ion microprobe facility staff, Page F. Z., Valley J. W., Channer D. M. D. and Jaques A. L. (2013) Anticorrelation between low $\delta^{13}\text{C}$ of eclogitic diamonds and high $\delta^{18}\text{O}$ of their coesite and garnet inclusions requires a subduction origin. *Geology* **41**, 455–458.
- Shieh Y. N. and Taylor H. P. (1969) Oxygen and carbon isotope studies of contact metamorphism of carbonate rocks. *J. Petrol.* **10**, 307–331.

- Skinner E. M. W., Apter D. B., Morelli C. and Smithson N. K. (2004) Kimberlites of the Man craton, West Africa. *Lithos* **76**, 233–259.
- Smart K. A., Heaman L. M., Chacko T., Simonetti A., Kopylova M., Mah D. and Daniels D. (2009) The origin of high-MgO diamond eclogites from the Jericho Kimberlite, Canada. *Earth Planet. Sci. Lett.* **284**, 527–537.
- Smart K. A., Chacko T., Stachel T., Tappe S., Stern R. A., Ickert R. B. and EIMF (2012) Eclogite formation beneath the northern Slave craton constrained by diamond inclusions: oceanic lithosphere origin without a crustal signature. *Earth Planet. Sci. Lett.* **319–320**, 165–177.
- Smit K. V., Shirey S. B. and Wang W. (2016) Type Ib diamond formation and preservation in the West African lithospheric mantle: Re–Os age constraints from sulphide inclusions in Zimmi diamonds. *Precambrian Res.* **286**, 152–166.
- Stachel T. and Harris J. W. (1997) Diamond precipitation and mantle metasomatism - evidence from the trace element chemistry of silicate inclusions in diamonds from Akwatia, Ghana. *Contrib. to Mineral. Petrol.* **129**, 143–154.
- Stachel T., Harris J. W. and Brey G. P. (1998) Rare and unusual mineral inclusions in diamonds from Mwadui, Tanzania. *Contrib. to Mineral. Petrol.* **132**, 34–47.
- Stachel T., Harris J., Aulbach S. and Deines P. (2002) Kankan diamonds (Guinea) III: $\delta^{13}\text{C}$ and nitrogen characteristics of deep diamonds. *Contrib. to Mineral. Petrol.* **142**, 465–475.
- Stachel T., Aulbach S., Brey G. P., Harris J. W., Leost I., Tappert R. and Viljoen K. S. (2004) The trace element composition of silicate inclusions in diamonds: a review. *Lithos* **77**, 1–19.

- Stachel T., Aulbach S. and Harris J. W. (2022) Mineral inclusions in lithospheric diamonds. *Rev. Mineral. Geochem.* **87**, 307–391.
- Thomson A. R., Kohn S. C., Bulanova G. P., Smith C. B., Araujo D. and Walter M. J. (2016) Trace element composition of silicate inclusions in sub-lithospheric diamonds from the Juina-5 kimberlite: evidence for diamond growth from slab melts. *Lithos* **265**, 108–124.
- Thomson Andrew R., Walter M. J., Kohn S. C. and Brooker R. A. (2016) Slab melting as a barrier to deep carbon subduction. *Nature* **529**, 76–79.
- Tompkins L. A. and Haggerty S. E. (1984) The Koidu kimberlite complex, Sierra Leone: geological setting, petrology and mineral chemistry. In *Developments in Petrology*, vol. 11, pp. 83–105
- Walter M. J., Bulanova G. P., Armstrong L. S., Keshav S., Blundy J. D., Gudfinnsson G., Lord O. T., Lennie A. R., Clark S. M., Smith C. B. and Gobbo L. (2008) Primary carbonatite melt from deeply subducted oceanic crust. *Nature* **454**, 622–626.
- Weill D. F. and Drake M. J. (1973) Europium anomaly in plagioclase feldspar: experimental results and semiquantitative model. *Science* **180**, 1059–1060.
- Zedgenizov D., Rubatto D., Shatsky V., Ragozin A. and Kalinina V. (2016) Eclogitic diamonds from variable crustal protoliths in the northeastern Siberian craton: trace elements and coupled $\delta^{13}\text{C}$ – $\delta^{18}\text{O}$ signatures in diamonds and garnet inclusions. *Chem. Geol.* **422**, 46–59.
- Zhang R. Y., Zhai S. M., Fei Y. W. and Liou J. G. (2003) Titanium solubility in coexisting garnet and clinopyroxene at very high pressure: The significance of exsolved rutile in garnet. *Earth Planet. Sci. Lett.* **216**, 591–601.

Chapter 4 Composition and evolution of the lithospheric mantle and its subducted components beneath the Koidu kimberlite, West African Craton

4.1 Introduction

Extensive studies have been conducted on kimberlite-borne mantle xenoliths from the Koidu kimberlite complex in Sierra Leone, which provide crucial information about the evolution of the subcontinental lithospheric mantle beneath the Man Shield of the West African Craton (Hills and Haggerty, 1989; Fung and Haggerty, 1995; Barth et al., 2001, 2002; Aulbach et al., 2019). Koidu is of particular interest as eclogites are the exclusive mantle xenoliths present (Tompkins and Haggerty, 1984). Eclogites are considered to be a minor constituent in the Earth's upper mantle (Schulze, 1989), but are locally significant as xenoliths at several mined kimberlites worldwide, such as Roberts Victor, Bellsbank and Lace in South Africa (MacGregor and Carter, 1970; Schulze and Helmstaedt, 1988; Viljoen, 1995), Orapa in Botswana (Robinson et al., 1984) and Zagadochnaya in Russia (Sobolev et al., 1968). Although no peridotite xenoliths were recovered from Koidu, the presence of peridotitic xenocrysts, such as Cr-rich subcalcic garnets, in heavy mineral concentrates suggests that sampling of strongly depleted harzburgites or dunites nevertheless occurred, but that such xenoliths may have disaggregated prior to or during kimberlite eruption (Skinner et al., 2004; Harder et al., 2013).

A Jurassic paleogeotherm for the Man Shield corresponding to a surface heat flow of 38 mW/m² (model geotherms of Hasterok and Chapman, 2011) was established through geothermobarometry on Koidu Cr-diopsides (Smit et al., 2016). This geotherm falls towards the lower end of the range of geothermal gradients exhibited by cratons worldwide (Hasterok and Chapman, 2011). Intersection of the 38 mW/m² conductive model geotherm with the graphite-

diamond transition (Day, 2012) and the mantle adiabat indicate that diamonds are stable above 850 °C (corresponding to a depth of 120 km) and that the base of the lithosphere is at approximately 220 km depth (Smit et al., 2016).

Despite evidence for an ultradeep origin (depth > 300 km) of a Koidu eclogite xenolith (Deines and Haggerty, 2000), no diamonds containing sublithospheric inclusions have been reported. Among the previously reported Koidu diamonds, only sulphide inclusions (from seven diamonds; Deines and Harris, 1995), plus one olivine, one garnet, two orthopyroxenes and two Mg-chromite inclusions (Meyer and Boyd, 1972) were analyzed for their major element compositions. In this study, I provide a more complete picture of the mineralogical composition of the mantle beneath the Man Shield of the West African Craton through a comprehensive investigation of inclusion-bearing diamonds and of some diamondiferous eclogite xenoliths from Koidu. Complementing previous studies on Koidu eclogite xenoliths and the geodynamic history of the region that they document, mineral inclusions in Koidu diamonds preserve information about the physical and chemical state of the lithospheric mantle at the time of diamond formation, prior to any subsequent metasomatic processes that modified xenolith samples.

A study of diamonds from Koidu is of particular interest because it is unique among diamond deposits worldwide through: (1) presence of mixed paragenesis (eclogitic-peridotitic) diamonds (Lai et al., 2022), and (2) a dominance of SiO₂ phase (coesite) inclusions (identified in 44% of diamonds in this study). Worldwide, the relative abundance of coesite inclusions in diamond is low ($\leq 2\%$; Stachel and Harris, 2008), although in some localities coesite-bearing diamonds can comprise a significant proportion, such as Renard in Canada (27%; Hunt et al., 2012), Guaniamo in Venezuela (22%; Sobolev et al., 1998), Argyle in Australia (19%; Jaques et al., 1989) and Helam in South Africa (17%; Mc Kenna et al., 2004).

4.2 Samples and analytical methods

A total of 105 diamonds with primary mineral inclusions were studied, of which 82 (78%) contained eclogitic inclusions, 18 (17%) contained peridotitic inclusions, and five (5%) contained co-occurring eclogitic and peridotitic inclusions. Characteristics of the host diamonds, including size, weight, colour, morphology, surface features, internal growth texture, as well as nitrogen concentrations and aggregation states were described by Lai et al. (2022). Diamonds were crushed to release mineral inclusions using a steel cracker. Recovered mineral inclusions are 20–400 μm in maximum dimension. For comparative purposes, six diamondiferous eclogite xenoliths (1.0–2.5 cm in maximum dimension) were crushed to recover fresh garnet and clinopyroxene. Three grains of each phase were picked. Inclusions and xenolith minerals were mounted in epoxy and polished for analysis.

Major and minor element compositions were determined by wavelength-dispersive spectrometry (WDS) using CAMECA SX100 and JEOL JXA-8900R electron probe microanalyzers (EPMA). Trace element compositions were determined using a Resonetics M-50-LR 193 nm ArF excimer laser ablation system, with a Laurin-Technic S-155 two-volume ablation cell, coupled with a Thermo Scientific Element IIXR inductively coupled plasma mass spectrometer (LA-ICP-MS). Spot size for laser ablation was chosen based on the morphology and dimension of the mineral inclusions, where the spot size was maximized to cover most of the area of each grain. The large grain dimension (1–2 mm) of xenolith minerals enabled a larger analytical spot size (130 μm). Details, including operating conditions, detection limits, reference materials and calibration methods, were described by Lai et al. (2022).

For trace Al, Ca and Cr analyses of olivine inclusions, the JEOL JXA-8900R EPMA was used, operating at an accelerating voltage of 20 kV. Reference materials include Frank Smith

pyrope (for Al), wollastonite (for Ca) and synthetic Cr₂O₃ (for Cr). A beam current of 20–100 nA and a beam diameter of 5 µm were used for the analysis of reference materials, with a counting time of 30 s on the peak. For olivine inclusions, the beam current was 200 nA and the beam diameter was 2–5 µm, with a counting time of 200 s each on the peak and for background measurements. Detection limits for Al, Ca, and Cr are estimated to be 6, 8 and 15 ppm, respectively.

For each diamondiferous eclogite xenolith, three garnet grains were analysed for their oxygen isotope composition, using a CAMECA IMS 1280 multicollector ion microprobe. The samples were mounted along with reference materials S0068 (pyrope garnet from the Gore Mountain area; Bartholomé, 1960) and S0088B (grossular garnet from the Jeffrey mine; Akizuki, 1989). The polished mount was coated with Au prior to scanning electron microscopy (SEM) to prevent charging. Characterization of garnet grains was carried out with a Zeiss EVO MA15 SEM instrument at a voltage of 20 kV and a beam current of 3–4 nA. Five measurement spots were set on each grain, based on the backscattered electron images of the grains, to assess their homogeneity. A primary ¹³³Cs⁺ beam of 20 keV with a current of 2 nA was focused to a beam diameter of approximately 12 µm during data acquisition. Oxygen isotope compositions are reported as δ¹⁸O_{VSMOW} in per mil (‰) [normalized difference of the ¹⁸O/¹⁶O ratio of the sample relative to that of Vienna Standard Mean Ocean Water (VSMOW), where ¹⁸O/¹⁶O_{VSMOW} = 2005.20 (±0.45) × 10⁻⁶; Baertschi, 1976]. To monitor the instrumental mass fractionation (IMF), S0068 (with δ¹⁸O_{VSMOW} = +5.72 ‰) and S0088B (with δ¹⁸O_{VSMOW} = +4.13 ‰) were analysed after every five and ten unknowns, respectively. The 95% confidence uncertainty estimates for δ¹⁸O_{VSMOW} of analysed garnet grains average ± 0.26 ‰, which includes errors related to within-spot counting statistics, between-spot (geometric) effects, correction for IMF, and matrix effects associated with Ca# [i.e., Ca/(Ca+Mg+Fe)]. Details of analytical methods are described in Ickert and Stern (2013).

4.3 Results

From 105 diamonds, 370 primary mineral inclusions were recovered, which include coesite (n = 80), omphacite (n = 79), kyanite (n = 53), olivine (n = 45), eclogitic garnet (n = 41), spinel (n = 41), sulphide (n = 27), rutile (n = 3) and corundum (n = 1) (Table C.1). Up to three mineral phases coexisted in single diamonds. Coesite, olivine and corundum inclusions were all colourless, while omphacite inclusions were mostly colourless or occasionally pale green, so these four phases could not usually be distinguished visually.

The diamondiferous eclogite xenoliths contain garnet and clinopyroxene in modal proportions between 60:40 and 40:60, consistent with mineral modes previously reported for diamond- or graphite-bearing eclogite xenoliths from Koidu (Hills and Haggerty, 1989). The xenoliths are characterized by subhedral garnets embedded in a matrix of clinopyroxene (Fig. C.1), similar to the texture of Group I eclogites from the Roberts Victor mine in South Africa (MacGregor and Carter, 1970). Garnets are mostly fresh, whereas clinopyroxenes are typically heavily altered, especially in a xenolith (KEC-40-coat) that also hosts an aggregate of multiple fibrous diamonds. In addition to diamond, accessory minerals in the eclogite xenoliths include amphibole and phlogopite.

4.3.1 Major element compositions of minerals

4.3.1.1 Peridotitic minerals

Olivine inclusions from 19 diamonds have a narrow range in molar Mg# [$100 \times \text{Mg}/(\text{Mg} + \text{Fe})$] between 92.2–94.7, with an average value of 94.0, which is higher than that of olivine inclusions in lithospheric diamonds from other localities on the West African Craton (Akwatia in Ghana and Kankan in Guinea; Stachel and Harris, 1997 and Stachel et al., 2000,

respectively) (Fig. 4.1). Two olivine inclusions from one diamond (130-34) have slightly higher CaO content compared to the others (0.05 vs 0.01–0.03 wt%; Table C.2). Olivine inclusions in four diamonds co-occur with omphacite, coesite or eclogitic garnet, and were previously reported as mixed paragenesis diamonds (Lai et al., 2022). Nickel contents (NiO = 0.30–0.39 wt%) in the olivine inclusions lie within the range for West African diamonds (Stachel and Harris, 1997; Stachel et al., 2000), and there is no difference between olivines from mixed paragenesis and purely peridotitic diamonds.

Spinel inclusions were recovered from eight diamonds. They occur as a single phase or together with olivine, except for two mixed paragenesis diamonds, where spinel occurs with omphacite or coesite (Lai et al., 2022). The composition of spinel from mixed paragenesis diamonds is not distinct from those occurring alone or with olivine. A spinel inclusion intergrown with olivine has a much higher molar Mg# [$100 \times \text{Mg}/(\text{Mg} + \text{Fe}^{2+})$; 89.5] than three non-touching spinel grains (average Mg# = 71.7) from the same diamond (147-1). Another spinel inclusion (diamond 136-1) with high Mg# (82.4) has a very low molar Cr# [$100 \times \text{Cr}/(\text{Cr} + \text{Al})$; 50.9]. Apart from this sample, all spinel inclusions have Cr# between 84.7 and 89.1, and Mg# (also excluding the spinel-olivine intergrowth) between 62.9 and 73.9 (Fig. 4.2). Titanium contents (TiO₂) in two spinel inclusions from diamond 135-3 are exceptionally high (average 2.8 wt%) compared to the other diamonds (0.04–0.26 wt%), and are the highest reported for West African diamonds (Stachel and Harris, 1997; Stachel et al., 2000).

4.3.1.2 Eclogitic minerals

Omphacite inclusions from 30 diamonds contain a jadeite component [$100 \times 2\text{Na}/(2\text{Na} + \text{Ca} + \text{Mg} + \text{Fe})$; Morimoto, 1988] of 29.2 to 76.5 mol% and have Mg# between 68.3 and 82.3 (Fig. 4.3). Except for two outliers (Cr# 7.3) in diamond 142-2, the Cr# of omphacite

inclusions is ≤ 0.6 . These two outliers also have the lowest jadeite component (29.2 and 29.5 mol%) and the highest FeO (6.3 vs 1.8–4.5 wt%) and K₂O (0.31 vs 0.05–0.25 wt%) compared to the others. Multiple omphacite inclusions in another diamond (130-1) have extremely high Na₂O, up to 10.5 wt%. Similarly high Na₂O contents in omphacite inclusions were previously only observed in placer diamonds from the northeastern Siberian Craton (Sobolev et al., 1999; Shatsky et al., 2015). Omphacites in two mixed paragenesis diamonds occur with olivine (Mg# 94.2) or Mg-chromite (Cr# 85.5) that have strongly depleted peridotitic signatures (Lai et al., 2022). Rutile was included in or exsolved from omphacites in three diamonds (130-12, 131-3 and 142-4). Omphacite from diamondiferous eclogite xenoliths (Hills and Haggerty, 1989 and this study) have jadeite components (32.2–46.4 mol%) at the low end of the inclusion population and generally higher Mg# (75.0–89.7) than the inclusions (Fig. 4.3). Based on molar proportions of Ca-Mg-Fe (Fig. 4.4), most omphacite inclusions overlap with the compositional field of Koidu low-MgO eclogites, whereas omphacites from xenoliths mostly lie within the field of Koidu gabbroic eclogites (Aulbach et al., 2019).

Garnet from 26 diamonds have the characteristic low Cr₂O₃ contents (≤ 0.02 to 0.28 wt%) of the eclogitic suite (Schulze, 2003) and range from low-Ca (G4; CaO = 3.6–< 6.0 wt%) to high-Ca (G3; CaO = 6.0–19.3 wt%) in composition (Grütter et al., 2004). A garnet inclusion in diamond 140-2 shows a minor excess of Si atoms over the available tetrahedral sites (3.03), indicative of a minor majorite component. The same garnet has the highest Mg# (79.0 vs 49.1–67.3), Cr₂O₃ (0.28 vs ≤ 0.02 to 0.17) and TiO₂ (0.86 vs 0.24–0.49 wt%) among the garnet suite. The CaO contents (3.6–11.1 wt%) of garnet inclusions in this study lie within the range reported for West African eclogitic diamonds (Stachel and Harris, 1997; Stachel et al., 2000), except for the very CaO-rich garnets (16.7–19.3 wt%; Lai et al., 2022) that co-occur with olivine in a mixed paragenesis

diamond (138-7). Garnets from diamondiferous eclogite xenoliths have slightly higher CaO (7.9–11.9 wt%) and Ca# (20.8–31.8 vs 9.3–51.4) than most inclusions (Fig. 4.5).

Kyanite is a rare inclusion in diamond, both worldwide and at any known locality, but it is exceptionally abundant in my sample suite, occurring in 17% (n = 18) of diamonds, indicating an unusually aluminous nature of the diamond source rocks (Spetsius, 2004; Shu et al., 2016). Two kyanites contained inclusions of sulphide and coesite (diamonds 128-7 and 130-15, respectively). Kyanite coexisted with eclogitic garnet in diamonds 128-2, 128-6, 137-1 and 144-1, but the garnets Ca#s (17.1–17.8) are too low to classify the assemblages as grosspyritic; grosspyrite is an unusual variant of eclogite consisting of three primary minerals, garnet, clinopyroxene and kyanite, where garnet must have Ca# > 50 (Sobolev et al., 1968; Spetsius, 2004). Significant impurities in the kyanite inclusions are TiO₂ (0.08–0.21 wt%), Cr₂O₃ (0.03–0.19 wt%), FeO (0.18–0.58 wt%) and MgO (≤ 0.02 to 0.18 wt%), which do not correlate with the type or composition of coexisting minerals.

Sulphide inclusions occur together with eclogitic silicate minerals or as lone inclusions in 13 diamonds. They have low Ni contents (0.27–2.3 wt%), indicating that also the lone sulphide inclusions are eclogitic (Bulanova et al., 1996). Most of the sulphide inclusions are compositionally homogeneous and fall in the fields for pyrrhotite to Ni-poor monosulphide solid solution (MSS) (Fig. 4.6). It is believed that sulphide was initially encapsulated as MSS during diamond formation (Deines and Harris, 1995). However, during cooling MSS readily undergoes exsolution to a fine-grained assemblage of different phases and, thus, even if a MSS composition is detected during analysis, exsolved phases could have been lost during sample preparation (polishing) or remained hidden below the polished surface (e.g., Taylor and Liu, 2009). Three sulphide inclusions in two diamonds (133-7 and 140-2) display small exsolved domains that

contain much higher Ni (up to 13.6 wt%) and Co (up to 1.2 wt%). Previous analysis of sulphide inclusions from Koidu diamonds indicated pyrrhotite as the dominant phase (Deines and Harris, 1995). The abundance of pyrrhotite is dependent on the bulk composition of the initial MSS, where Ni-poor compositions (indicating an eclogitic paragenesis) typically yield more pyrrhotite (Taylor and Liu, 2009). Other exsolved phases observed in sulphide inclusions elsewhere, including pentlandite, pyrite and chalcopyrite, are not identified in my samples.

Oxide mineral inclusions encompass coesite, rutile and corundum. *Coesite*, which is an uncommon inclusion in diamonds worldwide ($\leq 2\%$; Stachel and Harris, 2008), is the most abundant inclusion phase at Koidu and occurs in 46 diamonds. All of them are very pure SiO_2 . In two mixed paragenesis diamonds, coesite occurs with olivine and with olivine + spinel (Lai et al., 2022). On the West African Craton, coesite was previously only observed in one Kankan diamond (Stachel et al., 2000) and is absent in Akwatian diamonds (Stachel and Harris, 1997), documenting that silica-rich eclogitic substrates are not a widespread characteristic of the West African Craton. *Rutile* occurs in one diamond as three separate grains. Exsolved corundum is distributed sporadically as small needles (size = $0.5 \times 2 \mu\text{m}$) in two rutile grains, but is too small to be analyzed accurately. The corundum-free rutile inclusion has a homogeneous composition throughout the grain, with 98.4 wt% TiO_2 , 0.42 wt% Al_2O_3 , 0.38 wt% FeO and 0.32 wt% V_2O_3 , on average. A *corundum* inclusion was recovered from one diamond, where it occurs with two coesite inclusions. Its composition could not be determined accurately due to its morphology (needle-shaped) and small size ($5 \times 20 \mu\text{m}$). Corundum is a rare inclusion and has only been observed in diamonds from a few localities, e.g., Guaniamo in Venezuela (Sobolev et al., 1998), Venetia, Helam and Jagersfontein in South Africa (respectively Aulbach et al., 2002; Mc Kenna et al., 2004; Tappert et al., 2005).

4.3.2 Trace element compositions of minerals

In eclogites, clinopyroxene and garnet are the major hosts of trace elements such as rare earth elements (REE) and high field strength elements (HFSE). Trace element compositions for 39 omphacites (from 28 diamonds) and 33 eclogitic garnets (from 25 diamonds) were determined in this study. In addition and for comparison, omphacite and garnet from six diamondiferous eclogite xenoliths were also analyzed for their trace element compositions. Representative trace element compositions for inclusions and xenoliths are given in Table C.3.

The three garnets from mixed paragenesis diamond 138-7 have positive Eu anomalies with $[Eu/Eu^*]_N = 1.10\text{--}1.41$ ($Eu^* = [Sm_N \times Gd_N]^{0.5}$ and $_N =$ normalized to CI-chondrite composition of McDonough and Sun, 1995), are LREE-depleted and have distinctly lower $\sum HREE$ than the remaining Koidu inclusion garnets (Fig. 4.7a). They also are the only garnets with negative MREE–HREE slopes ($Gd_N/Lu_N > 1$) and their MREE–HREE contents fall in the field of garnets from Koidu gabbroic eclogite xenoliths (Aulbach et al., 2019; Fig. 4.7a). Seven diamonds have garnet inclusions with negative Eu anomalies ($[Eu/Eu^*]_N = 0.79\text{--}0.90$), while the remaining garnets have no discernible Eu anomalies. Two garnets with negative Eu anomalies and with the lowest Mg# (both 49.1; diamonds 138-12 and 143-1) have the highest $\sum REE$ and are unique through their flat $MREE_N\text{--}HREE_N$ slopes, compared to other garnet inclusions with variably positive $MREE_N$ slopes. All other garnets with negative or no discernible Eu anomalies are depleted in $LREE_N$, and generally have ~ 10 to $70\times$ chondritic MREE and HREE with flat $HREE_N$ (Fig. 4.7a). Most of these garnet inclusions have REE contents overlapping with the field of garnets from Koidu low-MgO eclogite xenoliths (Aulbach et al., 2019). Similar to garnet inclusions from diamond 138-7, garnet grains from all diamondiferous eclogite xenoliths have positive Eu anomalies ($[Eu/Eu^*]_N = 1.16\text{--}1.28$) and low $\sum HREE$ (Fig. 4.7b), falling in the compositional field

of gabbroic garnets from Koidu eclogite xenoliths (Aulbach et al., 2019).

Like their garnet counterparts, omphacite inclusions in mixed paragenesis diamond 133-6 have positive Eu anomalies ($[Eu/Eu^*]_N = 1.63\text{--}1.78$) (Fig. 4.8a). They are distinct from the other omphacite inclusions through their highly fractionated REE_N ($La_N/Yb_N = 422$), with MREE and HREE contents lower than typical eclogitic clinopyroxene inclusions in diamonds worldwide (Stachel and Harris, 2008). Omphacites in eight diamonds show negative Eu anomalies ($[Eu/Eu^*]_N = 0.74\text{--}0.86$), while most of the remaining omphacites have positive Eu anomalies ($[Eu/Eu^*]_N = 1.10\text{--}1.77$). Note that some omphacite inclusions with only weak positive Eu anomalies may also be a result of the combination of high $D_{HREE}(grt-cpx)$ in coexisting garnet which decreases HREE contents of omphacites and the whole-rock LREE-depletion which leads to development of humped omphacite REE_N patterns (Green et al., 2000) (Fig. 4.8a). Garnets coexisting with omphacites that have negative Eu anomalies also show negative Eu anomalies ($[Eu/Eu^*]_N = 0.85\text{--}0.89$), whereas garnets coexisting with omphacites that have weak positive Eu anomalies show no or slightly negative Eu anomalies ($[Eu/Eu^*]_N = 0.90$). All of these omphacites have humped REE_N patterns with LREE-depletion and negative $MREE_N\text{--}HREE_N$ slopes (Fig. 4.8a). The two omphacites with the lowest jadeite component (29.5 and 44.7 mol%; diamonds 142-2 and 142-4, respectively) have the highest $\sum REE$. Except for diamonds 133-6, 142-2 and 142-4, the HREE contents of omphacite inclusions overlap with the fields of omphacites from Koidu eclogite xenoliths, but more than two-thirds of the inclusion population have lower LREE compared to the xenolith omphacites of Aulbach et al. (2019). Omphacite grains from all diamondiferous eclogite xenoliths have small positive Eu anomalies ($[Eu/Eu^*]_N = 1.17\text{--}1.24$). They generally have higher LREE and lower HREE contents compared to omphacite inclusions with positive Eu anomalies, and overlap with the compositional field of Koidu gabbroic omphacites of Aulbach et al. (2019)

(Fig. 4.8b).

4.3.3 Reconstructed whole-rock compositions

Coexisting garnet and omphacite inclusions from six diamonds are used for bulk rock reconstructions based on a typical garnet/clinopyroxene ratio in eclogites of ~50:50 (Stachel et al., 2004). Since Koidu eclogites may be contaminated by kimberlite magma (Barth et al., 2001), the bulk rock compositions of the six studied diamondiferous eclogite xenoliths are also reconstructed, using relatively fresh garnet and omphacite grains and applying the same mineral modes. Jerde et al. (1993) demonstrated that calculated bulk eclogite REE patterns do not significantly change for variations in relative mineral mode of up to 30%, hence bulk rock compositions reconstructed using a garnet:cpx ratio of 50:50 are most suitable for comparison with published literature (with average garnet/clinopyroxene ratios for Koidu eclogites of 1.1 to 1.2; Hills and Haggerty, 1989; Aulbach et al., 2019).

Bulk rock compositions reconstructed from inclusions in diamond have lower MgO (6.6–9.6 vs 8.8–11.5 wt%) and CaO (5.5–9.6 vs 11.5–12.6 wt%), and higher Al₂O₃ (18.2–21.8 vs 15.2–16.9 wt%) and Na₂O (3.3–4.7 vs 2.6–3.3 wt%), compared to reconstructed diamondiferous eclogites (Table 4). The CaO-MgO-FeO proportions of bulk rocks reconstructed from inclusions in diamond are similar to Koidu low-MgO eclogites, but fall completely outside the compositional field of diamondiferous eclogites (Fig. 4.9).

Bulk rocks reconstructed from inclusions are depleted in LREE_N with subchondritic La, and have flat HREE_N slopes with 20 to 30× chondritic HREE (Fig. 4.10 and Table C.4). Two reconstructed bulk rocks (diamonds 138-12 and 143-1) show steep positive LREE_N slopes and negative Eu anomalies ([Eu/Eu*]_N=0.84–0.87). Similar to their constituent garnets (Fig. 4.7a),

these rocks also have the highest $\sum\text{REE}$ and lowest Mg# (55.4 and 53.5, respectively). Most reconstructed bulk rocks have MREE to HREE contents overlapping with the field of reconstructed Koidu low-MgO eclogites (Aulbach et al., 2019). The bulk rocks reconstructed from diamonds 137-1 and 138-9 have overall much lower LREE contents falling below the fields of Aulbach et al. (2019). These two samples, together with the bulk rocks reconstructed for diamonds 131-3 and 146-2, show a break in slope at Nd_N, with a shallower slope from La_N to Pr_N, followed by a steeper slope from Nd_N to Sm_N (Fig. 4.10). Reconstructed bulk compositions of the diamondiferous eclogites have small positive Eu anomalies ($[\text{Eu}/\text{Eu}^*]_{\text{N}} = 1.15\text{--}1.26$), consistent with their constituent garnets and omphacites, and their REE_N patterns again are similar to that of Koidu gabbroic eclogites of Aulbach et al. (2019) (Fig. 4.10).

4.3.4 Geothermobarometry

Temperatures and pressures of diamond formation for 19 olivine-bearing diamonds and six diamonds with non-touching pairs of eclogitic garnet and omphacite were estimated using Al-in-olivine thermometry (Bussweiler et al., 2017) and garnet-clinopyroxene Mg–Fe exchange thermometry (Krogh, 1988), respectively, both projected on a local model geotherm of 38 mW/m² (Smit et al., 2016). Olivine-bearing diamonds all plot within the diamond-stable portion of the lithospheric mantle ($T = 880\text{--}1240$ °C; $P = 3.9\text{--}6.1$ GPa; Fig. 4.11). The olivine inclusion with the highest CaO content (0.05 wt%; diamond 130-34) yields distinctly higher temperature (1240 °C) and pressure (6.1 GPa) compared to other olivine inclusions. Olivine inclusions in several diamonds, including mixed paragenesis diamonds 130-31 ($T = 1130$ °C; $P = 5.4$ GPa) and 138-7 ($T = 1140$ °C; $P = 5.5$ GPa), fall in the estimated temperature-pressure range for Koidu diamondiferous eclogite xenoliths, which excluding one outlier ($T = 1580$ °C) yield temperatures of 1040–1220 °C at pressures of 4.9–6.0 GPa, corresponding to 150–190 km depth. For two

diamonds calculated P-T values ($T = 1270\text{--}1320\text{ }^{\circ}\text{C}$; $P = 6.3\text{--}6.6\text{ GPa}$), based on eclogitic garnet and omphacite inclusions, fall within depth of the lithospheric mantle, whereas inclusions in four other eclogitic diamonds yield temperatures on the mantle adiabat or higher ($1358\text{--}1442\text{ }^{\circ}\text{C}$) (Fig. 4.11).

4.3.5 Oxygen isotope compositions

Oxygen isotope compositions were determined for three garnet grains from each of the six diamondiferous eclogite xenoliths. A few garnet grains have alteration along fractures, which were avoided during analysis. The inter-grain variability of $\delta^{18}\text{O}$ for garnets within each xenolith sample (average $2\sigma = 0.12\text{ }‰$) is smaller than analytical uncertainty ($2\sigma = \sim 0.26\text{ }‰$) and, consequently, average $\delta^{18}\text{O}$ values are reported for each xenolith (Table C.5) and used for discussion in the following section. Oxygen isotope compositions of all analyzed spots are given in Table C.6.

Garnet grains from diamondiferous eclogite xenoliths have $\delta^{18}\text{O}$ values between $+5.6$ and $+6.3\text{ }‰$, well within the $\delta^{18}\text{O}$ range of Koidu non-diamondiferous eclogite xenoliths ($+4.7$ to $+6.8\text{ }‰$; Deines and Haggerty, 2000; Barth et al., 2001, 2002), and largely overlap with the canonical mantle range ($+5.5 \pm 0.4\text{ }‰$; Matthey et al., 1994). Conversely, a subset ($n = 16$) of eclogitic garnet inclusions from Koidu diamonds have a much wider $\delta^{18}\text{O}$ range from $+5.4$ to $+12.1\text{ }‰$, with a mode of $+11.8\text{ }‰$ (see Chapter 3). Apart from the garnet ($\delta^{18}\text{O} = +5.4\text{ }‰$) in diamond 138-7 with positive Eu anomaly and the garnet ($\delta^{18}\text{O} = +6.3\text{ }‰$) in diamond 140-2 with a mild majorite component, other garnet inclusions have $\delta^{18}\text{O} \geq +9.9\text{ }‰$.

4.4 Discussion

4.4.1 Mantle substrates for diamond formation beneath the West African Craton

4.4.1.1 Peridotitic diamond substrates

The Mg# of olivine is a proxy for the degree of chemical depletion of lithospheric peridotites (Bernstein et al., 2007; Pearson and Wittig, 2008). Although olivine inclusions in Koidu diamonds lack coexisting garnet or clinopyroxene for the assignment to a specific paragenesis, in Akwatian diamonds (Ghana, West African Craton) only olivine inclusions with Mg# below 92.0 occurred with lherzolitic garnet or clinopyroxene (Stachel and Harris, 1997). Thus, the high Mg# (92.2–94.7) of Koidu olivine inclusions suggests derivation from harzburgitic or dunitic diamond substrates. Indeed, the presence of a spinel inclusion with high Mg# (82.4) and low Cr# (50.9) in diamond 136-1 is evidence for a dunitic diamond source, as spinel with Cr# much lower than 80 cannot have coexisted with orthopyroxene in the diamond stability field (Stachel and Harris, 2008). The complete absence of peridotitic orthopyroxene inclusions in this study further supports the inference of the presence of dunitic diamond substrates beneath Koidu. Exhaustion of orthopyroxene in peridotites requires high degrees of melt extraction (~40%; Bernstein et al., 2007), which occurred in the Archean to early Proterozoic, when the mantle potential temperatures were higher (Labrosse and Jaupart, 2007; Aulbach and Arndt, 2019).

Although indicator minerals from Koidu contain both dunitic/harzburgitic and lherzolitic garnets (Skinner et al., 2004; Harder et al., 2013), lherzolitic inclusions have not been found in Koidu diamonds. Dunites/harzburgites constitute the preferred substrates for peridotitic diamond formation not only at Koidu but globally, suggesting that carbon-bearing fluids preferentially react with highly depleted, clinopyroxene-free peridotite (Gurney, 1984; Stachel and Luth, 2015).

The unusually high TiO₂ in spinel inclusions from diamond 135-3 (2.8 wt% versus a

worldwide median of 0.09 wt%; Stachel et al., 2022) indicates localized but intense metasomatic re-enrichment. This event could be related to infiltration of ultramafic melt (proto-kimberlitic magmatism) into the local peridotitic diamond substrate (Smith et al., 2009), during or prior to diamond formation. This and similar metasomatic events may have refertilized the originally highly depleted peridotites in the lithospheric mantle of the West African craton and converted some dunites/harzburgites into lherzolites, as the garnet xenocrysts recovered from Koidu were mostly lherzolitic.

4.4.1.2 Eclogitic diamond substrates

Koidu is situated close to a craton margin, suggesting the formation of its predominantly eclogitic (78%) diamond population was associated with subduction of oceanic crusts at a convergent plate boundary, where oceanic crust metamorphosed to eclogite is the principal substrate for diamond formation (Sobolev, 1985; Jaques et al., 1989; Stachel et al., 2022). A subduction origin of Koidu eclogites has been supported by crustal signatures such as Eu anomalies and fractionated oxygen isotope compositions in their constituent minerals (Barth et al., 2001; Aulbach et al., 2019).

The presence of kyanite and corundum inclusions in Koidu diamonds indicates Al-rich eclogitic diamond substrates. Kyanite may form in eclogites through prograde metamorphism of plagioclase-rich protoliths, e.g., through the reaction $\text{anorthite} = \text{grossular} + \text{kyanite} + \text{coesite}$ (Schulze et al., 2000). Formation following this reaction could also explain the high CaO contents (15.8–21.1 wt%) in garnets from some kyanite-bearing eclogites (Hills and Haggerty, 1989). However, garnet inclusions coexisting with kyanite in Koidu diamonds have only moderate CaO contents (6.2–6.6 wt%). In addition, kyanite-associated garnet inclusions do not show discernible positive Eu anomalies, indicating that their derivation from plagioclase-rich gabbroic protoliths is

highly unlikely. Instead, the high $\delta^{18}\text{O}$ values (+11.8 and +11.9 ‰) in two of these garnet inclusions (in diamonds 137-1 and 144-1, respectively) suggests a basaltic protolith that had undergone extensive low-temperature seawater alteration (Gregory and Taylor, 1981). Some garnets in kyanite-bearing eclogites from the Lace kimberlite (Kaalvaal Craton) also have negative Eu anomalies indicative of basaltic protoliths; the Al-rich signature of these eclogites has, consequently, been attributed to metasomatism instead of a cumulate origin (Aulbach et al., 2016). Formation of kyanite in Koidu eclogitic diamond substrates is possibly related to infiltration of silicate melts derived from pelitic sediments into eclogites in a *mélange* zone (containing a mixture of pelitic sediment, oceanic crust and serpentinized peridotite). Melt infiltration would originally precipitate Al-rich clinopyroxene, which subsequently exsolves kyanite and garnet upon cooling (Smyth et al., 1989; Aulbach et al., 2016).

Coesite is the most abundant inclusion in Koidu diamonds (in 44% of diamonds). Although coesite is relatively uncommon in Koidu eclogite xenoliths (Hills and Haggerty, 1989), its common presence as inclusions suggests that the host eclogites for this mineral was not restites of Archean tonalite-trondjemite-granodiorite (TTG) melt extraction, as TTG formation requires high degrees of partial melting (20–40%; Rollinson, 1997; Schulze et al., 2000), which would completely remove free silica from eclogites. Coesite occurs in Koidu eclogites covering a wide range of compositions and depths of origin in the mantle: for example, a quartz (after coesite)-bearing eclogite (with garnet $\text{Mg}\# = 77.6$) reported in Hills and Haggerty (1989) yields a pressure of 3.7 GPa, whereas a coesite + omphacite + garnet ($\text{Mg}\# = 55.4$) assemblage in diamond 138-9 formed at pressure ≥ 6.9 GPa, with both pressures being derived through projection of garnet-clinopyroxene Mg–Fe exchange temperatures (Krogh, 1988) on a 38 mW/m² model geotherm. This wide distribution of coesite-bearing eclogites in the lithospheric mantle is inconsistent with

fractional crystallization of mafic magma at high pressures, as proposed by O'Hara and Yoder (1967), because coesite could only form from the silica-enriched residual magma after precipitation of garnet and clinopyroxene (Schulze and Helmstaedt, 1988). Thus, coesite is likely derived from subduction and prograde metamorphism of a silica-oversaturated basalt (e.g., quartz tholeiite), or simply a tholeiite through the reaction albite = jadeite + quartz, where quartz transforms into coesite at pressures > 2 GPa (Green and Ringwood, 1968; Bohlen and Boettcher, 1982; Schulze and Helmstaedt, 1988; Ryabchikov et al., 1996; Schulze et al., 2000).

Coexisting garnet and omphacite inclusions in six diamonds yield equilibration temperatures ≥ 1270 °C (Fig. 4.11), which are higher than for most eclogitic diamonds worldwide (median = 1207 °C; Stachel et al., 2022). The estimated pressures (≥ 6.3 GPa) for these diamonds suggest that they formed in the deepest parts of the lithospheric mantle (≥ 200 km). A comparable temperature-pressure range was estimated for the majority of eclogitic diamonds from Argyle, Australia, where the diamond substrates were also thought to reside near the base of the local lithosphere (Stachel et al., 2018). The presence of an eclogitic garnet inclusion with a minor majorite component (diamond 140-2) suggests the possibility that diamond formation occurred at even greater depth. Pressures of 7.8–8.2 GPa, corresponding to a depth of 250–260 km, were calculated for this sample using the majorite-in-garnet barometers of Collerson et al. (2010) and Beyer and Frost (2017), and combined with the occurrence of temperatures equal to or greater than the mantle adiabat for some eclogitic inclusion pairs, suggest that some Koidu eclogitic diamonds may have formed beneath the regional base of the lithosphere at ~220 km depth (Smit et al., 2016). Given the uncertainty of majorite-in-garnet barometry, derivation from the base of the lithosphere can, however, not be excluded for the majorite-bearing sample, with the high-temperature (> 1350 °C) eclogitic inclusions then relating to local thermal perturbations (i.e., advective events), in

which case a steady state geotherm is no longer applicable (Stachel et al., 2006; Stachel and Harris, 2008).

Diamond-bearing eclogite xenoliths from Koidu have a lower range of equilibrium temperatures and pressures ($T = 1040\text{--}1220\text{ }^{\circ}\text{C}$; $P = 4.9\text{--}6.0\text{ GPa}$; Fig. 4.11) compared to inclusions in diamond. Different origins of diamond-bearing xenoliths and inclusions in diamonds are also indicated by the presence of positive Eu anomalies ($[\text{Eu}/\text{Eu}^*]_{\text{N}} = 1.15\text{--}1.26$) in the xenoliths, indicating gabbroic protoliths, whereas reconstructed whole-rocks for inclusions in diamonds have negative or no Eu anomalies ($[\text{Eu}/\text{Eu}^*]_{\text{N}} = 0.84\text{--}1.01$), indicating basaltic protoliths (Fig. 4.10). The distinct oxygen isotope compositions of these samples further support separate protolith origins: garnets from xenoliths have low $\delta^{18}\text{O}$ values (+5.6 to +6.3 ‰; Table C.5), again typical for gabbroic protolith; garnet inclusions (coexisting with omphacite inclusions) have much higher $\delta^{18}\text{O}$ values (+11.3 to +12.0 ‰), characteristic of the uppermost basaltic layer of altered oceanic crust (AOC) (Gregory and Taylor, 1981). This observation of two distinct diamond substrates may suggest that gabbroic eclogites are the preferred substrates for eclogitic diamond formation at shallower depths in the lithospheric mantle, while at greater depths eclogitic diamonds mainly formed in association with basaltic eclogites. Note that gabbroic garnet or gabbroic omphacite inclusions are also present in my sample suite, but they do not coexist in individual diamonds, thus I cannot calculate the equilibrium temperatures and pressures, and hence the corresponding depths for these samples.

The overlapping temperature-pressure range for diamond-bearing gabbroic eclogites and peridotitic diamonds (Fig. 4.11) indicates that at least a subset of peridotitic and eclogitic diamonds precipitated at similar depths beneath the West African Craton. Olivine coexisting with eclogitic garnet inclusions in mixed paragenesis diamond 138-7 yields temperature and pressure ($T = 1140$

°C; $P = 5.5$ GPa) also falling in this range. The garnet inclusions from this diamond are also derived from a gabbroic protolith (Fig. 4.7a), consistent with the above inference of a shallower origin of diamonds associated with gabbroic compared to basaltic eclogite substrates (Fig. 4.11).

4.4.2 Evolution of subducted oceanic crust beneath the West African Craton

Whole-rocks reconstructed from garnet and omphacite inclusions in six Koidu diamonds match well with the MREE–HREE compositions of average normal mid-ocean ridge basalt (NMORB; Sun and McDonough, 1989) and lavas and sheeted dikes from the Oman ophiolite complex (Alabaster et al., 1982) (Fig. 4.12). The depletion in LREE of my Koidu inclusion samples indicates that they underwent partial melting in the garnet stability field, either during subduction or after emplacement into the subcratonic lithosphere, but not to the point where free silica (coesite) was completely eliminated.

Twenty to 30% batch melting of an NMORB starting composition in the eclogite stability field (Sun and McDonough, 1989; Green et al., 2000) results in residues that match the REE_N patterns of the reconstructed whole-rocks for samples 131-1 and 146-2 (Fig. 4.12a). The whole-rocks reconstructed from samples 137-1 and 138-9 appear to indicate lower degrees of melt extraction through higher MREE (Sm to Gd) contents, but show much stronger depletion in LREE than expected from 30% batch melting. However, diamond 138-9 contains a coesite inclusion, implying that its eclogitic substrate did not experience > 20% melt extraction (Schulze et al., 2000), unless the coesite is metasomatic in nature. Coesite could be formed by flooding of eclogites by a CO₂-rich fluid following the carbonation reaction: clinopyroxene + CO₂ = dolomite + coesite (Luth, 1993; Knoche et al., 1999). However, without the presence of dolomite inclusions in my sample suite, coesite formation by this mechanism is difficult to justify. In any case, a simple batch melting model clearly cannot explain the REE_N patterns of all reconstructed whole-rocks.

Residue compositions modelled as successive extraction of small-degree (5%) melt batches in the eclogite stability field (Fig. 4.12b) have steeper $LREE_N$ slopes compared to the single-stage batch melting model discussed above (Fig. 4.12a). Three to four stages of 5% batch melt extraction produce residues that match the REE_N patterns of the whole-rock reconstructed from diamonds 131-3, 137-1, 138-9 and 146-2. A mismatch for the lightest REE (La to Pr) for samples 131-3 and 146-2 may be attributed to metasomatic re-enrichment in LREE after melt depletion. The very steep $LREE_N$ slopes for samples 138-12 and 143-1, however, can still not be matched to any of the modelled compositions.

Given the low mobility of small melting increments of the broadly dacitic melts generated during metabasalt melting (Rapp et al., 1991; Wyllie, 1992), I consider fractional melting an unlikely scenario for the extreme LREE/MREE fractionation indicated by these two samples. Testing fractional melting models nevertheless for the whole-rocks reconstructed from diamonds 138-12 and 143-1 does not produce satisfying matches. The stronger LREE/MREE fractionation achieved through fractional melting can, however, yield satisfying matches if two additional parameters are adjusted: (1) the modal composition of the reconstructed whole-rocks (i.e., their garnet/omphacite ratio); and (2) the starting composition for melt extraction. Changing the garnet/omphacite ratio for the whole-rock reconstructed for sample 138-12 from 50:50 to 40:60 creates a very good match with the residue of 6% fractional melting of NMORB (Fig. 4.13). The whole-rock reconstructed from diamond 143-1 requires a starting composition with higher HREE contents than NMORB and, thus, basalt OM4289 from the Oman ophiolite complex (Alabaster et al., 1982) was chosen (Fig. 4.13). The REE_N pattern of the residue of 9% fractional melt extraction from OM4289 matches well with sample 143-1 (note, Pr was not reported for OM4289 by Alabaster et al. (1982)). The observation that adjusted fractional melting models can qualitatively

match the REE_N patterns in these reconstructed whole-rocks does, however, not invalidate my cautionary statement that extraction of infinitesimally small melt increments is a highly unlikely process during metabasalt melting. In reality, the two samples in question may also reflect a more complex evolution during protolith formation and subduction, as, e.g., dehydration of AOC during subduction can result in strong LREE-depletion (Beinlich et al., 2010; Rustioni et al., 2019; Aulbach et al., 2020).

Samples 138-12 and 143-1 do not show re-enrichment in LREE, suggesting that they were not affected by metasomatism before or during diamond formation, while the other four samples show various degrees of mild metasomatic re-enrichment in LREE after melt depletion. Negative Sr anomalies ($[\text{Sr}/\text{Sr}^*]_{\text{N}}=0.59\text{--}0.67$, where $\text{Sr}^* = [\text{Pr}_{\text{N}} \times \text{Nd}_{\text{N}}]^{0.5}$ and _N = normalized to CI-chondrite; McDonough and Sun, 1995) in samples 138-12 and 143-1 are correlated with their negative Eu anomalies, and together with high $\delta^{18}\text{O}$ value (+11.3 ‰) of garnet inclusion in diamond 138-12 unambiguously point to a basaltic protolith (Fig. 4.14). Strongly positive Sr anomalies ($[\text{Sr}/\text{Sr}^*]_{\text{N}} = 8.12\text{--}16.74$) in samples 131-3, 137-1, 138-9 and 146-2 (Fig. 4.14), however, cannot result from plagioclase accumulation in gabbroic protoliths, as these samples do not show positive Eu anomalies, and the garnet inclusions from these samples have high $\delta^{18}\text{O}$ values (+11.3 to +12.0 ‰) that indicate derivation from the uppermost layer of AOC. Thus, cryptic metasomatism (i.e., change in mineral compositions only; Dawson, 1984) is likely responsible for the addition of Sr and LREE, and a positive correlation between Sr and La is indeed observed in these four samples (Fig. 4.14 and Table C.4).

Major element compositional trends in garnet inclusions and garnets from Koidu eclogites related primarily to Ca# and Mg# (Fig. 4.5) could be due to igneous fractionation of MORB at mid ocean ridges and the heterogeneous nature of their mantle sources (e.g. Aulbach and Jacob, 2016;

Aulbach et al., 2020). Alternatively, some basaltic eclogites may experience partial melting subsequent to metasomatism, with the melt facilitating diffusional chemical exchange of eclogite with surrounding peridotites (Smart et al., 2009). This eclogite-peridotite interaction may have been coeval with diamond formation at Koidu, as revealed by a trend of decreasing Ca# with increasing Mg# in some eclogitic garnet inclusions (Fig. 4.5). The extent of chemical exchange may depend on the distance of garnets in eclogites from the eclogite-peridotite contact; for instance, garnet inclusions in diamonds 138-12 and 143-1, with the lowest Mg# (both 49.1) and relatively high Ca# (30.3 and 22.5, respectively), may have formed within eclogite at a location farther away from the interaction interface. The garnet inclusion with minor majorite component in diamond 140-2, having low Ca# (10.4) and the highest Mg# (79.0), may be a product of more extensive interaction between eclogite and ambient mantle peridotite, perhaps during redox freezing of slab-derived melts in the convecting sublithospheric mantle (Rohrbach and Schmidt, 2011). Diamond formation during eclogite-peridotite interaction is also consistent with covariations between the oxygen isotope and major element compositions of some garnet inclusions, where $\delta^{18}\text{O}$ values decrease with increasing Mg# and Cr#, and with decreasing Ca# (see Chapter 3).

The absence of diamond-bearing basaltic eclogite xenoliths in Koidu kimberlites may relate to their origin near the base of the lithosphere or beyond, with longer traveling distances to the surface and higher temperatures of mantle residence possibly causing complete disaggregation. Different protoliths for eclogites reconstructed from diamond inclusions (basaltic) and diamond-bearing eclogites (gabbroic) preclude direct comparison of their REE_N patterns. However, gabbroic garnet and omphacite inclusions (although they do not coexist in individual Koidu diamonds in this study) can be compared with the constituent garnet and omphacite grains from the diamond-bearing gabbroic eclogite xenoliths. For construction of REE_N patterns in Figs. 4.7b

and 4.8b, only the most pristine grains (with the lowest abundance of Rb and Ba, indicating minimal contamination by kimberlite) from the xenoliths were used. The higher LREE and lower HREE contents in garnet inclusions relative to xenolith garnets likely relate to crystal-chemical effects, as the much higher CaO contents (16.7–19.3 vs 7.7–11.9 wt%) of the inclusions facilitate higher LREE/HREE ratios (Harte and Kirkley, 1997; Aulbach et al., 2017) due to increased $D_{\text{LREE}}(\text{grt-cpx})$. Omphacite from xenoliths accordingly have higher LREE content compared to omphacite inclusions (Fig. 4.8b) suggesting that the diamond-bearing gabbroic eclogites were subjected to mantle metasomatism, likely by a carbonated, LREE-enriched ultramafic melt (Aulbach et al., 2019) that simultaneously increased the Mg# and decreased the Jd% of the omphacite grains (Fig. 4.3). This metasomatism may have introduced phlogopite, as seen in some diamond-bearing gabbroic eclogites (e.g. KEC-81-DB-1; Hills and Haggerty, 1989; Fig. C.2). Although phlogopite is a common mineral in Koidu kimberlites (Skinner et al., 2004), the low BaO content (0.26 wt%; Hills and Haggerty, 1989) of phlogopites in eclogite xenoliths indicates that their formation pre-dates kimberlite eruption, as kimberlitic phlogopites have much higher BaO contents (e.g. Heaman et al., 2006; Smart et al., 2009).

4.5 Conclusions

The high Mg# (92.2–94.7) of olivine inclusions and the presence of a spinel inclusion with a Cr# (50.9) too low to allow for equilibration with orthopyroxene suggest that the peridotitic diamond substrates in the lithospheric mantle beneath Koidu are highly-depleted dunites/harzburgites, likely having experienced more than 40% melt extraction leading to the exhaustion of orthopyroxene. Spinel inclusions with unusually high TiO₂ (2.8 wt%) in one diamond indicate metasomatic Ti re-enrichment, likely by infiltration of ultramafic (proto-

kimberlitic) melts into peridotitic diamond substrates. This melt metasomatic process may have converted some dunites/harzburgites back to lherzolites, which dominate the xenocryst population at Koidu (Skinner et al., 2004).

The principal diamond substrate beneath Koidu is eclogite (delivering 78% of all diamonds), and its formation was associated with subduction of oceanic crust at the margin of the West African Craton. Eclogitic garnet and omphacite inclusions with positive and negative Eu-anomalies in Koidu diamonds are indicative of diamond formation associated with gabbroic and basaltic layers of oceanic crust. Eclogites with gabbroic and basaltic protoliths may be the preferable eclogitic diamond substrates at shallower and deeper depths in the mantle, respectively, as geothermobarometry indicates diamond-bearing (gabbroic) eclogite xenoliths to have shallower equilibration conditions ($T = 1040\text{--}1220\text{ }^{\circ}\text{C}$; $P = 4.9\text{--}6.0\text{ GPa}$) than diamonds with coexisting (basaltic) garnet and omphacite inclusions ($T \geq 1270\text{ }^{\circ}\text{C}$; $P \geq 6.3\text{ GPa}$). The calculated temperature-pressure range of diamond-bearing gabbroic eclogites overlaps with that of peridotitic diamonds ($T = 880\text{--}1240\text{ }^{\circ}\text{C}$; $P = 3.9\text{--}6.1\text{ GPa}$), suggesting that at least a subset of eclogitic and peridotitic diamonds formed at similar depths beneath Koidu.

The following conclusions can be drawn based on the characteristics of eclogitic inclusions in diamonds and diamond-bearing eclogites from Koidu:

- (1) The presence of kyanite and corundum inclusions suggests that the host eclogites were Al-rich. However, they were unlikely to be derived from plagioclase-rich gabbroic protoliths, as the coexisting garnet inclusions have high $\delta^{18}\text{O}$ values (+11.8 to +11.9 ‰) indicative of low-pressure basaltic protoliths that experienced seawater alteration at low temperatures. Thus, kyanite formation may relate to infiltration of silicate melts derived from pelitic sediments into host eclogites.

- (2) Batch melting modelling of reconstructed whole-rock compositions, based on coexisting garnet and omphacite inclusions in six diamonds, suggests that the basaltic eclogite diamond substrates experienced a high-degree of melt extraction (> 20% batch melting). This contradicts the large abundance of coesite, in 44% of studied diamonds, as coesite should be removed at high-degree melting. Thus, it is possible that coesite was added to eclogites through metasomatism, e.g., coesite formed from carbonation of clinopyroxene in eclogites by a CO₂-rich fluid. Strong LREE/MREE fractionation for a subset of samples cannot be matched by single stage batch melting models and likely reflect repeated stages of batch melting (e.g., two to four stages of extraction of 5% melt increments).
- (3) Reconstructed whole-rocks from coexisting garnet and omphacite inclusions in four diamonds show various degrees of LREE re-enrichment after melt depletion. Strong positive Sr anomalies ($[Sr/Sr^*]_N = 8.12\text{--}16.74$) that positively correlate with La contents in reconstructed whole-rocks indicate a metasomatic event that affected the eclogitic substrates prior to or coeval with diamond formation.
- (4) Omphacites from diamond-bearing gabbroic eclogite xenoliths have higher LREE contents compared to gabbroic omphacite inclusions from diamonds, suggesting that the diamond-bearing gabbroic eclogites were metasomatized, possibly by infiltration of a carbonated, LREE-enriched ultramafic melt, which may have introduced phlogopite to these eclogite xenoliths. The diamond inclusions may have been shielded from these effects if the metasomatism post-dated diamond formation.

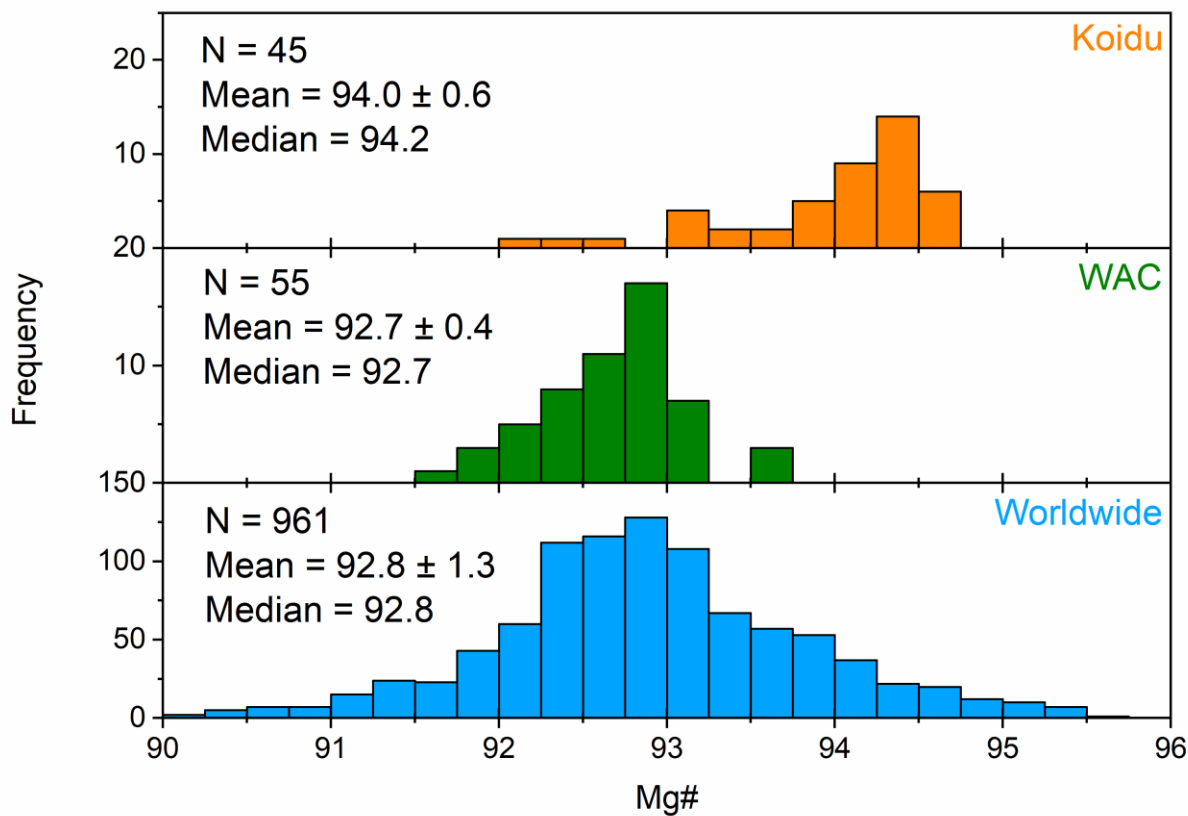


Figure 4.1 Histograms of molar Mg# [$100 \times \text{Mg}/(\text{Mg} + \text{Fe})$] of olivine inclusions in diamonds from Koidu (bin size = 0.25). Also shown are olivine inclusions in diamonds from Akwatia and Kan Kan (West African Craton) and diamonds worldwide. The number of analyzed olivine inclusion (N), the mean (± 1 standard deviation) and median values for each histogram are shown.

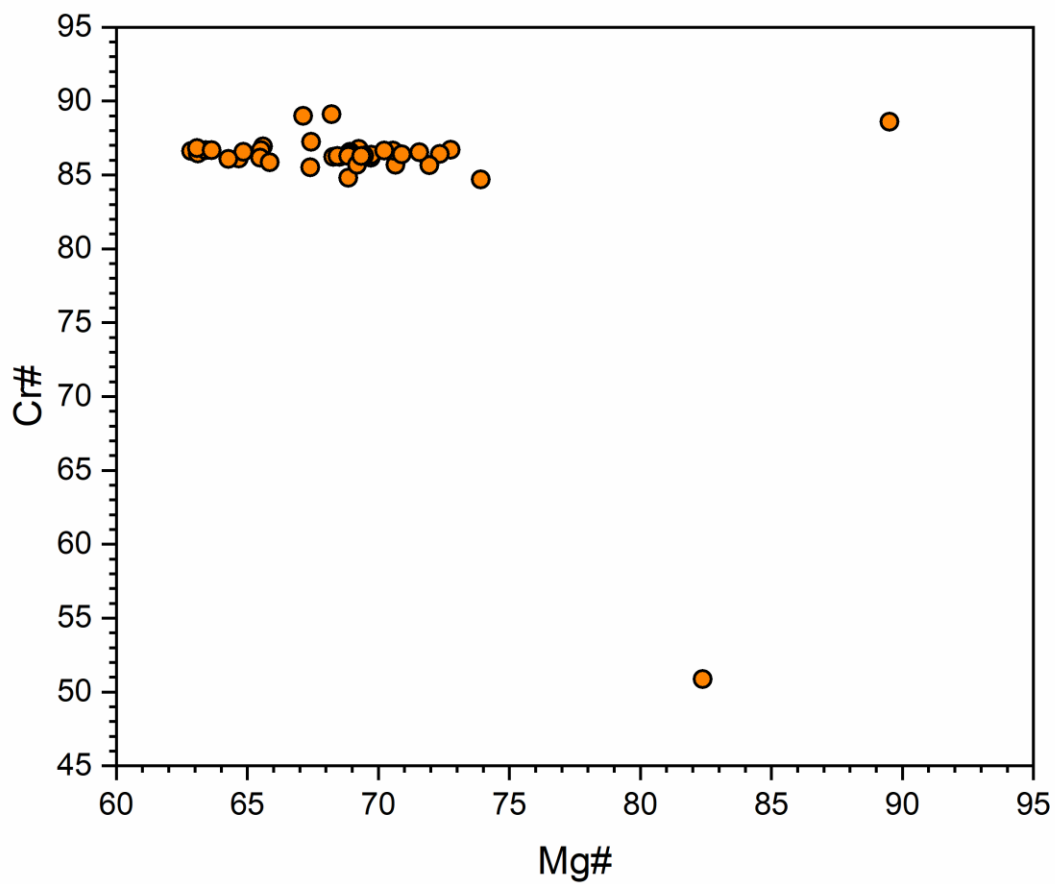


Figure 4.2 Molar Cr# [$100 \times \text{Cr}/(\text{Cr} + \text{Al})$] vs molar Mg# [$100 \times \text{Mg}/(\text{Mg} + \text{Fe}^{2+})$] of spinel inclusions in Koidu diamonds, where Fe^{2+} is calculated based on the stoichiometric method of Droop (1987).

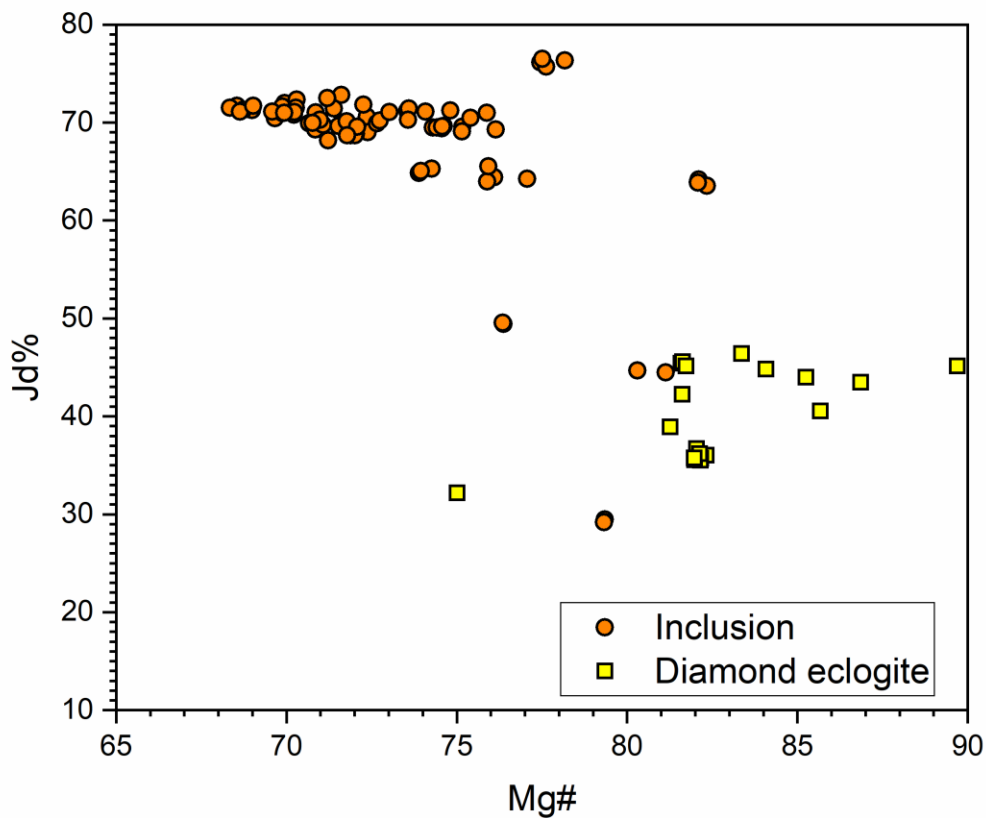


Figure 4.3 Jadeite component [Jd%; $100 \times 2\text{Na} / (2\text{Na} + \text{Ca} + \text{Mg} + \text{Fe})$] vs molar Mg# of omphacite inclusions in Koidu diamonds, compared with omphacites from Koidu diamondiferous eclogite xenoliths (including data from this study and Hills and Haggerty (1989)).

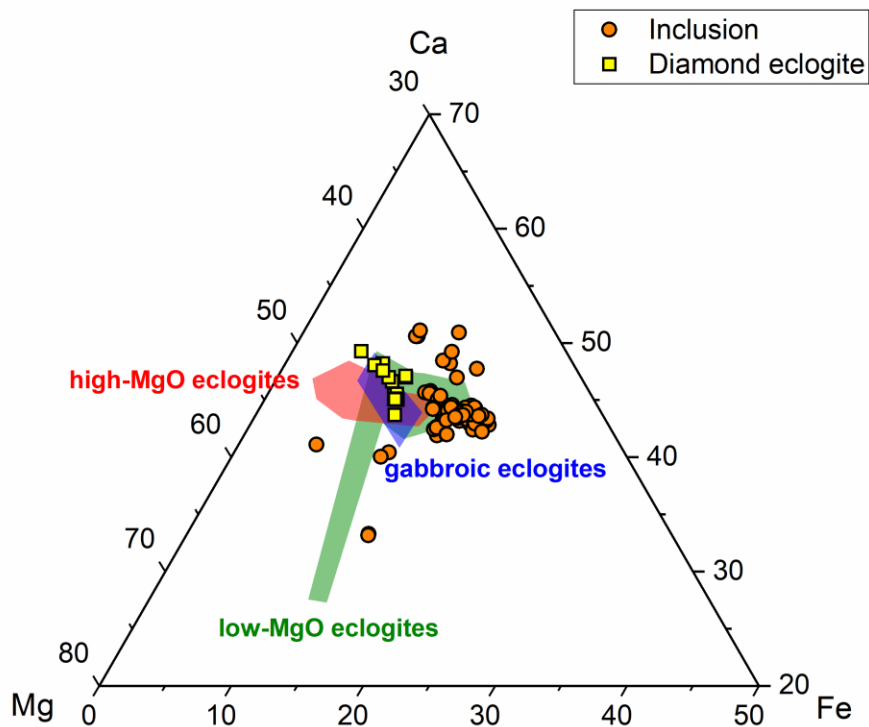


Figure 4.4 Ternary diagram of molar Ca-Mg-Fe of omphacite from Koidu included in diamonds and from Koidu diamondiferous eclogite xenoliths (Hills and Haggerty, 1989 and this study). Also shown are the compositional fields of omphacite grains from low-MgO (green), high-MgO (red) and gabbroic (blue) bimineralic eclogites (Aulbach et al., 2019).

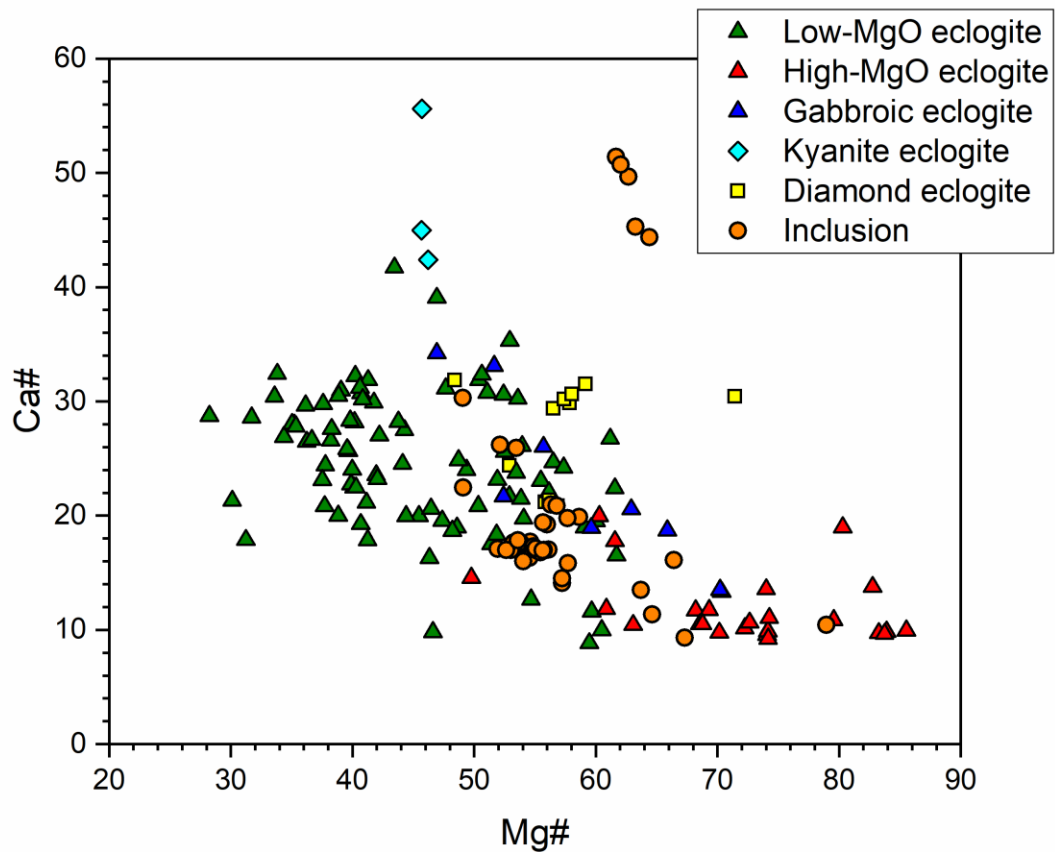


Figure 4.5 Molar Ca# vs Mg# of garnets from Koidu diamonds, diamondiferous eclogites (data from this study and Hills and Haggerty, 1989), kyanite eclogites (Hills and Haggerty, 1989) and bimineralec eclogites including low-MgO, high-MgO and gabbroic eclogites (Hills and Haggerty, 1989; Fung and Haggerty, 1995; Aulbach et al., 2019).

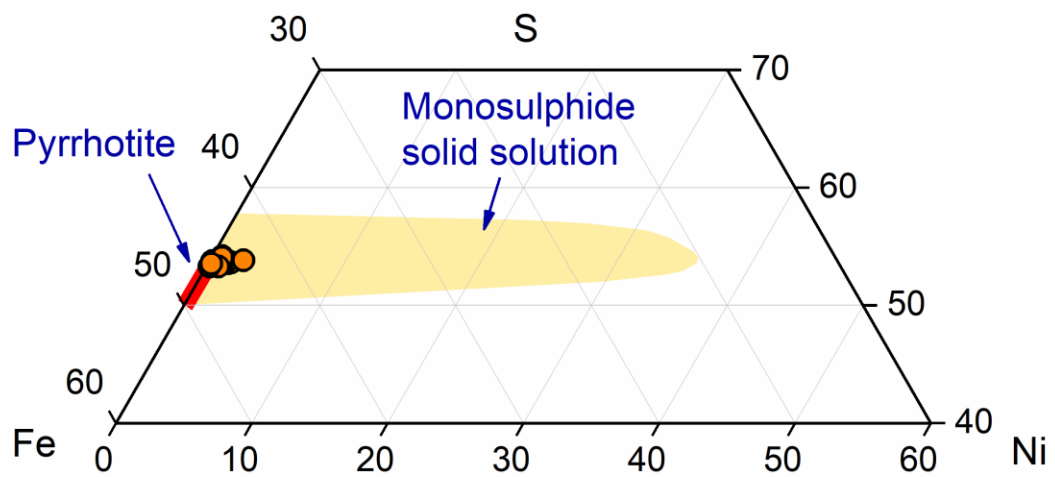
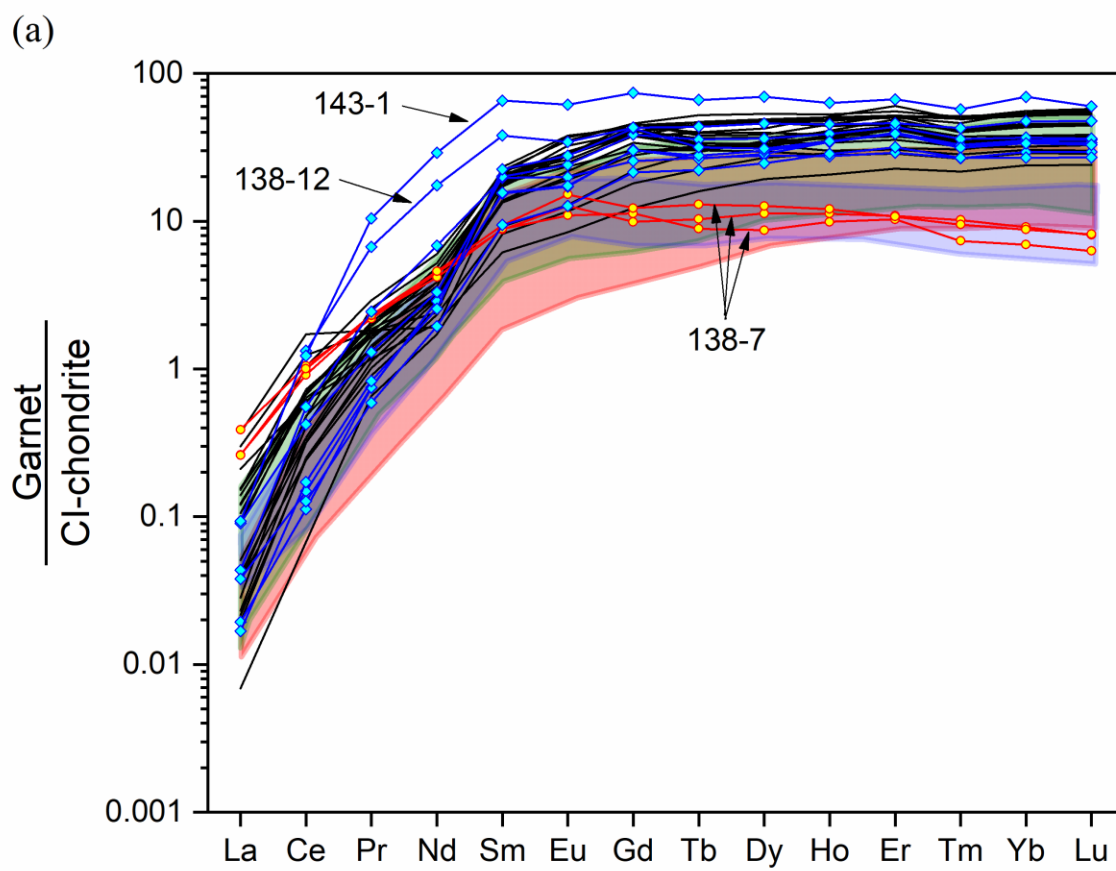


Figure 4.6 Fe-Ni-S (atomic proportions) quadrilateral for sulphide inclusions from Koidu. Compositional fields of pyrrhotite (red) and monosulphide solid solution (MSS; beige) are indicated.



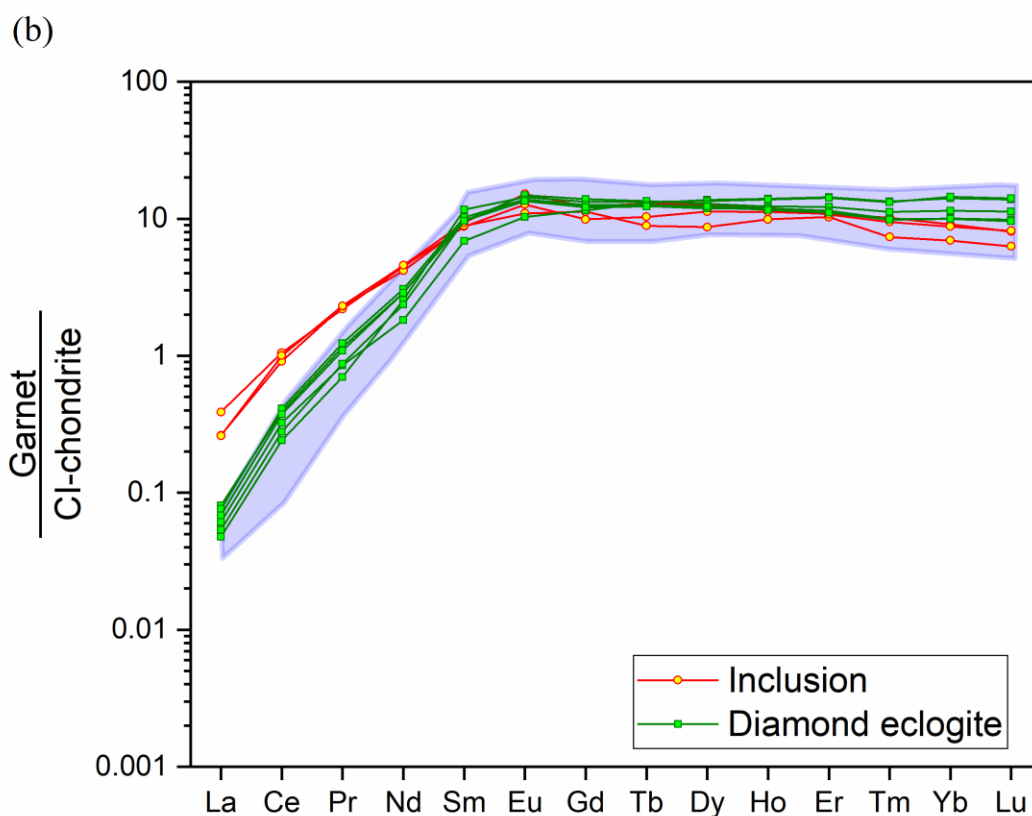
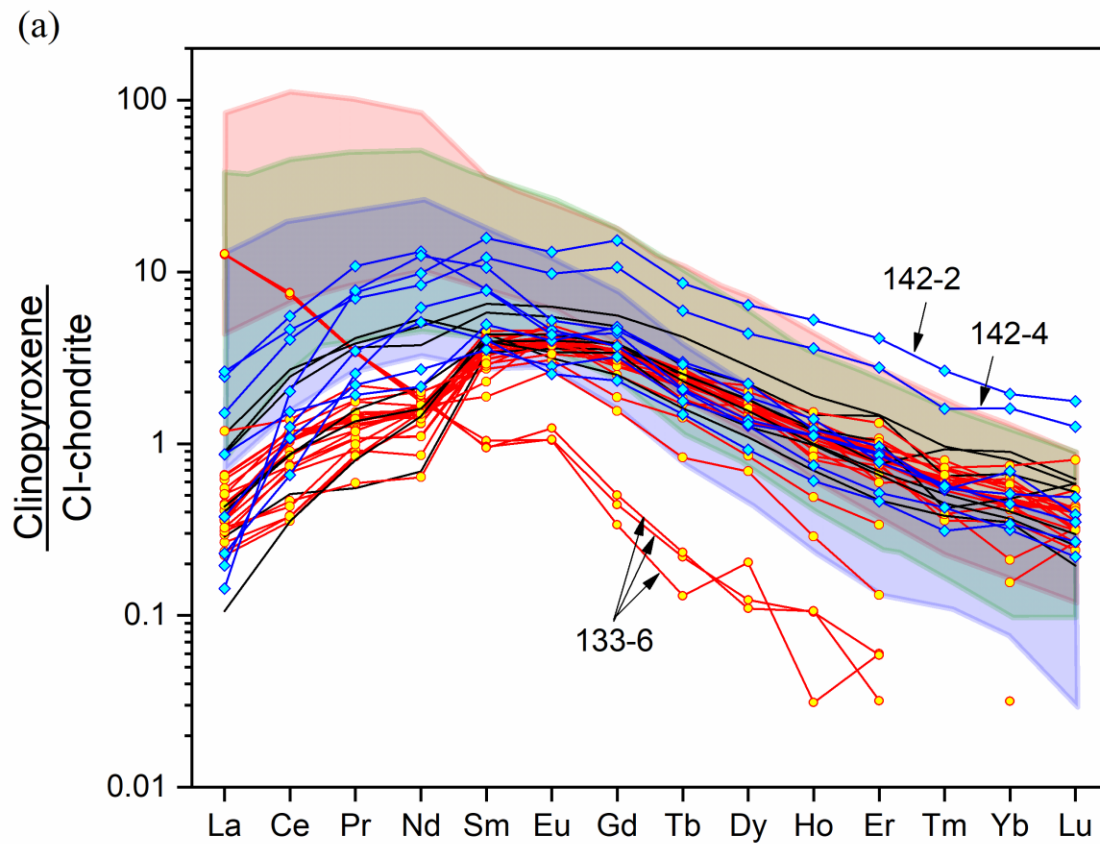


Figure 4.7 (a) REE concentrations in garnet inclusions from Koidu, normalized to CI-chondrite (McDonough and Sun, 1995). Garnet inclusions with positive, negative and no discernible Eu anomalies are represented by red, blue and black lines, respectively. Garnets in diamonds 138-12 and 143-1 have the highest $\sum\text{REE}$ and are characterized by flat $\text{MREE}_N\text{--HREE}_N$ slopes. Compositional fields of garnet grains from Koidu biminerals eclogites including low-MgO (green), high-MgO (red) and gabbroic eclogites (blue) are shown for comparison (Aulbach et al., 2019). (b) REE concentrations in garnets from Koidu diamondiferous eclogite xenoliths, normalized to CI-chondrite (McDonough and Sun, 1995). All garnets have positive Eu anomalies and low $\sum\text{HREE}$, similar to the garnet inclusions from the mixed paragenesis diamond 138-7 (shown in red), and fall in the compositional field of garnets from Koidu gabbroic eclogite xenoliths of Aulbach et al. (2019; blue).



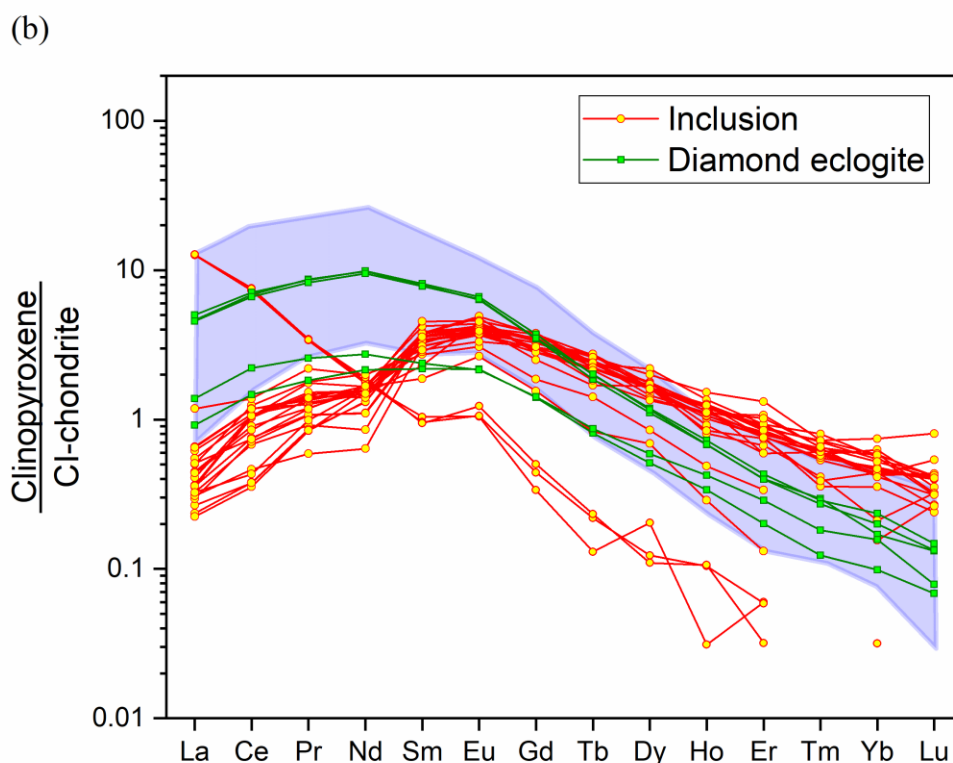


Figure 4.8 (a) REE concentrations in omphacite inclusions from Koidu diamonds, normalized to CI-chondrite (McDonough and Sun, 1995). Omphacite inclusions with positive, negative and no discernible Eu anomalies are represented by red, blue and black lines, respectively. Compositional fields of omphacites from biminerals eclogites, including low-MgO (green), high-MgO (red) and gabbroic eclogites (blue), are shown for comparison (Aulbach et al., 2019). Omphacites in diamonds 142-2 and 142-4 have the highest Σ REE, where their HREE contents are above the compositional fields of Aulbach et al. (2019). (b) REE concentrations in omphacite grains from Koidu diamondiferous eclogite xenoliths (green), normalized to CI-chondrite (McDonough and Sun, 1995). These omphacite grains have positive Eu anomalies and largely overlap with the compositional field of omphacites from Koidu gabbroic eclogite xenoliths of Aulbach et al. (2019). Compared to omphacite inclusions from Koidu diamonds (red) with positive Eu anomalies, omphacites from xenoliths generally have higher LREE and lower HREE contents.

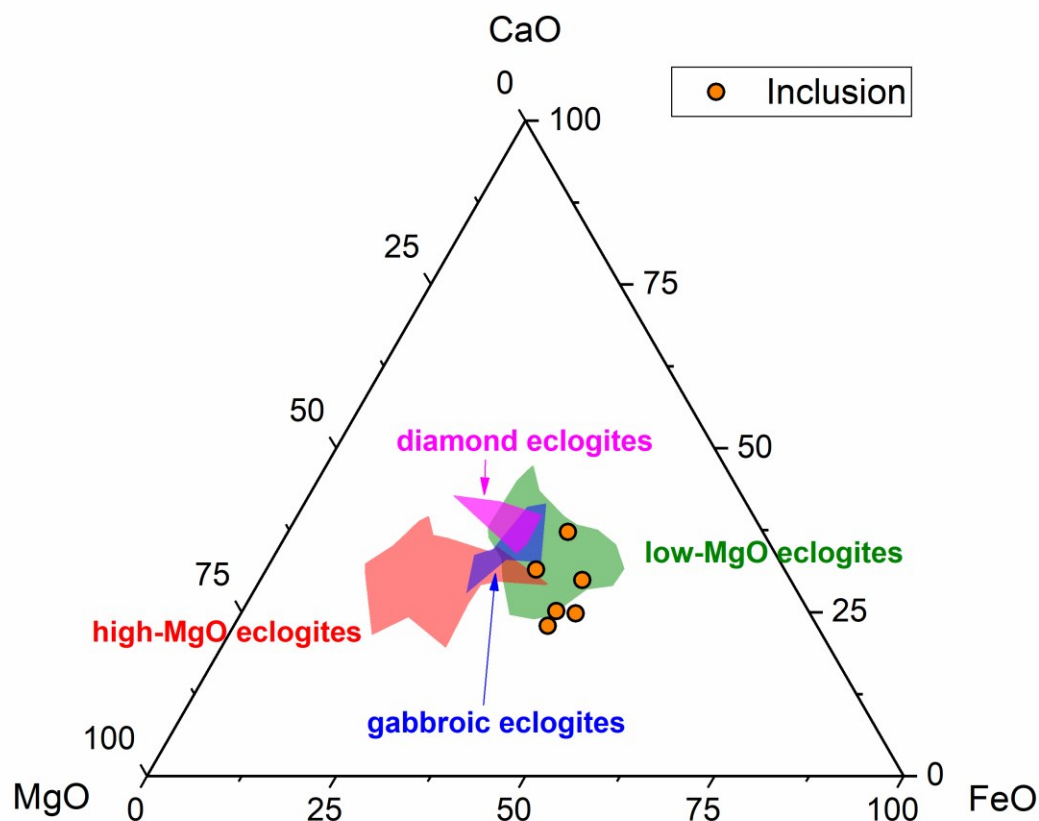


Figure 4.9 CaO-MgO-FeO (based on wt%) ternary diagram for bulk rock compositions reconstructed from coexisting garnet and omphacite inclusions in six Koidu diamonds. Also shown are the compositional fields of reconstructed biminerals eclogites, including low-MgO (green), high-MgO (red) and gabbroic eclogites (blue) (Aulbach et al., 2019), and reconstructed diamondiferous eclogites (magenta; data from this study and Hills and Haggerty, 1989).

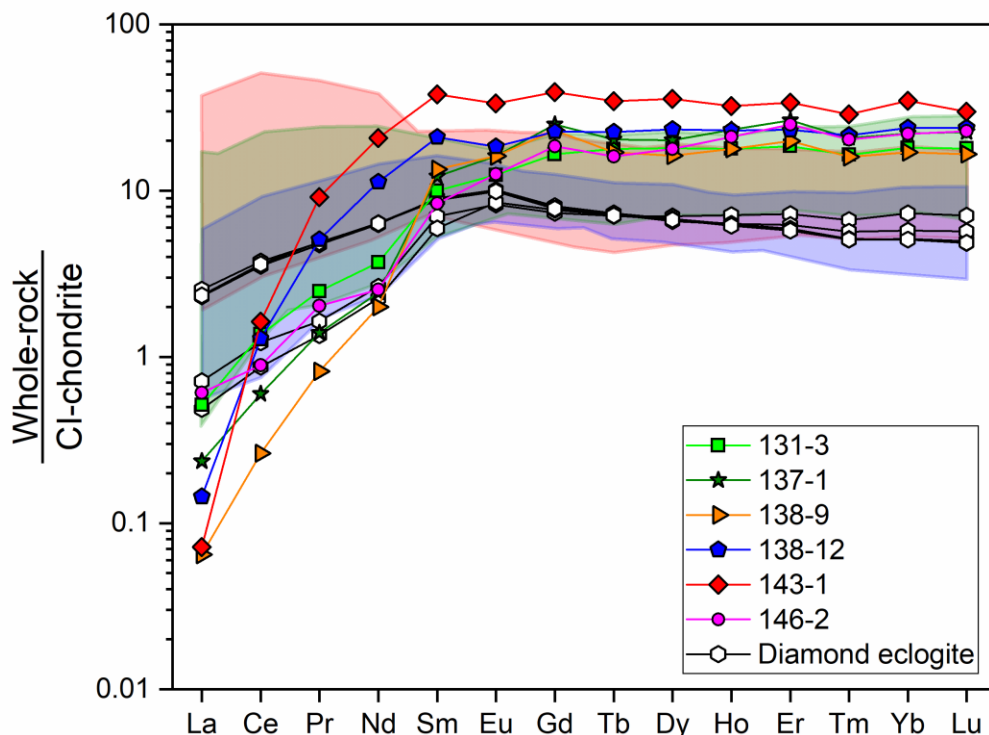


Figure 4.10 REE concentrations in whole-rocks reconstructed from coexisting garnet and omphacite inclusions assuming a modal ratio of 50:50. Two reconstructed bulk rocks (diamond 138-12 and 143-1) show negative Eu anomalies, the others have no discernible Eu anomalies. Compositional fields of bimineralic eclogites, including low-MgO (green), high-MgO (red) and gabbroic eclogites (blue), are shown for comparison (Aulbach et al., 2019). The whole-rock reconstructed from diamond 143-1 has the highest HREE contents, falling above the xenolith-based fields. All reconstructed bulk compositions have steep positive LREEN slopes, with samples 131-1, 137-1, 138-9 and 146-2 show an inflection at Nd, with shallower slopes from La to Pr. Also shown are whole-rocks reconstructed from garnet and omphacite in diamondiferous eclogite xenoliths, which have REE contents well within the compositional field of gabbroic eclogites of Aulbach et al. (2019).

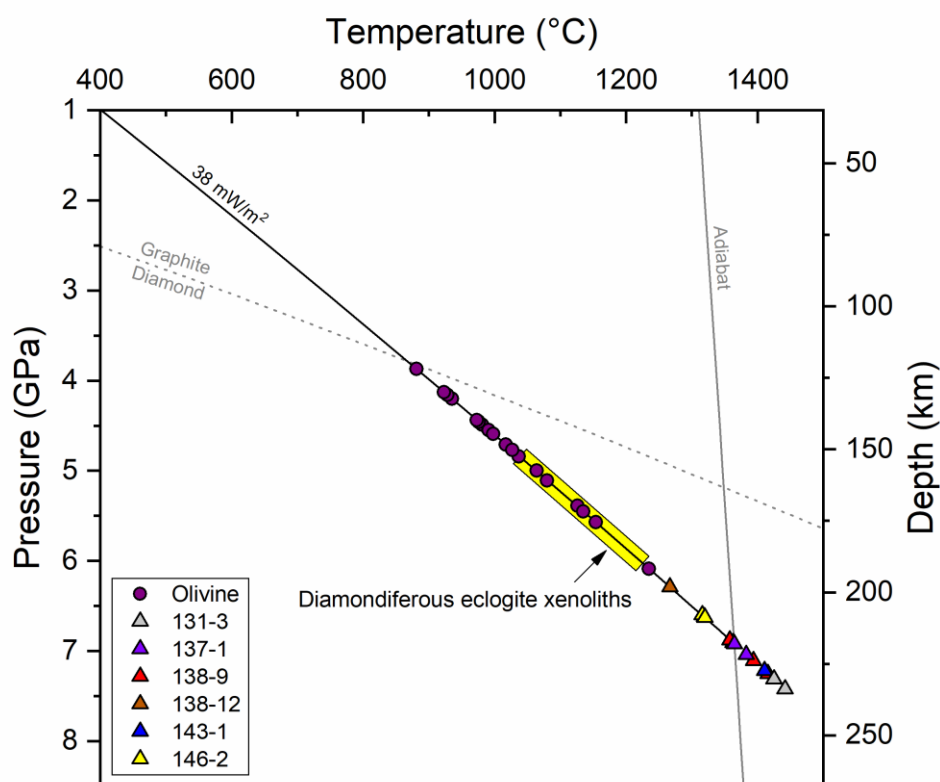
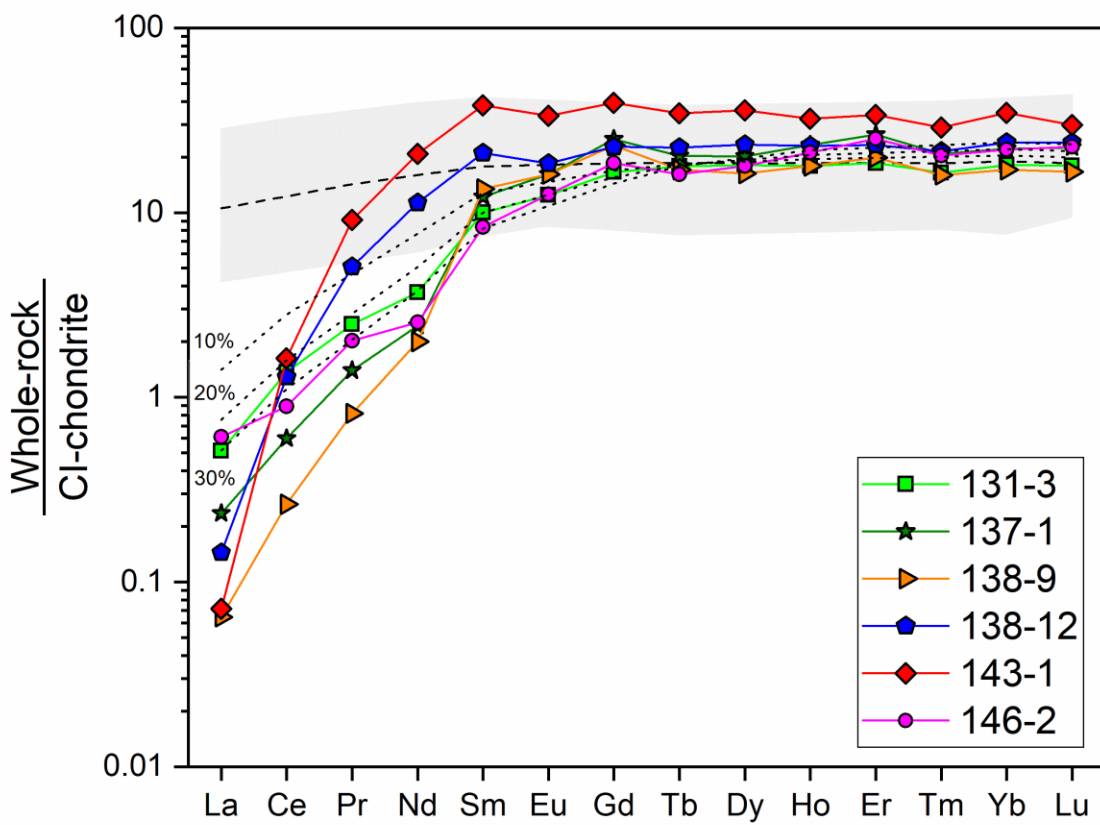


Figure 4.11 Equilibration temperatures for 19 forsteritic olivine-included diamonds and six diamonds with non-touching pairs of eclogitic garnet and omphacite inclusions, calculated using the Al-in-olivine (Bussweiler et al., 2017) and garnet-clinopyroxene Mg-Fe exchange thermometers (Krogh, 1988), respectively. Pressures are derived through projection of the two geothermometers on the local model geotherm of 38 mW/m² (Hasterok and Chapman, 2011), which was established based on geothermobarometry using Cr-diopside xenocrysts from the Koidu kimberlite complex (Smit et al., 2016). The graphite-diamond transition curve is from Day (2012). The mantle adiabat corresponding to a potential temperature of 1300 °C with a gradient of 0.3 °C/km is after Hasterok and Chapman (2011). All olivine-included diamonds and diamondiferous eclogite xenoliths (except for one outlier; field in yellow; mineral chemistry data from Hills and Haggerty, 1989 and this study) have equilibration temperatures within the diamond stability field, whereas four out of six eclogitic diamonds yield temperatures on the mantle adiabat or higher.

(a)



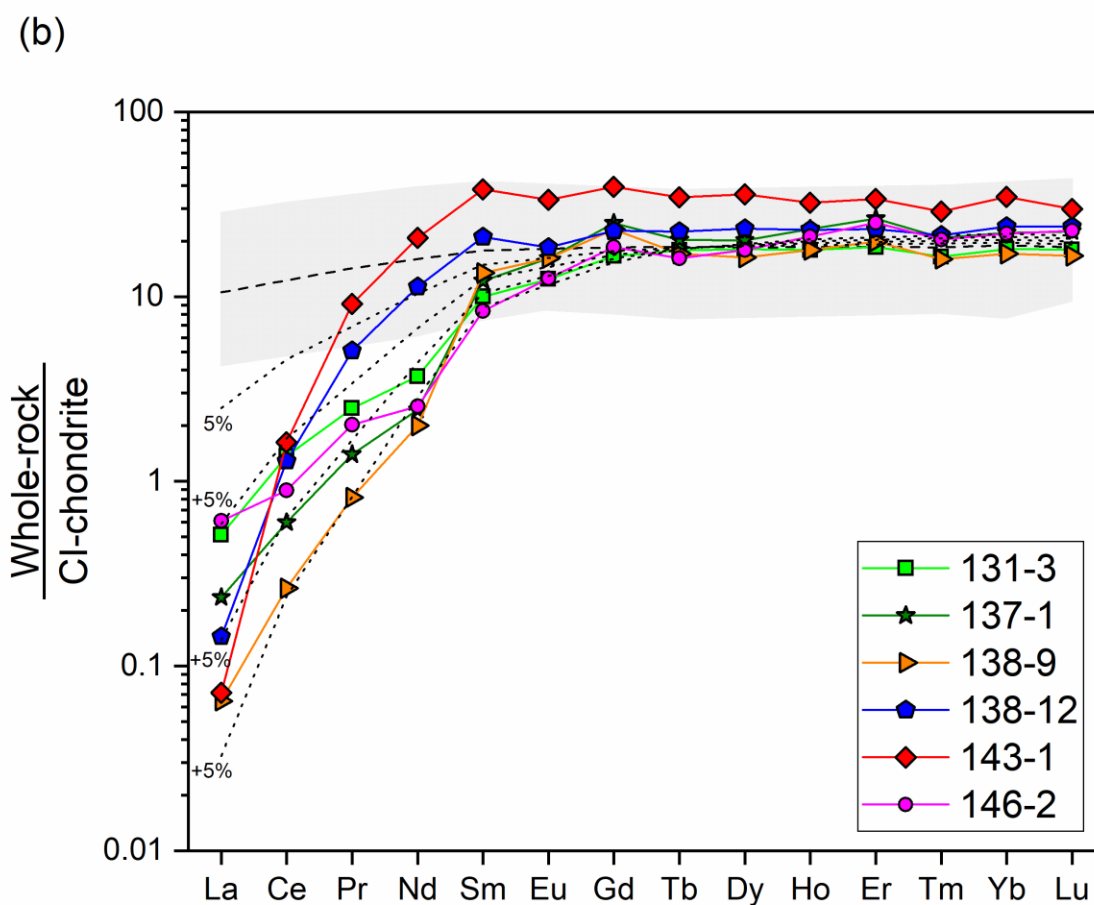


Figure 4.12 REE_N patterns of reconstructed whole-rocks from garnet and omphacite inclusions in six Koidu diamonds (garnet/omphacite ratio of 50:50) compared to the compositions of average NMORB (black dashed line; Sun and McDonough, 1989) and lavas and sheeted dikes from the Oman ophiolite complex (grey field; Alabaster et al., 1982; outliers removed). Also shown are residue compositions (dotted lines) from an NMORB starting composition after (a) 10 to 30% batch melt extraction in the eclogite stability field and (b) successive extraction of 5% batch melting increments. Mineral/melt partition coefficients are from Green et al. (2000).

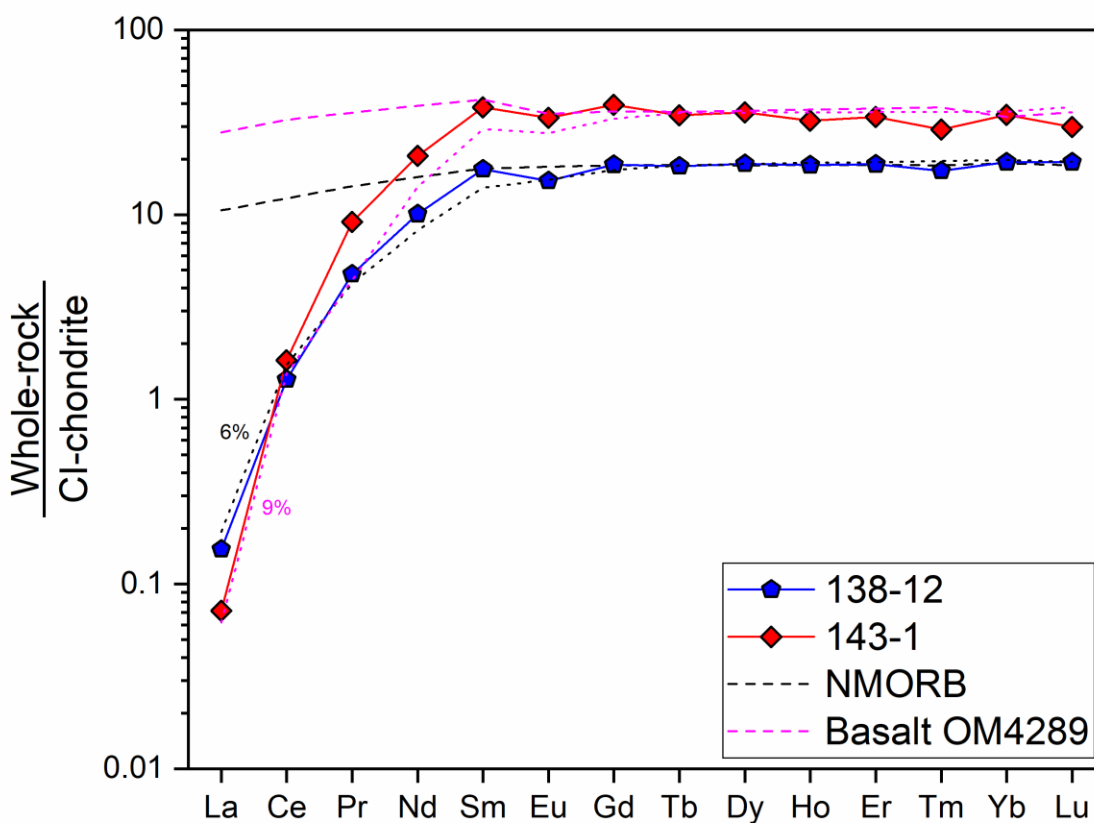


Figure 4.13 Fractional melting residues compared to REE_N patterns of reconstructed whole-rocks from diamonds 138-12 and 143-1. Garnet/omphacite ratio of sample 138-12 was adjusted to 40:60, to achieve a REE_N pattern similar to the residue (black dotted line) modelled for 6% fractional melting from NMORB (black dashed line). Basalt OM4289 from the Oman ophiolite complex (magenta dashed line) was chosen as the starting composition for melt depletion modelling of sample 143-1 and produces a good match for 9% fractional melting (magenta dotted line). Mineral/melt partition coefficients are from Green et al. (2000).

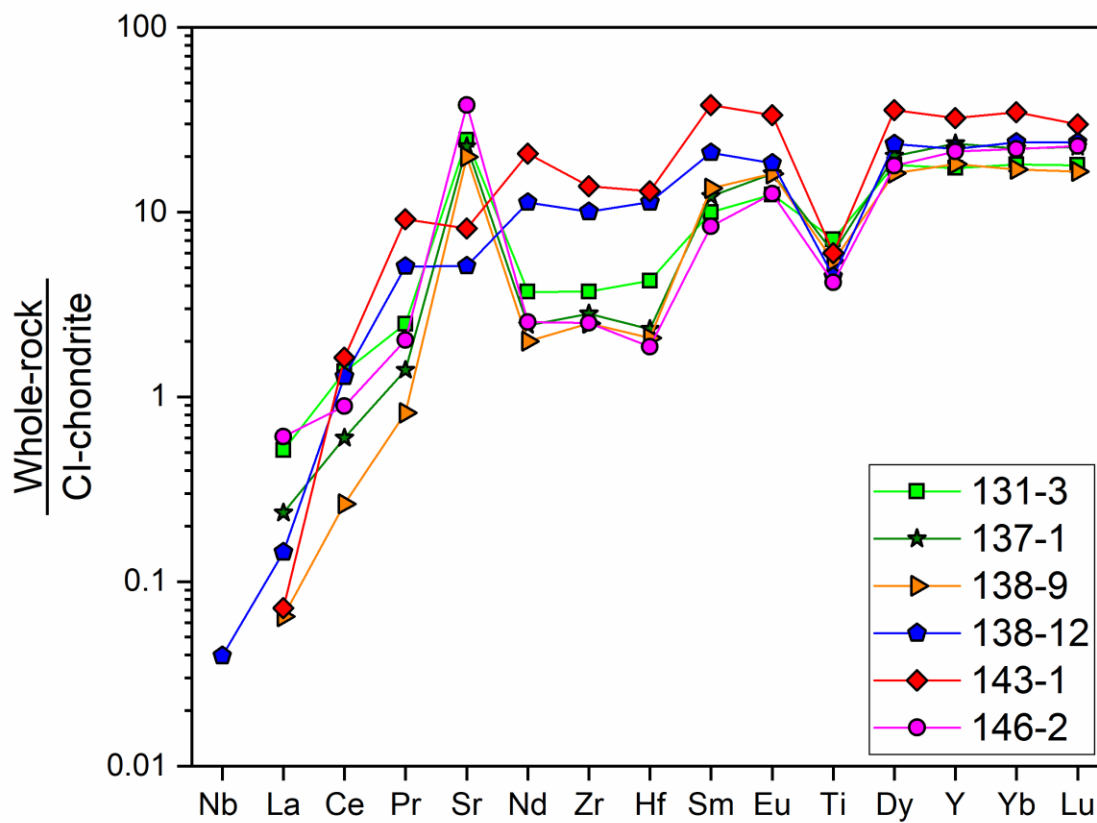


Figure 4.14 Extended trace element patterns for whole-rocks reconstructed from garnet and omphacite inclusions in six Koidu diamonds (garnet/omphacite ratio of 50:50), normalized to CI-chondrite (McDonough and Sun, 1995).

References

- Akizuki M. (1989) Growth structure and crystal symmetry of grossular garnets from the Jeffrey mine, Asbestos, Quebec, Canada. *Am. Mineral.* **74**, 859–864.
- Alabaster T., Pearce J. A. and Malpas J. (1982) The volcanic stratigraphy and petrogenesis of the Oman ophiolite complex. *Contrib. to Mineral. Petrol.* **81**, 168–183.
- Aulbach S. and Jacob D. E. (2016) Major- and trace-elements in cratonic mantle eclogites and pyroxenites reveal heterogeneous sources and metamorphic processing of low-pressure protoliths. *Lithos* **262**, 586–605.
- Aulbach S. and Arndt N. T. (2019) Eclogites as palaeodynamic archives: evidence for warm (not hot) and depleted (but heterogeneous) Archaean ambient mantle. *Earth Planet. Sci. Lett.* **505**, 162–172.
- Aulbach S., Stachel T., Viljoen K. S., Brey G. P. and Harris J. W. (2002) Eclogitic and websteritic diamond sources beneath the Limpopo Belt - Is slab-melting the link? *Contrib. to Mineral. Petrol.* **143**, 56–70.
- Aulbach S., Gerdes A. and Viljoen K. S. (2016) Formation of diamondiferous kyanite-eclogite in a subduction mélange. *Geochim. Cosmochim. Acta* **179**, 156–176.
- Aulbach S., Jacob D. E., Cartigny P., Stern R. A., Simonetti S. S., Wörner G. and Viljoen K. S. (2017) Eclogite xenoliths from Orapa: ocean crust recycling, mantle metasomatism and carbon cycling at the western Zimbabwe craton margin. *Geochim. Cosmochim. Acta* **213**, 574–592.
- Aulbach S., Höfer H. E. and Gerdes A. (2019) High-Mg and low-Mg mantle eclogites from

- Koidu (West African Craton) linked by Neoproterozoic ultramafic melt metasomatism of subducted archaean plateau-like oceanic crust. *J. Petrol.* **60**, 723–754.
- Aulbach S., Massuyeau M., Garber J. M., Gerdes A., Heaman L. M. and Viljoen K. S. (2020) Ultramafic carbonated melt- and auto-metasomatism in mantle eclogites: compositional effects and geophysical consequences. *Geochemistry, Geophys. Geosystems* **21**, 1–27.
- Baertschi P. (1976) Absolute ^{18}O content of standard mean ocean water. *Earth Planet. Sci. Lett.* **31**, 341–344.
- Barth M. G., Rudnick R. L., Horn I., McDonough W. F., Spicuzza M. J., Valley J. W. and Haggerty S. E. (2001) Geochemistry of xenolithic eclogites from West Africa, part I: A link between low MgO eclogites and archaean crust formation. *Geochim. Cosmochim. Acta* **65**, 1499–1527.
- Barth M. G., Rudnick R. L., Horn I., McDonough W. F., Spicuzza M. J., Valley J. W. and Haggerty S. E. (2002) Geochemistry of xenolithic eclogites from West Africa, part 2: origins of the high MgO eclogites. *Geochim. Cosmochim. Acta* **66**, 4325–4345.
- Bartholomé P. (1960) Genesis of the Gore Mountain garnet deposit, New York. *Econ. Geol.* **55**, 255–277.
- Beinlich A., Klemd R., John T. and Gao J. (2010) Trace-element mobilization during Ca-metasomatism along a major fluid conduit: eclogitization of blueschist as a consequence of fluid-rock interaction. *Geochim. Cosmochim. Acta* **74**, 1892–1922.
- Bernstein S., Kelemen P. B. and Hanghøj K. (2007) Consistent olivine Mg# in cratonic mantle reflects Archean mantle melting to the exhaustion of orthopyroxene. *Geology* **35**, 459–462.

- Beyer C. and Frost D. J. (2017) The depth of sub-lithospheric diamond formation and the redistribution of carbon in the deep mantle. *Earth Planet. Sci. Lett.* **461**, 30–39.
- Bohlen S. R. and Boettcher A. L. (1982) The quartz-coesite transformation: a precise determination and the effects of other components. *J. Geophys. Res.* **87**, 7073–7078.
- Bulanova G. P., Griffin W. L., Ryan C. G., Shestakova O. Y. and Barnes S. J. (1996) Trace elements in sulfide inclusions from Yakutian diamonds. *Contrib. to Mineral. Petrol.* **124**, 111–125.
- Bussweiler Y., Brey G. P., Pearson D. G., Stachel T., Stern R. A., Hardman M. F., Kjarsgaard B. A. and Jackson S. E. (2017) The aluminum-in-olivine thermometer for mantle peridotites — Experimental versus empirical calibration and potential applications. *Lithos* **272–273**, 301–314.
- Collerson K. D., Williams Q., Kamber B. S., Omori S., Arai H. and Ohtani E. (2010) Majoritic garnet: a new approach to pressure estimation of shock events in meteorites and the encapsulation of sub-lithospheric inclusions in diamond. *Geochim. Cosmochim. Acta* **74**, 5939–5957.
- Dawson J. B. (1984) Contrasting types of upper-mantle metasomatism? In *Kimberlites II: The Mantle and Crust-Mantle Relationships*, pp. 289–294.
- Day H. W. (2012) A revised diamond-graphite transition curve. *Am. Mineral.* **97**, 52–62.
- Deines P. and Harris J. W. (1995) Sulfide inclusion chemistry and carbon isotopes of African diamonds. *Geochim. Cosmochim. Acta* **59**, 3173–3188.
- Deines P. and Haggerty S. E. (2000) Small-scale oxygen isotope variations and petrochemistry

- of ultradeep (>300 km) and transition zone xenoliths. *Geochim. Cosmochim. Acta* **64**, 117–131.
- Droop, G. T. R. (1987) A general equation for estimating Fe³⁺ concentrations in ferromagnesian silicates and oxides from microprobe analyses, using stoichiometric criteria. *Mineral. Mag.* **51**, 431–435.
- Fung A. T. and Haggerty S. E. (1995) Petrography and mineral compositions of eclogites from the Koidu kimberlite complex, Sierra Leone. *J. Geophys. Res.* **100**.
- Green T. H. and Ringwood A. E. (1968) Genesis of the calc-alkaline igneous rock suite. *Contrib. to Mineral. Petrol.* **18**, 105–162.
- Green T. H., Blundy J. D., Adam J. and Yaxley G. M. (2000) SIMS determination of trace element partition coefficients between garnet, clinopyroxene and hydrous basaltic liquids at 2–7.5 GPa and 1080–1200°C. *Lithos* **53**, 165–187.
- Gregory R. T. and Taylor H. P. (1981) An oxygen isotope profile in a section of Cretaceous oceanic crust, Samail ophiolite, Oman: evidence for δ¹⁸O buffering of the oceans by deep (>5 km) seawater-hydrothermal circulation at mid-ocean ridges. *J. Geophys. Res. Solid Earth* **86**, 2737–2755.
- Grütter H. S., Gurney J. J., Menzies A. H. and Winter F. (2004) An updated classification scheme for mantle-derived garnet, for use by diamond explorers. *Lithos* **77**, 841–857.
- Gurney J. J. (1984) A correlation between garnets and diamonds in kimberlites. *Publ. Geol. Dep. Univ. Extension. Univ. West. Aust. Perth*, pp. 143–166.
- Harder M., Nowicki T. E., Hetman C. M., Freeman L. and Abedu B. (2013) Geology and

- evaluation of the K2 kimberlite, Koidu Mine, Sierra Leone, West Africa. *Proc. 10th Int. Kimberl. Conf.*, 191–208.
- Harte B. and Kirkley M. B. (1997) Partitioning of trace elements between clinopyroxene and garnet: data from mantle eclogites. *Chem. Geol.* **136**, 1–24.
- Hasterok D. and Chapman D. S. (2011) Heat production and geotherms for the continental lithosphere. *Earth Planet. Sci. Lett.* **307**, 59–70.
- Heaman L. M., Creaser R. A., Cookenboo H. O. and Chacko T. (2006) Multi-stage modification of the northern Slave mantle lithosphere: evidence from zircon- and diamond-bearing eclogite xenoliths entrained in Jericho Kimberlite, Canada. *J. Petrol.* **47**, 821–858.
- Hills D. V. and Haggerty S. E. (1989) Petrochemistry of eclogites from the Koidu kimberlite complex, Sierra Leone. *Contrib. to Mineral. Petrol.* **103**, 397–422.
- Hunt L., Stachel T., McCandless T. E., Armstrong J. and Muelenbachs K. (2012) Diamonds and their mineral inclusions from the Renard kimberlites in Quebec. *Lithos* **142–143**, 267–284.
- Ickert R. B. and Stern R. A. (2013) Matrix corrections and error analysis in high-precision SIMS $^{18}\text{O}/^{16}\text{O}$ measurements of Ca-Mg-Fe garnet. *Geostand. Geoanalytical Res.* **37**, 429–448.
- Jaques A., Hall A., Sheraton J., Smith C., Sun S.S., Drew R., Foudoulis C. and Ellingsen K. (1989) Composition of crystalline inclusions and C-isotopic composition of Argyle and Ellendale diamonds. *Ross J. al. Kimberlites Relat. rocks GSA Spec Publ 14, vol 2. Blackwell, Carlt.*, pp. 966–989.
- Jerde E. A., Taylor L. A., Crozaz G., Sobolev N. V. and Sobolev V. N. (1993) Diamondiferous eclogites from Yakutia, Siberia: evidence for a diversity of protoliths. *Contrib. to Mineral.*

Petrol. **114**, 189–202.

Knoche R., Sweeney R. J. and Luth R. W. (1999) Carbonation and decarbonation of eclogites: the role of garnet. *Contrib. to Mineral. Petrol.* **135**, 332–339.

Krogh E. J. (1988) The garnet-clinopyroxene Fe-Mg geothermometer - a reinterpretation of existing experimental data. *Contrib. to Mineral. Petrol.* **99**, 44–48.

Labrosse S. and Jaupart C. (2007) Thermal evolution of the Earth: secular changes and fluctuations of plate characteristics. *Earth Planet. Sci. Lett.* **260**, 465–481.

Lai M. Y., Stachel T., Stern R. A., Hardman M. F., Pearson D. G. and Harris J. W. (2022) Formation of mixed paragenesis diamonds during multistage growth – constraints from in situ $\delta^{13}\text{C}$ – $\delta^{15}\text{N}$ –[N] analyses of Koidu diamonds. *Geochim. Cosmochim. Acta* **323**, 20–39.

Luth R. W. (1993) Diamonds, eclogites, and the oxidation state of the earth's mantle. *Science* **261**, 66–68.

MacGregor I. D. and Carter J. L. (1970) The chemistry of clinopyroxenes and garnets of eclogite and peridotite xenoliths from the Roberts Victor Mine, South Africa. *Phys. Earth Planet. Inter.* **3**, 391–397.

Mattey D., Lowry D. and Macpherson C. (1994) Oxygen isotope composition of mantle peridotite. *Earth Planet. Sci. Lett.* **128**, 231–241.

Mc Kenna N., Gurney J. J., Klump J. and Davidson J. M. (2004) Aspects of diamond mineralisation and distribution at the Helam Mine, South Africa. *Lithos* **77**, 193–208.

McDonough W. F. and Sun S. S. (1995) The composition of the Earth. *Chem. Geol.* **120**, 223–253.

- Meyer H. O. A. and Boyd F. R. (1972) Composition and origin of crystalline inclusions in natural diamonds. *Geochim. Cosmochim. Acta* **36**, 1255–1273.
- Morimoto N. (1988) Nomenclature of pyroxenes. *Mineral. Petrol.* **39**, 55–76.
- O'Hara M. J. and Yoder H. S. (1967) Formation and fractionation of basic magmas at high pressures. *Scottish J. Geol.* **3**, 67–117.
- Pearson D. G. and Wittig N. (2008) Formation of Archaean continental lithosphere and its diamonds: the root of the problem. *J. Geol. Soc. London.* **165**, 895–914.
- Rapp R. P., Watson E. B. and Miller C. F. (1991) Partial melting of amphibolite/eclogite and the origin of Archean trondhjemites and tonalites. *Precambrian Res.* **51**, 1–25.
- Robinson D. N., Gurney J. J. and Shee S. R. (1984) Diamond eclogite and graphite eclogite xenoliths from Orapa, Botswana. *Dev. Petrol.* **11**, 11–24.
- Rohrbach A. and Schmidt M. W. (2011) Redox freezing and melting in the Earth's deep mantle resulting from carbon-iron redox coupling. *Nature* **472**, 209–214.
- Rollinson H. (1997) Eclogite xenoliths in west African kimberlites as residues from Archaean granitoid crust formation. *Nature* **389**, 173–176.
- Rollinson H. (2016) Archaean crustal evolution in West Africa: a new synthesis of the Archaean geology in Sierra Leone, Liberia, Guinea and Ivory Coast. *Precambrian Res.* **281**, 1–12.
- Rustioni G., Audétat A. and Keppler H. (2019) Experimental evidence for fluid-induced melting in subduction zones. *Geochem. Perspect. Lett.* **11**, 49–54.
- Ryabchikov I. D., Miller C. and Mirwald P. W. (1996) Composition of hydrous melts in equilibrium with quartz eclogites. *Mineral. Petrol.* **58**, 101–110.

- Schulze D. J. (1989) Constraints on the abundance of eclogite in the upper mantle. *J. Geophys. Res.* **94**, 4205–4212.
- Schulze D. J. (2003) A classification scheme for mantle-derived garnets in kimberlite: a tool for investigating the mantle and exploring for diamonds. *Lithos* **71**, 195–213.
- Schulze D. J. and Helmstaedt H. (1988) Coesite-sanidine eclogites from kimberlite: products of mantle fractionation or subduction? *J. Geol.* **96**, 435–443.
- Schulze D. J., Valley J. W. and Spicuzza M. J. (2000) Coesite eclogites from the Roberts Victor kimberlite, South Africa. *Lithos* **54**, 23–32.
- Shatsky V. S., Zedgenizov D. A., Ragozin A. L. and Kalinina V. V. (2015) Diamondiferous subcontinental lithospheric mantle of the northeastern Siberian Craton: evidence from mineral inclusions in alluvial diamonds. *Gondwana Res.* **28**, 106–120.
- Shu Q., Brey G. P., Hoefler H. E., Zhao Z. and Pearson D. G. (2016) Kyanite/corundum eclogites from the Kaapvaal Craton: subducted troctolites and layered gabbros from the mid- to early Archean. *Contrib. to Mineral. Petrol.* **171**, 1–24.
- Skinner E. M. W., Apter D. B., Morelli C. and Smithson N. K. (2004) Kimberlites of the Man craton, West Africa. *Lithos* **76**, 233–259.
- Smart K. A., Heaman L. M., Chacko T., Simonetti A., Kopylova M., Mah D. and Daniels D. (2009) The origin of high-MgO diamond eclogites from the Jericho kimberlite, Canada. *Earth Planet. Sci. Lett.* **284**, 527–537.
- Smit K. V., Shirey S. B. and Wang W. (2016) Type Ib diamond formation and preservation in the West African lithospheric mantle: Re–Os age constraints from sulphide inclusions in

- Zimmi diamonds. *Precambrian Res.* **286**, 152–166.
- Smith C. B., Pearson D. G., Bulanova G. P., Beard A. D., Carlson R. W., Wittig N., Sims K., Chimuka L. and Muchemwa E. (2009) Extremely depleted lithospheric mantle and diamonds beneath the southern Zimbabwe Craton. *Lithos* **112S**, 1120–1132.
- Smyth J. R., Caporuscio F. A. and McCormick T. C. (1989) Mantle eclogites: evidence of igneous fractionation in the mantle. *Earth Planet. Sci. Lett.* **93**, 133–141.
- Sobolev N. V. (1985) Ultramafic and eclogitic types of paragenesis of diamonds. Conference on native elements formation in endogenic processes. Extended abstracts. Acad Sci USSR, Siberian Division, Yakutsk (not paginated)
- Sobolev N. V., Kuznetsova I. K. and Zyuzin N. I. (1968) The petrology of grospydite xenoliths from the Zagadochnaya kimberlite pipe in Yakutia. *J. Petrol.* **9**, 253–280.
- Sobolev N. V., Yefimova E. S., Channer D. M. D., Anderson P. F. N. and Barron K. M. (1998) Unusual upper mantle beneath Guaniamo, Guyana shield, Venezuela: evidence from diamond inclusions. *Geology* **26**, 971–974.
- Sobolev N. V., Yefimova E. S. and Koptil V. I. (1999) Mineral inclusions in diamonds in the northeast of the Yakutian diamondiferous province. *Proc. VII Intern. Kimb. Conf. Cape Town.* **2**, 816–822.
- Spetsius Z. V. (2004) Petrology of highly aluminous xenoliths from kimberlites of Yakutia. *Lithos* **77**, 525–538.
- Stachel T. and Harris J. W. (1997) Syngenetic inclusions in diamond from the Birim field (Ghana) - a deep peridotitic profile with a history of depletion and re-enrichment. *Contrib.*

to *Mineral. Petrol.* **127**, 336–352.

Stachel T. and Harris J. W. (2008) The origin of cratonic diamonds — Constraints from mineral inclusions. *Ore Geol. Rev.* **34**, 5–32.

Stachel T. and Luth R. W. (2015) Diamond formation — where, when and how? *Lithos* **220–223**, 200–220.

Stachel T., Brey G. P. and Harris J. W. (2000) Kankan diamonds (Guinea) I: from the lithosphere down to the transition zone. *Contrib. to Mineral. Petrol.* **140**, 1–15.

Stachel T., Aulbach S., Brey G. P., Harris J. W., Leost I., Tappert R. and Viljoen K. S. (2004) The trace element composition of silicate inclusions in diamonds: a review. *Lithos* **77**, 1–19.

Stachel T., Banas A., Muehlenbachs K., Kurszlaukis S. and Walker E. C. (2006) Archean diamonds from Wawa (Canada): samples from deep cratonic roots predating cratonization of the Superior Province. *Contrib. to Mineral. Petrol.* **151**, 737–750.

Stachel T., Harris J. W., Hunt L., Muehlenbachs K. and Kobussen A. F. (2018) Argyle diamonds: how subduction along the Kimberley Craton edge generated the world's biggest diamond deposit. *Econ. Geol.* **20**, 145–167.

Stachel T., Aulbach S. and Harris J. W. (2022) Mineral inclusions in lithospheric diamonds. *Rev. Mineral. Geochemistry* **88**, 307–391.

Sun S. S. and McDonough W. F. (1989) Chemical and isotopic systematics of oceanic basalts: implications for mantle composition and processes. *Geol. Soc. Spec. Publ.* **42**, 313–345.

Tappert R., Stachel T., Harris J. W., Muehlenbachs K., Ludwig T. and Brey G. P. (2005) Diamonds from Jagersfontein (South Africa): messengers from the sublithospheric mantle.

Contrib. to Mineral. Petrol. **150**, 505–522.

Taylor L. A. and Liu Y. (2009) Sulfide inclusions in diamonds: not monosulfide solid solution.

Russ. Geol. Geophys. **50**, 1201–1211.

Tompkins L. A. and Haggerty S. E. (1984) The Koidu kimberlite complex, Sierra Leone:

geological setting, petrology and mineral chemistry. *Dev. Petrol.* **11**, 83–105.

Viljoen K. S. (1995) Graphite- and diamond-bearing eclogite xenoliths from the Bellsbank

kimberlites, Northern Cape, South Africa. *Contrib. to Mineral. Petrol.* **121**, 414–423.

Wyllie P. J. (1992) Experimental petrology: Earth materials science. In *Brown GC, Hawkesworth*

CJ, Wilson RCL (eds) Understanding Earth pp. 67–87.

Chapter 5 Conclusions

5.1 Volatile recycling recorded by diamonds

Combined *in-situ* $\delta^{13}\text{C}$ and $\delta^{15}\text{N}$ analyses of Koidu diamonds trace the source of diamond-forming fluids/melts beneath the West African Craton. The low $\delta^{13}\text{C}$ (down to -33.2 ‰) and high $\delta^{15}\text{N}$ (up to +10.1 ‰) values in eclogitic diamonds unambiguously require involvement of carbon and nitrogen derived from crustal sources. Formation of these eclogitic diamonds was related to subduction of oceanic crust beneath the West African Craton, possibly coeval with or subsequent to tectonic plate convergence in the Archean, although the exact timing of diamond formation has not been constrained.

A subset of these eclogitic diamonds have overgrowth layers with mantle-like $\delta^{13}\text{C}$ (-7.8 to -3.6 ‰) and $\delta^{15}\text{N}$ (-7.9 to -2.1 ‰) values, suggesting that a metasomatic fluid/melt carrying mantle-derived carbon and nitrogen infiltrated the source region. Low nitrogen aggregation states in the overgrowth layers (in contrast to the high nitrogen aggregation states in the cores) of these diamonds indicate that this pulse of fluid/melt was generated in close temporal proximity to kimberlite eruption, possibly associated with proto-kimberlitic magmatism.

Koidu peridotitic diamonds have mantle-like $\delta^{13}\text{C}$, although two-thirds of them have slightly elevated $\delta^{13}\text{C}$ of up to -1.1 ‰, which could be attributed to a subducted normal carbonate component. In $\delta^{15}\text{N}$ the peridotitic diamonds extend from mantle-like to strongly positive values (-4.2 to +9.7 ‰), indicating mixing of carbon and nitrogen from the convecting mantle with subducted components.

5.2 Diamond formation mechanisms

Koidu peridotitic diamonds contain olivine inclusions with high Mg# (92.2–94.7), documenting formation in highly depleted dunitic or harzburgitic substrates. Carbon and nitrogen isotope compositions of these diamonds indicate that their formation is associated with the infiltration of diamond-forming fluid/melt that may either derive from partial melting of carbonated peridotite located deeper in the lithospheric mantle and initiated by subduction-related fluids, or a mantle plume that carried signatures of deeply subducted crustal material.

Detailed investigation of a subset of Koidu diamonds with eclogitic garnet inclusions, including coupled $\delta^{13}\text{C}$ – $\delta^{15}\text{N}$ – $\delta^{18}\text{O}$ and elemental analyses, suggest three possible formation modes for eclogitic diamonds may have operated: (1) diamond formation in eclogitic substrates derived from gabbroic protoliths, with low primary concentrations of crustal carbon, may have relied on introduction of external carbon, either through asthenosphere-derived fluids/melts, or deserpentinization fluids; (2) in eclogitic substrates derived from basaltic protoliths, which contained high concentrations of ^{13}C -depleted crustal carbon (biogenic carbonate and organic matter) as a consequence of intense sea water alteration, diamond formation mainly involved inherited crustal carbon and likely was facilitated by melt generated during partial melting of eclogitic substrates, or by an external pulse of mantle-derived fluid/melt, which remobilized the subducted carbon for diamond precipitation; (3) diamonds in the sublithospheric mantle possibly precipitated when slab-derived fluids/melts infiltrated surrounding asthenospheric peridotite, as reflected by the elevated Mg# (79.0) and Cr# (0.90) in a mildly majoritic garnet inclusion, and in this case diamonds may have precipitated from mixing of both subducted and mantle carbon.

Mixed paragenesis diamonds are found in this study, in which two of them (containing mineral inclusions with clearly distinguishable colours) have eclogitic mineral inclusions located in the core and peridotitic mineral inclusions in the rim (one with omphacite + Mg-chromite, the other

with eclogitic garnet + forsteritic olivine). Positive Eu anomalies in omphacite and eclogitic garnet inclusions are indicative of derivation from eclogites with subducted gabbroic protoliths. Mg-chromite ($Cr\# = 85.5$; $Mg\# = 65.2$) and forsteritic olivine ($Mg\# = 94.5$) inclusions clearly originated from strongly depleted cratonic peridotites. Different origins of eclogitic and peridotitic inclusions located in the core and rim of these diamonds, respectively, indicate that the diamonds were initially formed in eclogitic substrates and then physically transported into peridotitic substrates for renewed diamond growth.

5.3 The lithospheric mantle beneath Koidu

This study of 105 Koidu diamonds reveals a dominance of eclogitic (78%) over peridotitic (17%) and mixed paragenesis (5%) diamonds. The eclogitic inclusion assemblage includes coesite, omphacite, kyanite, garnet, sulphide, rutile and corundum. The peridotitic inclusion assemblage includes olivine and spinel.

Kyanite and corundum are rare inclusions in diamonds. Their occurrence in diamonds indicates Al-rich eclogitic substrates, which likely resulted from infiltration of sediment-derived melts, as the high $\delta^{18}O$ values and lack of positive Eu anomalies in coexisting garnet inclusions preclude formation of kyanite from prograde metamorphism of plagioclase-rich (cumulate) protoliths. Both gabbroic and basaltic eclogites were substrates for diamond crystallization beneath Koidu, as diamond-bearing gabbroic eclogite xenoliths and diamond inclusions derived from both gabbroic and basaltic eclogites were recovered. Although diamond-bearing basaltic eclogite xenoliths have not been recovered at Koidu, six diamonds in this study contain coexisting garnet and omphacite inclusions derived from eclogites with basaltic protoliths, as indicated by negative Eu anomalies and occurrence of very high $\delta^{18}O$ values (+11.3 to +12.0 ‰). These inclusion pairs are used to reconstruct whole-rock major and trace element compositions. Geothermobarometry

indicates diamond-bearing gabbroic eclogite xenoliths resided at shallower depths (150–190 km) compared to inclusion pairs from six diamonds derived from basaltic eclogites (≥ 200 km). Coesite occurred in 44% of Koidu diamonds. The six reconstructed whole-rocks from garnet and omphacite inclusion pairs (one pair coexisted with coesite), however, indicate that their eclogite substrates were strongly depleted in LREE and probably experienced $> 20\%$ batch melting, which conflicts with the high abundance of coesite as it should have been completely removed during such high-degree melting. If coesite was indeed eliminated by melt extraction, its ubiquity in Koidu diamonds could be explained by subsequent metasomatism of the eclogitic diamond substrates, possibly through carbonation of clinopyroxene by a CO_2 -rich fluid. Among the six reconstructed whole-rocks, four (including the coesite-bearing example) have evidence for LREE re-enrichment after melt depletion as well as strong positive Sr anomalies that positively correlate with La contents. This metasomatic event may be related to the addition of coesite to eclogitic diamond substrates, if coesite is indeed metasomatic.

Olivine inclusions from Koidu diamonds have the higher average Mg# (94.0) compared to olivine inclusions in diamonds from Akwatia (average Mg# = 92.8) and Kankan (average Mg# = 92.1), also on the West African Craton. The high Mg# of Koidu olivine inclusions, together with (1) the absence of peridotitic orthopyroxene and clinopyroxene as diamond inclusions, and (2) the presence of a spinel inclusion with a low Cr# (50.9) that cannot have coexisted with orthopyroxene, are indicative of highly-depleted dunitic/harzburgitic diamond substrates in the lithospheric mantle. Removal of orthopyroxene from peridotites generally requires $> 40\%$ melt extraction, which may have occurred at the high mantle temperatures of the Archean or early Proterozoic. At least some of peridotitic diamond substrates were affected by a metasomatic event, as inferred by the spinel inclusions in one diamond with unusually high TiO_2 contents compared to other spinel inclusions

in this study (2.8 wt% vs 0.04–0.26 wt%), that likely was associated with proto-kimberlitic magmatism.

5.4 Future directions

In this study, I determined the carbon and nitrogen isotope compositions, nitrogen concentrations and nitrogen aggregation states of 105 diamonds, as well as the major element, trace element and oxygen isotope compositions of 370 mineral inclusions in these diamonds and of six diamond-bearing eclogite xenoliths. This large dataset provides reliable information about diamond formation in the lithospheric mantle and the geologic history on the West African Craton lithospheric mantle underpinning the Koidu area. However, the formation ages of Koidu diamonds are still unknown. Diamond formation and exhumation are usually triggered by tectonic events, such as rifting or assembly of supercontinents. Without knowing the ages of diamonds, we are only able to determine the relative sequence of melt depletion and metasomatic events of the diamond substrates. To better constrain the timing of localized mantle processes or large-scale tectonic events that are associated with diamond formation, geochronology is an essential tool. Eclogitic sulphide is a common inclusion in Koidu diamonds and suitable for Re–Os radiometric dating to constrain diamond ages. In addition, sulphur isotope compositions of these sulphide inclusions can be used to trace sulphur recycling, as surficial sulphides with mass-independently fractionated sulphur (associated with photochemical reactions in the atmosphere) occurred only before the Proterozoic oxygenation event.

Appendix A

Supplementary information including tables and figures for Chapter 2.

Table A.1. Characteristics of Koidu diamonds.

Sample	Weight (g)	Size (mm)	Morphology	Colour	Paragenesis	Total N (at.ppm)	%B	Type
128-1	0.0081	2	o	c	—	351	13	IaAB
128-2	0.0139	3	o	c	E	313	43	IaAB
128-3	0.0225	3	o-d	c	E	303	61	IaAB
128-4	0.0108	2	a	c	E	730	57	IaAB
128-5	0.0142	2	o	c	E	242	17	IaAB
128-6	0.0170	3	o	c	E	171	12	IaAB
128-7	0.0161	3	o	c	E	169 (rim); 298 (centre)	17 (rim); 51 (centre)	IaAB*
128-8	0.0101	2	o-d	c	E	193 (rim); 315 (centre)	0 (rim); 39 (centre)	IaAB*
128-9	0.0114	2	d	c	E	385	0	IaA
129-3	0.0275	4	o	c	E	131	18	IaAB
129-8	0.0136	2	o	c	E	70	9	IaA
129-13	0.0200	3	d	c	E	132	27	IaAB
130-1	0.0121	3	o	p.y.	E	748	62	IaAB
130-2	0.0198	3	o	c	E	117	1	IaA
130-3	0.0213	3	o	c	E	83 (rim); 190 (centre)	0 (rim); 33 (centre)	IaAB*
130-4	0.0231	3	o	c	P	122	0	IaA
130-5	0.0159	3	o	c	P	463	14	IaAB
130-6	0.0207	3	o	c	E	198	16	IaAB
130-7	0.0201	4	irr	c	E	34	7	IaA
130-8	0.0159	3	o-d	c	E	376	68	IaAB
130-9	0.0171	3	o	c	Mixed	290	59	IaAB
130-10	0.0212	3	o	c	E	306	6	IaA
130-11	0.0152	3	o	c	E	337	33	IaAB
130-12	0.0216	3	o	c	E	116	56	IaAB
130-13	0.0180	3	o	c	E	90	31	IaAB
130-14	0.0156	2	d	c	E	271	0	IaA
130-15	0.0102	2	o	c	E	146	6	IaA
130-17	0.0088	2	o	c	P	412	20	IaAB

130-18	0.0072	2	o-d	c	E	677	77	IaAB
130-20	0.0084	2	o	c	E	126	7	IaA
130-21	0.0150	2	o	c	P	77	65	IaAB
130-22	0.0120	2	o	c	E	98	10	IaA
130-23	0.0179	3	o	c	E	232	15	IaAB
130-24	0.0179	3	o	c	E	452	56	IaAB
130-25	0.0125	2	o	c	P	407	27	IaAB
130-26	0.0172	3	o	c	E	467	72	IaAB
130-27	0.0111	3	o	c	P	92	0	IaA
130-28	0.0225	3	o	c	—	40	0	IaA
130-29	0.0173	3	int	c	E	173	0	IaA
130-30	0.0088	2	o	c	E	58	0	IaA
130-31	0.0166	2	o	c	Mixed	237	62	IaAB
130-32	0.0131	2	o	c	E	305	55	IaAB
130-33	0.0106	2	o	c	P	50	0	IaA
130-34	0.0285	3	d	c	P	273	32	IaAB
130-35	0.0081	2	d	c	E	269	0	IaA
130-36	0.0196	3	o	c	—	200	10	IaAB
130-37	0.0163	4	d	c	E	28	0	IaA
131-1	0.0191	3	o	c	E	56	0	IaA
131-2	0.0145	2	o	c	E	128	38	IaAB
131-3	0.0174	2	o	c	E	319	53	IaAB
131-4	0.0116	2	o	c	E	167	9	IaA
131-5	0.0225	3	o-d	c	E	232	34	IaAB
132-1	0.0122	3	o	c	E	45	0	IaA
132-2	0.0194	3	o	c	E	53	17	IaAB
132-3	0.0209	2	o	c	E	109	2	IaA
132-4	0.0195	2	o	c	E	562	48	IaAB
132-5	0.0134	2	o	c	E	342	42	IaAB
132-6	0.0177	3	o	c	P	950	42	IaAB
132-7	0.0083	2	o	c	P	86	2	IaA
132-8	0.0160	3	o	c	E	49	3	IaA
132-9	0.0131	3	o	c	E	83	5	IaA

133-1	0.0155	3	o-d	c	E	61	9	IaA
133-2	0.0200	3	o	c	E	208	7	IaA
133-3	0.0209	3	o	c	E	282	59	IaAB
133-4	0.0205	3	o	c	E	70	2	IaA
133-5	0.0290	4	d	c	E	19	0	IaA
133-6	0.0101	2	o	c	Mixed	295	54	IaAB
133-7	0.0158	3	o	c	E	225	38	IaAB
133-8	0.0191	3	o	c	E	97	0	IaA
133-10	0.0151	2	o	c	E	65	10	IaAB
133-11	0.0166	2	o	c	E	86	27	IaAB
133-12	0.0113	2	o	c	E	328	55	IaAB
133-13	0.0165	3	o	c	E	124	18	IaAB
133-14	0.0184	3	o	c	E	272	48	IaAB
133-15	0.0196	3	o	c	—	238	32	IaAB
134-1	0.0217	3	o	c	P	37	6	IaA
134-2	0.0179	3	o	c	P	144	0	IaA
135-1	0.0193	2	o	c	E	289	42	IaAB
135-2	0.0190	3	o	c	P	91	10	IaAB
135-3	0.0096	3	irr	c	P	5	0	IaA
136-1	0.0169	3	o	c	P	40	3	IaA
137-1	0.0171	2	o	c	E	109	0	IaA
138-1	0.0059	2	o	c	E	189 (rim); 981 (centre)	34 (rim); 72 (centre)	IaAB*
138-2	0.0121	2	o	c	E	34	6	IaA
138-3	0.0187	3	o	c	E	712	65	IaAB
138-4	0.0191	3	o	c	E	424	56	IaAB
138-5	0.0144	3	o	c	E	414	6	IaA
138-6	0.0171	3	irr	c	E	150	42	IaAB
138-7	0.0087	2	o	c	Mixed	488	10	IaAB
138-8	0.0159	3	o	c	E	737	70	IaAB
138-9	0.0248	3	o	c	E	311	29	IaAB
138-10	0.0106	2	o	c	—	603	62	IaAB
138-11	0.0107	3	d	c	E	463	59	IaAB
138-12	0.0223	3	o	c	E	74	14	IaAB

139-1	0.0157	2	o	c	E	47	11	IaAB
140-1	0.0133	2	o	c	E	51	24	IaAB
140-2	0.0081	2	irr	l.b.	E	< 5	—	IIa
141-1	0.0057	2	o	c	—	198	7	IaA
142-1	0.0153	3	m	c	E	152	41	IaAB
142-2	0.0127	3	d	c	E	280	51	IaAB
142-3	0.0128	3	o	c	P	16	1	IaA
142-4	0.0091	2	d	c	E	65	22	IaAB
143-1	0.0159	3	o	c	E	96	10	IaAB
143-2	0.0154	3	o	c	E	517	55	IaAB
144-1	0.0119	3	o-d	c	E	29	0	IaA
145-1	0.0166	3	o	c	E	540	65	IaAB
146-1	0.0139	3	o	c	Mixed	199	0	IaA
146-2	0.0172	3	o	c	E	294	38	IaAB
147-1	0.0174	4	m	c	P	46	3	IaA
147-2	0.0101	2	o	c	P	37	0	IaA
148-1	0.0195	3	d	c	E	264	64	IaAB

Abbreviations:

Morphology – o: octahedron, d: dodecahedron, a: aggregate, irr: irregular, o-d: transitional octahedron-dodecahedron, m: macle, int: parallel intergrowth.

Colour – c: colourless, p.y.: pale yellow, l.b.: light brown.

Paragenesis – E: eclogitic, P: peridotitic, Mixed: mixed paragenesis.

*Type of diamond was determined by averaging the %B of the rim and core zones of the diamond.

Table A.2. Major element (wt%) compositions of mineral inclusions in other mixed paragenesis diamonds.

Sample	130-9-1	130-9-2	130-9-4	130-9-5	130-31-2	130-31-4	146-1-1
Mineral	omphacite	olivine	omphacite	olivine	coesite	olivine	olivine
Paragenesis	E	P	E	P	E	P	P
SiO ₂	56.22	41.58	55.75	41.32	100.56	41.00	41.42
TiO ₂	0.48	< 0.02	0.46	0.03	0.02	< 0.02	< 0.02
Al ₂ O ₃	18.80	< 0.02	18.76	0.03	< 0.02	< 0.02	< 0.02
Cr ₂ O ₃	0.08	0.02	0.08	0.06	< 0.02	0.04	0.02
FeO ^{total}	2.82	5.68	2.80	5.78	< 0.02	6.32	5.48
NiO	< 0.02	0.35	< 0.02	0.30	< 0.02	0.37	0.35
MnO	0.04	0.08	0.03	0.08	< 0.02	0.10	0.08
MgO	5.01	51.99	4.97	52.06	< 0.02	51.94	52.01
CaO	7.52	0.01	7.50	0.02	0.01	0.02	0.01
Na ₂ O	8.34	< 0.02	8.20	< 0.02	< 0.02	< 0.02	< 0.02
K ₂ O	0.15	< 0.02	0.14	< 0.02	< 0.02	< 0.02	< 0.02
Total	99.47	99.72	98.69	99.69	100.59	99.79	99.37
Mg#	76.1	94.2	76.1	94.1		93.6	94.4

Sample	146-1-3	146-1-5	146-1-6	146-1-8	146-1-9	146-1-10	146-1-12
Mineral	olivine	olivine	olivine	olivine	Mg-chromite	olivine	coesite
Paragenesis	P	P	P	P	P	P	E
SiO ₂	40.79	40.71	40.73	40.66	0.13	41.25	100.50
TiO ₂	< 0.02	< 0.02	< 0.02	< 0.02	0.08	< 0.02	< 0.02
Al ₂ O ₃	< 0.02	< 0.02	< 0.02	< 0.02	6.76	< 0.02	0.02
Cr ₂ O ₃	0.01	0.03	0.01	< 0.02	66.02	< 0.02	< 0.02
FeO ^{total}	5.43	5.43	5.50	5.44	13.14	5.58	< 0.02
NiO	0.35	0.34	0.35	0.35	0.09	0.36	< 0.02
MnO	0.07	0.08	0.09	0.08	0.35	0.08	< 0.02
MgO	51.81	51.33	51.95	50.91	14.33	51.73	< 0.02
CaO	0.01	0.01	0.01	0.01	< 0.02	0.01	< 0.02
Na ₂ O	< 0.02	< 0.02	< 0.02	< 0.02	< 0.02	< 0.02	< 0.02
K ₂ O	< 0.02	< 0.02	< 0.02	< 0.02	< 0.02	< 0.02	< 0.02
Total	98.48	97.93	98.64	97.44	100.88	99.01	100.53
Mg#	94.4	94.4	94.4	94.3	66.0	94.3	

$$\text{Mg\#} = 100 \times \text{Mg} / (\text{Mg} + \text{Fe})$$

Table A.3. Major element (wt%) compositions of mineral inclusions in diamond 133-6 and 138-7.

Sample	133-6*	133-6-4	138-7-1	138-7-2	138-7-3	138-7-4	138-7-6	138-7-7
Mineral	omphacite	Mg-chromite	garnet	garnet	garnet	garnet	garnet	olivine
Paragenesis	E	P	E	E	E	E	E	P
SiO ₂	55.75	< 0.02	40.97	41.85	41.00	39.46	40.26	41.98
TiO ₂	0.26	0.06	0.45	0.45	0.47	0.47	0.47	< 0.02
Al ₂ O ₃	18.94	7.32	23.21	21.94	22.98	23.86	23.27	< 0.02
Cr ₂ O ₃	0.01	64.46	0.04	0.04	0.02	0.03	0.02	0.07
FeO ^{total}	1.93	12.96	9.60	9.56	8.99	8.95	9.11	5.51
NiO	0.03	0.08	< 0.02	< 0.02	< 0.02	0.01	0.01	0.35
MnO	0.02	0.16	0.17	0.18	0.16	0.17	0.16	0.08
MgO	4.96	13.66	9.28	9.70	8.47	8.07	8.36	53.47
CaO	8.65	< 0.02	16.89	16.70	18.55	19.26	19.28	0.02
Na ₂ O	8.33	< 0.02	0.18	0.17	0.18	0.18	0.18	< 0.02
K ₂ O	0.22	< 0.02	< 0.02	< 0.02	< 0.02	< 0.02	< 0.02	< 0.02
Total	99.10	98.70	100.79	100.56	100.82	100.46	101.12	101.48
Mg#	82.2	65.2	63.2	64.4	62.7	61.7	62.1	94.5
Ca#			45.1	44.2	49.5	51.2	50.5	

Mg# = $100 \times \text{Mg} / (\text{Mg} + \text{Fe})$; Ca# = $100 \times \text{Ca} / (\text{Ca} + \text{Mg} + \text{Fe} + \text{Mn})$.

* Average values of multiple omphacites in diamond 133-6 are reported here.

Table A.4. Trace element (ppm) compositions of mineral inclusions in diamond 133-6 and 138-7.

Sample	133-6-1	133-6-2	133-6-3	138-7-1	138-7-3	138-7-6
Mineral	Omphacite	Omphacite	Omphacite	Garnet	Garnet	Garnet
La	2.988	3.000	3.016	0.092	0.062	0.062
Ce	4.480	4.642	4.622	0.644	0.559	0.615
Pr	0.315	0.321	0.317	0.203	0.213	0.215
Nd	0.800	0.827	0.870	2.050	1.910	2.090
Sm	0.154	0.142	0.140	1.300	1.314	1.392
Eu	0.059	0.060	0.069	0.716	0.617	0.854
Gd	0.067	0.088	0.100	1.970	2.240	2.440
Tb	0.005	0.008	0.008	0.373	0.321	0.468
Dy	0.050	0.030	0.027	2.770	2.138	3.120
Ho	0.002	0.006	0.006	0.614	0.540	0.660
Er	0.010	0.009	0.005	1.740	1.646	1.715
Tm	n.d.	n.d.	n.d.	0.252	0.182	0.234
Yb	n.d.	0.005	n.d.	1.470	1.116	1.414
Lu	n.d.	n.d.	n.d.	0.198	0.155	0.201
Sc	1.330	1.560	1.680	41.3	36.1	38.4
Ti	1553	1613	1618	2596	2889	2895
V	108	110	110	86.4	78.5	82.5
Ni	326	321	328	78.3	60.2	65.0
Rb	0.540	0.532	0.510	n.d.	n.d.	n.d.
Sr	135	134	133	5.97	4.02	4.05
Y	0.107	0.116	0.097	15.3	14.5	16.6
Zr	2.2	2.2	2.3	12.2	7.1	12.1
Nb	1.120	1.088	1.106	0.091	0.106	0.142
Ba	0.380	0.685	0.628	n.d.	n.d.	n.d.
Hf	0.137	0.131	0.158	0.233	0.146	0.251

n.d. = not determined.

Three omphacites (from diamond 133-6) and three eclogitic garnets (from diamond 138-7) with larger grain size were analyzed.

Table A.5. Summary of SIMS analysis of Koidu diamonds.

Paragenesis	No. of diamond	$\delta^{13}\text{C}_{\text{VPDB}}$ (‰)	[N] (at.ppm)	$\delta^{15}\text{N}_{\text{Air}}$ (‰)
Peridotitic	18	-6.0 to -1.1	0.4 to 920	-4.2 to +9.7
Eclogitic	82	-33.2 to -0.04	0.4 to 2200	-7.9 to +10.1
Mixed	5	-24.8 to -1.3	0.3 to 1050	-9.8 to +5.8

Table A.6. SIMS analysis of Koidu diamonds.

Sample	Spot #	Paragenesis	$\delta^{13}\text{C}_{\text{VPDB}}$ (‰)	2σ (‰)	[N] at.ppm	2σ (at.ppm)	$\delta^{15}\text{N}_{\text{Air}}$ (‰)	2σ (‰)
128-1	1	—	-4.9	0.2	185	6	2.1	1.9
128-1	2	—	-4.9	0.1	254	8	0.1	1.6
128-1	3	—	-5.7	0.2	297	9	-1.3	1.4
128-1	4	—	-6.3	0.1	29	1	—	—
128-1	5	—	-6.3	0.2	478	15	-2.4	1.2
128-1	6	—	-6.7	0.2	2	0	—	—
128-1	7	—	-6.7	0.1	20	1	—	—
128-2	1	E	-5.7	0.1	744	23	-6.7	1.1
128-2	2	E	-24.5	0.2	34	1	—	—
128-2	3	E	-24.6	0.2	1	0	—	—
128-2	4	E	-24.8	0.1	53	2	—	—
128-3	1	E	-29.6	0.1	1511	47	0.7	0.7
128-3	2	E	-29.3	0.1	1288	39	2.8	0.7
128-3	3	E	-28.8	0.1	330	11	-3.9	1.8
128-3	4	E	-24.9	0.1	32	1	—	—
128-3	5	E	-17.3	0.1	35	1	—	—
128-4	1	E	-6.8	0.1	789	25	-5.2	1.0
128-4	2	E	-26.3	0.1	4	0	—	—
128-4	3	E	-26.4	0.1	18	1	—	—
128-5	1	E	-26.8	0.1	1	0	—	—
128-5	2	E	-26.5	0.1	43	2	—	—
128-5	3	E	-26.6	0.1	76	3	-2.9	3.4
128-6	1	E	-24.1	0.1	38	2	—	—
128-6	2	E	-27.9	0.1	22	1	—	—
128-6	3	E	-26.7	0.2	2	0	—	—
128-6	4	E	-27.0	0.1	31	2	—	—
128-6	5	E	-24.9	0.1	71	3	—	—
128-6	6	E	-25.5	0.1	329	11	-4.1	1.6
128-7	1	E	-27.5	0.2	41	2	—	—
128-7	2	E	-27.6	0.1	3	0	—	—

128-7	3	E	-28.1	0.1	122	4	0.9	2.4
128-7	4	E	-28.4	0.1	3	0	—	—
128-8	1	E	-7.7	0.2	1408	44	-2.9	0.7
128-8	2	E	-27.6	0.1	34	1	—	—
128-8	3	E	-27.5	0.2	38	2	—	—
128-8	4	E	-27.8	0.1	237	8	-2.7	1.6
128-8	5	E	-27.6	0.1	47	2	—	—
128-8	6	E	-24.2	0.1	32	1	—	—
128-9	1	E	-6.6	0.1	743	23	-5.5	1.0
128-9	2	E	-6.3	0.1	924	28	-5.7	1.0
128-9	3	E	-6.0	0.1	827	25	-5.4	0.9
128-9	4	E	-25.1	0.1	24	1	—	—
128-9	5	E	-24.6	0.1	8	0	—	—
129-3	1	E	-26.3	0.1	18	1	—	—
129-3	2	E	-25.3	0.1	93	3	-5.0	2.7
129-3	3	E	-26.3	0.2	61	2	—	—
129-3	4	E	-26.3	0.1	37	2	—	—
129-3	5	E	-26.1	0.1	1	0	—	—
129-8	1	E	-27.9	0.1	11	1	—	—
129-8	2	E	-28.1	0.1	426	13	2.4	1.5
129-8	3	E	-27.9	0.2	146	5	2.3	2.3
129-13	1	E	-27.5	0.1	1	0	—	—
129-13	2	E	-27.7	0.1	33	1	—	—
130-1	1	E	-25.7	0.1	36	2	—	—
130-1	2	E	-26.0	0.1	768	24	-2.6	1.0
130-1	3	E	-25.9	0.1	28	1	—	—
130-1	4	E	-25.8	0.1	99	3	-4.6	2.8
130-2	1	E	-30.6	0.1	2	0	—	—
130-2	2	E	-29.9	0.1	146	6	-0.6	1.8
130-2	3	E	-30.9	0.1	7	0	—	—
130-2	4	E	-20.8	0.1	33	1	—	—
130-3	1	E	-25.2	0.1	40	2	—	—
130-3	2	E	-25.2	0.1	6	0	—	—

130-3	3	E	-25.3	0.1	33	2	—	—
130-3	4	E	-25.2	0.1	20	1	—	—
130-3	5	E	-21.2	0.1	25	1	—	—
130-4	1	P	-2.7	0.1	1	0	—	—
130-4	2	P	-2.7	0.1	83	3	-2.8	3.0
130-4	3	P	-2.6	0.1	47	2	—	—
130-5	1	P	-1.3	0.1	234	8	-1.4	1.8
130-5	2	P	-1.3	0.1	248	8	-1.2	1.9
130-6	1	E	-28.3	0.1	347	11	-0.5	1.5
130-6	2	E	-28.2	0.1	33	1	—	—
130-6	3	E	-28.4	0.1	4	0	—	—
130-6	4	E	-6.8	0.1	1029	31	-4.9	0.9
130-7	1	E	-32.9	0.1	1	0	—	—
130-7	2	E	-33.2	0.1	15	1	—	—
130-7	3	E	-33.1	0.1	17	1	—	—
130-8	1	E	-28.9	0.1	50	2	—	—
130-8	2	E	-29.0	0.1	2	0	—	—
130-8	3	E	-29.1	0.2	3	0	—	—
130-9	1	Mixed	-22.7	0.1	52	2	—	—
130-9	2	Mixed	-22.6	0.1	1	0	—	—
130-9	3	Mixed	-24.8	0.2	40	2	—	—
130-9	4	Mixed	-24.6	0.1	2	0	—	—
130-9	5	Mixed	-22.7	0.2	68	3	—	—
130-9	6	Mixed	-23.0	0.2	180	6	-4.1	2.1
130-10	1	E	-29.7	0.2	103	4	-2.0	2.8
130-10	2	E	-29.8	0.2	200	10	-0.1	1.8
130-10	3	E	-29.9	0.1	33	1	—	—
130-10	4	E	-29.8	0.1	19	1	—	—
130-10	5	E	-6.5	0.1	1136	35	-7.9	0.8
130-11	1	E	-29.4	0.1	1	0	—	—
130-11	2	E	-29.6	0.1	109	4	-3.6	2.5
130-11	3	E	-29.4	0.1	49	2	—	—
130-11	4	E	-29.5	0.2	628	20	-3.5	1.0

130-11	5	E	-29.5	0.1	29	1	—	—
130-11	6	E	-29.3	0.1	220	7	-1.3	1.8
130-11	7	E	-28.6	0.1	4	0	—	—
130-12	1	E	-27.3	0.1	36	1	—	—
130-12	2	E	-27.0	0.2	2	0	—	—
130-12	3	E	-27.2	0.1	1	0	—	—
130-12	4	E	-15.8	0.1	46	2	—	—
130-12	5	E	-15.8	0.1	47	2	—	—
130-13	1	E	-21.5	0.1	149	5	9.5	2.4
130-13	2	E	-27.0	0.2	26	1	—	—
130-13	3	E	-27.1	0.1	6	1	—	—
130-13	4	E	-23.1	0.1	100	4	6.1	2.7
130-13	5	E	-21.8	0.1	295	10	7.0	1.6
130-14	1	E	-6.0	0.1	905	28	-6.8	1.0
130-14	2	E	-20.3	0.1	102	4	6.7	2.7
130-14	3	E	-28.0	0.1	22	1	—	—
130-14	4	E	-28.1	0.2	1	0	—	—
130-15	1	E	-7.0	0.1	710	22	-5.9	1.0
130-15	2	E	-18.0	0.1	25	1	—	—
130-15	3	E	-21.2	0.1	62	2	—	—
130-15	4	E	-26.6	0.1	2	0	—	—
130-15	5	E	-26.6	0.1	60	3	—	—
130-17	1	P	-5.3	0.1	579	18	1.3	1.1
130-17	2	P	-5.3	0.1	579	18	1.3	1.2
130-17	3	P	-5.3	0.1	526	17	1.9	1.2
130-17	4	P	-5.4	0.1	414	14	0.3	1.3
130-18	1	E	-24.4	0.1	438	14	-3.1	1.2
130-18	2	E	-24.1	0.2	30	1	—	—
130-18	3	E	-24.3	0.1	2	0	—	—
130-18	4	E	-25.7	0.1	7	1	—	—
130-18	5	E	-25.1	0.1	1	0	—	—
130-20	1	E	-27.6	0.1	27	1	—	—
130-20	2	E	-27.6	0.1	16	1	—	—

130-21	1	P	-6.0	0.1	154	5	5.9	2.7
130-21	2	P	-4.6	0.2	0.4	0	—	—
130-21	3	P	-4.5	0.1	14	1	—	—
130-21	4	P	-4.5	0.1	1	0	—	—
130-22	1	E	-27.4	0.1	53	2	—	—
130-22	2	E	-28.9	0.1	46	2	—	—
130-22	3	E	-29.1	0.2	118	4	0.7	2.8
130-22	4	E	-29.0	0.1	35	1	—	—
130-22	5	E	-27.7	0.1	2	0	—	—
130-23	1	E	-5.6	0.1	746	23	-4.8	0.9
130-23	2	E	-20.2	0.1	13	1	—	—
130-23	3	E	-20.4	0.1	6	0	—	—
130-23	4	E	-26.2	0.1	62	2	—	—
130-23	5	E	-26.2	0.1	15	1	—	—
130-24	1	E	-27.5	0.1	10	1	—	—
130-24	2	E	-26.8	0.1	41	2	—	—
130-24	3	E	-27.1	0.1	82	3	-0.6	2.9
130-24	4	E	-27.1	0.1	75	3	—	—
130-24	5	E	-27.1	0.1	1	0	—	—
130-25	1	P	-2.4	0.1	206	7	2.7	1.9
130-25	2	P	-2.2	0.1	126	4	9.2	2.3
130-25	3	P	-5.0	0.1	549	17	2.8	1.1
130-25	4	P	-4.4	0.1	925	28	-1.5	0.9
130-26	1	E	-27.0	0.1	26	1	—	—
130-26	2	E	-26.9	0.1	1	0	—	—
130-26	3	E	-21.5	0.1	30	1	—	—
130-27	1	P	-2.6	0.1	393	12	-3.2	1.2
130-27	2	P	-2.7	0.1	446	14	-4.2	1.2
130-27	3	P	-2.6	0.1	590	18	-4.1	1.0
130-28	1	—	-22.7	0.2	23	1	—	—
130-28	2	—	-22.8	0.2	25	1	—	—
130-29	1	E	-6.9	0.1	937	29	-5.0	0.8
130-29	2	E	-24.5	0.2	32	1	—	—

130-29	3	E	-26.3	0.1	1	0	—	—
130-29	4	E	-26.6	0.1	39	2	—	—
130-29	5	E	-26.4	0.1	25	1	—	—
130-30	1	E	-29.4	0.1	3	0	—	—
130-30	2	E	-28.8	0.1	50	2	—	—
130-30	3	E	-19.2	0.1	32	2	—	—
130-31	1	Mixed	-4.7	0.2	0.3	0	—	—
130-31	2	Mixed	-4.2	0.1	171	6	5.8	1.9
130-31	3	Mixed	-4.6	0.1	11	1	—	—
130-32	1	E	-26.3	0.1	4	0	—	—
130-32	2	E	-26.3	0.1	377	13	-0.6	1.3
130-32	3	E	-26.0	0.1	40	2	—	—
130-32	4	E	-26.3	0.1	42	2	—	—
130-33	1	P	-5.5	0.1	48	2	—	—
130-33	2	P	-5.6	0.1	50	2	—	—
130-33	3	P	-5.4	0.2	47	2	—	—
130-34	1	P	-4.1	0.1	202	7	9.7	1.9
130-34	2	P	-4.3	0.1	19	1	—	—
130-34	3	P	-4.0	0.1	36	1	—	—
130-34	4	P	-3.9	0.1	160	8	0.0	1.9
130-35	1	E	-7.5	0.1	923	28	-6.5	0.9
130-35	2	E	-19.7	0.1	61	2	—	—
130-35	3	E	-25.4	0.1	47	2	—	—
130-35	4	E	-26.0	0.1	43	2	—	—
130-36	1	—	-3.6	0.1	11	1	—	—
130-36	2	—	-3.5	0.1	3	0	—	—
130-37	1	E	-28.4	0.1	89	4	1.9	2.6
130-37	2	E	-28.8	0.2	23	1	—	—
131-1	1	E	-26.4	0.2	52	2	—	—
131-1	2	E	-26.3	0.1	1	0	—	—
131-1	3	E	-26.6	0.1	64	3	—	—
131-1	4	E	-26.5	0.1	35	1	—	—
131-2	1	E	-16.6	0.1	95	3	9.9	2.6

131-2	2	E	-16.9	0.1	37	2	—	—
131-2	3	E	-24.8	0.1	39	2	—	—
131-3	1	E	-28.3	0.1	3	0	—	—
131-3	2	E	-29.0	0.1	772	25	-1.3	0.9
131-3	3	E	-28.9	0.1	324	12	-2.0	1.6
131-4	1	E	-15.1	0.1	99	4	2.9	2.7
131-4	2	E	-25.9	0.1	39	2	—	—
131-4	3	E	-26.3	0.1	2078	63	0.6	0.5
131-5	1	E	-25.7	0.1	76	3	1.1	3.2
131-5	2	E	-25.3	0.2	1	0	—	—
131-5	3	E	-25.3	0.1	46	2	—	—
132-1	1	E	-22.7	0.2	12	1	—	—
132-1	2	E	-30.0	0.1	10	1	—	—
132-2	1	E	-24.0	0.2	29	1	—	—
132-2	2	E	-24.1	0.2	36	2	—	—
132-2	3	E	-26.3	0.1	1	0	—	—
132-2	4	E	-26.0	0.1	15	1	—	—
132-3	1	E	-25.8	0.2	6	0	—	—
132-3	2	E	-26.0	0.1	31	1	—	—
132-4	1	E	-7.1	0.1	986	30	-5.5	0.8
132-4	2	E	-14.4	0.1	227	8	10.1	1.6
132-4	3	E	-25.4	0.1	345	11	-1.3	1.4
132-4	4	E	-25.4	0.1	352	12	-0.5	1.3
132-4	5	E	-6.7	0.1	2201	68	-2.6	0.5
132-4	6	E	-16.2	0.1	91	3	8.0	2.4
132-4	7	E	-25.2	0.2	102	4	8.1	2.4
132-4	8	E	-25.2	0.1	535	17	0.0	1.0
132-5	1	E	-7.0	0.1	853	27	-5.3	0.8
132-5	2	E	-24.6	0.1	30	1	—	—
132-5	3	E	-24.7	0.1	1	0	—	—
132-5	4	E	-24.7	0.1	3	0	—	—
132-6	1	P	-5.7	0.1	477	15	-2.2	1.1
132-6	2	P	-5.5	0.1	676	21	-2.1	1.1

132-7	1	P	-2.4	0.1	135	5	-1.0	2.4
132-7	2	P	-2.6	0.1	16	1	—	—
132-7	3	P	-2.7	0.1	311	10	2.2	1.5
132-8	1	E	-27.8	0.1	36	2	—	—
132-8	2	E	-27.7	0.2	33	1	—	—
132-9	1	E	-29.8	0.1	17	1	—	—
132-9	2	E	-29.7	0.1	10	1	—	—
132-9	3	E	-7.2	0.1	675	21	-6.3	1.0
133-1	1	E	-29.8	0.1	30	1	—	—
133-1	2	E	-29.6	0.1	4	0	—	—
133-2	1	E	-27.0	0.1	1	0	—	—
133-2	2	E	-24.5	0.1	23	1	—	—
133-2	3	E	-25.3	0.1	30	1	—	—
133-3	1	E	-27.7	0.1	260	9	-1.9	1.6
133-3	2	E	-27.7	0.1	5	0	—	—
133-3	3	E	-21.3	0.1	35	2	—	—
133-4	1	E	-28.6	0.1	452	16	-2.8	1.2
133-4	2	E	-28.4	0.1	45	2	—	—
133-4	3	E	-28.2	0.1	1	0	—	—
133-4	4	E	-28.2	0.1	109	4	-1.1	2.8
133-4	5	E	-16.7	0.1	28	1	—	—
133-6 (Fragment 1)	1	Mixed	-4.1	0.2	195	8	4.0	1.7
133-6 (Fragment 1)	2	Mixed	-3.8	0.1	174	6	3.3	1.8
133-6 (Fragment 1)	3	Mixed	-3.8	0.2	109	4	2.1	2.4
133-6 (Fragment 1)	4	Mixed	-3.8	0.2	95	3	2.3	2.4
133-6 (Fragment 1)	5	Mixed	-3.8	0.1	17	1	—	—
133-6 (Fragment 1)	6	Mixed	-4.4	0.1	113	4	2.8	2.2
133-6 (Fragment 1)	7	Mixed	-3.6	0.2	1	0	—	—
133-6 (Fragment 1)	8	Mixed	-3.6	0.1	7	0	—	—
133-6 (Fragment 1)	9	Mixed	-4.1	0.1	2	0	—	—
133-6 (Fragment 1)	10	Mixed	-4.5	0.2	616	19	-7.9	1.1
133-6 (Fragment 2)	1	Mixed	-3.9	0.1	58	2	-5.6	3.9
133-6 (Fragment 2)	2	Mixed	-3.9	0.1	50	2	-4.2	4.1

133-6 (Fragment 2)	3	Mixed	-4.8	0.1	50	2	-6.2	3.9
133-6 (Fragment 2)	4	Mixed	-4.3	0.1	51	2	-4.2	4.2
133-6 (Fragment 2)	5	Mixed	-4.2	0.1	9	1	—	—
133-6 (Fragment 2)	6	Mixed	-4.4	0.1	579	18	-7.6	1.0
133-6 (Fragment 2)	7	Mixed	-4.5	0.1	645	20	-7.9	1.0
133-6 (Fragment 2)	8	Mixed	-4.3	0.2	543	17	-7.1	1.1
133-6 (Fragment 3)	1	Mixed	-4.7	0.1	333	11	2.5	1.5
133-6 (Fragment 3)	2	Mixed	-4.5	0.2	327	10	3.0	1.4
133-6 (Fragment 3)	3	Mixed	-4.2	0.2	285	9	2.9	1.5
133-6 (Fragment 3)	4	Mixed	-3.7	0.2	71	3	-1.4	2.7
133-6 (Fragment 3)	5	Mixed	-3.7	0.1	16	1	—	—
133-6 (Fragment 3)	6	Mixed	-4.6	0.2	94	3	-1.2	2.6
133-6 (Fragment 3)	7	Mixed	-4.3	0.2	516	16	-6.7	1.1
133-6 (Fragment 3)	8	Mixed	-4.5	0.1	613	19	-7.4	1.0
133-6 (Fragmant 4)	1	Mixed	-3.7	0.1	87	3	4.8	2.5
133-6 (Fragmant 4)	2	Mixed	-4.0	0.1	1	0	—	—
133-6 (Fragmant 4)	3	Mixed	-4.4	0.1	82	3	2.5	3.1
133-6 (Fragmant 4)	4	Mixed	-4.2	0.1	747	24	-7.1	1.0
133-7	1	E	-28.5	0.1	51	2	—	—
133-7	2	E	-28.4	0.1	1	0	—	—
133-7	3	E	-22.5	0.1	59	2	—	—
133-7	4	E	-28.3	0.1	4	0	—	—
133-8	1	E	-22.4	0.1	34	1	—	—
133-8	2	E	-22.2	0.1	1	0	—	—
133-8	3	E	-22.3	0.1	1	0	—	—
133-8	4	E	-24.4	0.1	20	1	—	—
133-8	5	E	-7.8	0.1	1274	39	-3.4	0.8
133-10	1	E	-19.9	0.1	37	2	—	—
133-10	2	E	-24.4	0.1	69	3	-3.8	3.5
133-10	3	E	-24.3	0.1	40	2	—	—
133-10	4	E	-24.4	0.1	51	2	—	—
133-11	1	E	-26.3	0.1	51	2	—	—
133-11	2	E	-26.4	0.1	77	4	0.1	3.0

133-11	3	E	-26.3	0.1	7	0	—	—
133-11	4	E	-20.3	0.1	32	1	—	—
133-12	1	E	-28.8	0.1	294	10	-4.4	1.6
133-12	2	E	-28.8	0.1	91	4	-0.8	3.0
133-12	3	E	-28.8	0.1	17	1	—	—
133-12	4	E	-28.7	0.1	6	0	—	—
133-12	5	E	-18.6	0.1	4	0	—	—
133-13	1	E	-27.0	0.1	182	8	0.0	1.9
133-13	2	E	-27.1	0.1	98	4	-2.3	2.5
133-13	3	E	-21.9	0.1	45	2	—	—
133-13	4	E	-27.0	0.1	14	1	—	—
133-14	1	E	-21.3	0.2	1	0	—	—
133-14	2	E	-22.4	0.1	29	1	—	—
133-14	3	E	-22.5	0.1	2	0	—	—
133-14	4	E	-22.4	0.1	16	1	—	—
133-15	1	—	-30.0	0.1	21	1	—	—
133-15	2	—	-30.1	0.1	55	2	—	—
133-15	3	—	-30.1	0.1	1	0	—	—
134-1	1	P	-2.1	0.2	1	0	—	—
134-1	2	P	-1.9	0.1	28	1	—	—
134-1	3	P	-2.1	0.1	44	2	—	—
134-1	4	P	-2.2	0.1	76	3	-0.8	2.8
134-2	1	P	-1.1	0.1	240	8	-0.9	1.6
134-2	2	P	-2.3	0.1	27	1	—	—
135-1	1	E	-6.6	0.1	874	27	-6.5	0.8
135-1	2	E	-23.7	0.1	141	5	-3.0	2.0
135-1	3	E	-23.7	0.1	46	2	—	—
135-1	4	E	-23.7	0.1	26	1	—	—
135-1	5	E	-23.9	0.1	48	3	—	—
135-2	1	P	-2.2	0.1	26	1	—	—
135-2	2	P	-2.3	0.1	26	1	—	—
135-3	1	P	-4.9	0.1	1	0	—	—
135-3	2	P	-4.8	0.1	72	3	6.3	3.4

136-1	1	P	-2.5	0.1	272	9	5.4	1.7
136-1	2	P	-1.5	0.1	14	1	—	—
137-1	1	E	-28.0	0.1	43	2	—	—
137-1	2	E	-28.1	0.1	67	3	0.6	3.5
137-1	3	E	-28.0	0.1	1	0	—	—
137-1	4	E	-27.6	0.1	19	1	—	—
138-1	1	E	-26.0	0.1	41	2	—	—
138-1	2	E	-26.2	0.2	246	8	-4.4	1.6
138-1	3	E	-7.0	0.1	605	19	-5.7	1.0
138-1	4	E	-25.9	0.1	14	1	—	—
138-2	1	E	-28.2	0.1	30	1	—	—
138-2	2	E	-28.8	0.1	26	2	—	—
138-2	3	E	-28.0	0.1	26	1	—	—
138-2	4	E	-28.1	0.1	1	0	—	—
138-3	1	E	-23.3	0.1	39	2	—	—
138-3	2	E	-28.5	0.1	741	23	0.1	1.0
138-3	3	E	-28.7	0.1	877	27	-0.4	0.8
138-4	1	E	-26.0	0.1	17	1	—	—
138-4	2	E	-26.3	0.1	208	8	-5.3	1.7
138-4	3	E	-26.2	0.1	26	1	—	—
138-4	4	E	-26.6	0.1	1080	36	0.1	0.8
138-4	5	E	-26.4	0.1	4	0	—	—
138-5	1	E	-7.0	0.1	968	30	-5.8	0.8
138-5	2	E	-26.2	0.1	8	1	—	—
138-5	3	E	-26.6	0.1	419	14	-5.6	1.2
138-5	4	E	-26.6	0.1	443	14	-5.6	1.2
138-6	1	E	-21.9	0.1	109	4	-2.0	2.5
138-6	2	E	-22.0	0.2	12	1	—	—
138-6	3	E	-22.0	0.1	45	2	—	—
138-7 (Fragment 1)	1	Mixed	-4.1	0.1	132	5	-9.8	2.1
138-7 (Fragment 1)	2	Mixed	-4.3	0.2	432	14	-7.6	1.2
138-7 (Fragment 1)	3	Mixed	-5.0	0.2	556	17	-7.9	1.2
138-7 (Fragment 1)	4	Mixed	-5.0	0.1	492	15	-7.8	1.1

138-7 (Fragment 1)	5	Mixed	-5.0	0.1	378	12	-7.2	1.3
138-7 (Fragment 1)	6	Mixed	-5.0	0.1	612	20	-6.7	1.0
138-7 (Fragment 1)	7	Mixed	-4.8	0.1	720	22	-6.7	0.9
138-7 (Fragment 1)	8	Mixed	-4.5	0.1	362	12	-7.5	1.3
138-7 (Fragment 1)	9	Mixed	-5.0	0.1	546	17	-7.5	1.1
138-7 (Fragment 1)	10	Mixed	-5.1	0.2	771	25	-7.1	0.8
138-7 (Fragment 1)	11	Mixed	-5.3	0.1	1054	33	-6.7	0.8
138-7 (Fragment 1)	12	Mixed	-4.8	0.2	499	16	-6.4	1.2
138-7 (Fragment 1)	13	Mixed	-5.1	0.2	673	21	-6.7	1.0
138-7 (Fragment 1)	14	Mixed	-5.0	0.1	461	15	-6.9	1.1
138-7 (Fragment 1)	15	Mixed	-4.9	0.2	604	19	-7.3	0.9
138-7 (Fragment 1)	16	Mixed	-4.8	0.1	371	12	-6.6	1.1
138-7 (Fragment 1)	17	Mixed	-4.4	0.1	1	0	—	—
138-7 (Fragment 2)	1	Mixed	-4.3	0.2	512	16	-6.9	1.2
138-7 (Fragment 2)	2	Mixed	-4.9	0.2	603	19	-6.9	1.0
138-7 (Fragment 2)	3	Mixed	-4.6	0.2	460	15	-7.0	1.1
138-7 (Fragment 2)	4	Mixed	-4.6	0.1	436	14	-6.4	1.3
138-7 (Fragment 2)	5	Mixed	-4.4	0.2	73	3	-5.3	3.1
138-7 (Fragment 2)	6	Mixed	-4.2	0.2	515	16	-6.9	1.1
138-7 (Fragment 2)	7	Mixed	-4.2	0.1	391	12	-7.1	1.2
138-7 (Fragment 2)	8	Mixed	-4.3	0.2	39	2	—	—
138-7 (Fragment 2)	9	Mixed	-4.8	0.2	887	27	-5.9	0.9
138-7 (Fragment 2)	10	Mixed	-4.9	0.1	1009	31	-5.6	0.8
138-7 (Fragment 2)	11	Mixed	-4.9	0.1	1010	31	-6.6	0.8
138-7 (Fragment 2)	12	Mixed	-4.3	0.2	56	2	-8.5	4.0
138-7 (Fragment 3)	1	Mixed	-4.8	0.1	484	15	-6.9	1.2
138-7 (Fragment 3)	2	Mixed	-4.7	0.1	288	9	-7.1	1.6
138-7 (Fragment 3)	3	Mixed	-4.8	0.1	412	13	-6.8	1.2
138-7 (Fragment 3)	4	Mixed	-4.8	0.1	761	23	-6.1	1.0
138-7 (Fragment 3)	5	Mixed	-4.5	0.1	330	11	-8.2	1.4
138-7 (Fragment 3)	6	Mixed	-4.3	0.2	730	23	-6.7	1.0
138-7 (Fragment 3)	7	Mixed	-5.0	0.2	861	27	-6.8	0.8
138-7 (Fragment 3)	8	Mixed	-4.9	0.1	712	22	-6.4	0.9

138-7 (Fragment 3)	9	Mixed	-4.9	0.2	716	22	-7.3	0.9
138-7 (Fragment 3)	10	Mixed	-5.0	0.2	465	15	-7.2	1.4
138-7 (Fragment 3)	11	Mixed	-4.2	0.1	3	0	—	—
138-7 (Fragment 3)	12	Mixed	-4.6	0.1	450	14	-7.7	1.2
138-7 (Fragment 3)	13	Mixed	-4.7	0.2	720	23	-5.7	1.0
138-7 (Fragment 3)	14	Mixed	-5.3	0.1	558	18	-6.7	1.2
138-7 (Fragment 3)	15	Mixed	-4.1	0.1	398	13	-7.1	1.3
138-7 (Fragment 4)	1	Mixed	-4.8	0.1	502	16	-7.0	1.2
138-7 (Fragment 4)	2	Mixed	-4.9	0.1	888	27	-5.8	0.9
138-7 (Fragment 4)	3	Mixed	-4.3	0.1	279	9	-6.4	1.4
138-8	1	E	-28.2	0.1	17	1	—	—
138-8	2	E	-29.9	0.1	2	0	—	—
138-8	3	E	-31.1	0.1	991	30	2.1	0.8
138-9	1	E	-18.9	0.1	24	1	—	—
138-9	2	E	-26.3	0.1	5	0	—	—
138-9	3	E	-26.7	0.1	184	6	0.2	1.8
138-9	4	E	-6.9	0.1	1027	31	-5.5	0.8
138-10	1	—	-28.6	0.2	27	1	—	—
138-10	2	—	-28.8	0.1	132	6	-3.4	2.2
138-10	3	—	-28.6	0.1	123	4	-3.4	2.1
138-10	4	—	-7.1	0.1	809	26	-5.6	0.9
138-11	1	E	-29.4	0.1	6	0	—	—
138-11	2	E	-29.6	0.1	726	24	1.6	1.0
138-11	3	E	-29.7	0.1	392	13	1.0	1.3
138-11	4	E	-29.5	0.1	21	1	—	—
138-12	1	E	-28.7	0.1	12	1	—	—
138-12	2	E	-28.5	0.1	716	22	-1.3	0.9
138-12	3	E	-28.6	0.1	28	2	—	—
139-1	1	E	-6.0	0.1	682	21	-6.1	1.0
139-1	2	E	-30.2	0.1	11	1	—	—
140-1	1	E	-24.6	0.1	15	1	—	—
140-1	2	E	-24.2	0.1	2	0	—	—
140-1	3	E	-24.2	0.1	6	0	—	—

140-1	4	E	-24.2	0.1	25	1	—	—
140-1	5	E	-24.3	0.1	25	1	—	—
140-2	1	E	-1.8	0.1	1	0	—	—
140-2	2	E	-4.2	0.1	51	3	—	—
140-2	3	E	-4.2	0.1	84	5	—	—
140-2	4	E	0.0	0.1	1	0	—	—
141-1	1	—	-7.3	0.1	806	25	-5.5	0.8
141-1	2	—	-6.8	0.1	714	26	-4.6	0.8
142-1	1	E	-30.7	0.1	0.4	0	—	—
142-1	2	E	-30.5	0.1	3	0	—	—
142-1	3	E	-27.9	0.1	52	2	—	—
142-1	4	E	-26.6	0.1	30	1	—	—
142-2	1	E	-27.1	0.1	16	1	—	—
142-2	2	E	-27.1	0.1	54	2	—	—
142-2	3	E	-27.0	0.1	0.4	0	—	—
142-3	1	P	-1.8	0.1	66	2	4.6	4.0
142-3	2	P	-1.7	0.1	54	2	—	—
142-3	3	P	-1.5	0.1	97	3	1.6	2.3
142-4	1	E	-29.4	0.1	285	9	-1.9	1.4
142-4	2	E	-29.3	0.1	86	3	0.3	2.5
142-4	3	E	-29.1	0.1	60	2	—	—
143-1	1	E	-28.4	0.1	8	0	—	—
143-1	2	E	-28.3	0.1	1	0	—	—
143-1	3	E	-28.2	0.1	9	1	—	—
143-2	1	E	-6.0	0.2	1070	33	-4.5	0.8
143-2	2	E	-22.8	0.1	32	1	—	—
143-2	3	E	-25.7	0.1	30	1	—	—
143-2	4	E	-25.3	0.1	16	1	—	—
143-2	5	E	-25.5	0.1	584	18	-2.9	1.0
143-2	6	E	-25.3	0.1	1	0	—	—
144-1	1	E	-25.6	0.1	36	2	—	—
144-1	2	E	-25.7	0.1	0.4	0	—	—
144-1	3	E	-25.9	0.1	42	2	—	—

144-1	4	E	-25.8	0.1	7	0	—	—
145-1	1	E	-6.6	0.1	621	19	-5.5	1.1
145-1	2	E	-27.2	0.1	34	2	—	—
145-1	3	E	-28.1	0.1	4	0	—	—
145-1	4	E	-27.9	0.1	892	28	-3.7	0.8
145-1	5	E	-28.0	0.1	76	3	-5.3	2.5
145-1	6	E	-27.9	0.1	2	0	—	—
145-1	7	E	-27.9	0.1	9	1	—	—
146-1	1	Mixed	-1.6	0.2	66	2	—	—
146-1	2	Mixed	-1.3	0.1	344	11	-2.2	1.3
146-1	3	Mixed	-1.4	0.1	344	11	-2.3	1.3
146-2	1	E	-7.0	0.1	680	21	-4.8	0.9
146-2	2	E	-24.4	0.1	30	1	—	—
146-2	3	E	-26.8	0.1	1	0	—	—
146-2	4	E	-26.8	0.1	1	0	—	—
146-2	5	E	-26.9	0.1	33	1	—	—
147-1	1	P	-2.4	0.1	12	1	—	—
147-1	2	P	-2.5	0.2	83	3	1.6	2.8
147-1	3	P	-2.4	0.1	76	3	0.3	3.0
147-1	4	P	-2.3	0.2	77	3	0.9	2.6
147-2	1	P	-2.2	0.1	3	0	—	—
147-2	2	P	-2.1	0.1	2	0	—	—
147-2	3	P	-2.0	0.1	2	0	—	—
148-1	1	E	-25.6	0.1	1	0	—	—
148-1	2	E	-25.1	0.1	290	11	7.6	1.3
148-1	3	E	-24.9	0.1	—	—	—	—
148-1	4	E	-24.6	0.1	59	2	—	—
148-1	5	E	-23.3	0.1	203	7	7.8	1.8

Paragenesis – E: eclogitic, P: peridotitic, Mixed: mixed paragenesis. Parageneses of six diamonds with only epigenetic inclusions are not determined.

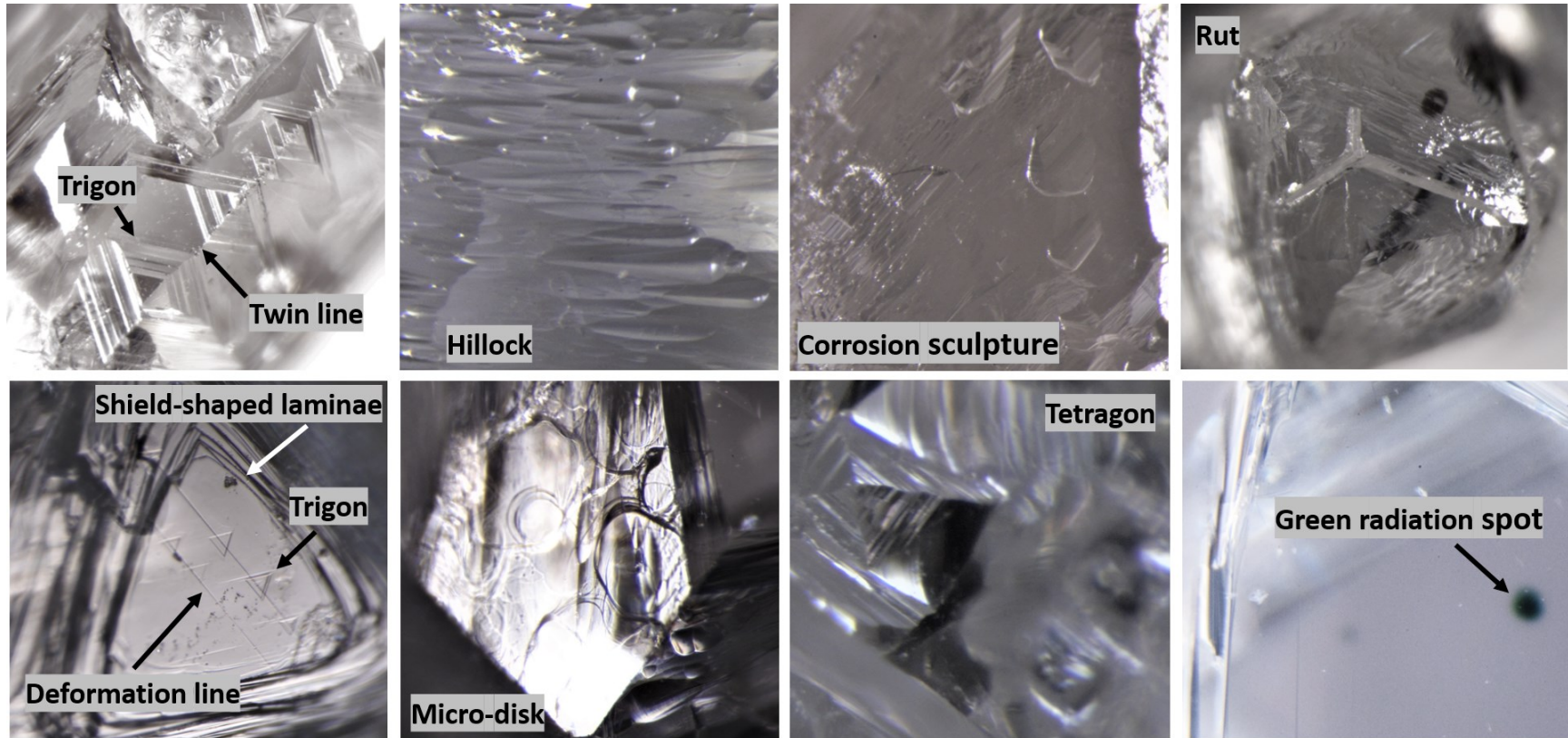


Fig. A.1. Common surface textures of Koidu diamonds.

Appendix B

Supplementary information including tables and figures for Chapter 3.

Table B.1. Major element composition (wt%) of garnet inclusions in 16 Koidu diamonds.

Sample	131-2-2	131-5-8	137-1-6	138-2-1	138-3-1	138-4-1	138-5-1	138-6-2
SiO ₂	40.53	40.29	40.22	41.02	40.91	40.38	41.26	40.06
TiO ₂	0.36	0.36	0.37	0.47	0.36	0.39	0.39	0.24
Al ₂ O ₃	22.68	22.67	21.99	23.08	23.48	22.94	23.27	22.72
Cr ₂ O ₃	0.02	0.05	0.04	0.15	0.07	0.04	0.08	0.11
FeO ^{total}	17.98	16.58	18.58	13.52	17.04	18.32	15.27	15.94
NiO	n.d.	0.01						
MnO	0.24	0.38	0.26	0.26	0.25	0.24	0.25	0.29
MgO	12.11	10.13	11.27	15.01	13.04	11.60	15.66	12.19
CaO	6.03	9.59	6.22	6.03	5.91	6.23	4.32	7.24
Na ₂ O	0.17	0.16	0.16	0.17	0.16	0.18	0.13	0.12
Total	100.11	100.23	99.09	99.71	101.22	100.31	100.63	98.92
Mg#	54.5	52.1	51.9	66.4	57.7	53.0	64.6	57.7
Ca#	16.3	26.2	17.1	16.1	15.8	17.0	11.4	19.8
Cr#	0.07	0.17	0.08	0.45	0.20	0.10	0.23	0.30

Sample	138-7-3	138-9-6	138-11-1	138-12-1	140-2-1	143-2-3	144-1-3	146-2-1
SiO ₂	41.00	40.70	41.38	40.48	42.56	40.59	40.38	40.56
TiO ₂	0.47	0.38	0.48	0.25	0.86	0.29	0.32	0.33
Al ₂ O ₃	22.98	22.38	23.13	22.88	21.09	22.85	22.94	23.38
Cr ₂ O ₃	0.02	0.04	0.17	0.04	0.28	0.05	0.05	0.04
FeO ^{total}	8.99	17.57	14.56	16.64	9.79	17.45	18.00	17.41
NiO	n.d.	n.d.	n.d.	n.d.	0.01	n.d.	n.d.	n.d.
MnO	0.16	0.22	0.26	0.41	0.27	0.24	0.23	0.35
MgO	8.47	12.26	16.83	9.00	20.61	12.33	11.67	13.06
CaO	18.55	6.21	3.57	11.08	4.24	6.29	6.58	5.39
Na ₂ O	0.18	0.16	0.14	0.13	0.13	0.14	0.14	0.14
Total	100.82	99.93	100.52	100.91	99.82	100.23	100.32	100.67
Mg#	62.7	55.4	67.3	49.1	79.0	55.7	53.6	57.2
Ca#	49.7	16.8	9.3	30.3	10.4	17.0	17.8	14.5
Cr#	0.07	0.14	0.47	0.12	0.90	0.17	0.15	0.12

Mg# = $100 \times \text{Mg}/(\text{Mg} + \text{Fe})$; Ca# = $100 \times \text{Ca}/(\text{Ca} + \text{Mg} + \text{Fe})$; Cr# = $100 \times \text{Cr}/(\text{Cr} + \text{Al})$.

Table B.2. Trace element concentration (ppm) of garnet inclusions in 16 Koidu diamonds.

Sample	131-2-2	131-5-8	137-1-6	138-2-1	138-3-1	138-4-1	138-5-1	138-6-2
La	0.005	0.010	0.010	0.021	0.023	0.010	0.009	0.009
Ce	0.149	0.339	0.198	0.428	0.392	0.295	0.148	0.091
Pr	0.104	0.227	0.134	0.159	0.123	0.129	0.084	0.070
Nd	1.347	3.115	1.497	1.483	1.392	1.470	1.067	1.316
Sm	3.100	2.914	3.017	2.672	1.976	3.260	1.362	2.311
Eu	2.084	1.118	1.593	1.322	1.120	1.978	0.724	0.977
Gd	8.880	5.080	9.180	6.060	5.840	9.100	4.360	6.000
Tb	1.688	0.967	1.373	1.087	1.164	1.887	1.061	1.002
Dy	11.420	6.810	9.460	7.270	8.030	13.090	8.560	7.360
Ho	2.404	1.504	2.473	1.529	1.635	2.896	1.976	1.875
Er	7.170	4.651	8.300	4.584	4.893	8.860	5.990	6.250
Tm	1.038	0.661	1.015	0.655	0.697	1.255	0.855	0.807
Yb	7.320	4.736	7.050	4.659	4.882	8.640	5.805	5.510
Lu	1.129	0.726	1.093	0.707	0.737	1.337	0.835	0.836
Sample	138-7-3	138-9-6	138-11-1	138-12-1	140-2-1	143-2-3	144-1-3	146-2-1
La	0.062	0.004	0.002	0.022	0.050	0.037	0.007	0.009
Ce	0.559	0.105	0.000	0.812	0.374	0.418	0.291	0.249
Pr	0.213	0.077	0.061	0.623	0.108	0.192	0.239	0.173
Nd	1.910	1.171	0.784	8.000	0.934	2.040	2.378	1.414
Sm	1.314	3.324	1.218	5.620	0.911	2.700	3.254	2.044
Eu	0.617	1.563	0.656	1.931	0.475	1.660	1.579	1.227
Gd	2.240	8.440	3.603	8.570	2.441	7.520	8.280	6.760
Tb	0.321	1.144	0.810	1.571	0.576	1.622	1.176	1.097
Dy	2.138	7.630	6.600	11.250	4.732	11.680	7.850	8.460
Ho	0.540	1.898	1.578	2.477	1.128	2.610	2.048	2.246
Er	1.646	6.240	5.000	7.370	3.634	8.170	6.750	7.850
Tm	0.182	0.775	0.756	1.054	0.535	1.217	0.836	0.988
Yb	1.116	5.420	5.470	7.640	3.835	8.790	6.070	6.980
Lu	0.155	0.810	0.822	1.171	0.593	1.380	0.941	1.109

Table B.3. Average $\delta^{18}\text{O}$ values and nitrogen concentrations, $\delta^{13}\text{C}$ and $\delta^{15}\text{N}$ values of garnet inclusions and their host diamonds, respectively.

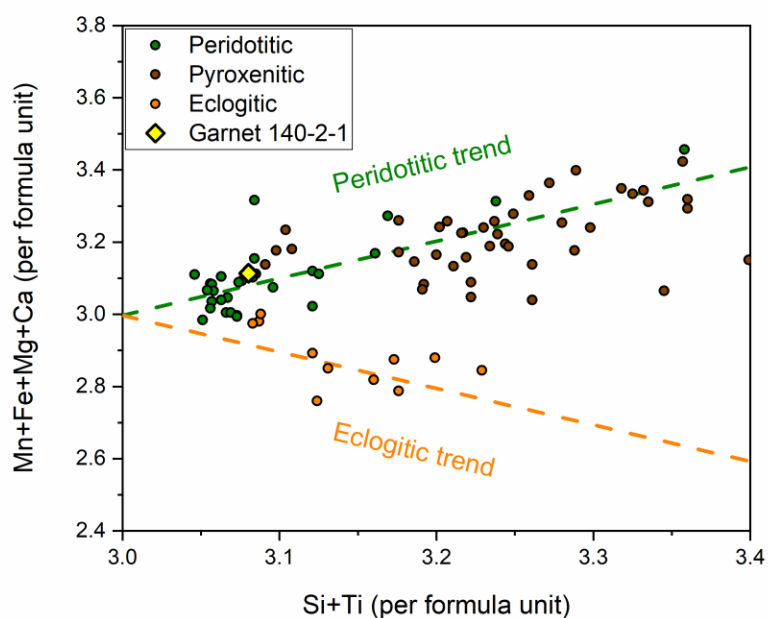
Sample	$\delta^{18}\text{O}_{\text{VSMOW}}$ (‰)	2σ (‰)	$\delta^{13}\text{C}_{\text{VPDB}}$ (‰)	2σ (‰)	$\delta^{15}\text{N}_{\text{Air}}$ (‰)	2σ (‰)	[N] (at.ppm)	2σ (at.ppm)
131-2-2	12.1	0.3	-19.4	0.1	9.9	2.6	57	2
131-5-8	10.8	0.3	-25.4	0.2	1.1	3.2	41	2
137-1-6	11.8	0.3	-27.9	0.1	0.6	3.5	33	2
138-2-1	11.8	0.3	-28.3	0.1	—	—	21	1
138-3-1	10.8	0.3	-26.8	0.1	-0.2	0.9	552	17
138-4-1	11.8	0.3	-26.3	0.1	-2.6	1.3	267	9
138-5-1 (rim)	10.3	0.3	-7.0	0.1	-5.8	0.8	968	30
138-5-1 (core)	10.3	0.3	-26.5	0.1	-5.6	1.2	290	10
138-6-2	11.1	0.3	-22.0	0.1	-2.0	2.5	55	2
138-7-3	5.4	0.3	-4.7	0.1	-6.9	1.2	515	16
138-9-6 (rim)	12.0	0.3	-6.9	0.1	-5.5	0.8	1027	31
138-9-6 (core)	12.0	0.3	-24.0	0.1	0.2	1.8	71	2
138-11-1	9.9	0.3	-29.6	0.1	1.3	1.2	286	10
138-12-1	11.3	0.3	-28.6	0.1	-1.3	0.9	252	8
140-2-1	6.3	0.3	-2.6	0.1	—	—	34	2
143-2-3 (rim)	11.3	0.3	-6.0	0.2	-4.5	0.8	1070	33
143-2-3 (core)	11.3	0.3	-24.9	0.1	-2.9	1.0	133	4
144-1-3	11.9	0.3	-25.7	0.1	—	—	21	1
146-2-1 (rim)	11.9	0.3	-7.0	0.1	-4.8	0.9	680	21
146-2-1 (core)	11.9	0.3	-26.2	0.1	—	—	16	1

Table B.4. SIMS analysis of garnet inclusions in 16 Koidu diamonds.

Sample	Spot #	$\delta^{18}\text{O}$ (VSMOW)	2σ (‰)
131-2-2	1	12.14	0.27
131-2-2	2	12.02	0.25
131-2-2	3	12.11	0.25
131-2-2	4	12.10	0.26
131-5-8	1	10.86	0.26
131-5-8	2	10.76	0.27
131-5-8	3	10.81	0.25
131-5-8	4	10.82	0.26
131-5-8	5	10.87	0.27
131-5-8	6	10.94	0.26
137-1-6	1	11.76	0.25
137-1-6	2	11.77	0.25
137-1-6	3	11.85	0.25
137-1-6	4	11.94	0.26
138-2-1	1	11.83	0.26
138-2-1	2	11.80	0.26
138-2-1	3	11.90	0.25
138-2-1	4	11.68	0.26
138-3-1	1	10.72	0.25
138-3-1	2	10.74	0.27
138-3-1	3	10.71	0.26
138-3-1	4	10.86	0.25
138-3-1	5	10.70	0.26
138-4-1	1	11.74	0.25
138-4-1	2	11.87	0.26
138-4-1	3	11.72	0.27
138-4-1	4	11.86	0.27
138-5-1	1	10.39	0.27
138-5-1	2	9.99	0.26
138-5-1	3	10.44	0.27
138-5-1	4	10.43	0.26
138-5-1	5	10.27	0.27
138-6-2	1	11.18	0.27
138-6-2	2	10.98	0.27
138-6-2	3	11.20	0.26
138-6-2	4	11.23	0.28
138-6-2	5	10.99	0.26
138-7-3	1	5.29	0.27

138-7-3	2	5.45	0.27
138-7-3	3	5.30	0.26
138-7-3	4	5.34	0.26
138-9-6	1	12.08	0.26
138-9-6	2	11.99	0.27
138-9-6	3	11.96	0.26
138-9-6	4	11.94	0.26
138-11-1	1	9.92	0.26
138-11-1	2	9.82	0.26
138-11-1	3	9.99	0.26
138-11-1	4	9.72	0.26
138-11-1	5	9.95	0.26
138-12-1	1	11.29	0.26
138-12-1	2	11.34	0.26
138-12-1	3	11.31	0.26
138-12-1	4	11.35	0.26
138-12-1	5	11.25	0.26
140-2-1	1	6.31	0.27
140-2-1	2	6.37	0.27
140-2-1	3	6.18	0.26
140-2-1	4	6.23	0.26
143-2-3	1	11.44	0.27
143-2-3	2	11.23	0.25
143-2-3	3	11.25	0.26
144-1-3	1	11.89	0.26
144-1-3	2	11.95	0.28
144-1-3	3	11.97	0.25
146-2-1	1	11.78	0.26
146-2-1	2	11.84	0.25
146-2-1	3	11.87	0.25
146-2-1	4	11.95	0.27

(a)



(b)

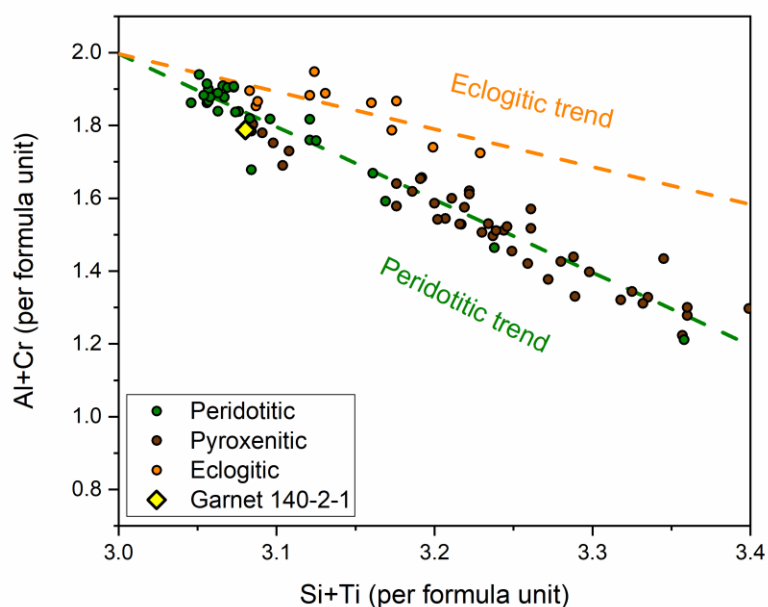


Fig. B.1. Major element composition of Koidu majoritic garnet 140-2-1. Also shown are compositions of majoritic garnet inclusions in diamonds worldwide (Kiseeva et al., 2013 and references therein). (a) Sum of divalent cations and (b) sum of trivalent cations as functions of (Si + Ti) per formula unit. Garnet 140-2-1 follows the trend of peridotitic majoritic substitution (after Kiseeva et al., 2016).

Appendix C

Supplementary information including tables and figures for Chapter 4.

Table C.1. Inclusion abundance in Koidu diamonds.

Mono-mineralic assemblages	n	Bi-mineralic assemblages	n	Tri-mineralic assemblages	n
Coesite (SiO ₂)	17	Cpx+SiO ₂	10	Grt+cpx+sul	2
Olivine (ol)	12	Ky+SiO ₂	5	Cpx+ky+SiO ₂	2
Eclogitic garnet (grt)	9	Grt+SiO ₂	4	Grt+sul+SiO ₂	1
Omphacite (cpx)	8	Ol+sp	3	Grt+ky+sul	1
Kyanite (ky)	5	Ky+sul	2	Grt+ky+SiO ₂	1
Spinel (sp)	3	Grt+cpx	2	Grt+cpx+ky	1
Sulphide (sul)	2	Grt+sul	2	Ol+sp+SiO ₂	1
Rutile (ru)	1	Grt+ky	1	Cpx+sul+SiO ₂	1
		Ol+SiO ₂	1	Grt+cpx+SiO ₂	1
		Ol+grt	1		
		Sul+SiO ₂	1		
		Corundum+SiO ₂	1		
		Sul+cpx	1		
		Cpx+sp	1		
		Cpx+ol	1		
Total diamonds	57		36		11

Table C.2. Major element compositions (wt%) of representative silicate and oxide inclusions from Koidu diamonds. Abbreviation of mineral follows Table C.1.

Sample	130-5-2	130-34-1	147-1-4	135-3-3	136-1-6	147-1-6	131-3-5	137-1-13
Mineral	ol	ol	ol	sp	sp	sp	cpx	cpx
Paragenesis	P	P	P	P	P	P	E	E
Assemblage	ol	ol	ol+sp	sp	ol+sp	ol+sp	grt+cpx+sul	ky+grt+cpx
SiO ₂	41.67	41.22	41.54	0.08	0.18	0.06	55.26	56.98
TiO ₂	b.d.l.	0.01	0.01	2.84	0.21	0.05	0.58	0.47
ZnO	n.d.	n.d.	n.d.	0.03	0.06	0.06	b.d.l.	0.02
Al ₂ O ₃	b.d.l.	b.d.l.	b.d.l.	5.16	26.69	7.25	13.91	20.51
V ₂ O ₃	n.d.	n.d.	n.d.	0.19	0.17	0.14	0.08	0.08
Cr ₂ O ₃	0.04	0.05	0.05	62.09	41.17	64.36	0.04	0.05
FeO ^{total}	5.21	7.70	5.59	15.17	11.25	13.39	4.50	2.93
NiO	0.37	0.38	0.35	0.18	0.18	0.07	b.d.l.	b.d.l.
MnO	0.07	0.10	0.08	0.31	0.22	0.31	0.06	0.03
MgO	52.36	51.36	52.67	14.68	18.83	14.89	7.33	3.82
CaO	0.02	0.05	0.01	b.d.l.	b.d.l.	b.d.l.	10.63	5.87
Na ₂ O	b.d.l.	b.d.l.	b.d.l.	0.01	b.d.l.	b.d.l.	6.48	9.11
K ₂ O	b.d.l.	b.d.l.	b.d.l.	b.d.l.	b.d.l.	b.d.l.	0.23	0.09
Total	99.74	100.87	100.30	100.74	98.95	100.58	99.10	99.96

Sample	138-9-1	138-12-2	142-2-3	143-1-2	146-2-2	128-6-1	131-3-1	137-1-6
Mineral	cpx	cpx	cpx	cpx	cpx	grt	grt	grt
Paragenesis	E	E	E	E	E	E	E	E
Assemblage	grt+cpx+SiO ₂	grt+cpx	cpx	grt+cpx+sul	grt+cpx	ky+grt	grt+cpx+sul	ky+grt+cpx
SiO ₂	55.84	56.26	54.80	55.62	56.59	40.29	40.16	40.22
TiO ₂	0.51	0.41	0.50	0.45	0.25	0.29	0.49	0.37
ZnO	b.d.l.	0.02	0.03	b.d.l.	b.d.l.	n.d.	n.d.	n.d.
Al ₂ O ₃	20.27	19.05	6.96	19.81	20.17	23.06	22.42	21.99
V ₂ O ₃	0.09	0.06	0.06	b.d.l.	0.08	n.d.	n.d.	n.d.
Cr ₂ O ₃	0.09	0.04	0.82	b.d.l.	0.09	0.06	0.05	0.04
FeO ^{total}	2.79	2.40	6.31	3.02	2.66	18.15	16.26	18.58
NiO	0.01	b.d.l.	0.01	b.d.l.	b.d.l.	0.01	b.d.l.	b.d.l.
MnO	0.03	0.03	0.09	0.02	0.05	0.25	0.29	0.26
MgO	4.17	4.24	13.59	3.86	4.15	11.60	11.76	11.27
CaO	6.13	8.06	11.83	6.83	5.69	6.48	7.72	6.22
Na ₂ O	9.06	8.32	4.07	8.65	9.24	0.15	0.16	0.16
K ₂ O	0.09	0.13	0.31	0.05	0.08	b.d.l.	b.d.l.	b.d.l.
Total	99.07	99.01	99.37	98.31	99.06	100.32	99.31	99.09

Sample	138-1-3	138-9-6	138-12-1	143-1-1	146-2-1	128-5-2	137-1-8	132-1-2
Mineral	grt	grt	grt	grt	grt	ky	ky	ru
Paragenesis	E	E	E	E	E	E	E	E
Assemblage	grt+SiO ₂	grt+cpx+SiO ₂	grt+cpx	grt+cpx+sul	grt+cpx	ky	ky+grt+cpx	ru
SiO ₂	40.27	40.70	40.48	39.34	40.56	37.07	35.79	b.d.l.
TiO ₂	0.34	0.38	0.25	0.31	0.33	0.17	0.18	98.44
ZnO	n.d.	n.d.	n.d.	n.d.	n.d.	n.d.	n.d.	n.d.
Al ₂ O ₃	23.17	22.38	22.88	22.35	23.38	61.86	63.38	0.42
V ₂ O ₃	n.d.	n.d.	n.d.	n.d.	n.d.	0.02	0.05	0.32
Cr ₂ O ₃	0.03	0.04	0.04	0.02	0.04	0.09	0.10	0.02
FeO ^{total}	18.13	17.57	16.64	18.19	17.41	0.36	0.31	0.38
NiO	b.d.l.	b.d.l.	b.d.l.	b.d.l.	b.d.l.	b.d.l.	b.d.l.	0.01
MnO	0.22	0.22	0.41	0.38	0.35	b.d.l.	b.d.l.	b.d.l.
MgO	11.96	12.26	9.00	9.84	13.06	0.18	0.11	b.d.l.
CaO	5.86	6.21	11.08	8.07	5.39	b.d.l.	b.d.l.	b.d.l.
Na ₂ O	0.15	0.16	0.13	0.16	0.14	b.d.l.	b.d.l.	b.d.l.
K ₂ O	b.d.l.	b.d.l.	b.d.l.	b.d.l.	b.d.l.	b.d.l.	b.d.l.	b.d.l.
Total	100.13	99.93	100.91	98.65	100.67	99.75	99.91	99.59

n.d. = not determined.

b.d.l. = below detection limit.

Table C.2. Major element compositions (wt%) of garnet and omphacite grains from Koidu diamond-bearing eclogite xenoliths.

Sample Mineral	KEC-40-coat grt	KEC-40-oct grt	KEC-80-DB-2-A grt	KEC-80-DB-2-B1 grt	KEC-80-DB-2-B2 grt	KEC-81-DB-1 grt
SiO ₂	40.24	40.30	40.25	40.28	40.20	39.69
TiO ₂	0.26	0.44	0.45	0.26	0.44	0.33
Al ₂ O ₃	22.53	22.14	22.28	22.48	22.26	22.19
Cr ₂ O ₃	0.05	0.06	0.05	0.05	0.05	0.04
FeO ^{total}	14.34	16.72	16.54	14.04	16.57	16.79
NiO	b.d.l.	b.d.l.	b.d.l.	b.d.l.	b.d.l.	b.d.l.
MnO	0.24	0.30	0.30	0.23	0.30	0.31
MgO	10.84	12.02	12.23	10.89	12.26	8.84
CaO	11.36	8.08	7.88	11.53	7.90	11.87
Na ₂ O	0.07	0.11	0.11	0.07	0.10	0.10
K ₂ O	b.d.l.	b.d.l.	b.d.l.	b.d.l.	b.d.l.	b.d.l.
Total	99.93	100.17	100.07	99.83	100.09	100.15

Sample Mineral	KEC-40-oct cpx	KEC-80-DB-2-A cpx	KEC-80-DB-2-B1 cpx	KEC-80-DB-2-B2 cpx	KEC-81-DB-1 cpx
SiO ₂	55.67	55.58	56.04	55.68	56.12
TiO ₂	0.40	0.40	0.25	0.41	0.28
Al ₂ O ₃	8.18	8.05	11.34	8.12	11.39
Cr ₂ O ₃	0.06	0.06	0.05	0.05	0.04
FeO ^{total}	4.12	4.21	2.81	4.21	3.47
NiO	0.04	0.04	0.04	0.04	0.03
MnO	0.03	0.03	0.03	0.03	0.03
MgO	10.64	10.84	9.22	10.80	8.67
CaO	15.03	15.09	13.61	15.03	13.12
Na ₂ O	5.19	5.11	6.24	5.17	6.40
K ₂ O	0.21	0.17	0.16	0.16	0.10
Total	99.57	99.59	99.81	99.70	99.65

b.d.l. = below detection limit.

Table C.3. Trace element compositions (ppm) of representative garnet and omphacite inclusions from Koidu diamonds.

Sample	131-1-1	131-3-1	137-1-6	138-4-2	138-9-6	138-11-1
Mineral	grt	grt	grt	grt	grt	grt
Sc	76.2	58.1	69.6	70.3	65.3	76.9
Ti	1987	2986	2334	2397	2508	2872
V	133	219	176	217	189	145
Ni	11.7	16.2	11.4	14.1	13.2	17.3
Rb	b.d.l.	b.d.l.	b.d.l.	b.d.l.	b.d.l.	b.d.l.
Sr	13.5	4.8	13.5	14.9	10.4	2.0
Y	80.6	51.9	71.9	78.5	55.8	42.8
Zr	19.5	18.0	13.5	25.5	13.3	27.0
Nb	b.d.l.	b.d.l.	b.d.l.	b.d.l.	b.d.l.	b.d.l.
Ba	b.d.l.	b.d.l.	b.d.l.	b.d.l.	b.d.l.	b.d.l.
La	0.088	0.006	0.010	0.010	0.004	0.002
Ce	1.054	0.195	0.198	0.295	0.105	b.d.l.
Pr	0.170	0.114	0.134	0.129	0.077	0.061
Nd	0.875	1.427	1.497	1.470	1.171	0.784
Sm	2.530	2.044	3.017	3.260	3.324	1.218
Eu	1.558	1.071	1.593	1.978	1.563	0.656
Gd	8.710	5.560	9.180	9.100	8.440	3.603
Tb	1.447	1.161	1.373	1.887	1.144	0.810
Dy	10.440	8.260	9.460	13.090	7.630	6.600
Ho	2.788	1.858	2.473	2.896	1.898	1.578
Er	9.640	5.690	8.300	8.860	6.240	5.000
Tm	1.210	0.791	1.015	1.255	0.775	0.756
Yb	8.320	5.700	7.050	8.640	5.420	5.470
Lu	1.311	0.870	1.093	1.337	0.810	0.822
Hf	0.291	0.340	0.169	0.382	0.180	0.527

Sample	138-12-1	143-1-1	146-2-1	130-1-2	131-3-5	137-1-11
Mineral	grt	grt	grt	cpx	cpx	cpx
Sc	69.6	81.3	64.4	5.6	10.8	6.8
Ti	1595	1897	2014	2248	4500	2983
V	149	153	149	718	578	540
Ni	1.7	b.d.l.	13.1	13.8	53.4	23.2
Rb	b.d.l.	b.d.l.	b.d.l.	b.d.l.	b.d.l.	b.d.l.
Sr	3.7	4.9	13.9	510	328	316
Y	68.1	99.7	65.1	0.626	2.260	1.779
Zr	50.9	77.6	15.5	6.5	11.2	8.0
Nb	0.002	b.d.l.	b.d.l.	b.d.l.	b.d.l.	b.d.l.
Ba	b.d.l.	b.d.l.	b.d.l.	b.d.l.	b.d.l.	b.d.l.
La	0.022	b.d.l.	0.009	0.130	0.207	0.102
Ce	0.812	0.755	0.249	0.645	1.305	0.535
Pr	0.623	0.970	0.173	0.163	0.337	0.125
Nd	8.000	13.310	1.414	0.760	1.710	0.731
Sm	5.620	9.700	2.044	0.278	0.860	0.582
Eu	1.931	3.470	1.227	0.149	0.308	0.224
Gd	8.570	14.700	6.760	0.309	0.960	0.760
Tb	1.571	2.390	1.097	0.030	0.102	0.092
Dy	11.250	17.100	8.460	0.170	0.550	0.443
Ho	2.477	3.450	2.246	0.016	0.080	0.067
Er	7.370	10.700	7.850	0.021	0.232	0.165
Tm	1.054	1.410	0.988	b.d.l.	0.016	0.010
Yb	7.640	11.170	6.980	b.d.l.	0.107	0.077
Lu	1.171	1.470	1.109	b.d.l.	0.013	0.014
Hf	0.962	1.450	0.232	0.267	0.560	0.310

Sample Mineral	138-9-1 cpx	138-12-2 cpx	142-2-1 cpx	142-4-1 cpx	143-1-2 cpx	146-2-2 cpx
Sc	6.1	7.9	15.6	15.8	8.2	6.2
Ti	3057	2353	3128	1929	3378	1647
V	601	417	425	531	490	521
Ni	27.4	8.6	102.1	87.3	9.6	30.2
Rb	b.d.l.	0.091	b.d.l.	b.d.l.	b.d.l.	b.d.l.
Sr	280	70	433	533	114	537
Y	1.465	0.913	7.830	4.965	1.620	1.790
Zr	6.6	25.7	16.7	8.6	28.2	3.7
Nb	b.d.l.	0.018	0.014	b.d.l.	b.d.l.	b.d.l.
Ba	0.082	0.452	0.701	1.004	b.d.l.	0.048
La	0.028	0.046	0.358	0.623	0.034	0.280
Ce	0.218	0.766	2.481	2.827	1.239	0.845
Pr	0.076	0.321	0.705	0.650	0.726	0.203
Nd	0.653	2.330	4.490	3.844	5.690	0.911
Sm	0.660	0.596	2.330	1.789	1.570	0.432
Eu	0.260	0.143	0.737	0.550	0.294	0.187
Gd	0.732	0.463	3.040	2.117	0.910	0.611
Tb	0.090	0.054	0.311	0.215	0.105	0.066
Dy	0.375	0.227	1.580	1.077	0.460	0.331
Ho	0.055	0.033	0.287	0.196	0.076	0.061
Er	0.120	0.074	0.657	0.443	0.125	0.163
Tm	0.014	0.008	0.066	0.040	0.014	0.016
Yb	0.075	0.055	0.313	0.258	b.d.l.	0.084
Lu	0.008	0.007	0.043	0.031	b.d.l.	0.010
Hf	0.283	1.371	0.643	0.351	1.220	0.152

b.d.l. = below detection limit.

Table C.3. Trace element compositions (ppm) of garnet and omphacite grains from Koidu diamond-bearing eclogite xenolith.

Sample	KEC-40-coat	KEC-40-oct	KEC-80-DB-2-A	KEC-80-DB-2-B1	KEC-80-DB-2-B2	KEC-81-DB-1
Mineral	grt	grt	grt	grt	grt	grt
Sc	47.4	51.9	50.8	45.6	52.2	56.4
Ti	1529	2670	2727	1601	2732	2004
V	123	103	101	152	103	132
Ni	38.7	36.0	33.0	35.2	33.4	28.5
Rb	0.008	0.003	b.d.l.	0.002	0.006	0.005
Sr	0.8	0.9	0.8	0.8	0.9	1.1
Y	20.0	16.6	16.4	19.8	16.9	17.1
Zr	15.7	19.7	19.6	28.0	20.7	15.8
Nb	0.093	0.072	0.050	0.037	0.055	0.001
Ba	0.002	0.005	b.d.l.	b.d.l.	0.004	0.009
La	0.015	0.016	0.019	0.011	0.018	0.013
Ce	0.199	0.229	0.240	0.148	0.252	0.171
Pr	0.079	0.101	0.107	0.065	0.114	0.081
Nd	0.83	1.312	1.315	1.169	1.406	1.081
Sm	1.020	1.426	1.444	1.721	1.514	1.433
Eu	0.582	0.760	0.759	0.810	0.776	0.836
Gd	2.287	2.413	2.441	2.644	2.518	2.773
Tb	0.472	0.445	0.448	0.479	0.455	0.486
Dy	3.384	3.019	2.934	3.302	3.036	3.169
Ho	0.762	0.634	0.647	0.756	0.650	0.670
Er	2.298	1.776	1.789	2.268	1.825	1.958
Tm	0.331	0.244	0.244	0.325	0.246	0.277
Yb	2.263	1.608	1.615	2.325	1.607	1.837
Lu	0.340	0.236	0.242	0.346	0.236	0.278
Hf	0.307	0.306	0.332	0.374	0.317	0.301

Sample Mineral	KEC-40-oct cpx	KEC-80-DB-2-A cpx	KEC-80-DB-2-B1 cpx	KEC-80-DB-2-B2 cpx	KEC-81-DB-1 cpx
Sc	14.7	14.9	9.9	14.7	12.0
Ti	2510	2531	1611	2554	1663
V	283	283	291	283	332
Ni	311	330	274	317	243
Rb	0.013	0.023	0.009	0.011	0.042
Sr	234	237	103	232	100
Y	0.873	0.922	0.499	0.902	0.421
Zr	15.7	25.0	10.4	16.4	8.2
Nb	0.133	0.135	0.081	0.134	0.015
Ba	0.252	0.284	0.068	0.261	0.178
La	1.096	1.185	0.327	1.079	0.218
Ce	4.205	4.355	1.352	4.075	0.900
Pr	0.806	0.797	0.239	0.768	0.169
Nd	4.499	4.514	1.250	4.337	0.980
Sm	1.175	1.200	0.352	1.154	0.323
Eu	0.357	0.372	0.121	0.360	0.122
Gd	0.690	0.739	0.283	0.695	0.279
Tb	0.067	0.072	0.031	0.073	0.029
Dy	0.273	0.292	0.145	0.286	0.126
Ho	0.037	0.040	0.023	0.037	0.019
Er	0.064	0.069	0.046	0.064	0.032
Tm	0.007	0.007	0.004	0.007	0.003
Yb	0.027	0.038	0.025	0.032	0.016
Lu	0.003	0.004	0.002	0.003	0.002
Hf	0.716	0.846	0.544	0.810	0.556

b.d.l. = below detection limit.

Table C.4. Major element (wt%) and trace element (ppm) compositions of reconstructed whole-rocks from garnet and omphacite inclusions.

Sample	131-3	137-1	138-9	138-12	143-1	146-2
SiO ₂	47.73	48.25	48.26	48.37	47.48	48.58
TiO ₂	0.46	0.42	0.38	0.33	0.38	0.29
Al ₂ O ₃	18.18	21.14	21.32	20.97	21.08	21.78
Cr ₂ O ₃	0.05	0.05	0.06	0.04	0.01	0.07
FeO ^{total}	10.38	10.76	10.19	9.52	10.60	10.03
NiO	b.d.l.	b.d.l.	b.d.l.	b.d.l.	b.d.l.	b.d.l.
MnO	0.17	0.14	0.13	0.22	0.20	0.20
MgO	9.55	7.52	8.17	6.62	6.85	8.61
CaO	9.17	6.03	6.17	9.57	7.45	5.54
Na ₂ O	3.33	4.63	4.60	4.23	4.40	4.69
K ₂ O	0.12	0.05	0.05	0.07	0.03	0.04
Sc	34.8	38.2	35.7	38.8	44.8	35.3
Ti	3130	2659	2395	1974	2638	1831
V	424	358	389	283	321	335
Ni	38.6	17.3	20.3	5.1	4.8	21.6
Rb	b.d.l.	b.d.l.	b.d.l.	0.046	b.d.l.	b.d.l.
Sr	178.3	164.6	144.3	37.0	59.3	275.5
Y	27.2	36.8	28.6	34.5	50.7	33.5
Zr	14.2	10.7	9.6	38.3	52.9	9.6
Nb	b.d.l.	b.d.l.	b.d.l.	0.010	b.d.l.	b.d.l.
Ba	0.043	b.d.l.	0.103	0.226	b.d.l.	0.024
La	0.122	0.056	0.015	0.034	0.017	0.144
Ce	0.837	0.367	0.161	0.789	0.997	0.547
Pr	0.230	0.130	0.076	0.472	0.848	0.188

Nd	1.692	1.114	0.914	5.165	9.500	1.163
Sm	1.479	1.800	1.987	3.108	5.635	1.238
Eu	0.701	0.909	0.907	1.037	1.882	0.707
Gd	3.298	4.970	4.593	4.517	7.805	3.686
Tb	0.644	0.733	0.615	0.812	1.248	0.582
Dy	4.442	4.952	4.005	5.739	8.780	4.396
Ho	0.975	1.270	0.976	1.255	1.763	1.153
Er	2.962	4.233	3.178	3.722	5.413	4.007
Tm	0.405	0.513	0.394	0.531	0.712	0.502
Yb	2.909	3.564	2.745	3.848	5.585	3.532
Lu	0.442	0.554	0.409	0.589	0.735	0.560
Hf	0.438	0.240	0.215	1.167	1.335	0.192

b.d.l. = below detection limit.

Table C.4. Major element (wt%) and trace element (ppm) compositions of reconstructed whole-rocks from constituent garnet and omphacite in xenoliths.

Sample	KEC-40 Oct	KEC-81 DB1	KEC-80 DB2 (A)	KEC-80 DB2 (B1)	KEC-80 DB2 (B2)
SiO ₂	47.99	47.90	47.91	48.16	47.94
TiO ₂	0.42	0.31	0.42	0.25	0.42
Al ₂ O ₃	15.16	16.79	15.16	16.91	15.19
Cr ₂ O ₃	0.06	0.04	0.05	0.05	0.05
FeO ^{total}	10.42	10.13	10.38	8.43	10.39
NiO	0.02	0.01	0.02	0.02	0.02
MnO	0.17	0.17	0.17	0.13	0.17
MgO	11.33	8.76	11.54	10.06	11.53
CaO	11.56	12.49	11.48	12.57	11.47
Na ₂ O	2.65	3.25	2.61	3.16	2.64
K ₂ O	0.11	0.05	0.09	0.08	0.08
Sc	27.7	32.9	34.2	33.5	33.3
Ti	1606	2629	1833.5	2643	2590
V	221	192	232	193	193
Ni	155	182	136	175	173
Rb	0.006	0.012	0.024	0.008	0.008
Sr	51.9	119.1	50.6	116.3	117.3
Y	10.1	8.7	8.8	8.9	8.7
Zr	19.2	22.3	12.0	18.5	17.7
Nb	0.059	0.093	0.008	0.094	0.103
Ba	0.034	0.141	0.094	0.132	0.128
La	0.169	0.602	0.115	0.549	0.556
Ce	0.750	2.298	0.536	2.164	2.217
Pr	0.152	0.452	0.125	0.441	0.454

Nd	1.210	2.915	1.031	2.872	2.906
Sm	1.037	1.322	0.878	1.334	1.301
Eu	0.465	0.566	0.479	0.568	0.559
Gd	1.464	1.590	1.526	1.607	1.552
Tb	0.255	0.260	0.258	0.264	0.256
Dy	1.724	1.613	1.647	1.661	1.646
Ho	0.390	0.343	0.344	0.344	0.336
Er	1.157	0.929	0.995	0.944	0.920
Tm	0.165	0.125	0.140	0.127	0.126
Yb	1.175	0.826	0.926	0.820	0.818
Lu	0.174	0.123	0.140	0.119	0.120
Hf	0.473	0.607	0.442	0.580	0.526

b.d.l. = below detection limit.

Table C.5. Average $\delta^{18}\text{O}$ values of garnet grains in six Koidu diamondiferous eclogites.

Sample	$\delta^{18}\text{O}_{\text{VSMOW}}$ (‰)	2σ (‰)
KEC-40-coat	5.89	0.26
KEC-40-oct	5.63	0.26
KEC-80-DB-2-A	5.66	0.26
KEC-80-DB-2-B1	5.78	0.26
KEC-80-DB-2-B2	5.63	0.26
KEC-81-DB-1	6.33	0.26

Table C.6. SIMS analysis of garnet grains in six Koidu diamondiferous eclogites.

Sample	Spot #	$\delta^{18}\text{O}_{\text{VSMOW}}$ (‰)	2σ (‰)
KEC-40-coat (grain 1)	1	5.89	0.26
KEC-40-coat (grain 1)	2	5.87	0.27
KEC-40-coat (grain 1)	3	5.83	0.26
KEC-40-coat (grain 1)	4	5.85	0.25
KEC-40-coat (grain 1)	5	5.92	0.27
KEC-40-coat (grain 2)	1	5.82	0.27
KEC-40-coat (grain 2)	2	5.88	0.27
KEC-40-coat (grain 2)	3	5.86	0.24
KEC-40-coat (grain 2)	4	5.77	0.26
KEC-40-coat (grain 2)	5	5.97	0.24
KEC-40-coat (grain 3)	1	5.98	0.32
KEC-40-coat (grain 3)	2	5.99	0.27
KEC-40-coat (grain 3)	3	5.90	0.24
KEC-40-coat (grain 3)	4	5.93	0.27
KEC-40-oct (grain 1)	1	5.61	0.27
KEC-40-oct (grain 1)	2	5.61	0.27
KEC-40-oct (grain 1)	3	5.65	0.24
KEC-40-oct (grain 1)	4	5.58	0.25
KEC-40-oct (grain 1)	5	5.66	0.28
KEC-40-oct (grain 2)	1	5.64	0.26
KEC-40-oct (grain 2)	2	5.65	0.25
KEC-40-oct (grain 2)	3	5.74	0.25
KEC-40-oct (grain 2)	4	5.65	0.25
KEC-40-oct (grain 2)	5	5.64	0.25
KEC-40-oct (grain 3)	1	5.67	0.27
KEC-40-oct (grain 3)	2	5.58	0.26
KEC-40-oct (grain 3)	3	5.64	0.26
KEC-40-oct (grain 3)	4	5.61	0.24
KEC-40-oct (grain 3)	5	5.50	0.26
KEC-80-DB-2-A (grain 1)	1	5.67	0.26
KEC-80-DB-2-A (grain 1)	2	5.71	0.26
KEC-80-DB-2-A (grain 1)	3	5.55	0.27
KEC-80-DB-2-A (grain 1)	4	5.68	0.25
KEC-80-DB-2-A (grain 1)	5	5.67	0.25
KEC-80-DB-2-A (grain 2)	1	5.63	0.24
KEC-80-DB-2-A (grain 2)	2	5.67	0.29
KEC-80-DB-2-A (grain 2)	3	5.72	0.27
KEC-80-DB-2-A (grain 2)	4	5.65	0.27

KEC-80-DB-2-A (grain 2)	5	5.77	0.26
KEC-80-DB-2-A (grain 3)	1	5.61	0.24
KEC-80-DB-2-A (grain 3)	2	5.61	0.24
KEC-80-DB-2-A (grain 3)	3	5.65	0.28
KEC-80-DB-2-A (grain 3)	4	5.56	0.25
KEC-80-DB-2-A (grain 3)	5	5.69	0.26
KEC-80-DB-2-B1 (grain 1)	1	5.73	0.30
KEC-80-DB-2-B1 (grain 1)	2	5.82	0.24
KEC-80-DB-2-B1 (grain 1)	3	5.78	0.24
KEC-80-DB-2-B1 (grain 1)	4	5.76	0.27
KEC-80-DB-2-B1 (grain 1)	5	5.82	0.26
KEC-80-DB-2-B1 (grain 2)	1	5.66	0.26
KEC-80-DB-2-B1 (grain 2)	2	5.80	0.25
KEC-80-DB-2-B1 (grain 2)	3	5.77	0.27
KEC-80-DB-2-B1 (grain 2)	4	5.73	0.25
KEC-80-DB-2-B1 (grain 2)	5	5.74	0.26
KEC-80-DB-2-B1 (grain 3)	1	5.78	0.26
KEC-80-DB-2-B1 (grain 3)	2	5.77	0.27
KEC-80-DB-2-B1 (grain 3)	3	5.80	0.25
KEC-80-DB-2-B1 (grain 3)	4	5.91	0.28
KEC-80-DB-2-B1 (grain 3)	5	5.87	0.25
KEC-80-DB-2-B2 (grain 1)	1	5.64	0.25
KEC-80-DB-2-B2 (grain 1)	2	5.65	0.27
KEC-80-DB-2-B2 (grain 1)	3	5.69	0.26
KEC-80-DB-2-B2 (grain 1)	4	5.71	0.25
KEC-80-DB-2-B2 (grain 1)	5	5.67	0.25
KEC-80-DB-2-B2 (grain 2)	1	5.61	0.27
KEC-80-DB-2-B2 (grain 2)	2	5.77	0.27
KEC-80-DB-2-B2 (grain 2)	3	5.56	0.24
KEC-80-DB-2-B2 (grain 2)	4	5.62	0.28
KEC-80-DB-2-B2 (grain 2)	5	5.50	0.25
KEC-80-DB-2-B2 (grain 3)	1	5.56	0.25
KEC-80-DB-2-B2 (grain 3)	2	5.52	0.24
KEC-80-DB-2-B2 (grain 3)	3	5.64	0.26
KEC-80-DB-2-B2 (grain 3)	4	5.70	0.27
KEC-80-DB-2-B2 (grain 3)	5	5.63	0.25
KEC-81-DB-1 (grain 1)	1	6.33	0.24
KEC-81-DB-1 (grain 1)	2	6.26	0.26
KEC-81-DB-1 (grain 1)	3	6.32	0.28
KEC-81-DB-1 (grain 1)	4	6.44	0.26
KEC-81-DB-1 (grain 1)	5	6.27	0.26

KEC-81-DB-1 (grain 2)	1	6.43	0.29
KEC-81-DB-1 (grain 2)	2	6.34	0.26
KEC-81-DB-1 (grain 2)	3	6.40	0.24
KEC-81-DB-1 (grain 2)	4	6.28	0.26
KEC-81-DB-1 (grain 2)	5	6.31	0.26
KEC-81-DB-1 (grain 3)	1	6.39	0.26
KEC-81-DB-1 (grain 3)	2	6.28	0.26
KEC-81-DB-1 (grain 3)	3	6.32	0.24
KEC-81-DB-1 (grain 3)	4	6.35	0.26
KEC-81-DB-1 (grain 3)	5	6.32	0.24



Fig. C.1. Example of a Koidu diamondiferous eclogite xenolith (KEC-80-DB-2) with subhedral garnets in a matrix of clinopyroxene. An octahedral diamond is embedded in clinopyroxene.

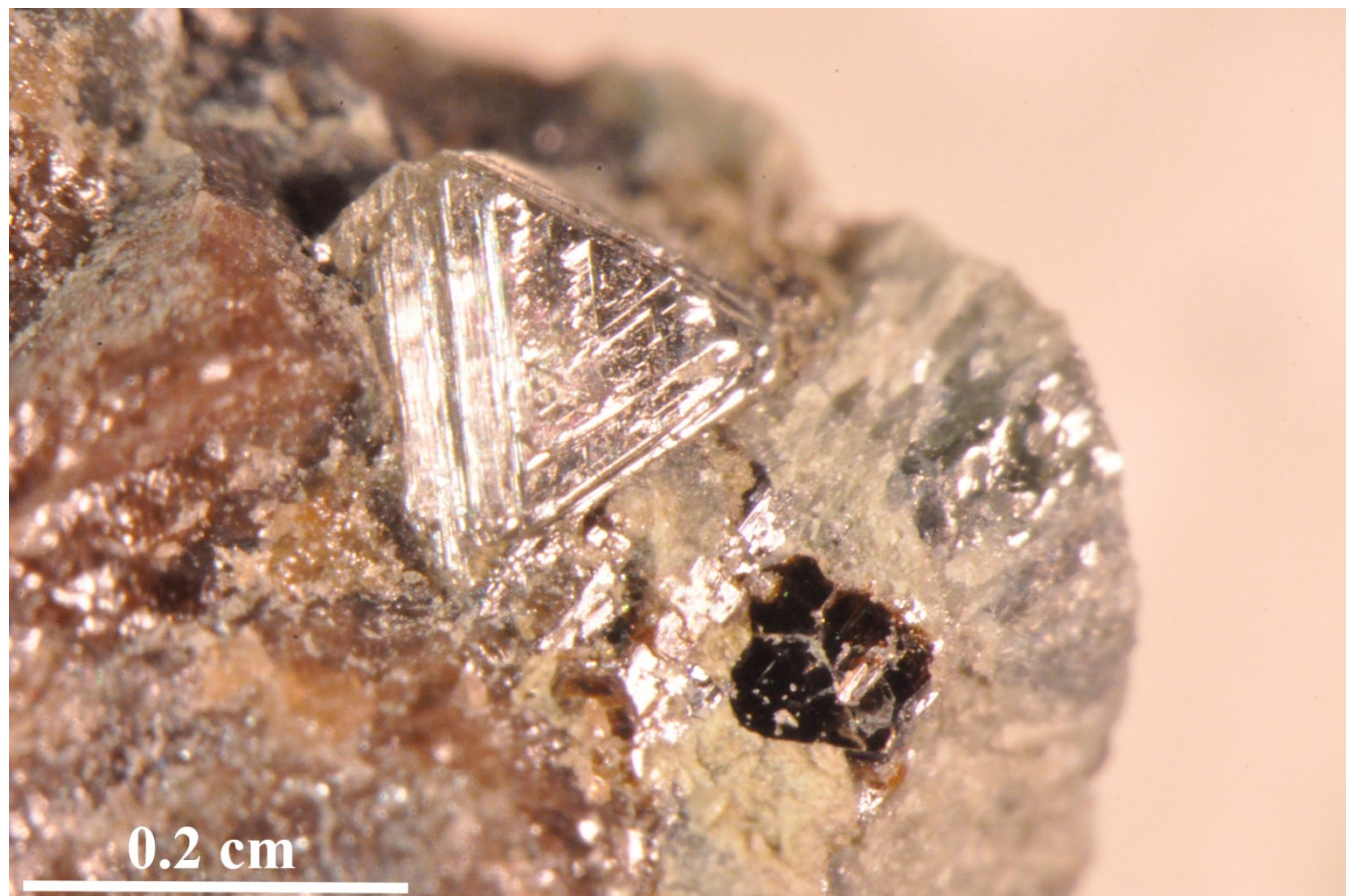


Fig. C.2. Example of a Koidu diamondiferous eclogite xenolith (KEC-81-DB-1) with accessory phlogopite.

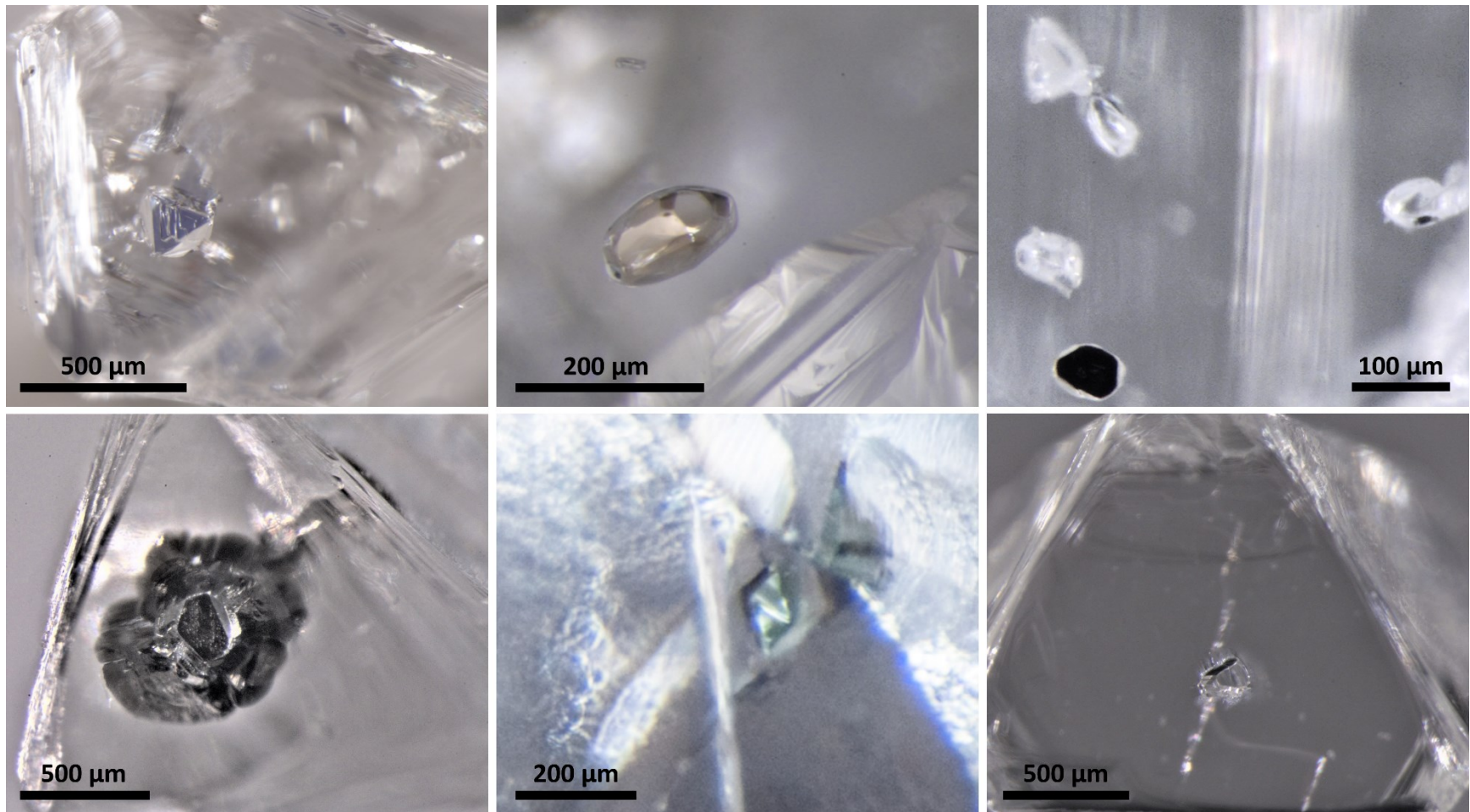


Fig. C.3. Common mineral inclusions in Koidu diamonds. Top row (from left to right): kyanite; eclogitic garnet; Mg-chromite and olivine. Bottom row (from left to right): sulphide; omphacite; coesite.